STATIC, ROTORDYNAMIC, AND THERMAL CHARACTERISTICS OF A FOUR PAD SPHERICAL-SEAT TILTING PAD JOURNAL BEARING WITH FOUR METHODS OF DIRECTED LUBRICATION

A Thesis

by

DAVID MICHAEL COGHLAN

Submitted to the Office of Graduate and Professional Studies of
Texas A&M University
in partial fulfillment of the requirements for the degree of

MASTER OF SCIENCE

Chair of Committee,	Dara W. Childs
Committee Members,	Luis A. San Andrés
	Ray W. James
Head of Department,	Andreas A. Polycarpou

August 2014

Major Subject: Mechanical Engineering

ABSTRACT

Static, dynamic, and thermal characteristics (measured and predicted) are presented for a 4-pad, spherical-seat, TPJB with 0.5 pivot offset, 0.6 L/D, 101.6 mm nominal diameter, and 0.3 preload in the LBP orientation. One bearing is tested four separate times in the following four different lubrication configurations: (1) flooded single-orifice (SO) at the bearing shell, (2) evacuated leading edge groove (LEG), (3) evacuated spray-bar blocker (SBB), and (4) evacuated spray-bar (SB). The LEG, SBB, and SB are all considered methods of "directed lubrication". These methods rely on lubrication injected directly to the pad/rotor interface. The same set of pads is used for every test to maintain clearance and preload; each method of lubrication is added as an assembly to the bearing.

Test conditions include surface speeds and unit loads up to 85 m/s and 2.9 MPa respectively. Static data includes measured bearing clearances prior to operation (cold) and immediately after operation (hot), rotor-bearing eccentricities and attitude angles, and a new approach to locating the hot center of a bearing. Dynamic data includes: (1) impedance values calculated from measured accelerations, displacements, and excitation forces; and (2) four sets (one set for each bearing configuration) of direct and cross-coupled rotordynamic coefficients derived from measurements and fit to a frequency independent KCM model.

Thermal data include measured temperatures from sixteen bearing thermocouples along with inlet, outlet, stator housing, and ambient thermocouples. Twelve of the bearing thermocouples are embedded in the babbitt layer of the pads while the remaining four are oriented at the leading and trailing edge of the loaded pads exposed to the lubricant. Bearing thermocouples provide a circumferential and axial temperature gradient.

The pivot stiffness (pad and pivot in series) is measured and incorporated into predictions. Measured static, dynamic, and thermal values are compared to predictions

from XL_TPJB, a computer code developed at the Texas A&M University Turbomachinery Lab for predicting bearing performance.

Measurements show significant cross-coupled stiffness terms with opposite signs and magnitudes that are 20-50% of the direct terms, a max axial temperature gradient of 9.6 °C, and attitude angles as high as 29°; all of these indicate that the tilt motion of the pad may be impeded by friction between the spherical pivot and the pad.

Temperature measurements show directed lubrication, coupled with an evacuated bearing housing, reduces max bearing temperatures up to 13.9 °C for the LEG, 10.2 °C for the SBB, and 12.8 °C for the SB. Although the SB and SBB reduce the max bearing temperature as intended, they can also cause an increase in temperatures at the leading and trailing edges of the loaded pads. The LEG typically reduced temperatures at all locations. Compared to the base case of the flooded SO, directed lubrication reduces the max bearing temperature. Additionally, the dynamics of the system can also be significantly impacted. Using directed lubrication can reduce direct stiffness by up to 18% for the LEG, 25% for the SBB, and 20% for the SB. Similarly, the direct damping can be reduced by up to 24% for the LEG, 45% for the SBB, and 34% for the SB.

DEDICATION

To my Family

ACKNOWLEDGMENTS

On a weekly basis Dr. Dara Childs, David Tschoepe, Michael Murphey, and Jennifer Gaines assisted me with this project. Thank you. Your advice, help, and humor made this project enjoyable. I would also like to thank Dr. San Andres, Yujiao Tao, Yingkun Lee, Stephen Phillips, Ray Mathews, Dr. John Kocur, Tom Shoup, Dr. John Nicholas, Dr. Ray James, and the Turbomachinery Research Consortium (TRC). Thank you all for your time and support.

NOMENCLATURE

$\boldsymbol{A_{ij}}$	Frequency dependent stator acceleration [L/T^2]
c_{ij}	Non-dimensional damping [--]
C_{ij}	Damping coefficients [FT/L]
C_b	Radial bearing clearance [L]
C_p	Radial pad clearance [L]
D	Bearing diameter [L]
$\boldsymbol{D_{ij}}$	Frequency dependent relative motion [L]
e	Total magnitude of journal eccentricity [L]
e_x, e_y	Components of journal eccentricity in x and y directions [L]
$\boldsymbol{F_{ij}}$	Frequency dependent stator excitation force [F]
F_s	Applied static load [F]
F_r	Reaction force to applied static load [F]
f_{bx}, f_{by}	Bearing reaction forces [F]
f_x, f_y	Excitation forces [F]
f_w	Whirl-frequency ratio [--]
$\boldsymbol{H_{ij}}$	Frequency dependent impedance (dynamic stiffness) [F/L]
$\boldsymbol{j}$	Imaginary operator ($\sqrt{-1}$) [--]
K_{eq}	Equivalent stiffness [--]
k_{ij}	Non-dimensional stiffness [--]
K_{ij}	Stiffness coefficients [F/L]
L	Pad axial length [L]
M_s	Mass of assembled bearing and stator [M]
M_p	Pad dimensionless preload [--]
M_{ij}	Virtual mass coefficients [M]
N	Number of impedances to be averaged [--]
n	Number of shake frequencies analyzed [--]
Q_d	Downstream fluid film flow rate in a feed groove [L^3/T]

Q_s	Supply fluid film flow rate in a feed groove [L^3/T]
Q_u	Upstream fluid film flow rate in a feed groove [L^3/T]
R_b	Bearing radius [L]
R_p	Pad radius [L]
R_s	Shaft radius [L]
T_d	Downstream feed groove fluid film temperature [Θ]
T_{max}	Max bearing temperature [Θ]
T_s	Oil inlet (supply) temperature [Θ]
T_u	Upstream feed groove fluid film temperature [Θ]
$\ddot{x}_s, \ddot{y}_s$	Stator acceleration in the *x* and *y* directions [L/T^2]
$\Delta x, \Delta y$	Relative displacement in the *x* and *y* directions [L]
ε	Total magnitude of journal eccentricity ratio [--]
$\varepsilon_x, \varepsilon_y$	Components of journal eccentricity ratio in *x* and *y* directions [--]
θ	Bearing circumferential coordinate [Angle]
λ	Thermal mixing coefficient [--]
Λ	Excitation frequency squared [T^{-2}]
ϕ	Attitude angle [Angle]
ω	Rotational speed of journal [T^{-1}]
ω_n	First critical speed [T^{-1}]
Ω	Excitation frequency [T^{-1}]

Subscripts

i	Direction of response, $i = x, y$
j	Direction of excitation, $j = x, y$
	(For example, K_{xy} corresponds to stiffness in the *x*-direction produced by displacement in the *y*-direction)

Abbreviations

DE	Drive end
LBP	Load between pad
LEG	Leading edge groove
LOP	Load on pivot
NDE	Non-drive end
OSI	Onset speed of instability
SB	Spray-bar
SBB	Spray-bar blocker
SO	Single-orifice
TPJB	Tilting-pad journal bearing
WFR	Whirl frequency ratio

TABLE OF CONTENTS

LIST OF FIGURES

LIST OF TABLES

INTRODUCTION

Hydrodynamic fluid film bearings are commonly used in turbomachinery to provide low friction load support between the rotating journal and the stationary ground. Relative motion between the journal and the bearing is required to drag the viscous lubricant into a convergent wedge and create hydrodynamic pressure, which supports the journal. Figure 1 shows a tilting-pad journal bearing (TPJB), a subset of hydrodynamic fluid film bearings.

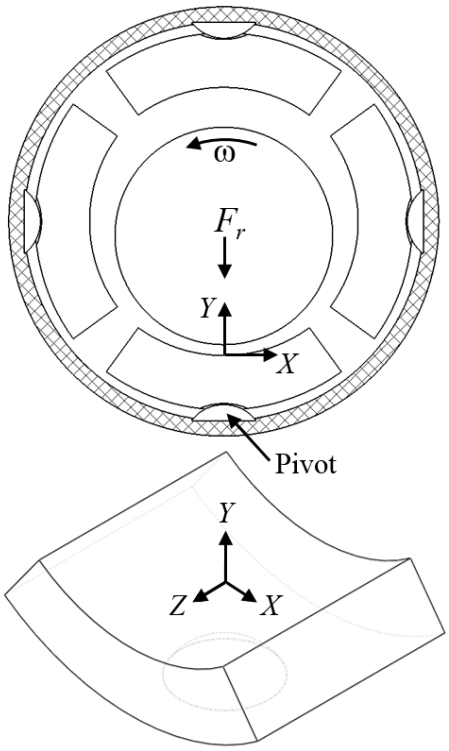

Figure 1: 4-Pad Spherical-Seat TPJB in Load-On-Pivot Orientation

In Figure 1 the force from the rotor weight, F_r, is directed downwards through the pad pivot; a load-on-pivot (LOP) orientation. The bearing can also be oriented so that the force from the rotor weight is between pad pivots; a load-between-pivot (LBP)

orientation. The bearing in Figure 1 has a spherical-seat pivot, which allows the pad to tilt radially about the *Z*-axis, and transversely about the *X*-axis. The radial rotation is typical of TPJBs and allows the resultant force from the hydrodynamic pressure to pass through the pivot, which increases stability and can improve the dynamic response of a rotor-bearing system. A spherical pivot also enables the pad to tilt axially to correct for any axial misalignment between the bearing and the shaft. This axial degree of freedom is not typical of all TPJBs. Figure 2 shows definitions for several geometric bearing parameters including the shaft radius, R_s, bearing radius, R_b, pad radius, R_p, pivot arc angle, θ_{PIVOT}, and pad arc angle, θ_{PAD}. In Figure 2 the bearing center and the journal center are concentric.

Shaft Radius	R_s
Bearing Center	Ⓑ
Bearing Radius	R_b
Pad Center	Ⓟ
Pad Radius	R_p
Pivot Arc Angle	θ_{PIVOT}
Pad Arc Angle	θ_{PAD}

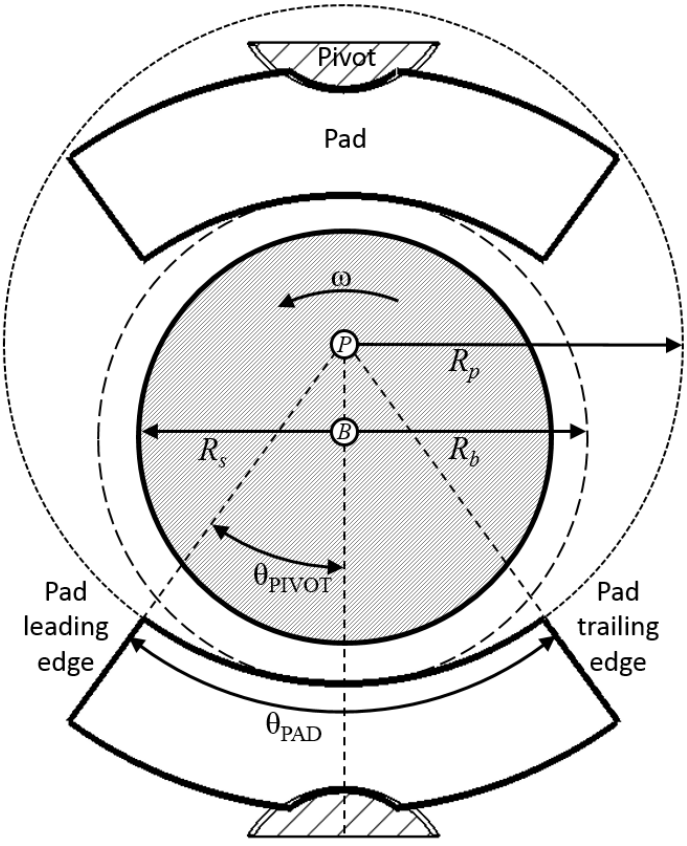

Figure 2: Definition of Geometric Bearing Parameters

The shaft radius, bearing radius, and pad radius are used to define the radial bearing clearance, C_b, and radial pad clearance, C_p.

$$C_b = R_b - R_s \tag{1}$$

$$C_p = R_p - R_s \tag{2}$$

The pivot offset defines the location of the pivot relative to the leading edge of the pad,

$$Pivot\,Offset = \frac{\theta_{PIVOT}}{\theta_{PAD}} \tag{3}$$

where θ_{PIVOT} is the angle from the pad leading edge to the pivot, and θ_{PAD} is the total arc length of the pad. Pad dimensionless preload, M_p, is

$$M_p = 1 - \frac{C_b}{C_p} \tag{4}$$

and is used to compare the pad curvature to bearing curvature. A positive preload is typical and helps provide a convergent fluid film even when the journal is operating concentrically with the bearing. Negative preloads are avoided since divergent fluid films are typically undesirable.

The fluid film can be modeled by the springs, dampers, and mass terms in Figure 3.

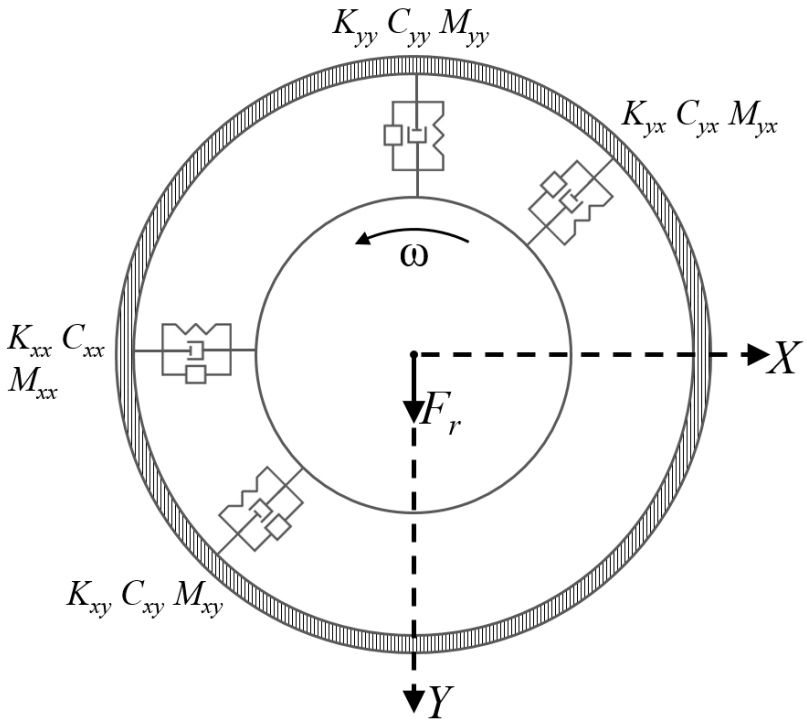

Figure 3: Spring, Mass, Damper (KCM) Model for Fluid Film Support

K_{ij}, C_{ij}, and M_{ij} are the stiffness, damping, and virtual mass terms, respectively, and collectively known as the rotordynamic coefficients. Rotordynamic coefficients are separated into direct terms, $i = j$, and cross-coupled terms, $i \neq j$. Cross-coupled stiffness and cross-coupled virtual mass terms can be destabilizing. A KCM model, which is used to model the bearing reaction forces, f_{bx}, f_{by}, for small amplitude motions about a static equilibrium position is

$$-\begin{Bmatrix} f_{bx} \\ f_{by} \end{Bmatrix} = \begin{bmatrix} K_{xx} & K_{xy} \\ K_{yx} & K_{yy} \end{bmatrix} \begin{Bmatrix} \Delta x \\ \Delta y \end{Bmatrix} + \begin{bmatrix} C_{xx} & C_{xy} \\ C_{yx} & C_{yy} \end{bmatrix} \begin{Bmatrix} \Delta \dot{x} \\ \Delta \dot{y} \end{Bmatrix} + \begin{bmatrix} M_{xx} & M_{xy} \\ M_{yx} & M_{yy} \end{bmatrix} \begin{Bmatrix} \Delta \ddot{x} \\ \Delta \ddot{y} \end{Bmatrix} \tag{5}$$

where $\Delta x, \Delta y$ are the relative displacements between the bearing and rotor in the X and Y axes respectively; $\Delta \dot{x}, \Delta \dot{y}, \Delta \ddot{x}, \Delta \ddot{y}$ are the relative velocities and accelerations. A KC model can also be used where the virtual mass terms are neglected.

In 1964, Lund [1] pioneered the prediction of rotordynamic coefficients using a KC model and assuming a pad response frequency that is synchronous with running speed. Coefficients found using this method are “synchronously reduced coefficients” [2]. In 1978, Lund stated that the damped natural frequency should be used instead of the synchronous frequency, which prompted research into the frequency dependence of TPJB coefficients [2] . Rodriguez [3], Dmochowski [4], Carter [5], Harris [6], Kulhanek [7], Delgado et al. [8], and Tschoepe [9], investigated the frequency dependence of rotordynamic coefficients for TPJBs using a KCM model; for each, the KCM model fit the data well resulting in frequency independent coefficients.

Dynamic data for spherical-seat TPJBs have been presented by Harris [6], Wygant et al. [10] [11], and Pettinato and De Choudhury [12]-[13]. In 2008, Harris [6] presented static and dynamic data for a 4-pad, spherical-seat TPJB in a LBP orientation with a bearing diameter of 101.6 mm, L/D = 1, and a 65% pivot offset. Harris concluded that the frequency-independent KCM model “did a good job of fitting the experimental dynamic-stiffness coefficients.” Harris measured dynamic data at excitation frequencies from 20-350 Hz for rotor surface speeds of 21, 31, 42, 53, and 63 m/s; and unit loads of 0.7, 1.4, and 1.9 MPa. Harris concluded that significant cross-coupled stiffness was present (15-35% of direct coefficients), although it should be insignificant for a TPJB (theoretically). However, the measured bearing clearance was highly elliptical (unintended) with a radial clearance of 99.57 μm in one axis and 54.61 μm in the perpendicular axis, likely indicating that the bearing was significantly crushed prior to testing. Distorting the intended shape of the bearing likely had a significant effect on the static and dynamic characteristics of the bearing, and results from Harris might not be representative of the typical characteristics of a spherical-seat TPJB.

In 1999, Wygant et al. [10]-[11] presented static and dynamic data for two separate bearings, identical except for pivot type, one a spherical-seat and the other a rocker-back. Each was a 5-pad bearing, with a nominal diameter of 70 mm, L/D = 0.75, 0.32 preload, 50% pivot offset, and tested in the LOP orientation. They measured dynamic data at synchronous excitation frequencies of 15, 27.5, and 37.5 Hz for the

corresponding (low) surface speeds of 3.3, 6.1, and 8.3 m/s; and (low) unit loads of 0.061-0.073 MPa. They conclude that significant cross-coupled stiffness was measured for the spherical-seat bearing but not for the rocker-back bearing. They attribute the spherical-seat cross-coupled stiffness to impeded tilt motion of the pad due to friction between the pad and pivot; measured finite attitude angles further support this conclusion.

In 1999, Pettinato and De Choudhury [12]-[13] presented static, dynamic, and temperature data for two 5-pad bearings in the LBP orientation. The bearings differed in pivot type, pad arc angle, and pad thickness; both have a diameter of 126.9 mm, L/D = 0.3, C_b = 95 µm, preload = 0.35, and a 50% pivot offset. The spherical-seat bearing has a 55.5° pad arc angle, and the key-seat bearing (shown in Figure 4) has a 65° pad arc angle.

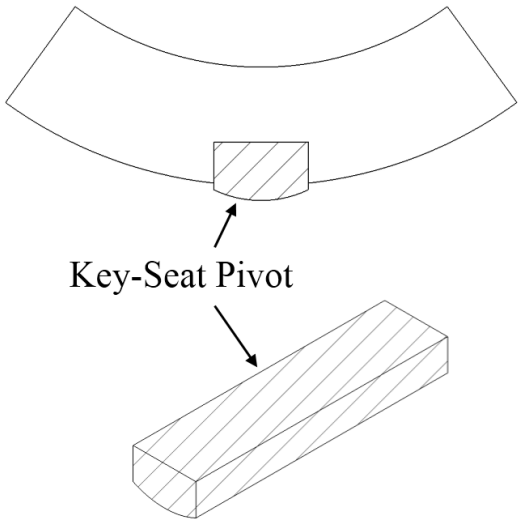

Figure 4: Key-Seat Pivot

Dynamic coefficients from Pettinato and De Choudhury are limited to direct stiffness and direct damping terms. No cross-coupled terms are calculated or presented, although the authors state that the static data "suggests the presence of cross-coupling forces."

The measured direct stiffness and damping were typically greater for the key-seat bearing than for the spherical-seat bearing, and the spherical-seat bearing showed a higher attitude angle than the key-seat bearing.

Besides pivot type the lubrication method is also important. Changing the method of lubrication can change how efficiently cool inlet oil is supplied to the pad surface. Figure 5 shows a TPJB and the thermal mixing that occurs between pads.

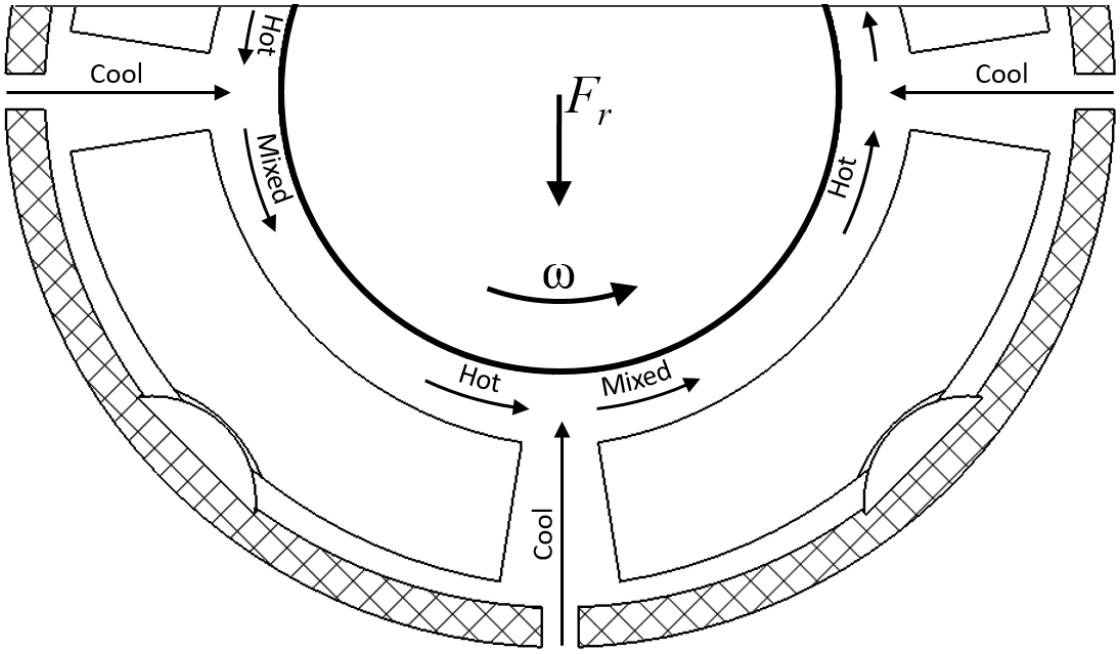

Figure 5: Thermal Mixing and Hot Oil Carry-Over in a TPJB

As oil moves from the leading edge to the trailing edge of a pad, the temperature of the lubricant will increase. The hot oil from the upstream pad mixes with the cool oil from the bearing inlet and the mixed oil enters the leading edge of the downstream pad; this is hot oil carry-over. From San Andrés [14], the amount of hot oil carry-over is quantified by the thermal mixing coefficient, λ, with a typical value of 0.80. The flow balance for the thermal mixing in Figure 5 is

$$Q_d = Q_s + \lambda Q_u \tag{6}$$

where Q_d, Q_s, and Q_u are the downstream (hot oil), supply (cool oil), and upstream (mixed oil) fluid film flow rates respectively [14]. The energy balance for the thermal mixing is

$$\begin{gathered} Q_d T_d = Q_s T_s + \lambda Q_u T_u \\ T_u > T_d > T_s \end{gathered} \tag{7}$$

where T_d, T_s, and T_u are fluid film temperatures at the downstream, supply, and upstream locations respectively [14]. Nicholas [15] presents several design limits for bearings, including the max bearing babbitt temperatures of Eq. (8). He states that the bearing babbitt will melt around 235 °C; however, it will become soft and will "wipe or smear" around 121 °C.

$$\begin{aligned} T_{\max} &\leq 85°C \text{ design (analytical prediction)} \\ T_{\max} &\leq 93°C \text{ test acceptance} \\ T_{\max} &\leq 110°C \text{ alarm} \\ T_{\max} &\leq 121°C \text{ trip} \end{aligned} \tag{8}$$

Nicholas continues, stating that a high bearing temperature can be the limiting factor when attempting to operate turbomachinery at higher speeds and loads.

Various methods of lubricating fluid film bearings have been introduced to allow operation at more severe conditions. Figure 6 shows four different lubricant feed methods for a TPJB. The lubricant flow path is shown along with the rotational direction of the journal, ω.

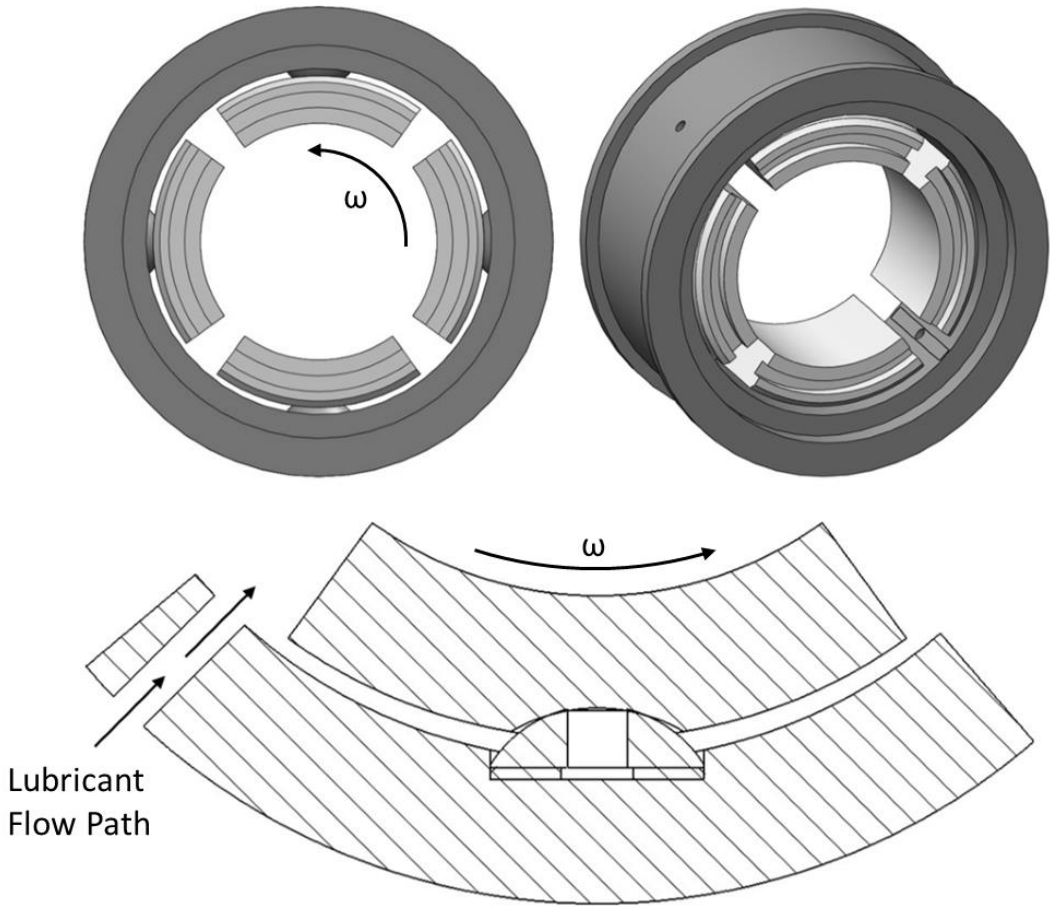

(a): Single Orifice Feed Type (Conventional)

Figure 6: Bearing Feed Types: (a) Single Orifice, (b) Spray-Bar Blocker, (c) Leading Edge Groove, and (d) Spray-Bar (figure continued on the following pages)

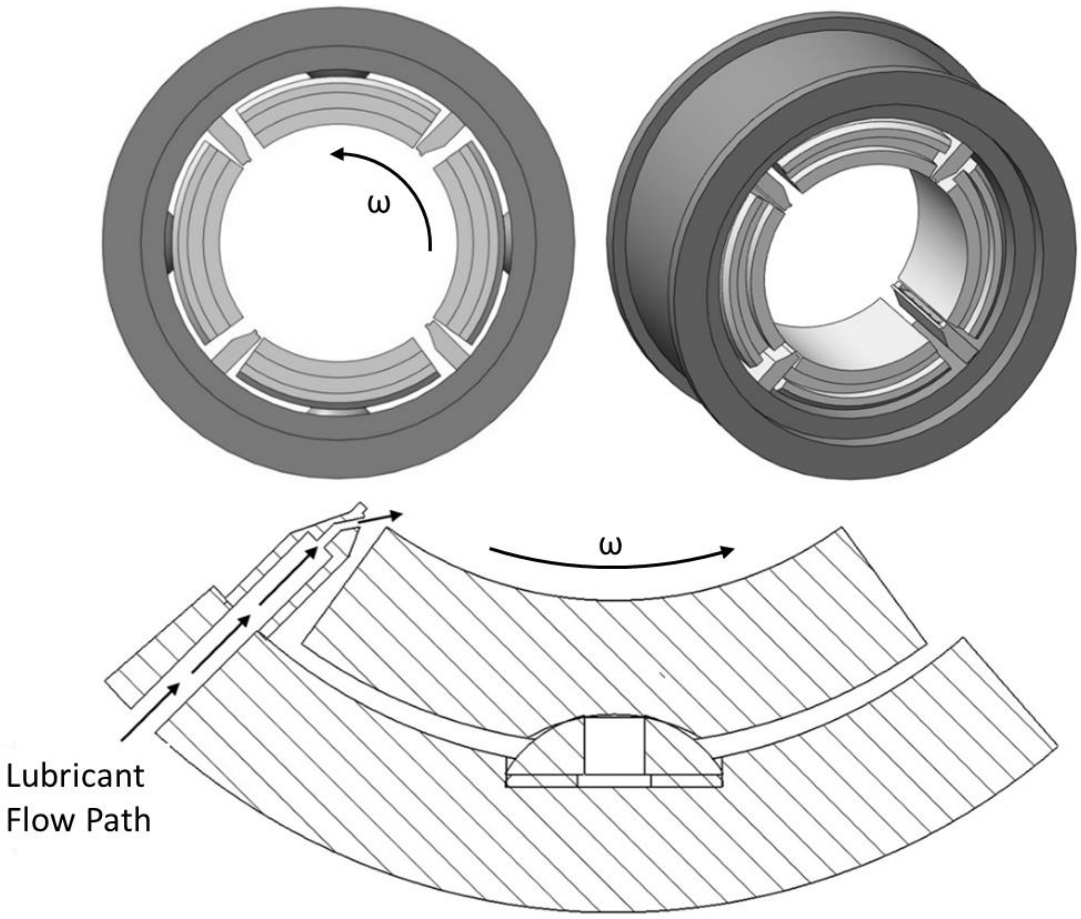

(b): Spray-Bar Blocker Feed Type

Figure 6 Continued.

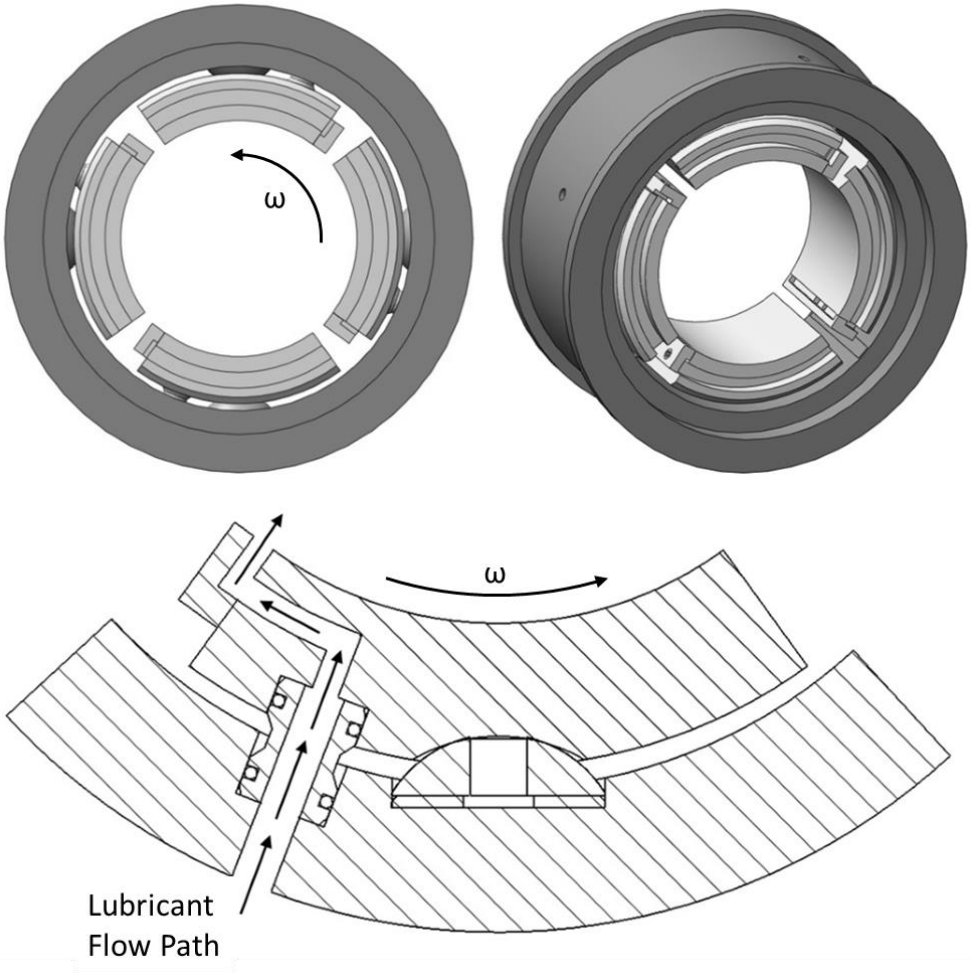

(c): Leading Edge Groove Feed Type

Figure 6 Continued.

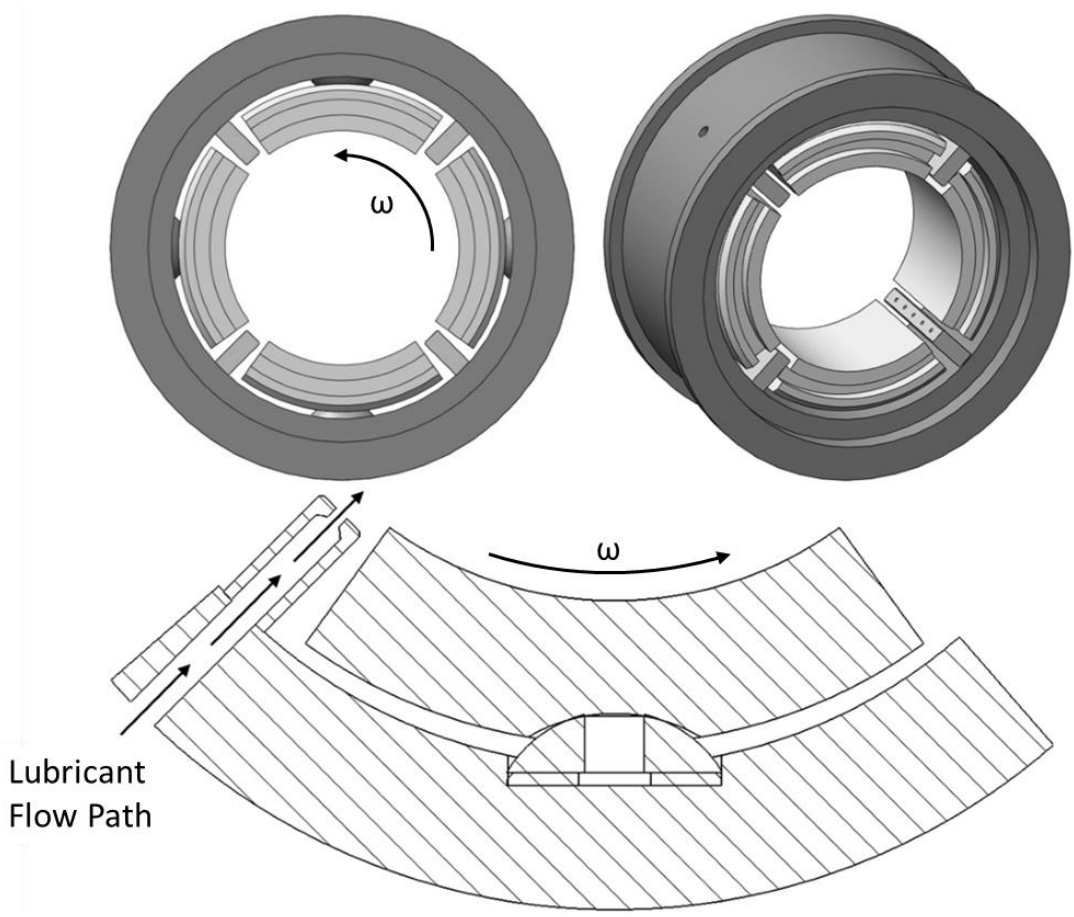

(d): Spray-Bar Feed Type

Figure 6 Continued.

The single orifice (SO) feed is the conventional method for providing lubricant to a fluid film bearing. A bearing with a single orifice feed will typically be configured with end seals ("flooded configuration") resulting in a pressurized housing by restricting the exit oil flow [15]. Using a single orifice feed at the bearing shell without end seals ("evacuated housing") is typically avoided as it can promote bearing starvation (insufficient oil to provide a constant film between rotor and pad). The spray-bar blocker (SBB) is a patented feed type described in [16]. The SBB feeds cool inlet oil close to the pad surface and incorporates a "scraper" feature, which aims to decrease (block) the hot oil carry-over. The leading edge groove (LEG) is comprised of a groove that runs axially

along the leading edge of the pad with cool inlet oil directly (usually) supplied to the groove. The spray-bar (SB) introduces cool inlet oil close to the pad surface similar to the SBB; however, the SB was not designed to prevent hot oil carry-over. The SBB, LEG, and SB are all methods of directed lubrication; methods that aim to deliver cool inlet oil directly to the pad surface.

Directed lubrication was first utilized in journal bearings by Sasaki et al. [17] in 1987 in the form of a spray-bar. In 1991, Tanaka [18] showed that by using "spot lubrication" (similar to a spray-bar) and removing the floating ring end seals (an evacuated housing) the max bearing temperature could be decreased by up to 10 °C. Operating a bearing with an evacuated housing allows hot oil to exit freely reducing bearing temperatures [18].

Nicholas [19] discusses the use of the spray-bar blocker and provides several examples of its use in actual-application, temperature-reducing TPJBs. However, all of the examples use the spray-bar blockers in conjunction with other methods of temperature reduction including 65% offset pivots (DeCamillo and Brockwell [20] reduced temperatures by 20 °C using offset pivots), by-pass cooling [21], and chrome-copper pads. These combinations make it difficult to quantify the spray-bar blocker's direct contribution to temperature reductions. All of the examples presented by Nicholas are for spherical-seat bearings. The load/speed combinations (very high speeds and loads) successfully utilizing the spray-bar blockers presented by Nicholas are; 2.4 MPa at 76.2 m/s, 3.4 MPa at 86.9 m/s, 5.3 MPa at 106.7 m/s, and 3.2 MPa at 128 m/s.

The spherical-seat bearing that Harris [6] tested was also equipped with spray-bar blockers, 65% offset pivots, chrome-copper pads, and by-pass cooling. He tested at a max rotor surface speed of 63 m/s in the LBP orientation with a unit load of 1.9 MPa and a max temperature of 71 °C. Harris does not discuss the clearance of the end seals; however, it is apparent from images that the inner end seal clearance was substantially larger than the outer seal. This seal arrangement is similar to the one used by Nicholas [19] in his examples (seal arrangement shown in Figure 7). No comparison is made between a conventional flooded bearing and the reduced-temperature bearing.

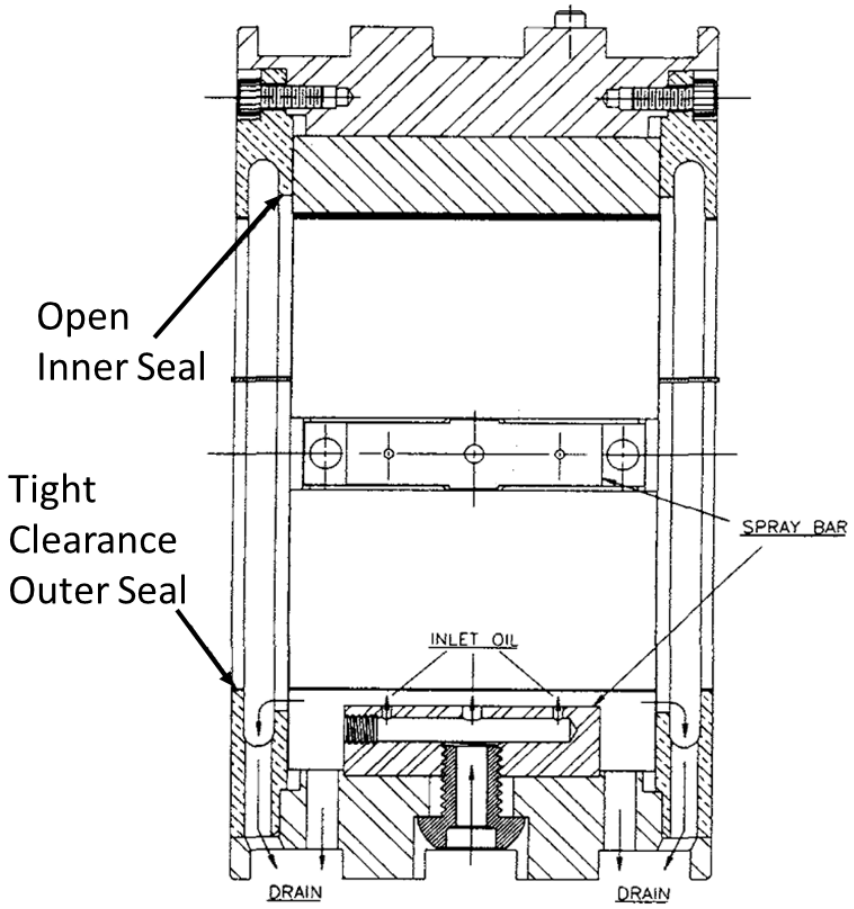

Figure 7: Seal Arrangement Used By Nicholas and Harris - Adapted from [15]

Dmochowski et al. [22] compare a rocker-pivot TPJB with an LEG to an identical bearing with a conventional SO feed, both with a 98 mm inner diameter. Each bearing has 5 pads with L/D = 0.387, 60% pivot offsets, 0.25 preload, and a radial bearing clearance of 76 μm. The pivot is "contoured both circumferentially and axially to allow the pads to adjust to conditions of axial misalignment" [22]. Temperatures are measured for both the LOP and LBP orientations up to speeds of 85 m/s and loads of 3.0 MPa. Dmochowski et al. do not state whether the bearings had evacuated or flooded housings. The description states that each bearing had "two aluminum alloy end plates" (end seals) but the clearance is not reported. Dmochowski et al. conclude that, below a certain threshold surface speed, the LEG and the conventionally lubricated bearing have

negligible differences in max pad temperature. That threshold surface speed is 26 m/s for a LBP orientation and 46 m/s for a LOP orientation. The largest difference in max pad temperature occurred at 85 m/s and 3.0 MPa; 20 °C for LBP and 10 °C for LOP, both in favor of the LEG design.

Continuing the work of Dmochowski et al. [22], Brockwell et al. [23] compare an LEG bearing with two other similar bearings, both conventional SO bearings. The results of the comparison are shown in Table 1. All bearings in Table 1 have 5-pads with C_b = 76.2 µm, C_p = 101.6 µm, and M_p = 0.25.

Table 1: Temperature Results from Brockwell et al. [23]

Load On Pad Orientation		
Feed Type	Pivot Offset	Max Temperature
LEG	60%	95 °C
SO	60%	111 °C
SO	50%	103 °C

Load Between Pad Orientation		
Feed Type	Pivot Offset	Max Temperature
LEG	60%	92 °C
SO	60%	116 °C
SO	50%	104 °C

Table 1 shows that the LEG can reduce temperatures up to 16 °C in the LOP orientation, and 24 °C in the LBP orientation. Brockwell et al. conclude that using an LEG bearing can reduce temperatures up to 24 °C through a reduction of the hot oil carried over from one pad to the next. The configuration of the end seals is not discussed.

Nicholas [15] presents results for a flooded bearing with inlet nozzles that is retrofitted to operate in an evacuated condition with spray-bars. Both the original bearing and the retrofit are 4-pad, 101.6 mm diameter bearings. The operating speed range is 21 m/s to 88 m/s, and the orientation is LBP. The load, pivot offset, and pivot type are not given. The seal clearance is not given but Nicholas states that the inner end seals are "wide open." He concludes that using spray-bars with an evacuated housing results in an approximate 10% decrease in pad temperatures, for a maximum reduction of approximately 20 °C for the hottest case.

In 1990, Harangozo et al. [24] compared the effects of the following three different methods of lubrication: (1) conventional (SO) flooded, (2) spray-bar (SB) evacuated, and (3) LEG evacuated. Their 4-pad TPJB had spherical seat pivots, a 127 mm diameter, L/D = 1, and a preload range of $-0.75 < M_p < -0.62$. For the evacuated housing, the labyrinth end seals are replaced with pad retaining rings; geometric details are not given. Tests are conducted up to surface speeds of 47 m/s and unit loads of 1.3 MPa. Their LEG differs from others in that the lubricant travels through the center of the spherical seat pivot and then through a channel in the pad to reach the LEG. They conclude that the temperatures for the loaded pads are lower for the evacuated spray-bar design than for the flooded SO design, and that the LEG runs cooler than the spray-bar except at high speeds. These results are not directly applicable to most bearings since a negative preload is usually undesirable as it will cause a divergent fluid film when a convergent one is typically desired.

In 2005 Dmochowski and Blair [25] addressed concerns over the effect an evacuated housing would have on the static and dynamic properties of a TPJB. Tests were conducted on a 5-pad TPJB in LBP orientation with a 98.6 mm diameter, L/D = 0.4, preload = 0.3, and 50% pivot offset. The pivot type is not stated explicitly but appears to be a rocker-back. Tests were conducted up to surface speeds of 76 m/s and unit loads of 1.5 MPa. Static, dynamic, and thermal data are presented for the same bearing with two different radial end seal clearances; a flooded clearance of 152.4 μm, and an evacuated clearance of 3175 μm (feed type is not specified). They conclude that "enlarging the

bore of the bearing end seals caused a significant reduction in bearing operating temperatures…as much as 15 °C at the higher speed." The dynamic data presented contains direct coefficients (no cross-coupled coefficients are presented) found using the power spectral density (PSD) method from Rouvas et al. [26]. Dmochowski and Blair state that an increase in the seal clearance leads to a reduction in the stiffness and damping, primarily in the direction perpendicular to load. With a unit load of 1.5 MPa the reduction is approximately 20-30% for the stiffness and damping coefficients in the direction perpendicular to load.

This thesis presents static, dynamic, and thermal measurements for a 4-pad, spherical-seat, TPJB in the LBP orientation. The bearing has a 0.6 L/D, 0.3 preload, 50% pivot offset, and 101.6 mm diameter. Four sets of data are presented, one for each of the following methods of lubrication: flooded SO at the bearing shell, evacuated LEG, evacuated SBB, and evacuated SB. These configurations are compared to determine which results in the lowest temperatures, and how the different configurations impact the dynamic properties of the rotor-bearing system. Each method of lubrication is added as an assembly to the bearing so that the same set of pads is used for each of the four configurations; ideally maintaining the clearance and preload across each configuration. Data sets are presented for surface speeds up to 85 m/s and loads up to 2.9 MPa. XL_TPJB [27], a computer code developed by Dr. San Andrés and Yujiao Tao, is used for static, dynamic, and thermal predictions to compare with the measured data.

TEST RIG AND BEARING DESCRIPTION

Figure 8 shows the bearing test rig at the Texas A&M Turbomachinery Lab; described in detail by Kaul [28]. This is a "floating bearing" test rig following the design pioneered by Glienecke [29] in 1966. The rotor is assumed stationary, and the bearing is perturbed relative to the rotor to measure the dynamic properties.

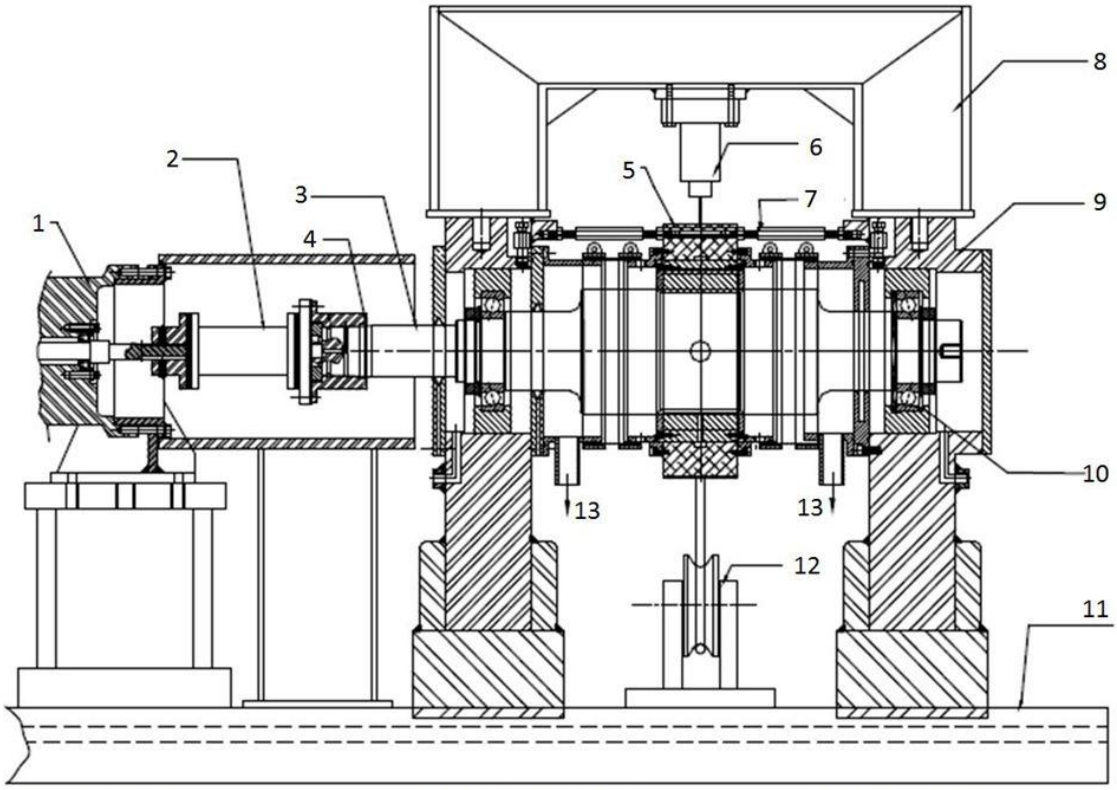

1. Air Turbine
2. Coupling
3. Test Rotor
4. Hydraulic Hub
5. Bearing Housing
6. Hydraulic Shaker
7. Pitch Stabilizer
8. Shaker Mounting Frame
9. Pedestal
10. Ball Bearing
11. Test Rig Base
12. Pulley
13. Test Oil Outlet

Figure 8: Side View of Bearing Test Rig Adapted from [7]

The air turbine drives the test rotor and has a maximum speed of 17,000 rpm. The turbine is connected to the test rotor by a flexible disc-pack coupling and a hydraulically fitted hub.

The test rotor is made of AISI 4140 steel with a measured diameter of 101.59 mm at the test bearing film lands. Axial alignment of the bearing relative to the rotor is achieved by six pitch stabilizers that prevent movement of the bearing in the axial direction but provide minimal support in the radial direction. Pedestals support the rotor through two angular contact ball bearings. The ball bearings are lubricated using an oil mist system, and buffer seals are used to prevent axial leakage of oil from the test bearing into the ball bearing chambers. Figure 9 is the test rig viewed from the non-drive end (NDE). The raw static and dynamic measurements are in this "bearing fixed" coordinate system. Data presented in this thesis has been converted to a conventional right-handed coordinate system where the rotor weight acts with gravity, and the journal rotation is counter-clockwise.

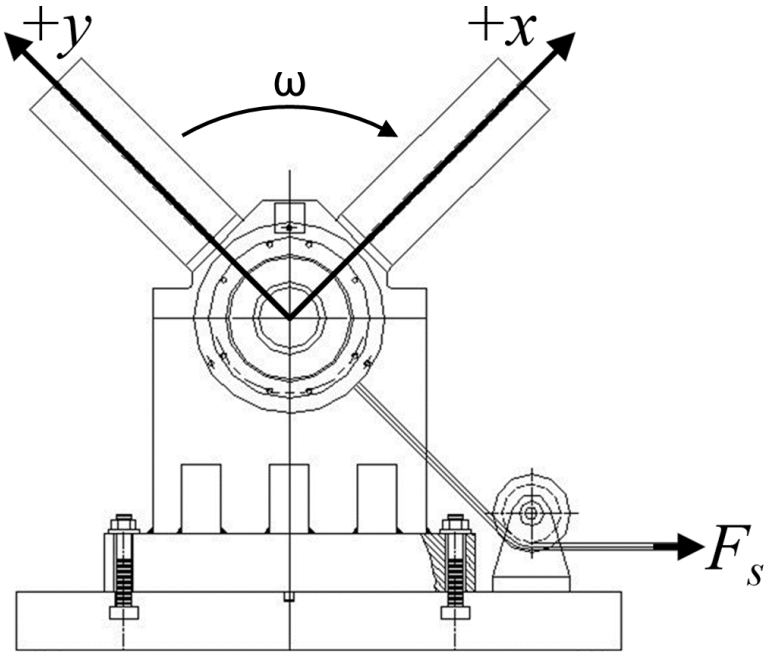

Figure 9: Front View of Test Rig from the NDE
(Rotor Rotation is Clockwise Viewed from NDE)

F_s is the static load applied to the bearing via a cable pulled by a large spring and pneumatic piston. As F_s is increased, the stationary rotor will appear to move in the $+y$ direction (since the coordinate system of Figure 9 is fixed to the bearing).The spring and pneumatic loader can apply a maximum load of 17.8 kN.

The test bearing is lubricated with ISO VG46 weight oil. The oil system delivers flow rates from 8–68 L/min (2-18 gpm). The oil system incorporates a heat exchanger and two adjustable valves, which control a hot stream and cold stream of oil. The two streams are mixed by adjusting the two valves, allowing the inlet oil temperature to be controlled within ±1 °C.

The test bearing is installed in a split-housing stator, which clamps about the bearing. A crush test is conducted to determine the amount of interference between the OD of the test bearing and the ID of the stator. This ensures that the stator does not distort the intended shape of the bearing. For this test bearing, the crush test indicated a 6 µm radial interference fit. The bearing is located in the stator by a pin which also prevents rotation of the bearing. The stator has attachments for the pitch stabilizers, eddy-current probes, accelerometers, pressure transducers, pneumatic loading attachment, and hydraulic shakers.

Figure 10 shows the non-drive end (NDE) of the test bearing with the hydraulic shaker heads and stingers attached.

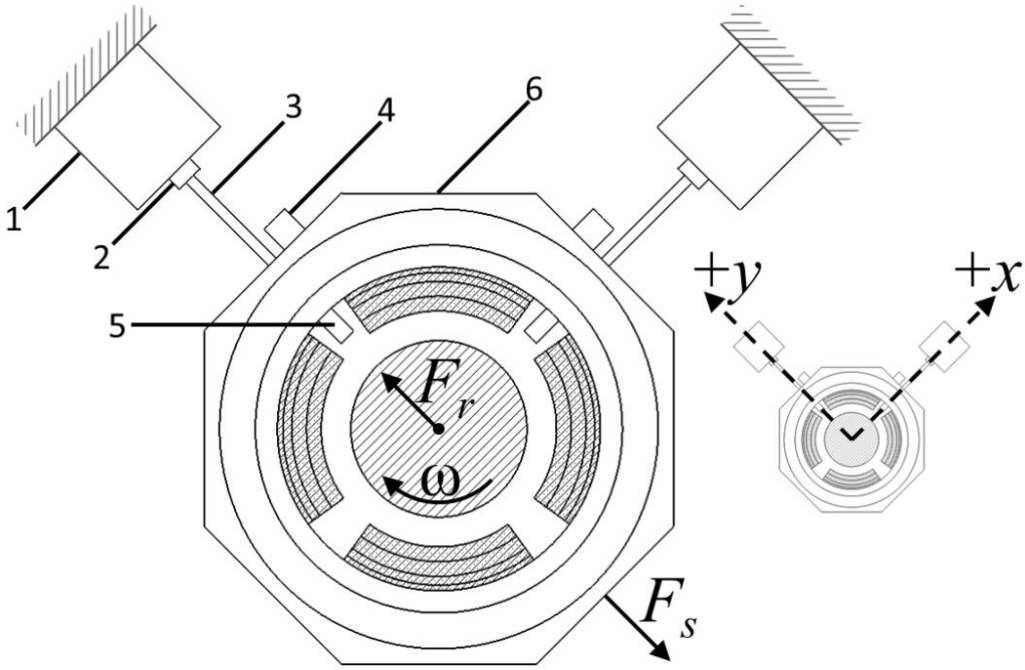

1 – Hydraulic Shaker
2 – Force Transducer
3 – Stinger
4 – Accelerometer
5 – Eddy Current Probe
6 – Location of Stator Thermocouple

Figure 10: Hydraulic Shaker/Stinger Setup for Bearing Excitation

The hydraulic shaker heads (1) are used to perturb the bearing about the rotor via the stingers (3). The input force of the shakers and the acceleration of the stator housing are measured in two orthogonal directions by the accelerometers (4) and the force transducers (2). The relative displacement between the bearing and the shaft is measured with two sets of perpendicular eddy current probes (5). One set is on the drive-end (DE), and the other on the NDE (a total of four probes). Comparing one set of eddy current probes to the other allows for axial alignment of the bearing and shaft. The eddy current probes have a measurement error of ±4 μm. The *x*-shaker can provide tensile and compressive forces up to 4450 N and the *y*-shaker can provide tensile forces of 4450 N, and compressive forces of 11,125 N. Each shaker can operate at excitation frequencies

up to 1000 Hz. The coordinate system of Figure 10 is the same “bearing fixed” system as Figure 9 for the raw data only.

Two static pressure probes measure the pressure of the lubricant at the inlet and NDE outlet. Specifically, the inlet probe measures the pressure in the feed groove that runs along the outer circumference of the bearing shell, and the outlet probe measures the pressure of the lubricant immediately after the end seals (immediately upstream of the “Test Oil Outlet” shown in Figure 8). Two thermocouples are placed in the same location as the pressure probes to measure the inlet and outlet temperatures of the lubricant, the outlet temperature is also measured at the DE of the bearing.

Lufkin RMT manufactured the test bearing, which is similar to the bearing tested by Harris [6]; however, this bearing does not have by-pass cooling, chrome-copper pads, or pad leading edge chamfers. As manufactured, the test bearing is a 4-pad TPJB, spherical-seat 50% offset pivot, L/D = 0.6, 0.3 mean preload, with a bearing bore of 101.77±0.0127 mm for a radial clearance of 90±6.4 μm (101.59 mm rotor diameter). The bearing clearance was measured at 94±8 μm in one axis and 95±8 μm in the perpendicular direction, indicating no significant bearing crush as Harris [6] experienced (the clearance measurement method is discussed later). The 1018 steel pad axial length is 61 mm with a pad arc angle of 72°. The bearing can be configured with the four different feed types (SO, LEG, SBB, SB) shown in Figure 6 with either a flooded or evacuated housing; the same set of pads is used for each configuration. Figure 11 and Figure 12 show the flooded and evacuated configurations, respectively.

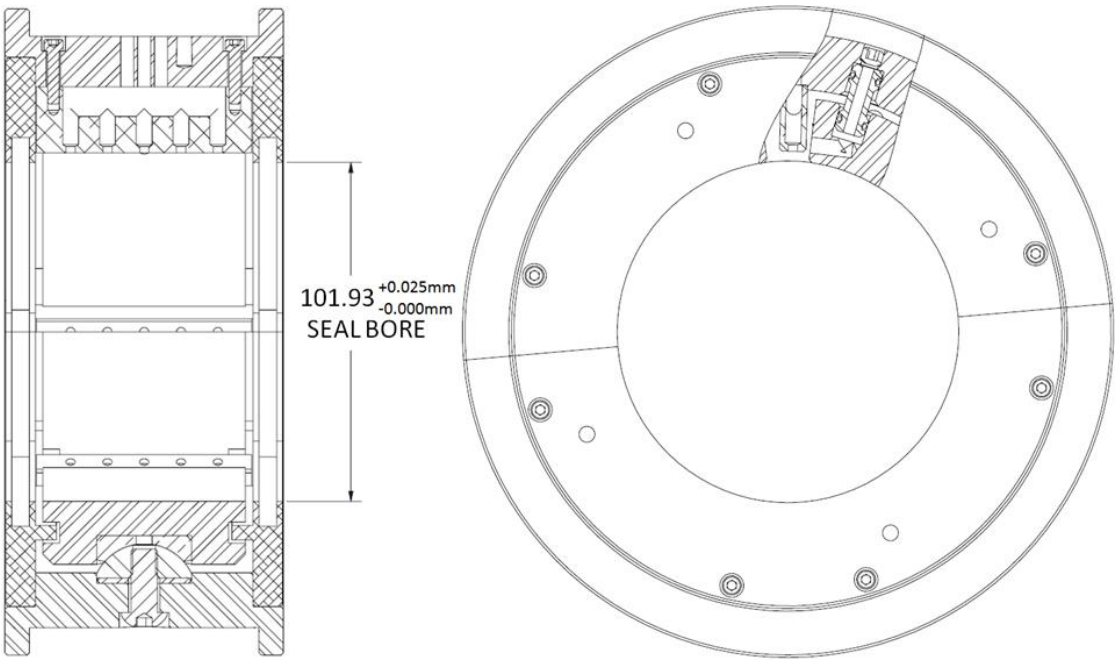

Figure 11: Flooded Bearing Configuration with Labyrinth End Seals Installed (Nominal End Seal Bore 101.93mm)

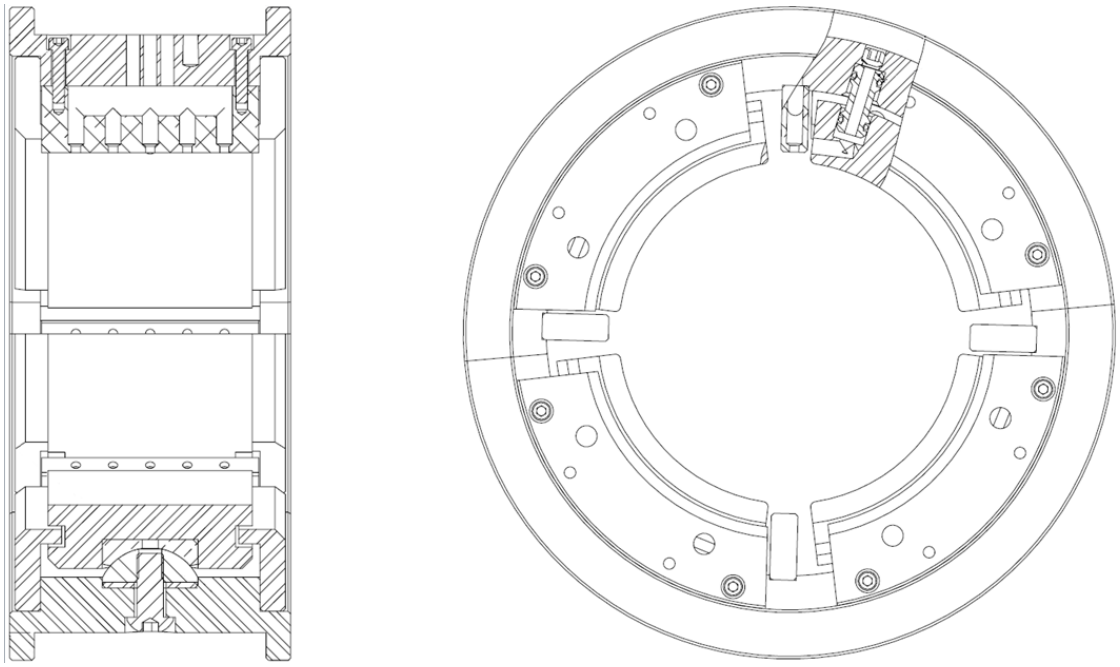

Figure 12: Evacuated Bearing Configuration with Pad Retainers Installed

The evacuated configuration (Figure 12) uses eight separate pad retainers; two for each pad, one for the DE and one for the NDE. Using separate pad retainers results in a large gap between each pad set. Some evacuated designs simply increase the bore of the end seals, which eliminates the gap between pads. Dmochowski and Blair [25] simply enlarge the clearance of the end seals from 152.4 µm for flooded, to 3175 µm for evacuated.

The bearing has 12 babbitt layer thermocouples and 4 exposed thermocouples (3, 8, 9, 14). The thermocouple layout was designed to measure differences at the pad leading and trailing edge caused by the different methods of lubrication. The bearing thermocouples are J-Type with an error of ±1.1 °C. The temperature of the bearing housing (stator) is also measured (location shown in Figure 10), along with the ambient temperature of the test cell. The ambient temperature measurement is made immediately adjacent to the stator housing.

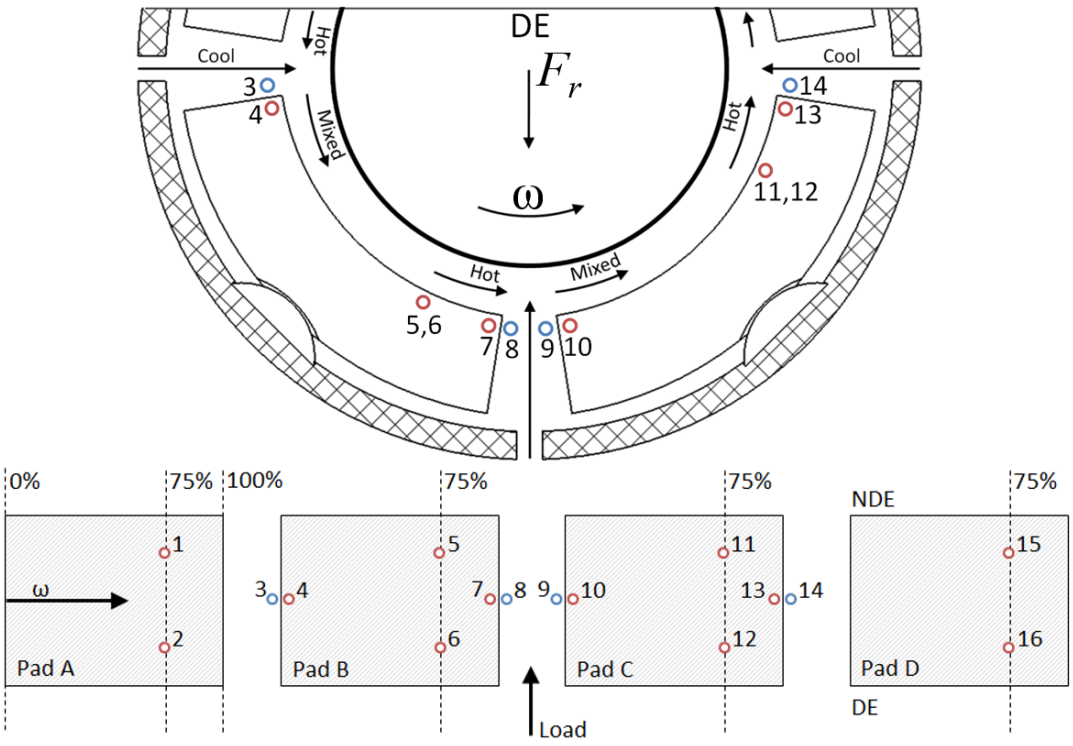

Figure 13: Bearing Thermocouple Layout (Babbitt Layer and Exposed)

EXPERIMENTAL PROCEDURE

Bearing Clearance Measurement

Prior to all testing, the "cold clearance" of the bearing is measured; this is accomplished with the bearing installed on the test rig using the eddy current probes shown in Figure 10. The hydraulic shakers are used to precess the bearing about the rotor, establishing the absolute clearance of the bearing. This procedure is done with no oil in the system and a stationary (non-rotating) rotor prior to testing with the bearing at the ambient temperature ("cold"). The force used to precess the bearing is small to minimize elastic deflection of the rotor and test bearing. The resulting shape for a 4-pad bearing is (approximately) a square, where each side is a pad (Figure 14).

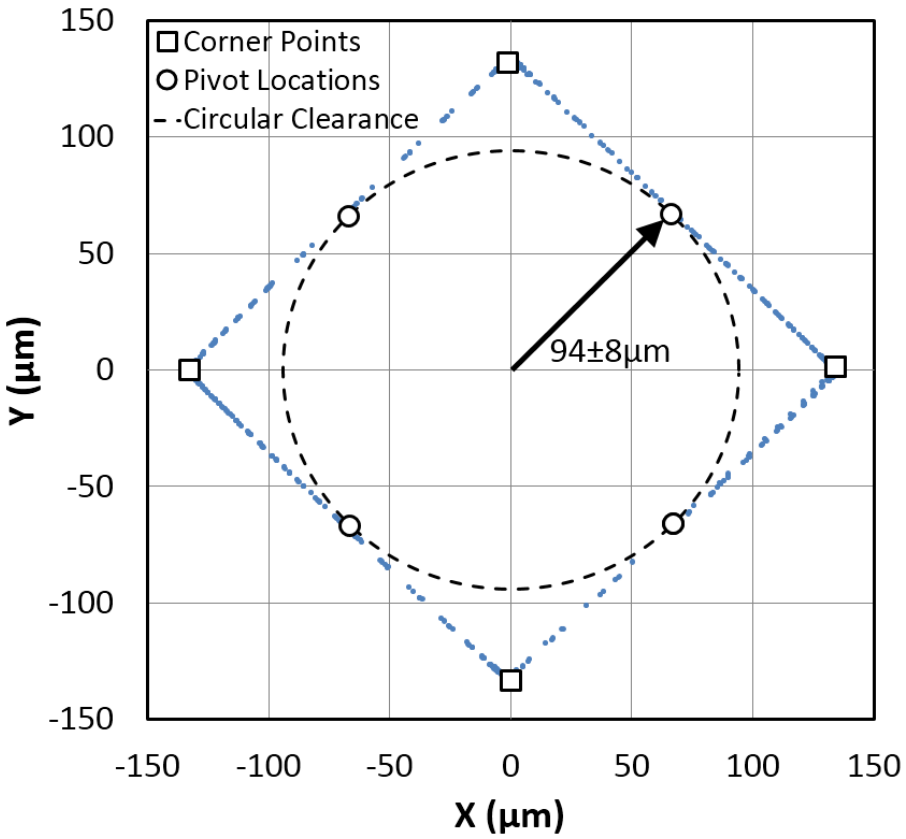

Figure 14: Measured Bearing Cold Clearance

The corner points of the clearance square are then used to determine the midpoint of each side, or pad. The middle of each side is the location of the pad pivot since this bearing has a 50% pivot offset. The four pad-pivot locations are then used to determine a best-fit circle, which is recorded as the circular clearance of the bearing. Note that in the LBP orientation it is possible to exceed the circular bearing clearance without contact between the bearing and the shaft. Appendix A contains cold clearance measurements for each of the four bearing configurations tested.

Dynamic Excitation Test

After the clearance measurement, the lubricant flow rate is set, followed by the rotor speed and static load. From startup, it takes approximately three hours to reach steady state temperature conditions. The nominal speed and load combinations tested, along with feed types, are listed in Table 2. Following the recommendations of Lufkin RMT, the flow rates for the flooded and evacuated configurations are 38 LPM (10 gpm) and 42 LPM (11 gpm) respectively. Refer to Appendix B for the measured conditions during the dynamic tests. The lubricant is an ISO VG46 with a nominal inlet temperature of 49 °C.

Table 2: Feed Types Tested with Speed/Load Combinations

Lubricant Feed Types (ISO VG46)				Rotational Speed: rpm	Surface Speed: m/s	Load: MPa
Flooded: Single Orifice (SO)	Evacuated: Leading Edge Groove (LEG)	Evacuated: Spray-Bar Blocker (SBB)	Evacuated: Spray-Bar (SB)	7000	38	0.7
						2.1
						2.9
				10,000	53	0.7
						2.1
						2.9
				13,000	69	0.7
						2.1
						2.9
				16,000	85	0.7
						2.1
						2.9

Once a steady-state condition is attained, the bearing is excited in two orthogonal directions (*x* and *y* of Figure 10); in each direction, the bearing is excited using a pseudo-random multi-frequency waveform with frequency components from 10-250 Hz in 10 Hz increments. During the excitation, voltage is recorded from the accelerometers ($\ddot{x}_S, \ddot{y}_S$), force transducers (f_x, f_y), and eddy current probes (Δx, Δy) shown in Figure 10. These values are recorded in the time domain at a sampling frequency of 10,000 Hz then transferred to the frequency domain via Fast Fourier Transform. The result is a set of frequency domain accelerations ($\boldsymbol{A_x}$, $\boldsymbol{A_y}$), excitation forces ($\boldsymbol{F_x}$, $\boldsymbol{F_y}$), and bearing/rotor relative displacements ($\boldsymbol{D_x}$, $\boldsymbol{D_y}$). The bearing mass, M_s, is determined prior to testing during the baseline testing (explained in detail later). These measured values are used to solve for the impedances, $\boldsymbol{H_{ij}}$.

Equation (9) is the bearing housing equation of motion and is rewritten symbolically in Eq. (10).

(External Forces)+(Fluid Film Forces) = (Bearing Mass)(Bearing Acceleration) (9)

$$\begin{Bmatrix} f_x \\ f_y \end{Bmatrix} + \begin{Bmatrix} f_{bx} \\ f_{by} \end{Bmatrix} = \begin{Bmatrix} M_s \ddot{x}_s \\ M_s \ddot{y}_s \end{Bmatrix} \tag{10}$$

Combining Eq. (5) and Eq. (10) gives Eq. (11) in the time-domain, which is shown in the frequency domain in Eq. (12). The subscripts indicate the response direction and the direction of excitation. For example, K_{ij} denotes stiffness in the *i* direction produced by an excitation (or displacement) in the *j* direction.

$$\begin{Bmatrix} f_x - M_s \ddot{x}_s \\ f_y - M_s \ddot{y}_s \end{Bmatrix} = \begin{bmatrix} K_{xx} & K_{xy} \\ K_{yx} & K_{yy} \end{bmatrix} \begin{Bmatrix} \Delta x \\ \Delta y \end{Bmatrix} + \begin{bmatrix} C_{xx} & C_{xy} \\ C_{yx} & C_{yy} \end{bmatrix} \begin{Bmatrix} \Delta \dot{x} \\ \Delta \dot{y} \end{Bmatrix} + \begin{bmatrix} M_{xx} & M_{xy} \\ M_{yx} & M_{yy} \end{bmatrix} \begin{Bmatrix} \Delta \ddot{x} \\ \Delta \ddot{y} \end{Bmatrix} \tag{11}$$

$$\begin{Bmatrix} \boldsymbol{F_x} - M_s \boldsymbol{A_x} \\ \boldsymbol{F_y} - M_s \boldsymbol{A_y} \end{Bmatrix} = \begin{bmatrix} \boldsymbol{H_{xx}} & \boldsymbol{H_{xy}} \\ \boldsymbol{H_{yx}} & \boldsymbol{H_{yy}} \end{bmatrix} \begin{Bmatrix} \boldsymbol{D_x} \\ \boldsymbol{D_y} \end{Bmatrix} \tag{12}$$

$$\boldsymbol{H_{ij}} = \left(K_{ij} - \Omega^2 M_{ij}\right) + \boldsymbol{j}\left(\Omega C_{ij}\right) \tag{13}$$

The impedance[1] values, $\boldsymbol{H_{ij}}$, are the only unknowns of matrix Eq. (12), which has two equations and four unknowns. To determine $\boldsymbol{H_{ij}}$ explicitly, two excitations in orthogonal directions must be applied to the bearing [26]. The impedance values are determined explicitly with matrix Eq. (14), which has four equations and four unknowns.

$$\begin{bmatrix} \boldsymbol{F_{xx}} - M_s \boldsymbol{A_{xx}} & \boldsymbol{F_{xy}} - M_s \boldsymbol{A_{xy}} \\ \boldsymbol{F_{yx}} - M_s \boldsymbol{A_{yx}} & \boldsymbol{F_{yy}} - M_s \boldsymbol{A_{yy}} \end{bmatrix} = \begin{bmatrix} \boldsymbol{H_{xx}} & \boldsymbol{H_{xy}} \\ \boldsymbol{H_{yx}} & \boldsymbol{H_{yy}} \end{bmatrix} \begin{bmatrix} \boldsymbol{D_{xx}} & \boldsymbol{D_{xy}} \\ \boldsymbol{D_{yx}} & \boldsymbol{D_{yy}} \end{bmatrix} \tag{14}$$

The impedance values from Eq. (14) contain contributions from the fluid film and from the test rig.

$$\boldsymbol{H_{ij}} = \boldsymbol{H_{ij}^{FLUID\ FILM}} + \boldsymbol{H_{ij}^{TEST\ RIG}} \tag{15}$$

To determine the impedance of the fluid film (the item of interest) the contribution of the test rig must be eliminated. This is accomplished by a baseline test. Prior to operation (no lubricant, non-rotating rotor), a static load of 2 kN is applied to the bearing, which is then centered about the rotor, and a dynamic excitation test is conducted over the frequency range discussed previously. This is a baseline test, and without the fluid-film contribution the impedance from the baseline test is the impedance contribution of the test rig.

$$\boldsymbol{H_{ij}^{BASELINE}} = \boldsymbol{H_{ij}^{TEST\ RIG}} \tag{16}$$

[1] Impedance is formally defined as the ratio of force to velocity; however, it is commonly used for the dynamic-stiffness coefficients of bearings.

The baseline contribution is then subtracted from Eq. (15) to yield to impedance of the fluid film only. Using the baseline impedance data, the stator mass (M_s) is determined by changing it iteratively until the direct virtual mass terms, M_{xx} and M_{yy}, equal zero. Using this method, and the coordinate system in Figure 10, the stator mass, M_s, is 25 kg in the *x*-axis and 32 kg in the *y*-axis. Weighing the bearing and stator housing resulted in approximately the same values. The static-loader assembly is likely responsible for the additional mass in the *y*-axis. Throughout the remainder of this thesis $\boldsymbol{H_{ij}}$, K_{ij}, C_{ij}, and M_{ij} will be used to refer to the impedance, stiffness, damping, and virtual mass of the fluid film unless stated otherwise. With the complex impedance of the fluid film calculated explicitly, the stiffness, damping, and virtual mass of the fluid film is calculated using Eq. (17) and (18) where Ω is the excitation frequency in rad/s.

$$\text{Re}\ (\boldsymbol{H_{ij}}) = K_{ij} - \Omega^2 M_{ij} \tag{17}$$

$$\text{Im}\ (\boldsymbol{H_{ij}}) = \Omega\, C_{ij} \tag{18}$$

Dynamic Excitation: Curve Fitting and Uncertainty

For repeatability, the bearing is excited with the multi-frequency waveform 320 times in each orthogonal direction (320 in the *x*-axis and 320 in the *y*-axis). This results in 320 response waveforms for the stator acceleration, rotor/bearing displacement, and input force in each orthogonal direction. Every 20 response waveforms are averaged, resulting in 16 sets of response data. Each of the 16 is used to calculate an impedance value, $\boldsymbol{h_{ij}}$. The impedance values are then summed together and divided by the number of sets, N = 16, to obtain the average impedance, $\boldsymbol{H_{ij}}$.

$$\boldsymbol{H_{ij}} = \frac{1}{N}\sum_{k=1}^{N}\left(\boldsymbol{h_{ij}}\right)_k \tag{19}$$

Eqs. (17, 18) are used with the average impedance values to extract the rotordynamic coefficients. Rearranging Eq. (17) and setting $\Omega^2 = \Lambda$ gives Eq. (20); a linear function of Λ.

$$\mathrm{Re}\ (\boldsymbol{H_{ij}}) = K_{ij} + \Lambda(-M_{ij}) \tag{20}$$

The equation for damping, Eq. (18), is already a linear function so no manipulation is needed. Eqs. (18, 20) match the form of Eq. (21); Eqs. (22, 23) are used to identify the coefficients *a* and *b* using a least-squares method [30]. The measured values are x_i, y_i, and *n* is the number of experimental observations. For this case, the "measured" values are the impedance values, $\boldsymbol{H_{ij}}$, and the number of observations is equal to the number of excitation frequencies that are analyzed.

$$y = mx + b \tag{21}$$

$$a = \frac{\sum y_i \sum x_i^2 - \sum x_i \sum x_i y_i}{n\sum x_i^2 - \left(\sum x_i\right)^2} \tag{22}$$

$$b = \frac{n\sum x_i y_i - \sum x_i \sum y_i}{n\sum x_i^2 - \left(\sum x_i\right)^2} \tag{23}$$

Using the standard error of the *y*-data about the fit, $s_{y/x}$, and the value, S_{xx}^2, percent confidence intervals for the intercept and the slope are found with Eqs. (26, 27). The t-statistic, t, is 1.96 corresponding to a 95% confidence interval.

$$s_{y/x} = \left(\frac{1}{(n-2)} \sum_{i=1}^{n} \left[y_i - y(x_i) \right]^2 \right)^{1/2} \tag{24}$$

$$S_{xx}^2 = \sum_{i=1}^{n} x_i^2 - \frac{1}{n}\left(\sum_{i=1}^{n} x_i\right)^2 \tag{25}$$

$$b \pm t\frac{s_{y/x}}{S_{xx}} \qquad \text{(c\%)} \tag{26}$$

$$a \pm t s_{y/x}\sqrt{\frac{1}{n} + \frac{\left[\left(\frac{1}{n}\right)\sum x_i\right]}{S_{xx}^2}} \qquad \text{(c\%)} \tag{27}$$

Appendix B contains the rotordynamic coefficients from Eqs. (22, 23), along with the confidence intervals from Eqs. (26, 27).

Whirl-Frequency Ratio (WFR)

The whirl-frequency ratio, WFR, for a bearing is the ratio of the first critical speed, ω_n, to the onset speed of instability, OSI. A transition from positive to negative damping defines the OSI.

$$WFR = \frac{\omega_n}{\text{OSI}} \tag{28}$$

The WFR quantifies the destabilizing effect of a bearing for a given system [31]. If the first critical speed of a system is known, the WFR can be used to determine the onset speed of instability. For example, a bearing with WFR = 0.5 produces instability at a speed twice ($WFR^{-1} = 2$) the first critical speed, and a bearing with WFR = 0.25 produces instability at four times ($WFR^{-1} = 4$) the first critical speed. A plain cylindrical journal bearing typically has WFR = 0.5 [32]. Lund [33] presents the following method to evaluate WFR for a rigid rotor supported on plain journal bearings.

$$WFR = \sqrt{\frac{(K_{eq} - k_{xx})(K_{eq} - k_{yy}) - k_{xy}k_{yx}}{c_{xx}c_{yy} - c_{xy}c_{yx}}}$$
$$K_{eq} = \frac{c_{xx}k_{yy} + c_{yy}k_{xx} - c_{yx}k_{xy} - c_{xy}k_{yx}}{c_{xx} + c_{yy}} \tag{29}$$
$$k_{ij} = \frac{C_b}{F_s}K_{ij}$$
$$c_{ij} = \frac{C_b\omega}{F_s}C_{ij}$$

Lund's method neglects the contribution of virtual mass terms. San Andrés [32] presents an alternative method, which is identical to Lund's method except for the inclusion of the virtual mass terms. However, Lund's method is used in this thesis since the measured virtual mass terms typically have very high uncertainties (specifically the cross-coupled terms).

Static and Thermal Testing

At the completion of a dynamic excitation test, the system is returned to steady state, and the static operating conditions are measured. This includes all thermocouple temperatures, rotor position for the DE and NDE (which are averaged), lubricant pressure drop from inlet to outlet, applied load, rotor speed, and lubricant flow rate. For the static and thermal testing, the sampling rate is 2 Hz over a period of 30 sec, resulting in 60 data points from each sensor. The average of each is reported in Appendix C along with 95% confidence intervals. The confidence intervals are for the 60 samples only; they do not include the error of the sensors. The confidence intervals of Appendix C are included primarily as validation that a steady state condition was reached. In all cases, except for rotor speed, the confidence intervals are much lower than the accuracy of the sensors.

Measured eccentricity and static load values are used to calculate the approximate static stiffness, K_{STATIC}. The static stiffness should be approximately equal to the measured direct stiffness in the loaded direction, K_{yy}, from the dynamic measurements. K_{STATIC} is compared to K_{yy} in the dynamic results section to validate the test results.

$$K_{STATIC} = \left(\frac{\partial F_s}{\partial e_y} \right)_{SS} \approx \left(\frac{\Delta F_s}{\Delta e_y} \right)_{SS} \tag{30}$$

Hot Clearance Measurement

After static, dynamic, and thermal testing a "hot clearance" measurement is made. From steady state operation, the static load is removed ($F_s = F_r = 0$), the drive turbine is shut off ($\omega = 0$), the lubricant flow is terminated, and the bearing clearance is measured (method described previously). This is done as quickly as possible, with an average execution time of about 20 sec. In Figure 15, the hot clearance is approximately 20% smaller than the cold clearance and serves as an estimate of the operational clearance of the bearing. Changes in clearance are primarily due to the thermal expansion of the journal and bearing.

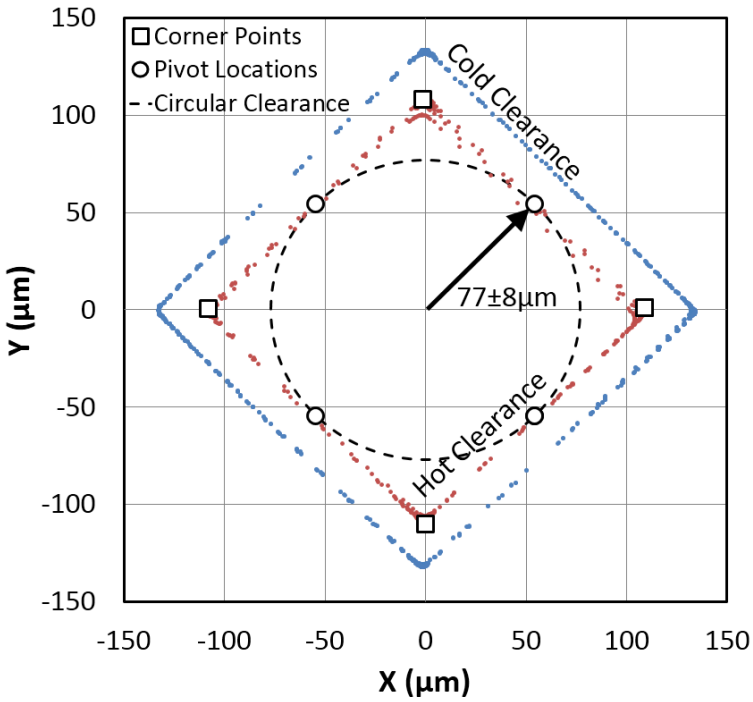

Figure 15: Hot and Cold Bearing Clearances

Since hot clearance measurements are time consuming (the rig must be shut down, restarted, and then returned to steady state to continue testing) they are only made at the highest load for each test speed. Limited measurements indicate that hot clearance measurements are more dependent on speed than load; hot clearances were measured for a constant speed at different loads and the difference was typically negligible.

Pivot Stiffness Measurement

The pivot stiffness was measured at the conclusion of static, dynamic, and thermal testing; pivot stiffness is the stiffness of the pad and pivot in series. The bearing is installed on the test rig in the LOP orientation, and the *y*-shaker (shown in Figure 10) is used to push the bearing into the rotor. This is similar to the method used by Harris [6] except a hydraulic shaker is used to apply the force instead of the static loader. The load from the *y*-shaker is increased from 0-4750 N, and the elastic deflection is recorded with the eddy current probes. The slope of the force versus deflection curve is the stiffness of

the pad and pivot in series. Kirk and Reedy [34] discuss the importance of incorporating the pivot stiffness into a predictive model. Figure 16 shows the measured pivot stiffness

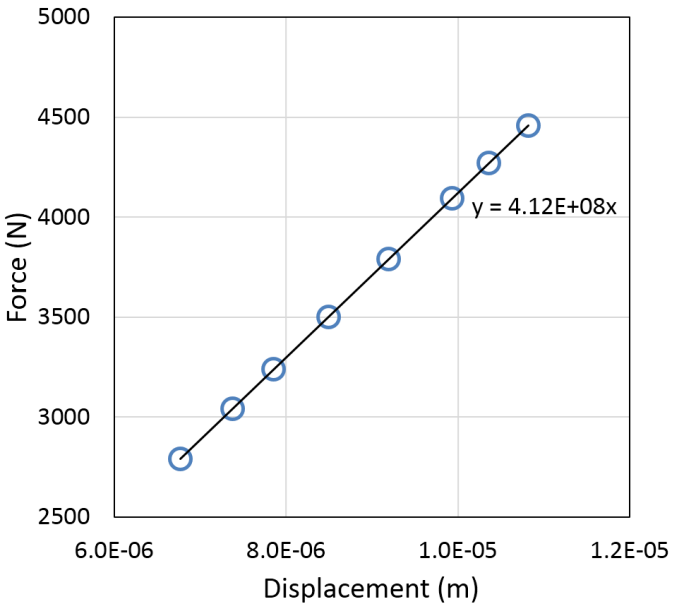

Figure 16: Measured Pad-Pivot Stiffness and Deflection Equation

The measured pivot stiffness of Figure 16 is 412 MN/m (approximated by a linear fit), which is slightly larger than the 350 MN/m measured by Harris [6], and less than half the 841 MN/m pivot stiffness measured by Tschoepe [9].

XL_TPJB: Bearing Performance Predictions

XL_TPJB was developed by Ms. Yujiao Tao and Dr. San Andrés at the Texas A&M University Turbomachinery Lab to predict bearing performance. A detailed description of XL_TPJB is given in [27]. XL_TPJB uses a thermohydrodynamic analysis with the selected options in Table 3, bearing properties in Table 4, and lubricant properties in Table 5.

Table 3: XL_TPJB Analysis Options

Analysis Type	Vary Load
Pad Option	Equal Pads
Fluid Inertia Option	Include Fluid Inertia Effects
Frequency Analysis Type	Nonsynchronous
Thermal Analysis Type (Adiabatic Journal and Pads)	4 (Haussen)
Pivot Option	User-Defined Load-Deflection Function (W = 4.12E+8x)
Clearance Option	Hot Bearing and Pad Clearances

Table 4: User Input Bearing Properties for XL_TPJB

Bearing Properties	
Rotor Diameter (m)	0.10159
Bearing Axial Length (m)	0.06100
Number of pads on bearing	4
Pad leading edge (°)	9.00
Preload	0.30
Pivot Offset	0.50
Pad Arc Length (°)	72.00
Pad Clearance (m)	1.24E-04
Temperature at Cold Condition (°C)	21.0
Shaft Thermal Expansion Coefficient (AISI 4140 Steel) [1/°C]	1.23E-05
Pad Thermal Expansion Coefficient (1018 Steel) [1/°C]	1.30E-05
Measured Pad Mass (kg)	6.35E-01
*Moment of Inertia about Pivot ($kg.m^2$)	4.59E-04
*Mass Center Location (m)	1.31E-02
Measured Pad Thickness (m)	1.90E-02

*Obtained from SolidWorks Model

Table 5: User Input Lubricant Properties for XL_TPJB

Fluid Properties (ISO VG46)	
Ambient Pressure (bar)	0.00
Cavitation Pressure (bar)	0.00
Supply Temperature (°C)	48.89
Viscosity at T_{supply} (cP)	2.56E+01
Density (kg/m^3)	843.5
Specific Heat (J/[kg °C])	2084.7
Thermal conductivity (Watt/[m °C])	0.1243
Viscosity Temperature Coefficient	0.0431

The user inputs listed in Tables 3-5 are constant for all predictions while the load, supply pressure, and shaft speed change for each test condition (shown in Appendix D). Frequencies from 9.77 to 166 Hz (in increments of 9.77 Hz) are used for the input excitation frequencies.

XL_TPJB does not include inputs to specifically address (model) the different methods of directed lubrication in this thesis (LEG, SBB, SB). However, the thermal mixing coefficient, λ, can be adjusted in an attempt to model the different feed types. Typically, a larger value of λ will yield higher max temperatures, higher direct stiffness, and lower direct damping. For this thesis, one set of predictions is provided using λ = 0.8. Predictions were also made for λ = 0.4, 0.5, 0.6, 0.7 and 0.9; however, these results are not shown because they did not provide a significant improvement in predictions. Overall, λ = 0.8 provided the best correlation between measurements and predictions for all four bearing configurations.

STATIC AND THERMAL RESULTS

Clearance Measurements

In 2008 Harris [6] tested a spherical seat bearing with the same test rig used here. Figure 17 is a re-creation of the highly elliptical bearing clearance reported by Harris, and also shows the direction of the split-housing stator clamping force.

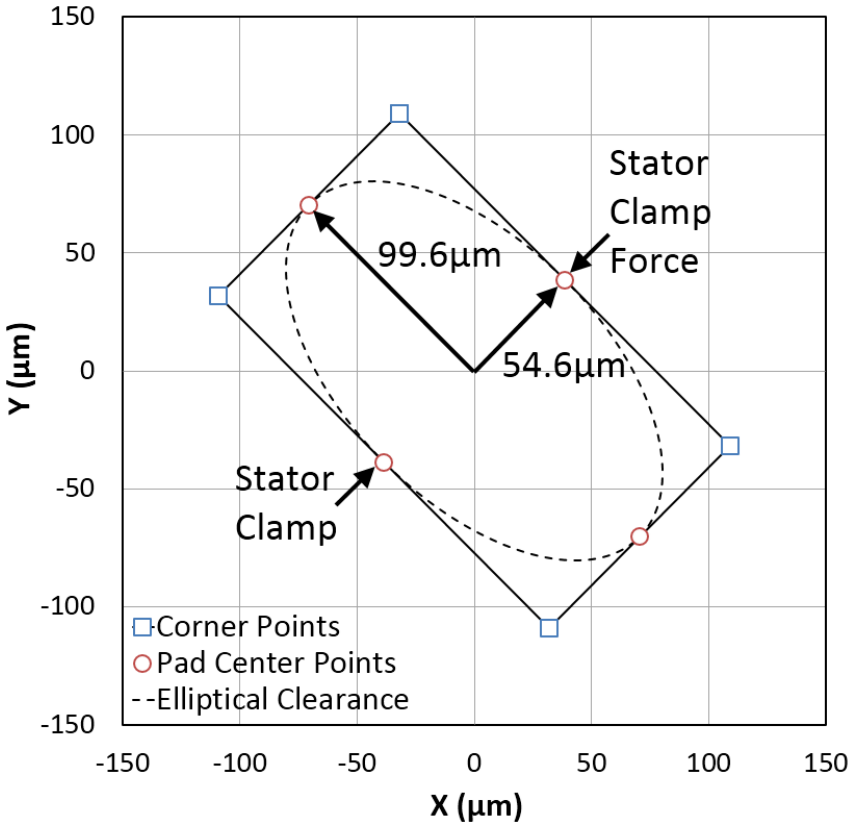

Figure 17: Re-creation of Crushed Harris [6] Clearance in LBP Orientation

Harris reports a nominal diametral bearing clearance of 190.5 µm, but measured an elliptical clearance with a diameter of 109.2 µm in the minor axis. The stator clamp force is in the same direction as the minor axis indicating that the bearing was likely crushed

by approximately 81.3 µm. Distorting the intended shape of the bearing likely had a significant effect on the static and dynamic performance of the bearing/rotor system.

For this study, care was taken to preserve the intended shape of the bearing and avoid the bearing crush that Harris experienced. Figure 18 shows the measured cold clearance for each of the four bearing configurations.

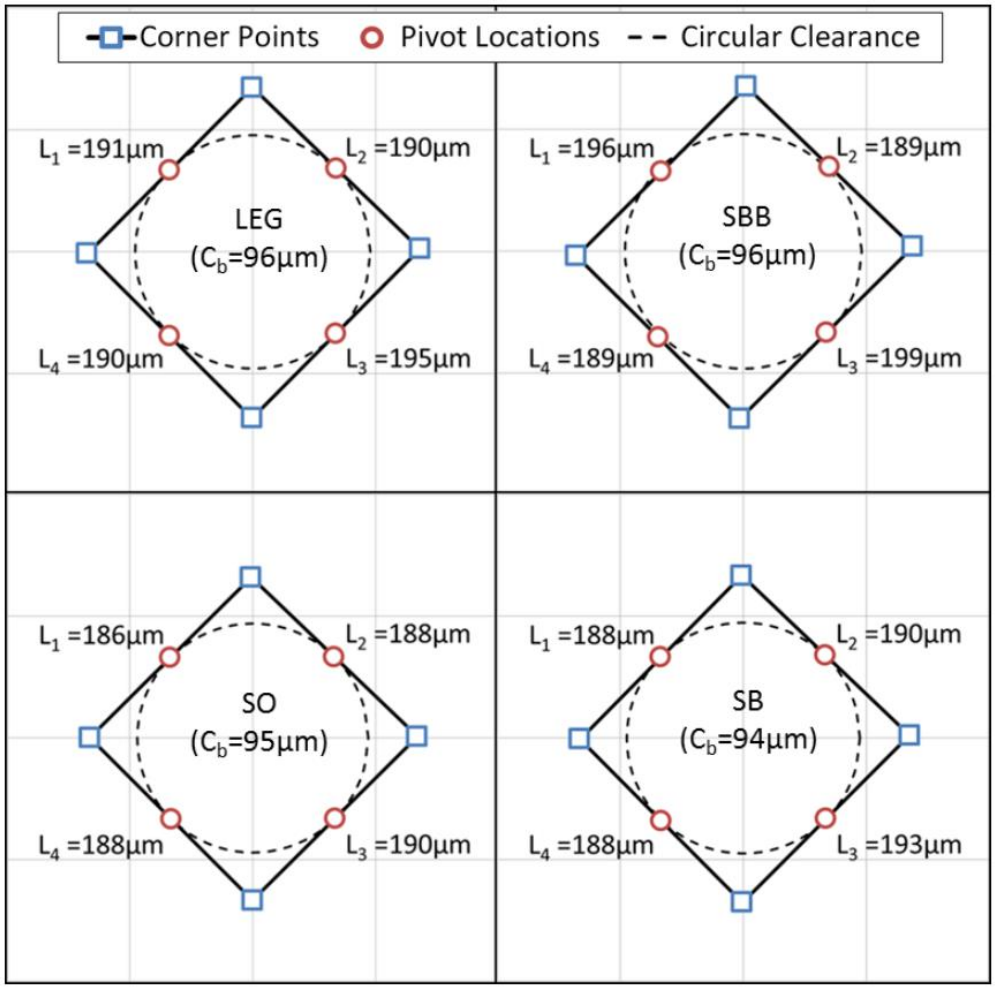

Figure 18: Measured Cold Clearance and Circular Clearance Estimate for Each Bearing Configuration (Good Repeatability and Symmetry for all Four Configurations)

The measured cold clearance for each configuration is highly symmetric with almost identical side lengths. The largest difference occurs for the SBB configuration with a diametral clearance of 199 μm in one axis and 189 μm in the other. The measured side lengths of Figure 18 have a systematic error of ±8 μm due to the limitations of the eddy current probes.

One hot clearance is measured for each test speed; immediately after testing at the highest load (2.9 MPa). The LEG always has the largest hot clearance, and the SO always has the smallest. Table 6 shows the radial hot-clearance circular estimates in micrometers for each bearing configuration. Hot clearance measurements were explained previously in the section on experimental procedures. The LEG always has the largest hot clearance and the SO always has the smallest.

Table 6: Radial Hot Clearance Circular Estimates in Micrometers

Feed Type	7 krpm	10 krpm	13 krpm	16 krpm
LEG	87	86	85	85
SBB	84	82	82	82
SB	84	82	81	81
SO	83	80	78	77

Figure 19 shows the radial hot-clearance circular estimates as a function of speed. During testing, the LEG typically ran cooler than the others and the SO configuration ran the hottest. The max temperature increased as speed increased. Typically, the hotter the bearing the smaller the clearance. Temperature measurements are discussed later. Currently, XL_TPJB calculates the hot clearance of the bearing independent of feed type; however, Table 6 and Figure 19 show that the hot clearance of the bearing is dependent on feed type. To accurately predict performance it is likely that feed type will need to be incorporated into models if attempting to model bearings with directed

lubrication and evacuated housings. The corner points, pivot locations, and circular clearance estimates are presented in Appendix A for both hot and cold clearances.

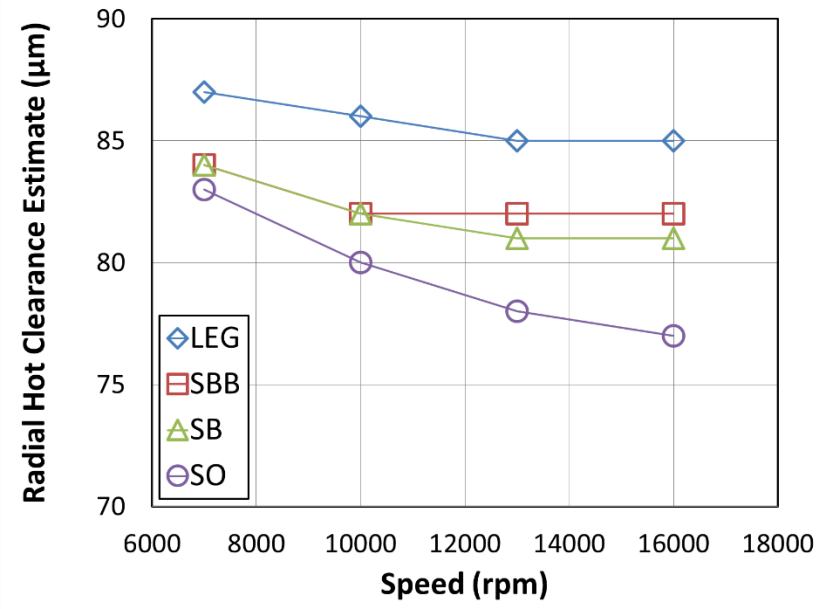

Figure 19: Radial Hot Clearance Circular Estimates as a Function of Speed

Static Equilibrium Journal Position

The position of the journal relative to the bearing center is defined with the eccentricity, e, and attitude angle, ϕ; Figure 20 shows definitions for both. The components of the eccentricity are e_x and e_y respectively. The attitude angle is defined to be positive in the direction of shaft rotation starting from the direction of the applied load.

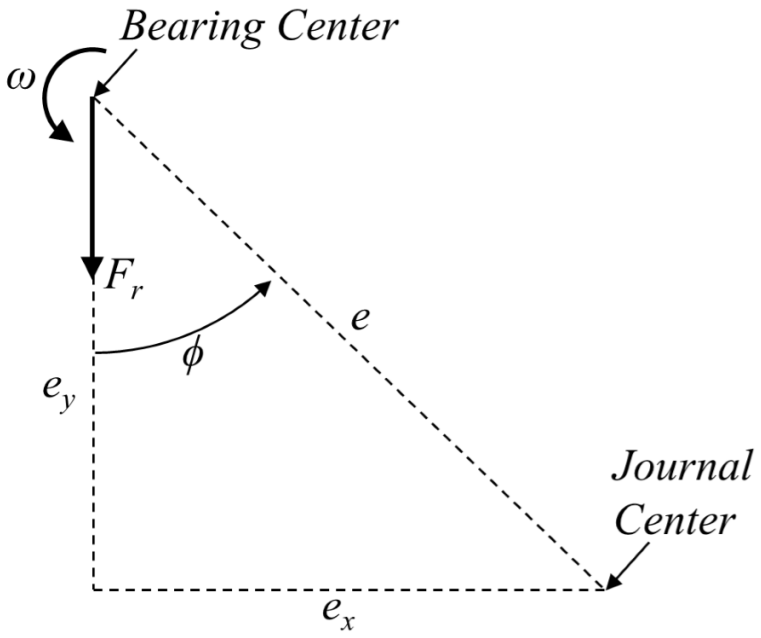

Figure 20: Geometric Definition of Journal Eccentricity and Attitude Angle

The position of the rotor is measured directly with eddy current probes, resulting in a set of *XY* data points for each static equilibrium position. To determine the eccentricity and attitude angles, the *XY* data points must be referenced to the hot bearing center (the bearing center during operation). In previous work with this test rig the hot bearing center was defined as the position of the journal with an applied static load of zero [7], [9]. Using this definition assumes that the weight of the bearing, stator housing, and static load attachment are all counteracted by the stingers/shakers to cancel out the gravity load. Wygant [35] uses a different method stating that "The hot center cannot be found by applying a net load of zero on the housing. It is impossible to completely cancel out the gravity load and run at a zero load condition. So, while the shaft is rotating, the same force magnitude is applied between each set of pads. The average of the proximity probes DC voltage signal from each loading condition is then considered to be the bearings geometric center." Figure 21 shows Wygant's method of determining the hot bearing center.

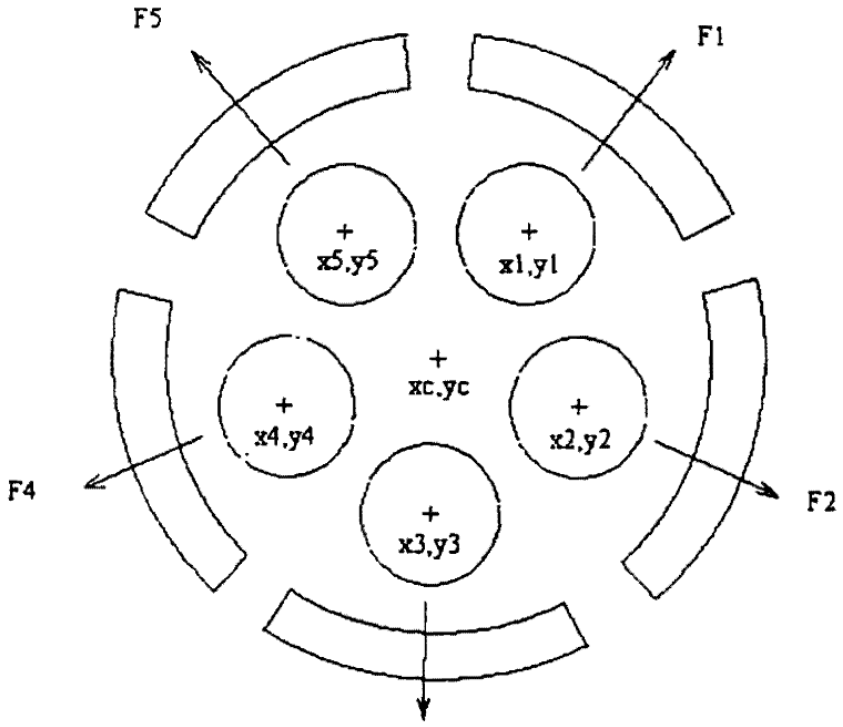

Figure 21: Hot Bearing Center Locating Technique from Wygant [35]

For this study a new method is used; the hot clearance measurements are used to define the hot bearing center. For example, at a steady state of 85 m/s and 2.9 MPa, the measured *XY* journal position, in micrometers, is (-75.81, -0.37) referenced to the tips of the eddy current probes. The system is then shut down, and the hot clearance is measured, providing a bearing-centric reference frame for the measured journal position. The pivot points are used to determine a best-fit circle and the center point of the circle-fit defines the hot bearing center. This new method assumes the difference between the operational center and the measured hot clearance center is small. Figure 22 shows the journal position and the bearing hot center, (-90.66, 60.31), determined from the hot clearance and best-fit circle. All points in Figure 22 are in a reference frame defined by the eddy current probes of Figure 10.

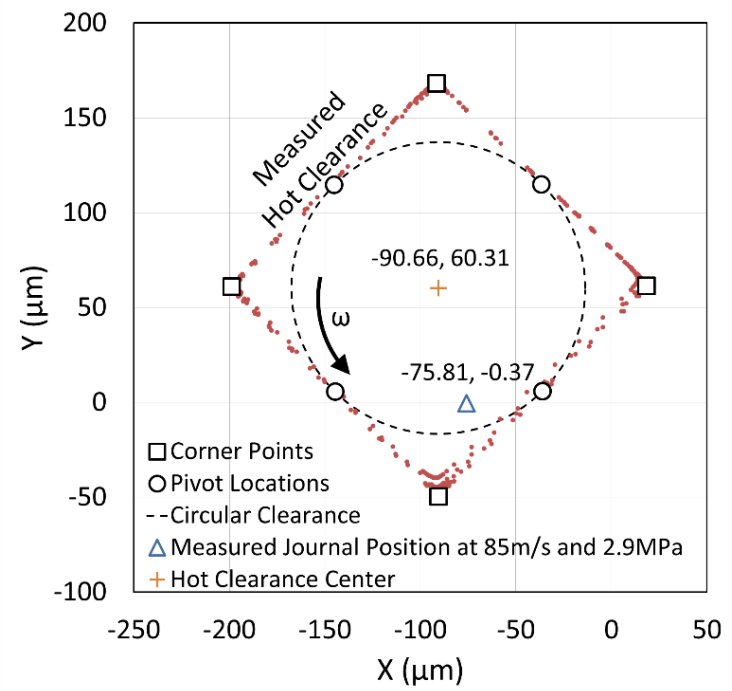

Figure 22: Example for Determination of Hot Bearing Center, Journal Eccentricity, and Attitude Angle (Raw Data Referenced to Eddy Current Probes)

Using the data in Figure 22, the journal eccentricity and attitude angle at 85 m/s and 2.9 MPa are:

$$e_x = -90.66 - (-75.81) = -14.85\,\mu m$$
$$e_y = 60.31 - (-0.37) = 60.68\,\mu m$$
$$e = \sqrt{e_x^2 + e_y^2} = 62.47\,\mu m$$
$$\phi = \tan^{-1}\left(\frac{e_x}{e_y}\right) = -13.75°$$

The attitude angle is ϕ = 13.75° (not -13.75°) since it is defined in Figure 20 to be positive in the direction of shaft rotation.

Figure 23 shows the center of the hot bearing clearance and the position of the journal with zero applied load, both referenced to the eddy current probes. One of these

points must be chosen as the hot bearing center to determine the eccentricity and attitude angle of the measured journal loci. Figure 24 compares the eccentricities and attitude angles that result from using each definition of the hot bearing center. The data set used in Figure 24 is from a previous test on a rocker-back pad; it is essentially one set of data analyzed two different ways. The new method (using the hot clearance center) results in larger magnitude (more negative) *y*-eccentricities, more positive *x*-eccentricities, and more positive attitude angles. Depending on the method used, the results may be significantly different; for example, at the lowest load (0.7 MPa) the attitude angle is about -10° using the old method and about 5° using the new method.

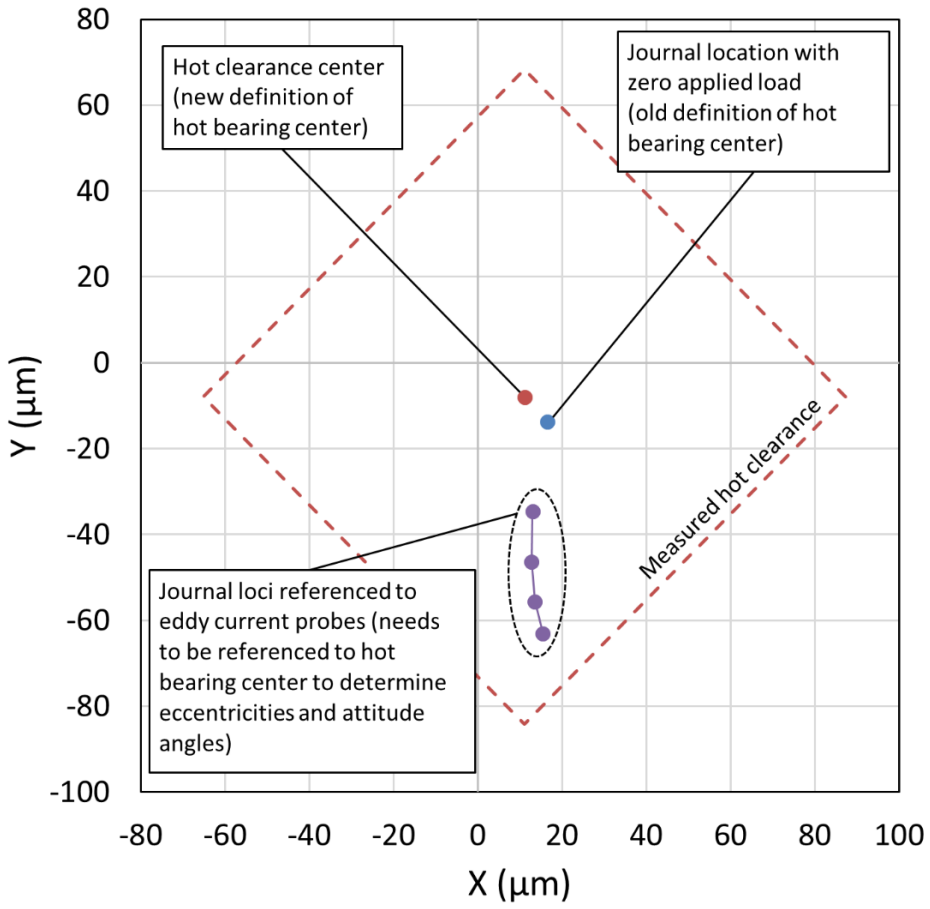

Figure 23: Hot Bearing Center - Location of Hot Clearance Center Relative to the Journal Position at Zero Load

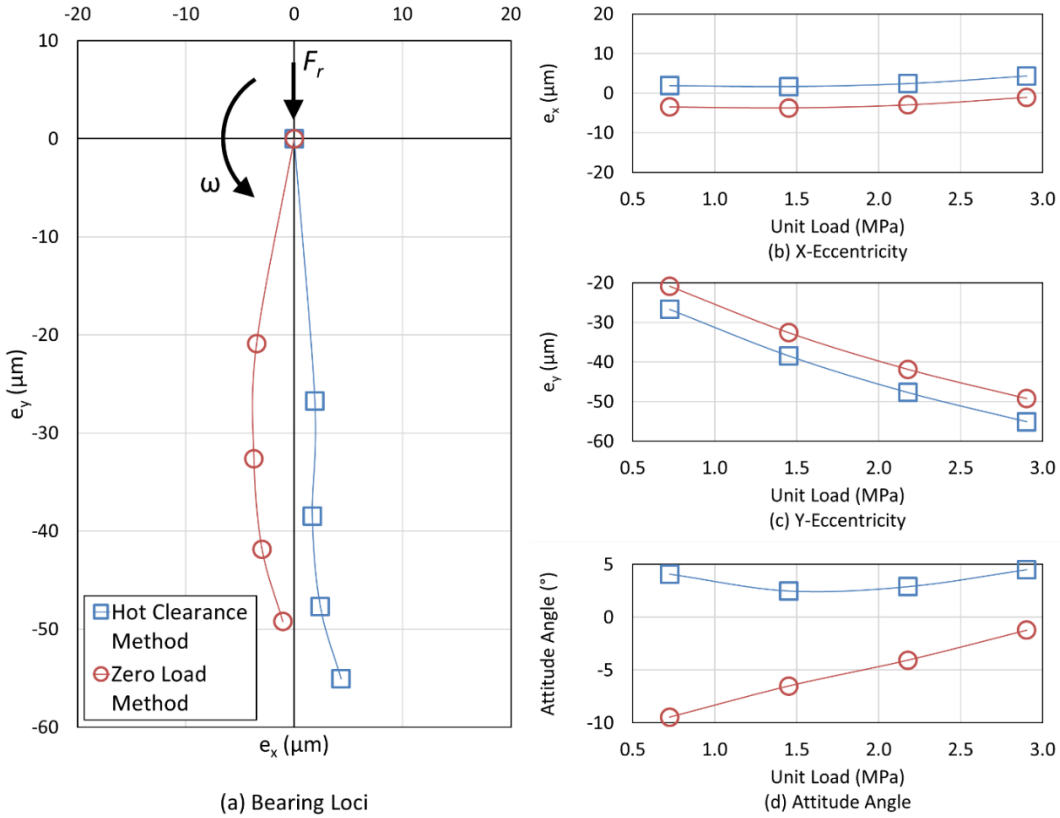

Figure 24: Hot Bearing Center - Comparison of Definitions (Data from Previously Tested Rocker-Back Bearing)

Figure 25 shows the journal position as a function of load for all configurations. The clearance used in Figure 25 is a perfect circle (not measured) with a radius of 94 µm (approximately the magnitude of the cold clearances shown in Figure 18). As expected, the magnitude of the journal *y*-eccentricity increases as load increases, and decreases as speed increases. The predicted eccentricity is greater than measured in the loaded direction (e_y), and less than measured in the perpendicular direction (e_x). Typically, the measured *y*-eccentricity is approximately the same across all four bearing configurations; except for the LEG at 38 m/s, which has a lower magnitude *y*-eccentricity than the other three bearing configurations. Figure 25 shows a significant attitude angle for most test cases, which implies the presence of stiffness cross-coupling, and indicates that the tilt-motion of the pad is impeded by friction.

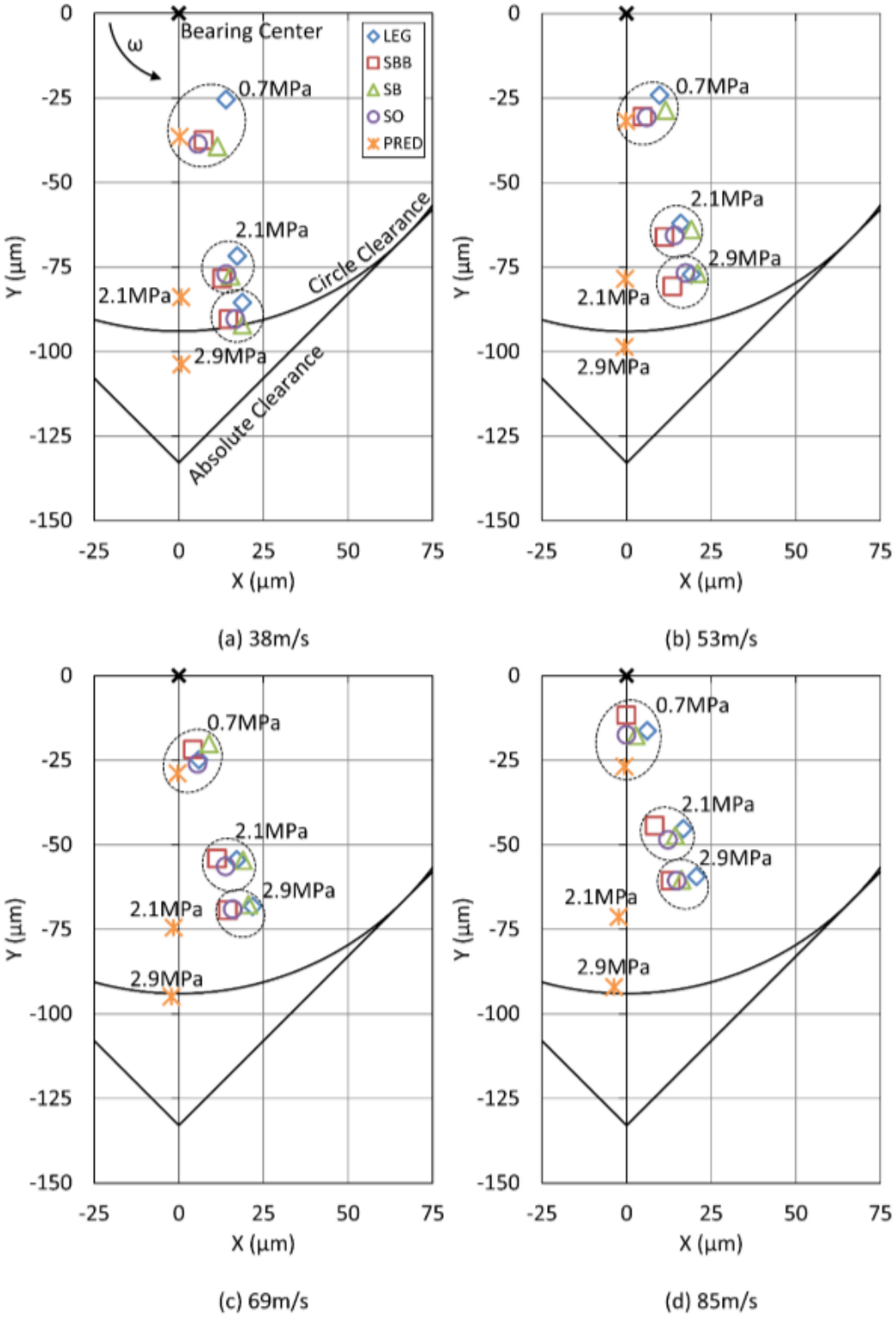

Figure 25: Journal Position as a Function of Load for Surface Speeds of (a) 38, (b) 53, (c) 69, and (d) 85 m/s

Figure 26 shows the measured *x*-eccentricity as a function of load for each bearing configuration. Predictions for e_x are approximately zero for all cases and are not shown. Typically, the LEG and SB configurations have a larger *x*-eccentricity than the SBB and SO configurations; of which, the SBB usually has the lowest. The significant *x*-eccentricities lead to finite attitude angles for most test conditions indicating stiffness cross-coupling and an impeded tilt-motion of the pads. Using the same test rig, Tschoepe [9] measured attitude angles that were less than 10° (except for one case) for a 4-pad, rocker-back, TPJB in the LBP orientation.

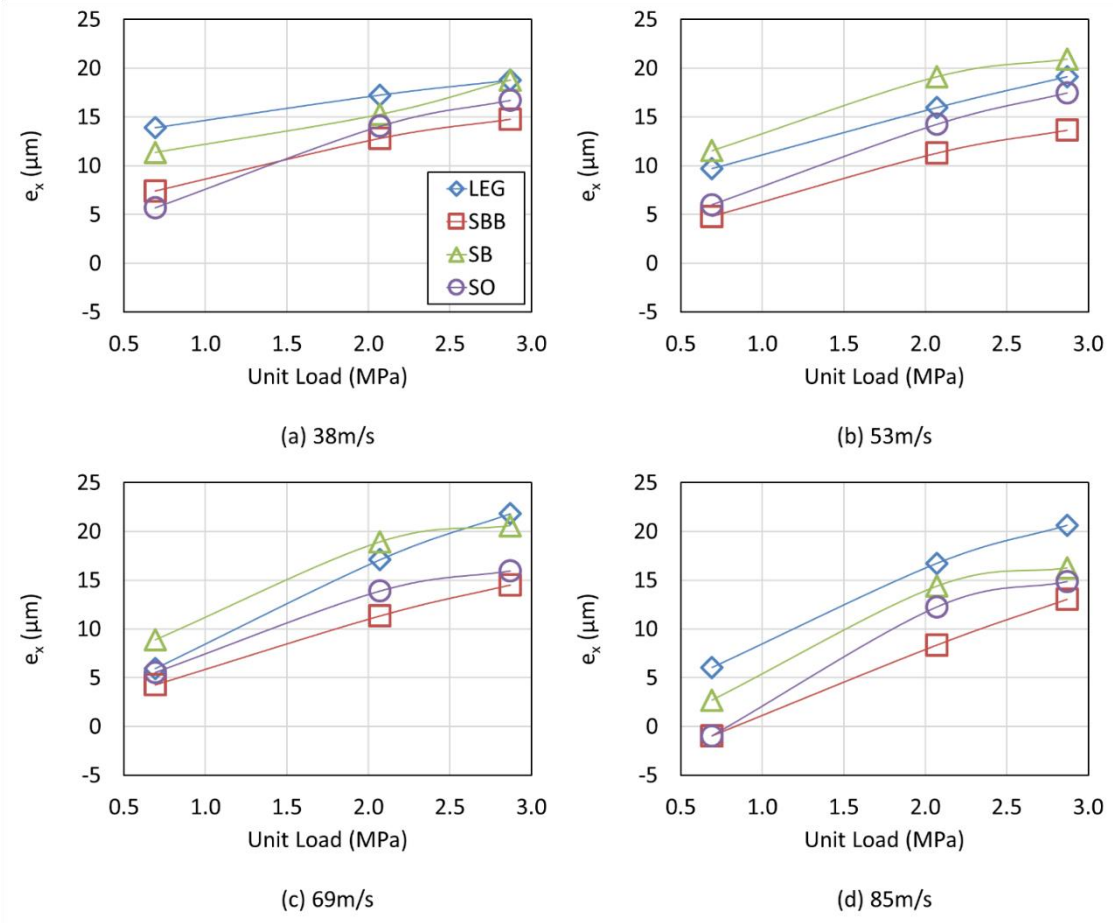

Figure 26: *X*-Eccentricity as a Function of Load for Surface Speeds of (a) 38, (b) 53, (c) 69, and (d) 85 m/s

Figure 27 shows measured attitude angles as a function of load. Typically the SBB has the lowest attitude angles while the LEG or SB have the highest. The max attitude angle for each configuration is 29° for the LEG, 24° for the SB, 14° for the SO, and 12° for the SBB. Predicted attitude angles are approximately zero and are not shown.

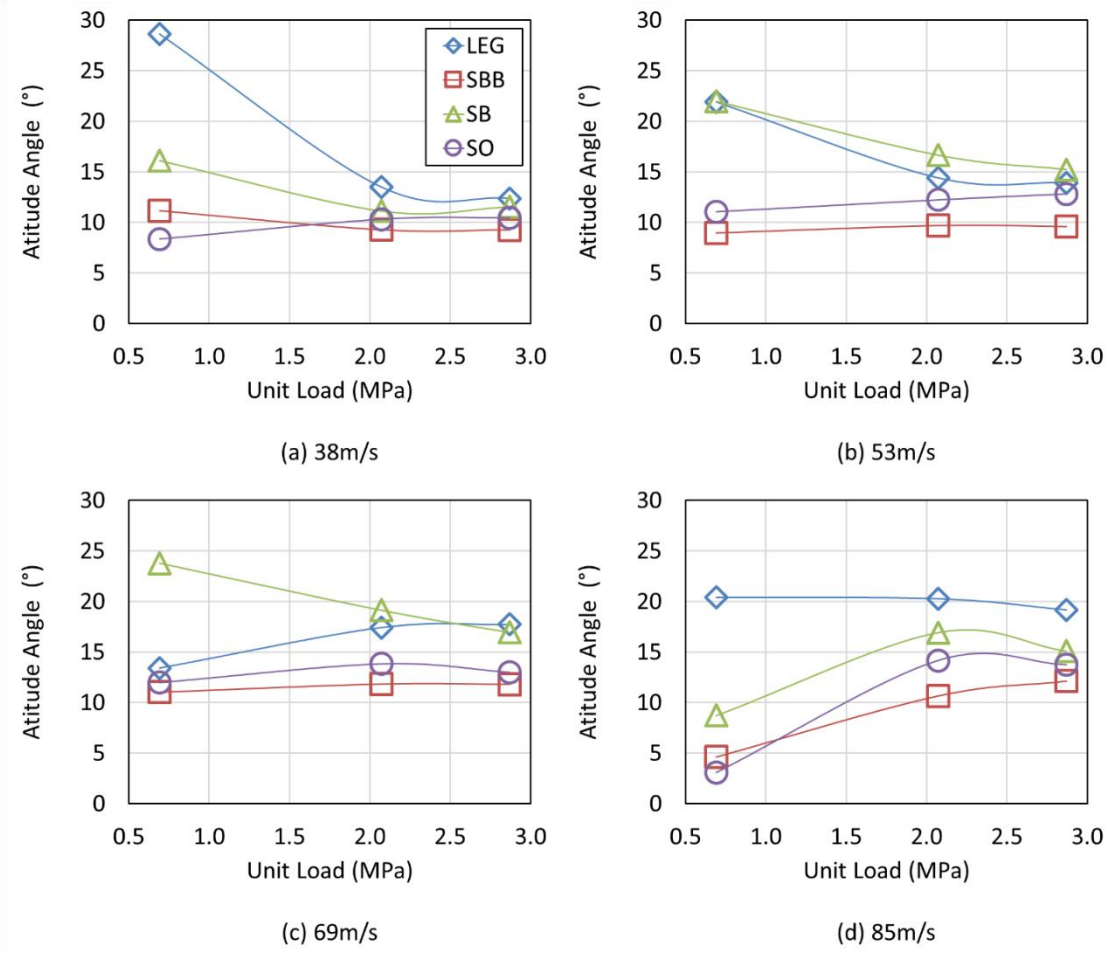

Figure 27: Attitude Angle as a Function of Load for Surface Speeds of (a) 38, (b) 53, (c) 69, and (d) 85 m/s

Harris [6], Wygant [10], and Pettinato and De Choudhury [12] also measured finite attitude angles for spherical-seat bearings, contrary to predictions. Figure 28 shows the

journal loci measured by Harris for a speed of 4000 rpm; the trend in attitude angle is typical of his measurements. For a rocker-back bearing, Wygant measured journal loci with a "straight line path" (low attitude angles) while he obtained a "curved path" (high attitude angles) for a spherical-seat bearing. Wygant states that this was the only significant difference between the two bearings. The reported uncertainty in the eccentricity measurements ranges from 4.6 to 21.3%. Wygant continues by stating that the measured film thickness profiles (measured via "on-shaft proximity probes") also indicate that the tilt motion of the spherical seat pad is impeded; possibly from increased friction in the spherical-seat pivot. Pettinato and De Choudhury compare measurements for a key-seat and a spherical-seat bearing; they conclude that the spherical seat bearing shows a higher attitude angle suggesting the presence of stiffness cross-coupling.

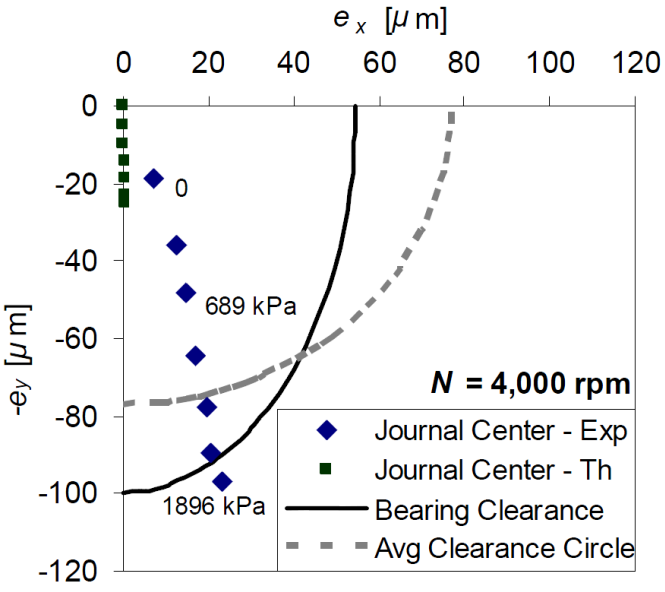

Figure 28: Journal Loci Adapted from Harris [6]

Temperature Measurements

Figure 29 shows the layout of the bearing thermocouples; 3, 8, 9, and 14 are exposed to the lubricant while all others are embedded babbitt layer thermocouples. All

thermocouples are type J with a measurement error of ±1.1 °C. Thermocouples are placed at 75% of the pad length from the leading edge; according to API 670 [36], the max temperatures in tilting pad bearings are in this vicinity.

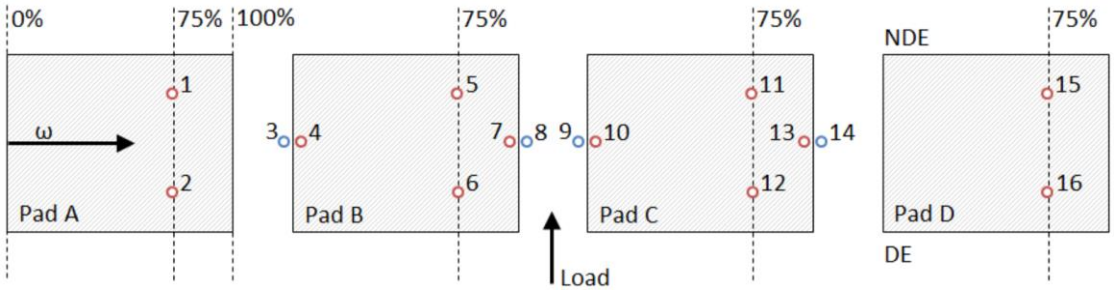

Figure 29: Bearing Thermocouple Layout

Figure 30 shows the measured and predicted temperature rise for the thermocouples of Figure 29 over the entire speed range with a constant load of 2.1 MPa. Figure 30 also shows the max bearing temperatures and their locations. For example, Figure 30a shows that at 2.1 MPa and 38 m/s the LEG has a max temperature rise of 36.5 °C, and the max temperature occurs at the 75% location of the 2nd loaded pad. For the axial thermocouple sets, only the maximum temperature rise is shown. As with Harris [6], the temperature rise is presented to minimize differences caused by small deviations (±0.5 °C) in inlet temperature. For example, if the measured inlet temperature is 50.5 °C, and the measured temperature for the #7 thermocouple (from Figure 29) is 56.3 °C, the temperature rise (5.8 °C) is presented instead of the raw temperature of 56.3 °C. Predictions are not available for the exposed thermocouples since XL_TPJB does not predict temperatures between pads.

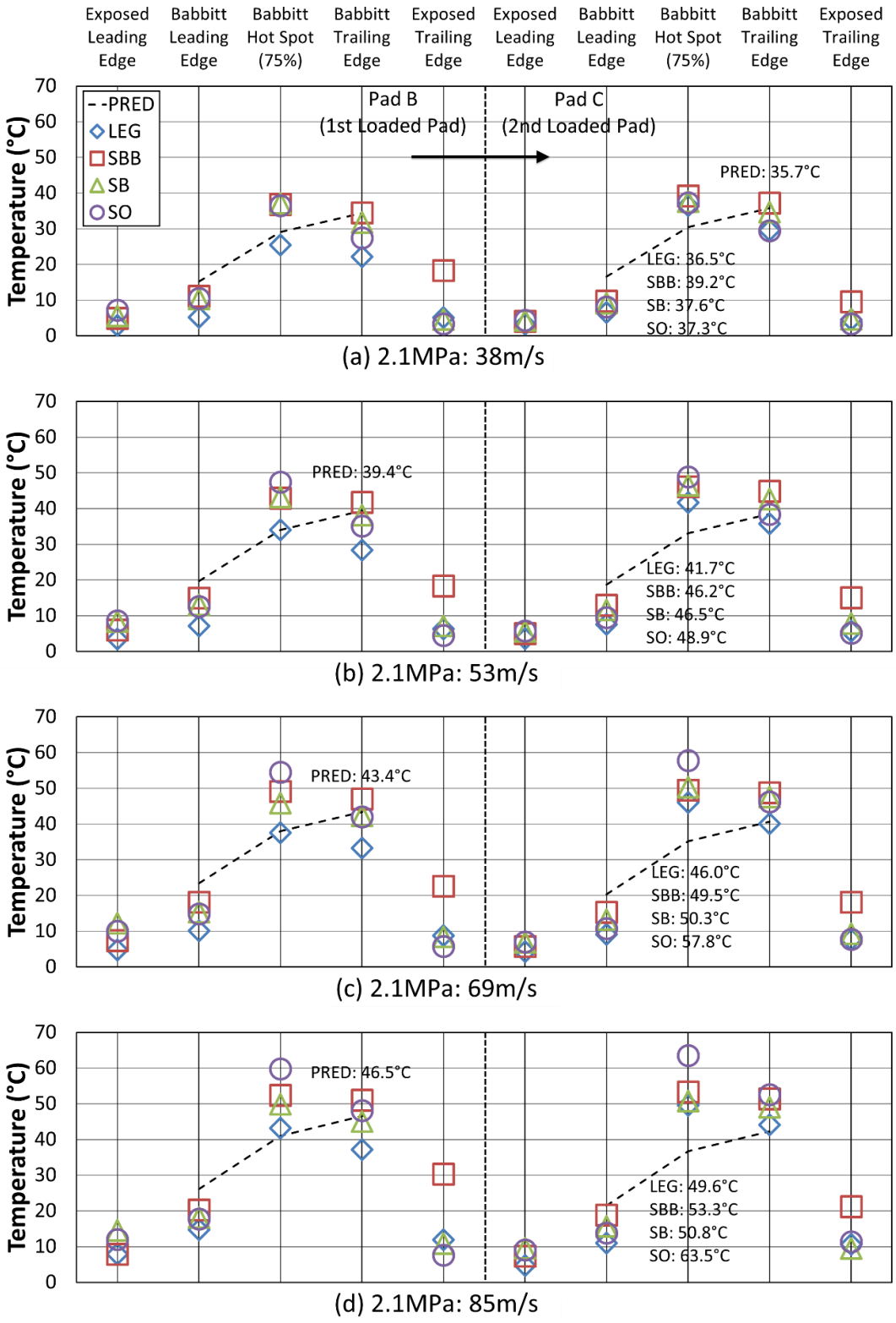

Figure 30: Temperature Profiles for the Loaded Pads with a Unit Load of 2.1 MPa

For most cases in Figure 30, the maximum measured temperature occurs at Pad C (2nd loaded pad) at the 75% location, and the maximum predicted temperature occurs at the trailing edge of either Pad B or C. For both loaded pads, the trailing edge temperature measurements (babbitt layer and exposed) are hotter for the SBB than for the LEG, SB, or SO configurations. The SBB is designed to block hot oil carry-over from Pad B to Pad C. It is likely that blocking the hot oil carry-over causes the hot oil to "back-up"; increasing the temperature at the trailing edge of the pads. The LEG significantly lowers the babbitt temperature of Pad B at the 75% and trailing edge locations; however, the cooling effect of the LEG is diminished for the second loaded pad though it does still provide a reduction in temperatures. The temperature profile trends are similar for loading cases of 0.7 MPa and 2.9 MPa and are included in Appendix E. Typically, the LEG offers the greatest reduction in max temperatures followed by the SB and then the SBB.

Figure 31 shows the measured (babbitt) temperature rise for the 2nd loaded pad (Pad C) as a function of speed for the 0.7 MPa load at three different locations. Typically, the highest measured temperatures occurred at the 2nd loaded pad. Figure 31a shows the measured temperature rise at the leading edge of Pad C. The LEG configuration produces the lowest leading edge temperatures followed by the SO configuration. Contrary to expectations, the SBB and SB produce higher temperatures at the leading edge than the SO (with the SBB being the highest). Figure 31b shows the temperature rise at the 75% location of Pad C; the LEG temperatures are lower than all others and the SO temperatures are highest. Figure 31c shows the temperature rise at the trailing edge of Pad C; the LEG is the coolest followed by the SO, SB, and SBB.

Figure 31 essentially shows the cooling effect of an evacuated housing. Of the four configurations, the one with the highest temperatures is the only flooded configuration (SO) even though the flooded SO configuration has consistently lower temperatures at the leading and trailing edge of the pad. The temperature trends are approximately the same for the 1st loaded pad (Pad B). The trends in Figure 31 for the 0.7 MPa load are generally the same for the other loads (2.1 and 2.9 MPa). Figure 31 shows that the SB

and SBB configurations do decrease temperatures at the 75% location of the 2nd loaded pad (typically the location of max temperatures) when compared to the SO. However, it is likely due more to the evacuated housing than introducing cool oil at the leading edge or blocking hot oil carry-over since the leading edge temperatures are actually hotter than the SO. Using the SB and SBB configurations increase leading and trailing edge pad temperatures (compared to the SO configuration) but the directed lubrication allows the use of an evacuated housing resulting in cooler temperatures at the 75% pad location. Figure 31 shows that the LEG typically provides the greatest temperature reduction while the SBB provides the least.

Figure 31 also shows temperature predictions from XL_TPJB. At the leading edge the predicted temperature is always higher (hotter) than measured, while the predicted temperature is typically lower (cooler) than measured at the trailing edge and the 75% location. Low temperature predictions at the 75% location can be problematic as this is typically the location of the measured max bearing temperature. Under-predicting max bearing temperatures can lead to bearings being operated hotter than intended. Max bearing temperatures are examined more closely in Figure 32.

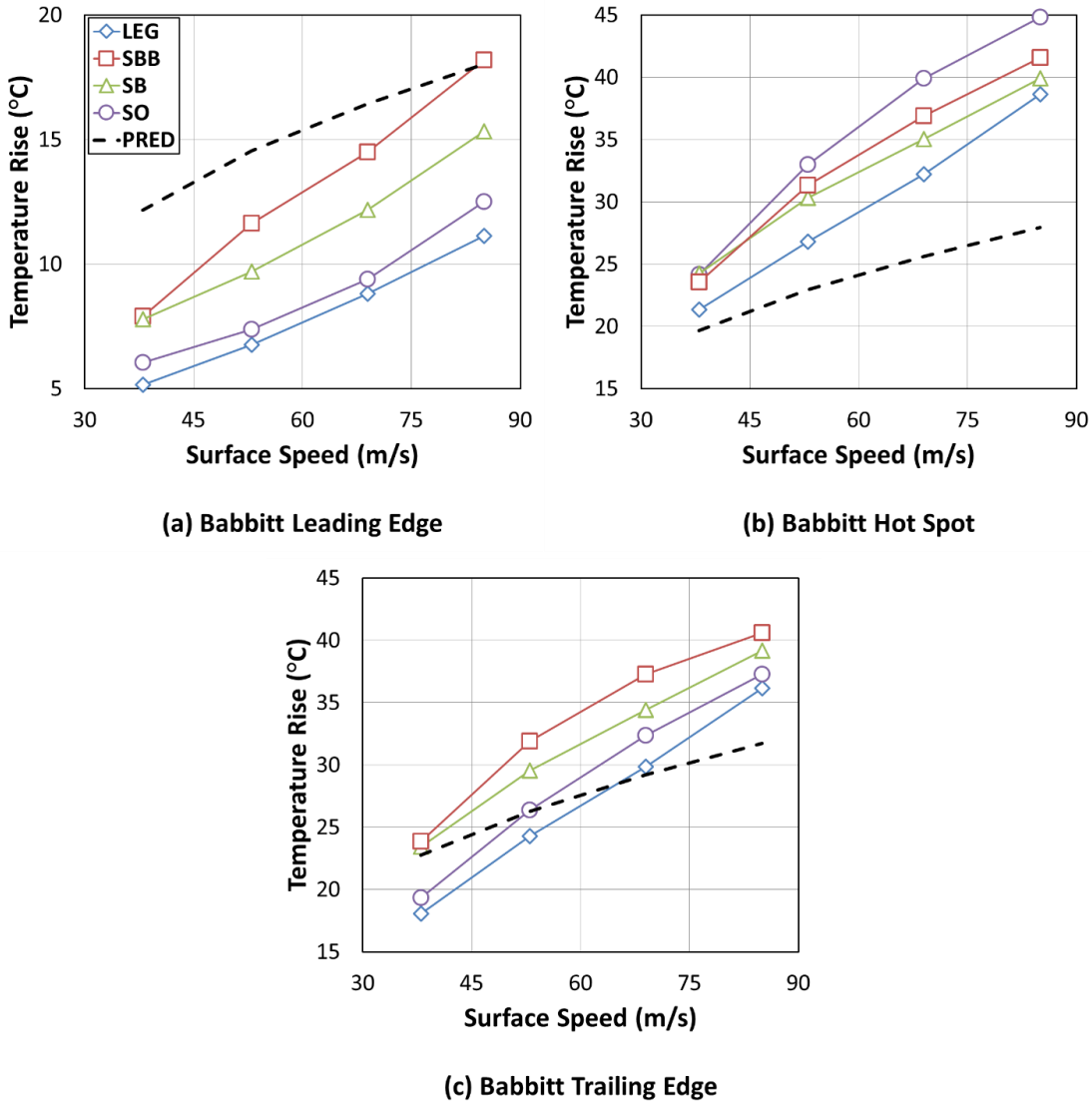

Figure 31: Pad C (2nd Loaded Pad) at 0.7 MPa - Measured Temperature Rise at the (a) Babbitt Leading Edge, (b) 75% Babbitt Location, and (c) Babbitt Trailing Edge

Figure 32 shows the measured and predicted maximum temperature rise for each configuration (typically the 75% location of the 2nd loaded pad). The predicted max temperature rise correlates well with measurements at the lowest speed but is significantly lower (cooler) than measurements as speed increases. At 38 m/s the max difference between the predictions and measurements is 2.4 °C, this increases to 8.3 °C

at 53 m/s, 12.4 °C at 69 m/s, and 14.3 °C at 85 m/s. Typically, the temperature predictions correlate best with the LEG measurements and worst with the SO measurements. The SO typically produces the highest max temperatures while the LEG yields the lowest.

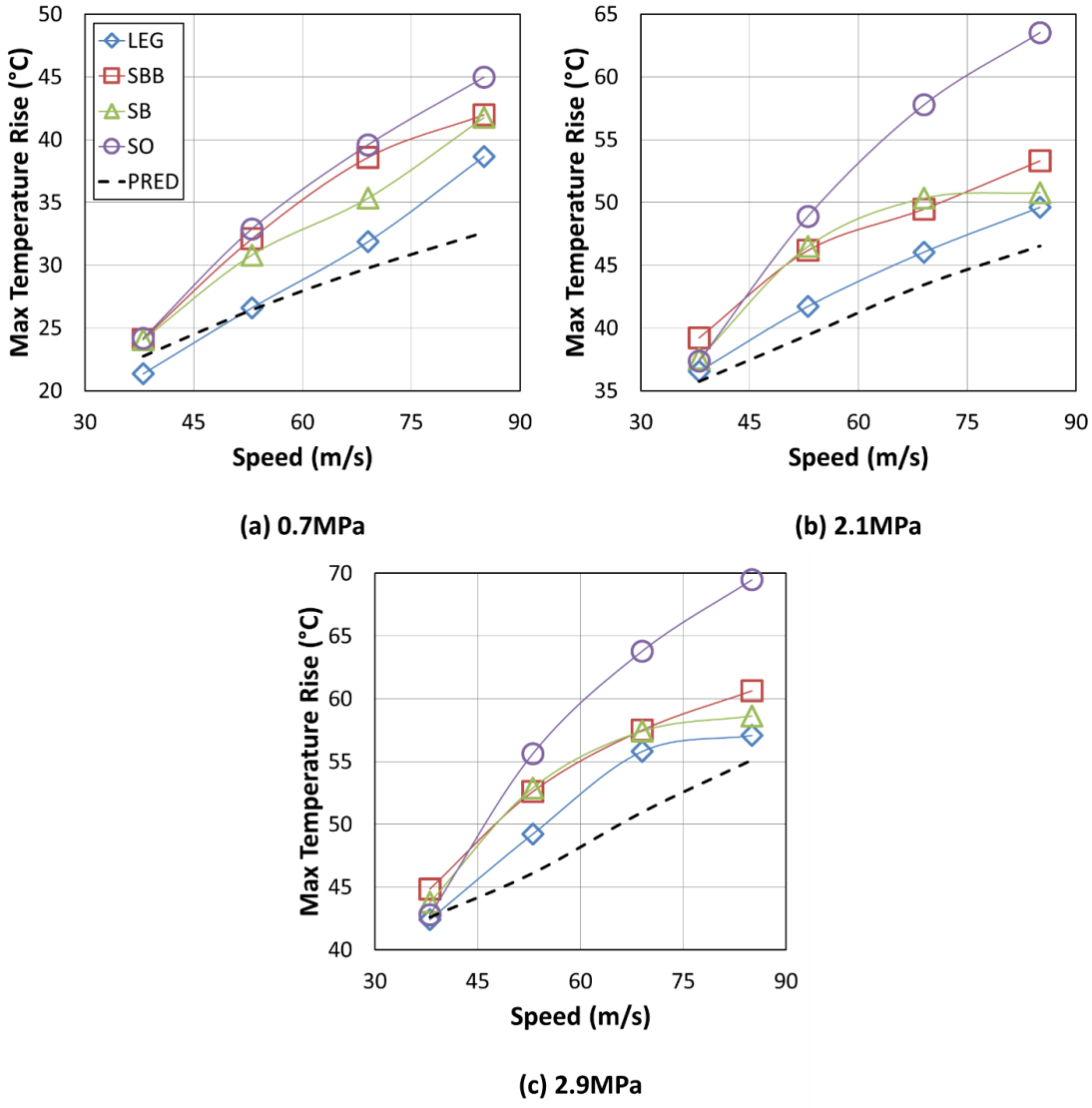

Figure 32: Maximum Temperature Rise as a Function of Speed (Measured and Predicted)

From Figure 32, the LEG typically outperforms the other feed types, decreasing the maximum temperature by up to 13.9 °C; compared to 10.2 °C for the SBB and 12.8 °C for the SB. On average, the LEG provides a temperature reduction of 7 °C; compared to 3.4 °C for the SBB and 4.3 °C for the SB over the speed and load range tested.

From Figure 29, thermocouple sets 1-2, 5-6, 11-12, 15-16 are used to measure the axial temperature gradient for each pad. Harris [6] also measured the axial temperature gradient; however, he states that the average axial temperature difference across each pad was only 1.2 °C so he presents only the average of each axial set. For this study, using the average of each axial set would be misleading. For example, the average of all axial sets is 2.1 °C; however, the maximum axial difference for Pads A through D are 5.1 °C, 9.6 °C (1st loaded), 7.2 °C (2nd loaded), and 3.1 °C respectively. There is no clear trend to the measured axial temperature gradients, but the difference can be large, and it can vary significantly with speed and load. Table 7 shows the minimum and maximum measured axial temperature gradients. For example, while testing the SO configuration (bottom row of Table 7) an axial temperature difference of 0 °C was measured for Pad C (fourth column of Table 7) at one operating condition, and an axial temperature gradient of 7.2 °C was measured for the same pad at a different operating condition. Similar to the presence of significant attitude angles in Figure 25, an axial temperature gradient suggests that the tilt motion of the spherical seat pad may be impeded.

Table 7: Minimum and Maximum Measured Axial Temperature Differences

Feed Type	Min and Max Axial Difference Pad A (°C)	Min and Max Axial Difference Pad B (°C)	Min and Max Axial Difference Pad C (°C)	Min and Max Axial Difference Pad D (°C)
LEG	0.0 - 1.1	0.7 - 6.9	0.9 - 3.9	0.0 - 3.1
SBB	0.6 - 5.1	3.0 - 9.6	0.0 - 1.9	0.1 - 2.0
SB	0.2 - 3.1	4.4 - 8.3	0.0 - 0.8	0.6 - 2.3
SO	0.2 - 1.9	0.2 - 6.3	0.0 - 7.2	0.0 - 1.5

DYNAMIC RESULTS

Calculation of rotordynamic coefficients was discussed previously in the experimental procedures. Figure 33 shows measured impedance values for the SBB configuration at 53 m/s and 0.7 MPa. Impedance values are included in Appendix F along with 95% confidence intervals for all test cases. For the data in Figure 33 the largest confidence interval is ±5 MN/m, which shows the excellent repeatability of the impedance measurements. The trends and repeatability of the impedance values in Figure 33 are representative of the majority of the measured impedance values in this thesis.

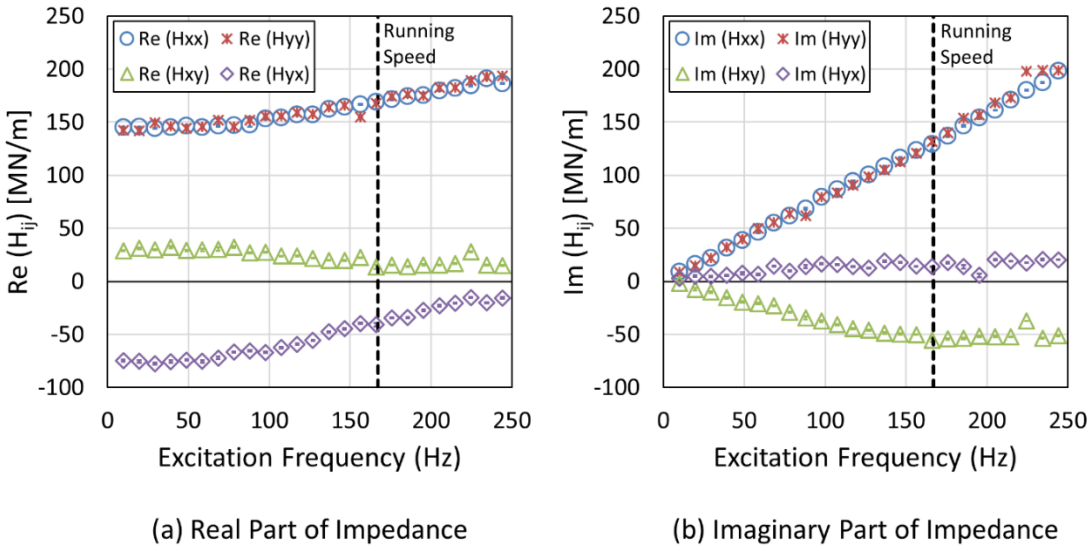

Figure 33: Measured Impedance Values for the SBB at 53 m/s and 0.7 MPa

A KCM model, Eq. (5), is used to capture the frequency dependence of the impedance coefficients. The rotordynamic coefficients are obtained from a least-squares linear regression of the measured impedance values. If the impedance values are not fit well by a KCM model the confidence intervals from Eqs. (26, 27) will be large. It does

not indicate poor repeatability in the measured impedance values, just that the impedances are poorly curve fitted. Appendix F contains measured impedance values and 95% confidence intervals from Eq. (19). Table 8 shows the average 95% confidence interval from Eqs. (26, 27) as a percentage for each of the rotordynamic coefficients. The direct stiffness and direct damping are both fit well by the KCM model with uncertainties of 2 to 5%. The cross-coupled stiffness and direct virtual mass terms are fit reasonably well by a KCM model with uncertainties of 9 to 47%. Cross-coupled damping and cross-coupled virtual mass terms are not shown in the body of this thesis due to large uncertainties in C_{yx} and M_{xy}, their values and uncertainties are in Appendix B.

Table 8: 95% Confidence Intervals of Measured Rotordynamic Coefficients as a Percentage of the Coefficient Magnitude

K_{xx}	K_{xy}	K_{yx}	K_{yy}
2%	47%	9%	4%
C_{xx}	C_{xy}	C_{yx}	C_{yy}
4%	15%	129%	5%
M_{xx}	M_{xy}	M_{yx}	M_{yy}
38%	777%	43%	37%

Direct Stiffness: K_{yy} & K_{xx}

Figure 34 shows predicted and measured values for K_{yy} as a function of speed for three different loads. Figure 34a shows K_{yy} for a constant load of 0.7 MPa; the measured stiffness increases linearly with speed and is approximately equal for all four feed types (LEG, SBB, SB, SO). Figure 34b shows K_{yy} for a constant load of 2.1 MPa. For the LEG, SBB, and SB, the measured stiffness decreases slightly while the stiffness for the SO configuration is approximately constant with speed. At 2.1 MPa the measured stiffness is highest for the SO and lowest for the SBB, which decreases with speed at a

faster rate than either the LEG or SB. Figure 34c shows K_{yy} for a constant load of 2.9 MPa; the measured stiffness decreases with speed and is approximately equal for the LEG, SBB, and SB, while the stiffness for the SO configuration is the highest and approximately constant with speed. Harris [6] shows an increase in K_{yy} with speed (for the speed range of 21-64 m/s) for 0.7 and 1.4 MPa loads, and a constant (approximately) K_{yy} for a 1.9 MPa load. None of the data presented by Harris shows K_{yy} decreasing with speed; contrary to Figure 34bc, which show significant decreases in K_{yy} for the SBB configuration (the same feed type tested by Harris). Variations in trends between this study and Harris [6] are attributed to bearing crush (large for Harris), different L/D ratios, by-pass cooling, leading-edge chamfers, end-seal configurations, and different lubricants (VG32 vs. VG46).

At 0.7 MPa in Figure 34a, predicted K_{yy} increases with speed at approximately the same rate as the measured values and is 1.0 to 1.2 times the measured values (recall measured K_{yy} is approximately equal across the four configurations at 0.7 MPa). At 2.1 MPa in Figure 34b, predicted K_{yy} is approximately constant (increases slightly) with speed. This matches the measured trend for the SO but does not match the measured trends for the LEG, SB, and SBB, which decrease with speed. However, even with the difference in trends, the predictions still correlate well with the measurements. For the 2.1 MPa load (Figure 34b), the ratio of predicted to measured K_{yy} is 0.9 for the SO, 1.0 to 1.1 for the LEG and SB, and 1.0 to 1.2 for the SBB. At 2.9 MPa in Figure 34c the trends are similar to the 2.1 MPa case; predicted K_{yy} and measured SO K_{yy} are approximately constant with speed while measured K_{yy} decreases with speed for the LEG, SBB, and SB. At 2.9 MPa, the ratio of predicted to measured K_{yy} is 0.9 for the SO, and 0.9 to 1.1 for the LEG, SBB, and SB. Overall, predictions for K_{yy} correlate very well with measurements; however, the predicted trend correlates best with the SO measurements.

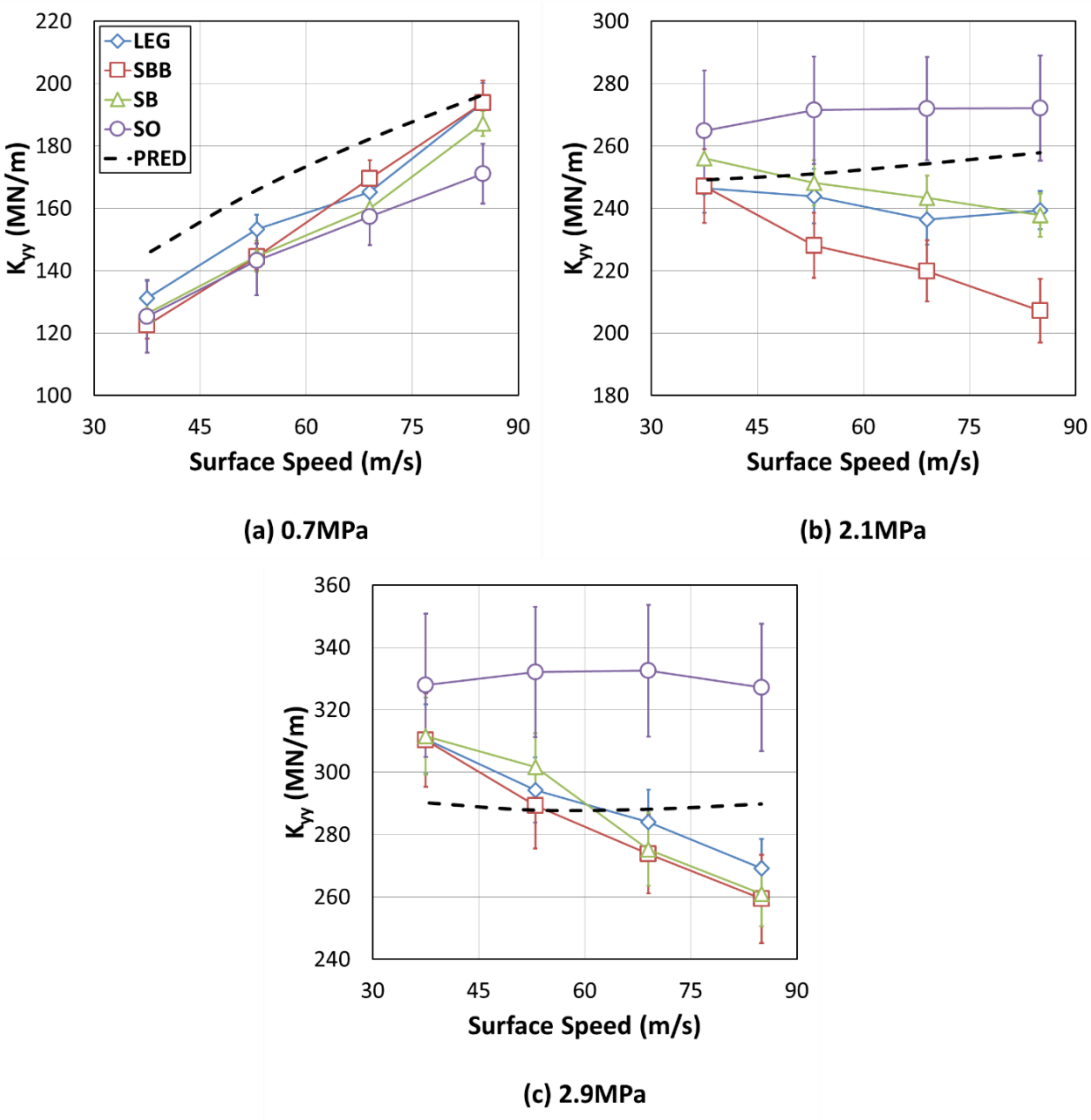

Figure 34: K_{yy} - Measured and Predicted Direct Stiffness in the Loaded Direction as a Function of Speed for Unit Loads of (a) 0.7, (b) 2.1, and (c) 2.9 MPa

Figure 35 shows K_{yy} as a function of load for four different surface speeds. Figure 35a shows K_{yy} for a constant surface speed of 38 m/s; the measured stiffness increases linearly with load and is approximately equal across all four configurations (LEG, SBB, SB, SO). Figure 35b shows K_{yy} for a constant surface speed of 53 m/s; the measured stiffness increases approximately linearly for all four configurations, is highest for the

flooded SO configuration, and is approximately equal for the three methods of directed lubrication. Figure 35c shows K_{yy} for a surface speed of 69 m/s; the measured stiffness continues to increase with load but is lower for the evacuated configurations (LEG, SBB, SB) than for the flooded SO. Figure 35d shows K_{yy} for a surface speed of 85 m/s; measured stiffness for the SO, SB, and LEG continues to increase linearly with speed while the stiffness for the SBB has changed to a distinct nonlinear trend. The measured stiffness for the SO configuration continues to be higher than the other three configurations.

Figure 35 shows predicted K_{yy}, which increases linearly (approximately) with load for surface speeds of 38, 53, 69, and 85 m/s. Measurements for the SO correlate well with predictions for K_{yy} as a function of load; the ratio of predicted to measured K_{yy} for the SO is 0.9 to 1.2 and the trends (a linear increase with load) are similar. As a function of load, predicted K_{yy} correlates very well with measurements for the LEG and SB. Typically, the slope of predicted K_{yy} is approximately equal to the slope of measured K_{yy} for the LEG and SB (K_{yy} for the LEG and SB are approximately equal at most test conditions). The ratio of predicted to measured K_{yy} for the LEG and SB is 0.9 to 1.2. Of the four configurations tested, the measurements for the SBB have the worst correlation with the predicted trend for K_{yy}. As the speed increases, measured K_{yy} for the SBB becomes increasingly non-linear (contrary to the predicted linear increase). This is the only configuration that shows a non-linear trend in K_{yy} as a function of load. Despite the opposing trends, the correlation between K_{yy} predictions and measurements is good for the SBB with a ratio of predicted to measured values from 0.9 to 1.2.

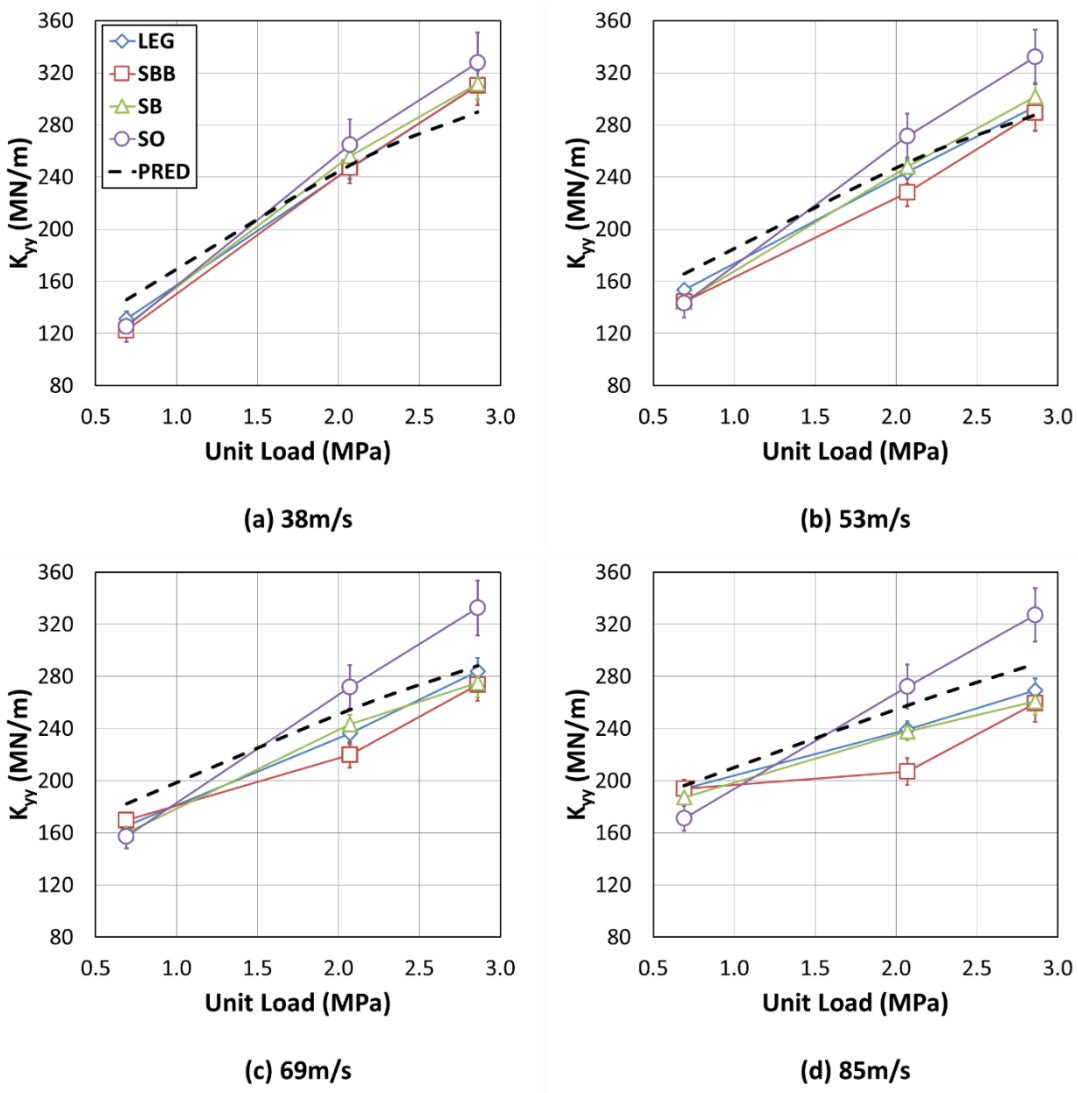

Figure 35: K_{yy} - Measured and Predicted Direct Stiffness in the Loaded Direction as a Function of Load for Speeds of (a) 38, (b) 53, (c) 69, and (d) 85 m/s

Figure 36 shows predicted and measured K_{xx} as a function of speed. Figure 36a shows K_{xx} for a constant load of 0.7 MPa; the trends and values in measured stiffness values are approximately the same as those for K_{yy} in Figure 26a. Figure 36b shows K_{xx} for a constant load of 2.1 MPa; the measured stiffness increases (slightly) with speed for the flooded SO, decreases for the evacuated SBB, and is approximately constant for the evacuated LEG and SB (which are approximately equal). The measured stiffness is

greatest for the flooded SO configuration and lowest for the evacuated SBB configuration. Figure 36c shows K_{xx} for a constant load of 2.9 MPa; the measured stiffness decreases slightly with speed for the three configurations with directed lubrication, and increases slightly for the flooded SO configuration. Harris [6] shows an increase in K_{xx} with speed (for the speed range of 21-64 m/s) for 0.7, 1.4, and 1.9 MPa loads. None of the data presented by Harris shows K_{xx} decreasing with speed; contrary to what is shown here in Figures 27bc, which show significant decreases in K_{xx} for the SBB configuration. Reasons for possible discrepancies were discussed previously. Figures for K_{xx} as a function of speed are relegated to Appendix G as the trends are almost identical to those in Figure 35 for K_{yy}.

XL_TPJB predicts isotropic direct stiffness coefficients, so predictions shown in Figure 36 are the same as those in Figure 34. Figure 36a shows predicted K_{xx} at 0.7 MPa that increases with speed at approximately the same rate as the measured values. At 0.7 MPa measured values for K_{xx} are approximately equal across the four configurations (LEG, SBB, SB, and SO). At 0.7 MPa the ratio of predicted to measured K_{xx} ranges from 1.0 to 1.2. Figure 36b shows predicted K_{xx} for a load of 2.1 MPa where it is approximately constant (it increases slightly) as speed increases. At 2.1 MPa, predicted K_{xx} is greater than all measured values. It correlates best with the measured values for the SO and worst with the SBB. At 2.1 MPa the ratio of predicted to measured K_{xx} ranges from 1.0 to 1.1 for the SO, 1.2 for the LEG and SB, and 1.2 to 1.4 for the SBB. Figure 36c shows predicted K_{xx} for a load of 2.9 MPa. Similar to the loading case of 2.1 MPa, the predicted values for K_{xx} (at 2.9 MPa) correlate best with measured values for the SO and worst with the SBB. At 2.9 MPa the ratio of predicted to measured K_{xx} ranges from 1.0 to 1.1 for the SO, 1.2 for the LEG and SB, and 1.2 to 1.3 for the SBB. Overall the predictions for K_{xx} (and K_{yy} as discussed previously) correlate best with the SO measurements.

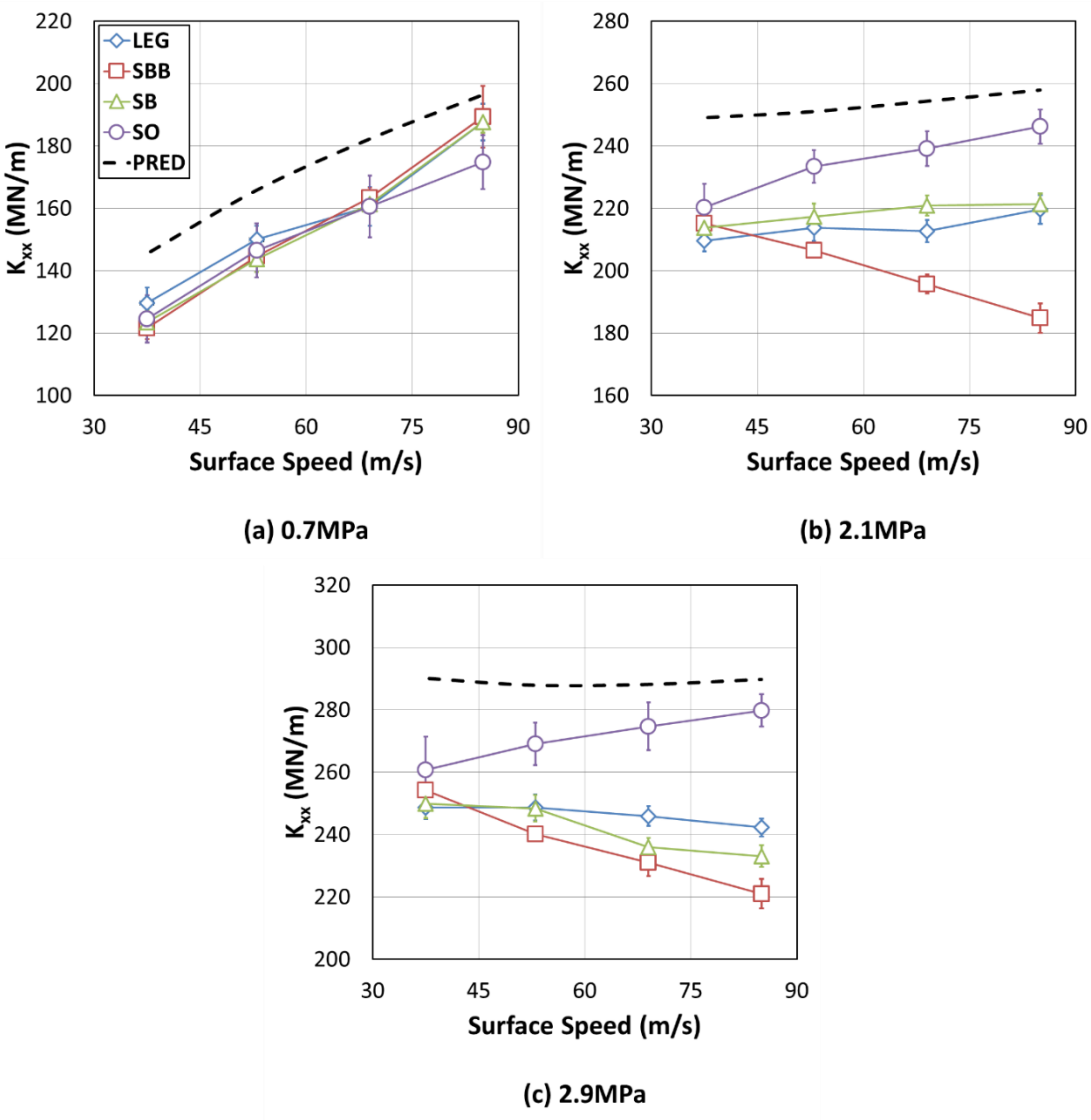

Figure 36: K_{xx} - Measured and Predicted Direct Stiffness in the Direction Perpendicular to Load as a Function of Speed for Unit Loads of (a) 0.7, (b) 2.1, and (c) 2.9 MPa

Table 9 shows factors (K_{xx} / K_{yy}) comparing the measured values of K_{xx} and K_{yy}; a value of one indicates stiffness isotropy (K_{xx} = K_{yy}), and a value below unity indicates that K_{yy} is greater than K_{xx}. In 1933, D.M. Smith [37] reported that direct stiffness orthotropy could raise the onset speed of instability; he states that "The speed of transition to instability is raised by increasing the relative intensity of damping on the

bearing supports and by rendering the bearing supports unsymmetrical." Typically, a system with bearings in the LOP configuration will have more stiffness orthotropy than in the LBP configuration. All four configurations have approximately the same level of stiffness orthotropy at any given speed or load. For the 0.7 MPa load the measured direct stiffness is isotropic for all four configurations with $K_{xx}/K_{yy} = 1.0$. At 2.1 MPa the direct stiffness is slightly orthotropic with $K_{xx}/K_{yy} = 0.9$ (on average). The stiffness orthotropy is greatest at 2.9 MPa with $K_{xx}/K_{yy} = 0.8$ (on average). Table 9 shows that increasing the load increases the stiffness orthotropy, which can have a stabilizing effect on a system. For this study, K_{xx} is always less than, or equal to, K_{yy}. Tschoepe [9] measured the same trend for the LBP orientation with a 4-pad rocker-back TPJB. However, Harris [6] measured the opposite trend with K_{xx} greater than, or equal to, K_{yy}. Harris measured K_{xx}/K_{yy} from 1.0 to 1 .3 so the level of orthotropy was similar to the results in Table 9, but the larger stiffness was in the direction perpendicular to load.

Table 9: Stiffness Orthotropy Factors - K_{yy}/K_{xx}

Factor: (Measured K_{xx})/(Measured K_{yy})					
Load (MPa)	Surface Speed (m/s)	LEG	SBB	SB	SO
0.7	38	1.0	1.0	1.0	1.0
	53	1.0	1.0	1.0	1.0
	69	1.0	1.0	1.0	1.0
	85	1.0	1.0	1.0	1.0
2.1	38	0.9	0.9	0.8	0.8
	53	0.9	0.9	0.9	0.9
	69	0.9	0.9	0.9	0.9
	85	0.9	0.9	0.9	0.9
2.9	38	0.8	0.8	0.8	0.8
	53	0.8	0.8	0.8	0.8
	69	0.9	0.8	0.9	0.8
	85	0.9	0.9	0.9	0.9

Figure 37 shows the trends in measured direct stiffness (K_{yy}) as a function of load for the four different feed types. Figure 37a shows K_{yy} for the SO at four different speeds; the stiffnesses increase linearly with load and are approximately equal at higher loads. Figure 37b shows K_{yy} for the evacuated SBB configuration; the stiffness increases with load but the trend becomes increasingly nonlinear as speed increases above 38 m/s.

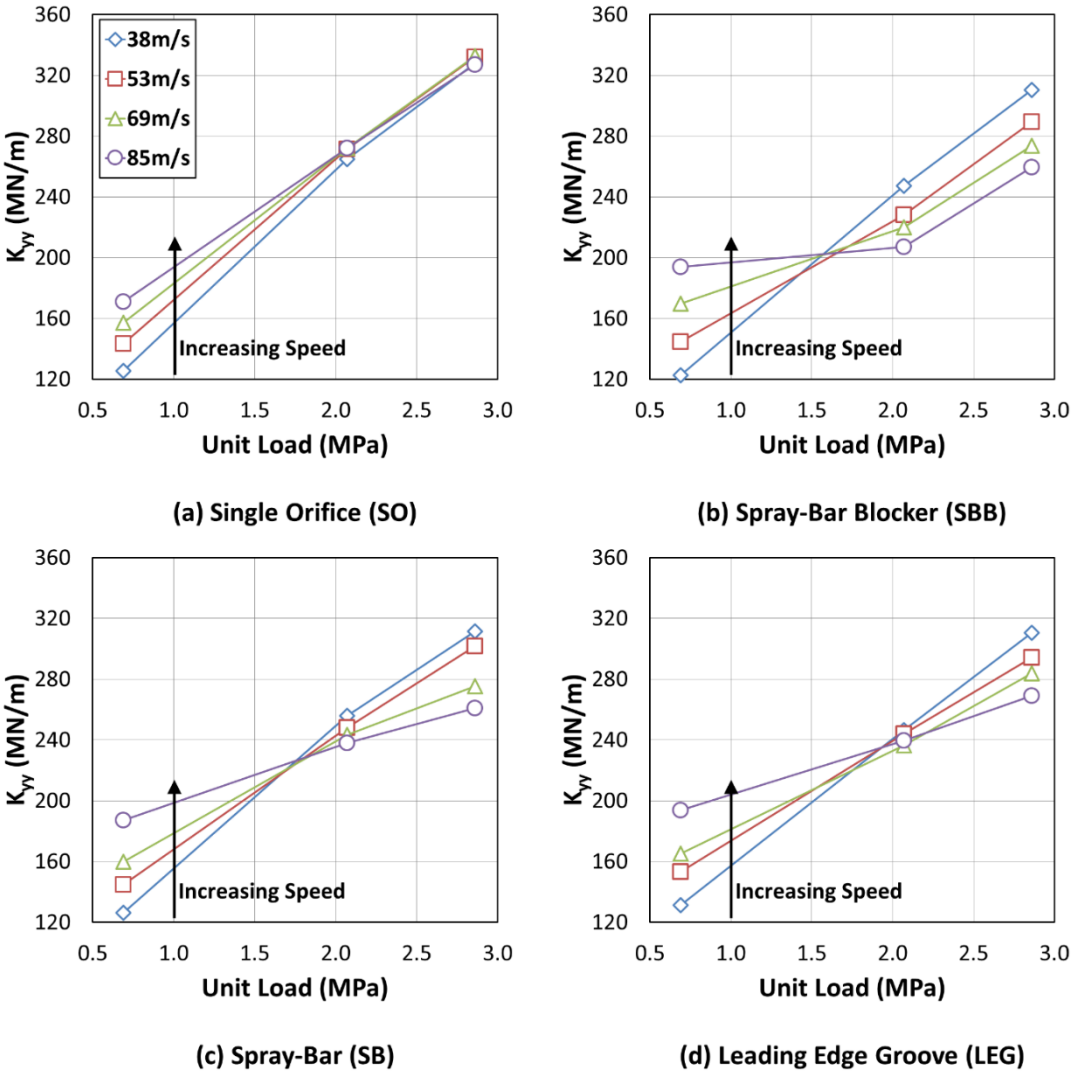

Figure 37: K_{yy} – Measured Direct Stiffness Trends for the (a) SO, (b) SBB, (c) SB, and (d) LEG.

Figure 37cd show K_{yy} for the evacuated SB and LEG configurations (respectively); the trends and values for these two methods of directed lubrication are approximately equal and linear over the speed and load range tested. The stiffness for all four configurations increase with speed at the lowest load (0.7 MPa); however, for all methods of directed lubrication (Figure 37bcd) the stiffness decreases with speed at the highest load (2.9 MPa). Figure 37 illustrates that using directed lubrication can significantly affect the trend in measured direct stiffness. Trends in K_{xx} are similar to K_{yy} and are not shown here.

Cross-Coupled Stiffness: K_{xy} & K_{yx}

Figure 38 shows measured values for the cross-coupled stiffness terms (K_{xy} and K_{yx}) as a function of speed. Predictions for the cross-coupled stiffness correlate poorly with measurements and are not shown in Figure 38, but are included in Appendix B; XL_TPJB predicts cross-coupled stiffness coefficients that are approximately zero. The measured cross-coupled stiffness terms are significant with magnitudes that are approximately 20-50% of the measured direct stiffness coefficients; Harris [6] reported lower magnitudes of 15-35%. Figure 38a shows measured cross-coupled stiffness terms for a constant load of 0.7 MPa; K_{xy} is negative and K_{yx} is positive over the entire speed. Cross-coupled stiffness terms with opposing signs will amplify forward whirl in a rotor/bearing system and can be destabilizing [31]. Wygant et al. [11] also measured cross-coupled stiffness terms with opposing signs. Figure 38b shows cross-coupled stiffness values for a load of 2.1 MPa; K_{yx} is negative for all four configurations over the entire speed range, K_{xy} is negative at lower speeds but transitions to positive values at higher speeds for all but the SO configuration. The result is destabilizing cross-coupled stiffness terms for the three configurations with directed lubrication for some test conditions at 2.1 MPa. Figure 38c shows cross-coupled stiffness for the 2.9 MPa load; K_{xy} and K_{yx} are negative for all configurations over the entire speed range. In Figure 38, K_{xy} and K_{yx} are always offset from each other contrary to the predicted values, which are always zero (approximately) and isotropic.

Figure 39 shows measured cross-coupled stiffness terms as a function of load. The most significant trend is: for all speed conditions, K_{xy} decreases with load, starting at a positive value and decreasing to a negative value as the load increases. Since K_{yx} is always negative, increasing the load essentially pushes K_{xy} negative resulting in a more stable system (cross-coupled stiffness terms with same signs).

Referring back to Figure 27 (measured attitude angles), there is no obvious correlation between the measured attitude angles and the measured cross-coupled stiffness in Figure 38 and 39. Typically, all test conditions had a positive measured attitude angle. The test cases with destabilizing (opposing-sign) cross-coupled stiffness, and the cases with same-sign cross-coupled stiffness terms can both have significant attitude angles. However, the measured stiffness orthotropy from Table 9 does correlate with the stability results in Figure 38 and 39. Typically, the test cases with less direct stiffness orthotropy also have cross-coupled stiffness terms with opposing signs. For example, at 0.7 MPa and 85 m/s the SO has $K_{xx}/K_{yy} = 1.0$ and cross-coupled stiffness terms with opposing signs; however, at 2.9 MPa and 69 m/s the SO has $K_{xx}/K_{yy} = 0.8$ and same-sign cross-coupled stiffness terms. Typically, the low-load/high-speed test cases had the least amount of stiffness orthotropy and opposing-sign cross-coupled stiffness with the greatest difference between terms ($K_{xy} - K_{yx}$).

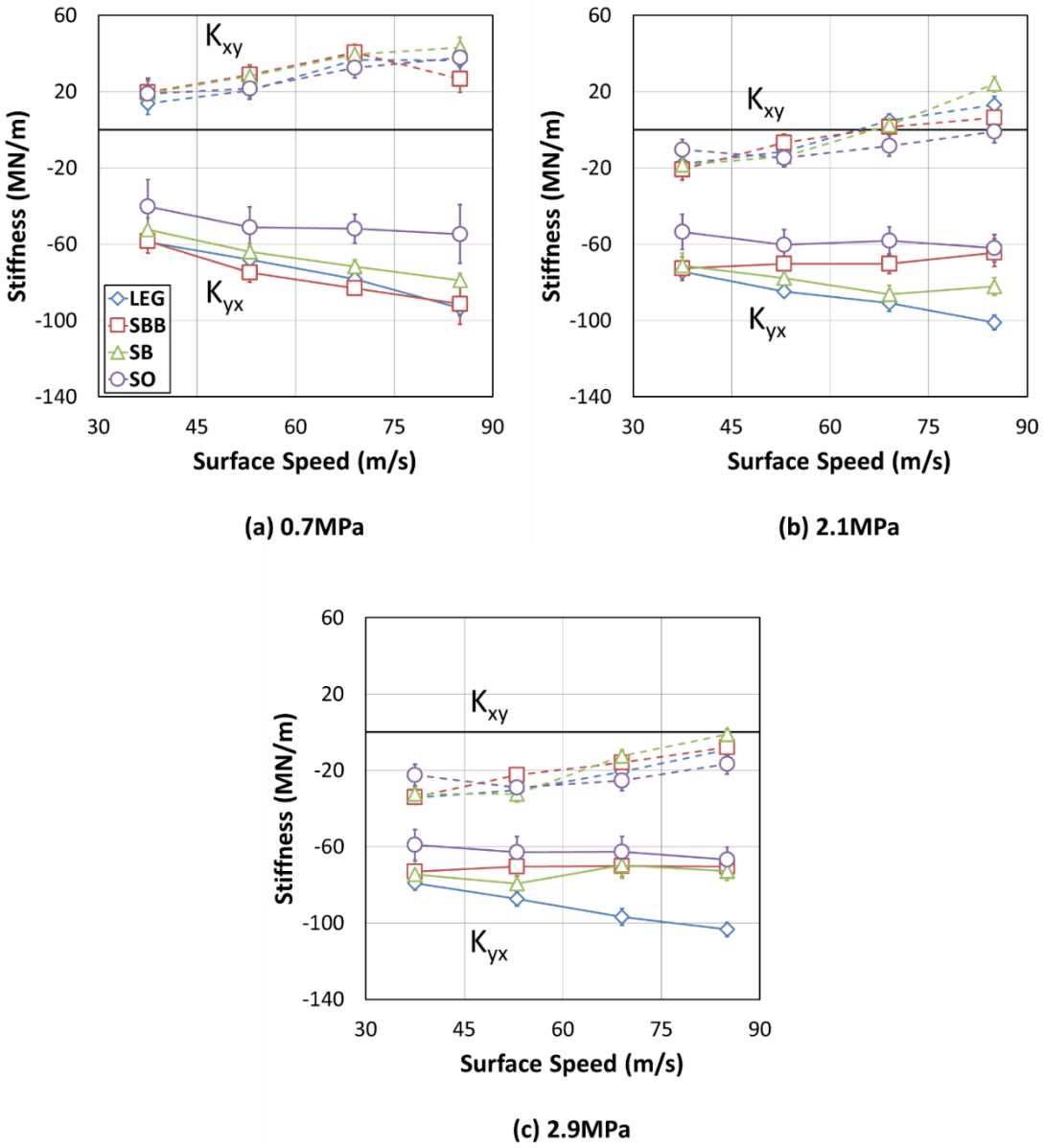

Figure 38: K_{xy} & K_{yx} - Measured Cross-Coupled Stiffness as a Function of Speed for Unit Loads of (a) 0.7, (b) 2.1, and (c) 2.9 MPa (Not Shown: Predicted $K_{xy} \approx K_{yx} \approx$ Zero)

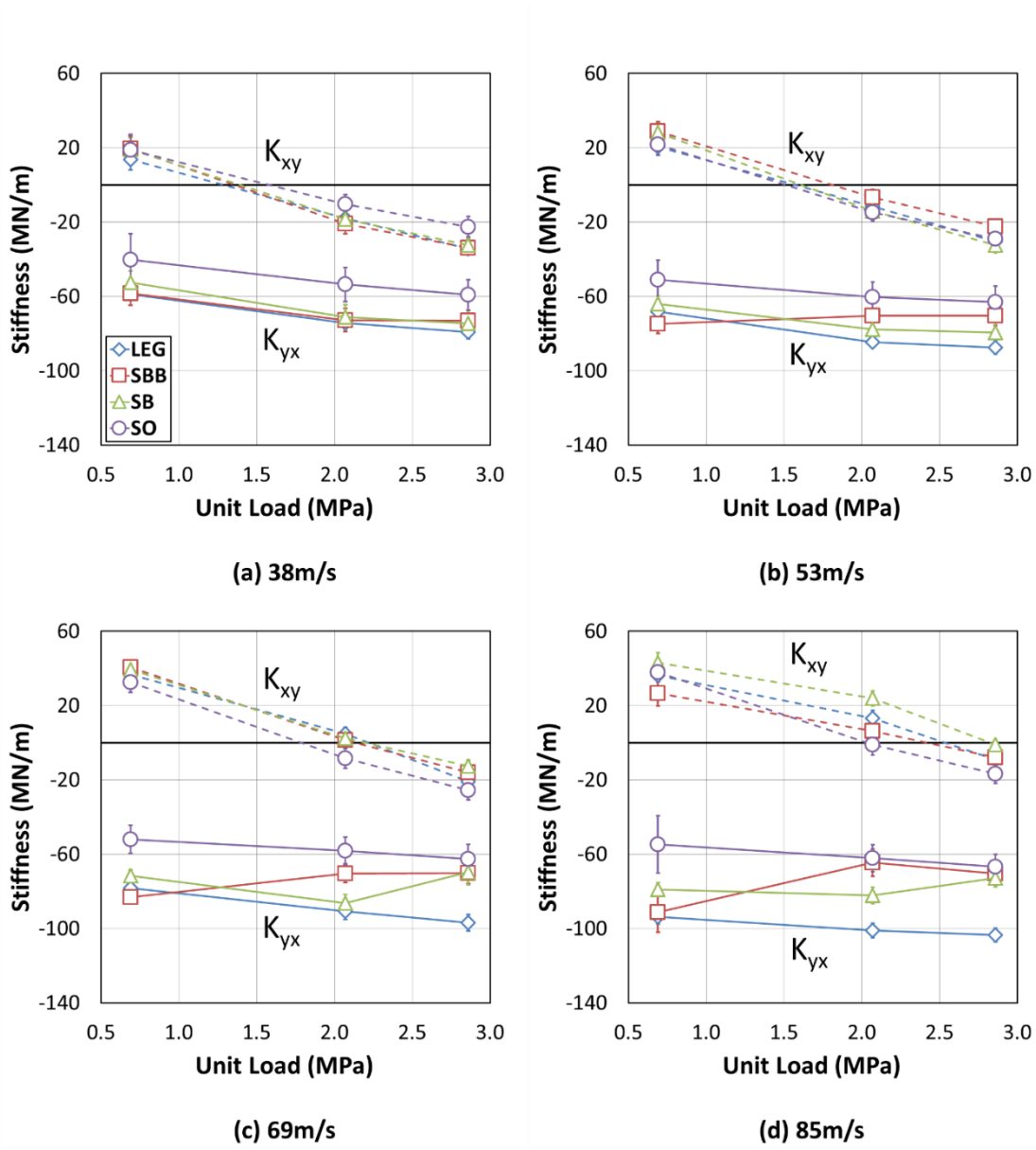

Figure 39: K_{xy} & K_{yx} - Measured Cross-Coupled Stiffness as a Function of Load for Speeds of (a) 38, (b) 53, (c) 69, and (d) 85 m/s (Not Shown: Predicted $K_{xy} \approx K_{yx} \approx$ Zero)

Direct Damping: C_{yy} & C_{xx}

Figure 40 shows predicted and measured C_{yy} as a function of surface speed for the three test loads. Figure 40a shows C_{yy} for a constant load of 0.7 MPa; the measured damping is approximately the same across the four configurations at low speeds but is significantly different at high speeds with the SO having the greatest damping and the SBB the least. Figure 40b shows C_{yy} for the 2.1 MPa load. The measured damping is approximately the same for all configurations at surface speeds of 38 and 53 m/s, but C_{yy} is different at surface speeds of 53 and 85 m/s where the SO has the greatest damping and the SBB has the lowest. Figure 40c shows C_{yy} for a load of 2.9 MPa; the difference in damping between the four configurations continues to be most noticeable at high speeds, but the difference between configurations is less for the 2.9 MPa load than for the 0.7 and 2.1 MPa cases. The largest difference in C_{yy} occurs at the low-load/high-speed combination of 0.7 MPa and 85 m/s. At this condition, the LEG, SBB, and SB provide 24, 42, and 26% less damping, respectively, than the SO at the same conditions.

Figure 41 shows predicted and measured C_{yy} as a function of load. Figure 41ab show C_{yy} for surface speeds of 38 and 53 m/s respectively. As a function of load, there are no major differences between the trends or values for the measured damping across the four bearing configurations. Figure 41cd show C_{yy} for surface speeds of 69 and 85 m/s respectively. The difference in measured damping for each of the four configurations is much more significant than at the lower surface speeds of 38 and 53 m/s. At the lowest load, the flooded SO provides substantially greater damping than the other methods, especially the evacuated SBB, which provides the least amount of damping across the entire load range. At 85 m/s the measured damping for the SBB is less than the SO by a factor of 0.6 at 0.7 MPa and 0.8 at 2.9 MPa; typically the correlation between configurations is better at higher loads.

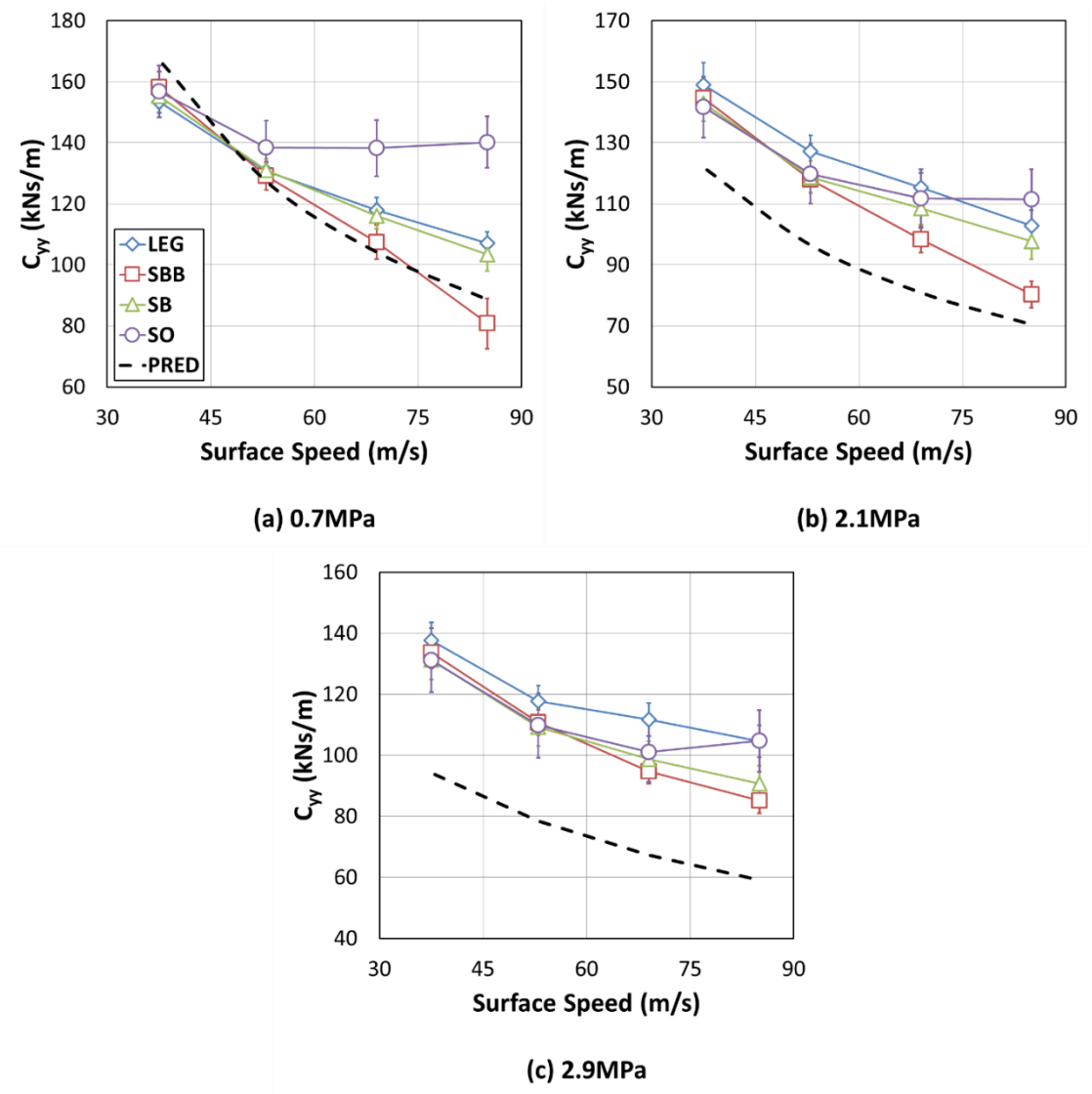

Figure 40: C_{yy} - Measured and Predicted Direct Damping in the Loaded Direction as a Function of Speed for Unit Loads of (a) 0.7, (b) 2.1, and (c) 2.9 MPa

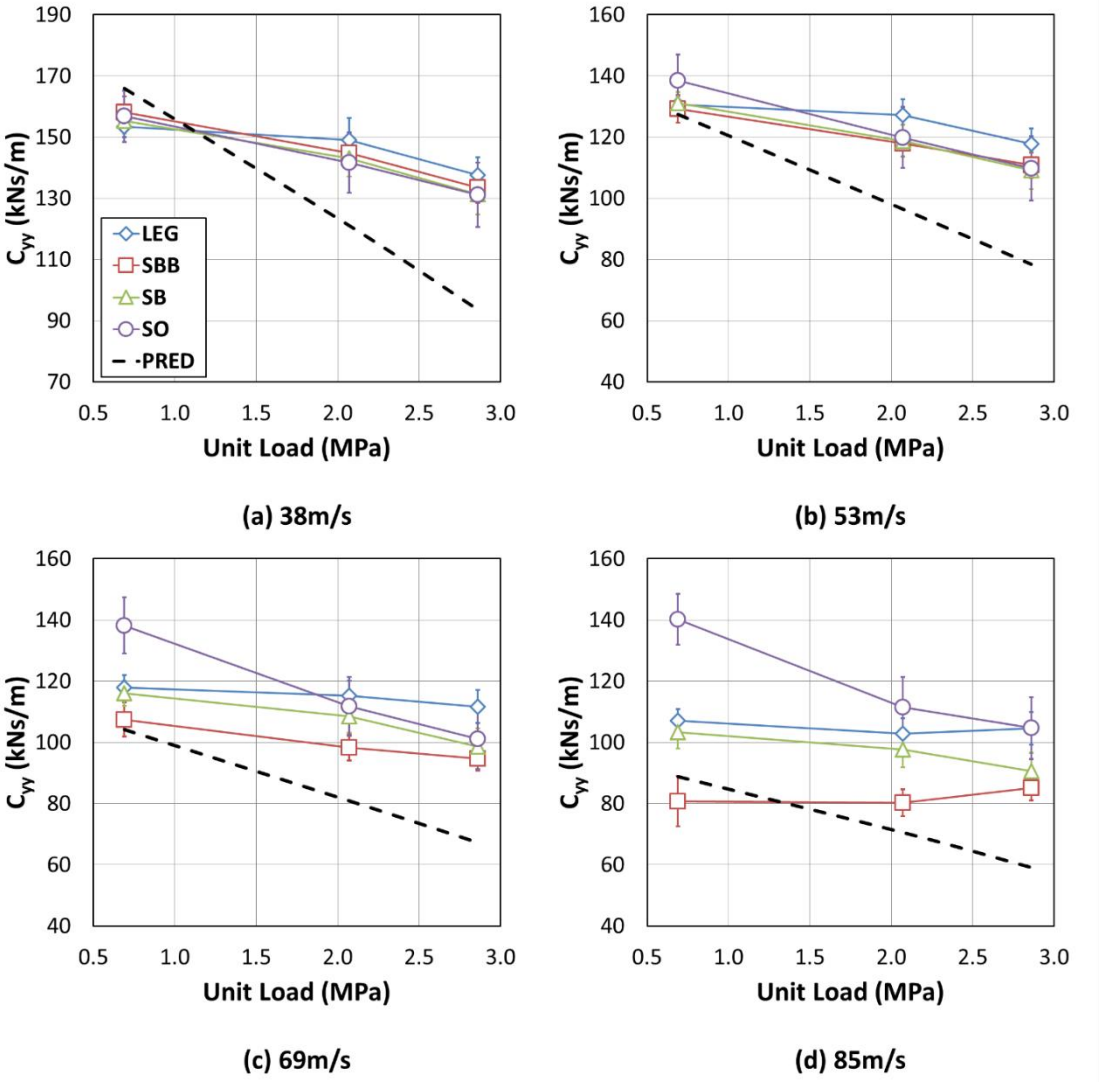

Figure 41: C_{yy} - Measured and Predicted Direct Damping in the Loaded Direction as a Function of Load for Speeds of (a) 38, (b) 53, (c) 69, and (d) 85 m/s

Table 10 compares the measured and predicted values for C_{yy}. Typically, the predictions correlate best with measurements at low loads and low speeds. The following ratios of predicted to measured C_{yy} are presented with low-speed (38 m/s) ratios first, followed by the ratios at high surface speeds (85 m/s). At 0.7 MPa the ratio of predicted to measured C_{yy} ranges from 1.1 to 0.6 for the SO, 1.1 to 0.8 for the LEG, 1.0 to 1.1 for the SBB, and 1.1 to 0.9 for the SB. At 2.1 MPa, C_{yy} ratios are 0.9 to 0.6 for the SO, 0.8

to 0.7 for the LEG and SB, and 0.8 to 0.9 for the SBB. At the highest load of 2.9 MPa the correlation between predicted and measured C_{yy} is the worst with ratios of 0.7 to 0.6 for the SO and LEG, and 0.7 for the SBB and SB. Overall, the predicted values for C_{yy} correlate best with the SBB and worst with the SO.

Table 10: Comparison Factors for Measured and Predicted C_{yy}

Factor: (Predicted C_{yy})/(Measured C_{yy})					
Load (MPa)	Surface Speed (m/s)	LEG	SBB	SB	SO
0.7	38	1.1	1.0	1.1	1.1
	53	1.0	1.0	1.0	0.9
	69	0.9	1.0	0.9	0.8
	85	0.8	1.1	0.9	0.6
2.1	38	0.8	0.8	0.8	0.9
	53	0.8	0.8	0.8	0.8
	69	0.7	0.8	0.7	0.7
	85	0.7	0.9	0.7	0.6
2.9	38	0.7	0.7	0.7	0.7
	53	0.7	0.7	0.7	0.7
	69	0.6	0.7	0.7	0.7
	85	0.6	0.7	0.7	0.6

Figure 42 shows the direct damping (C_{yy}) measured by Harris [6] as a function of surface speed (Figure 42a) and load (Figure 42b). Figure 42a shows damping that decreases with speed at a rate of approximately 15.8 kNs/m for every 10 m/s of surface speed increase. This trend presented by Harris (who also had a SBB) is almost identical to the trend for the SBB shown here in Figure 40ab, which show similar decreases in damping of 16.5 kN/s and 13.8 kN/s (respectively) for every 10 m/s of surface speed increase. Figure 42b shows damping from Harris that is approximately constant with

load. For this study, the damping for the SBB configuration decreases slightly with load except at 85 m/s (shown in Figure 41d) where it is approximately constant with load.

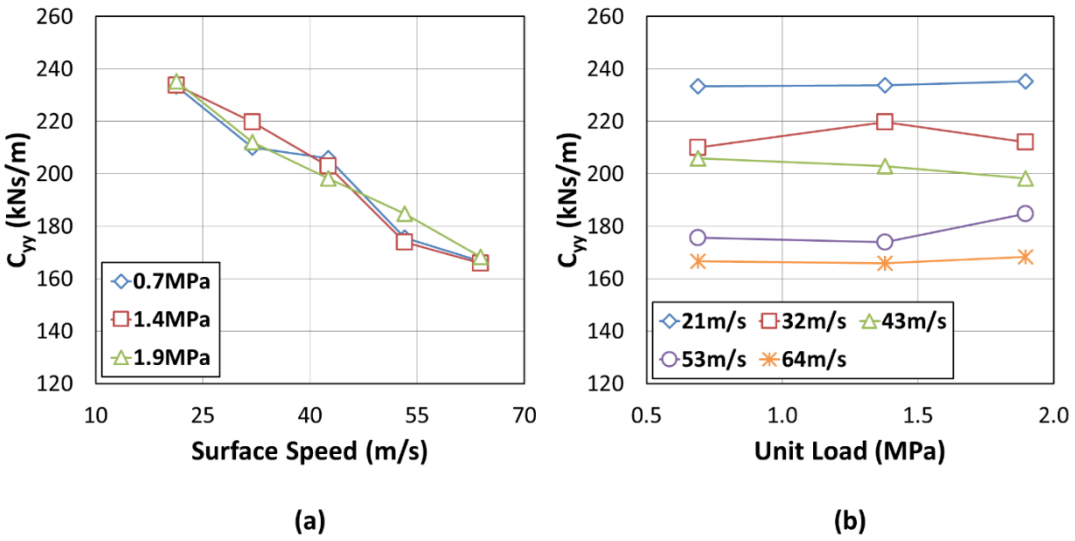

Figure 42: C_{yy} - Direct Damping in the Loaded Direction from Harris [6] as (a) a Function of Speed and (b) a Function of Load

Figure 43 shows predicted and measured values for C_{xx}. The configuration with the SBB typically has the lowest damping of all four configurations followed by the SB, LEG, and SO. Figure 43a shows C_{xx} for a load of 0.7 MPa; the trend for each configuration is approximately the same as those for C_{yy} shown previously in Figure 40a. The greatest difference between measured values of C_{xx} occurs at the low-load/high-speed condition of 0.7 MPa and 85 m/s. At this condition, the LEG, SBB, and SB produce 20, 45, and 29% less damping than the SO at the same conditions. Figure 43b shows C_{xx} for a load of 2.1 MPa. The SBB continues to supply the lowest damping while the SO provides the highest. Figure 43c shows C_{xx} for a load of 2.9 MPa. The measured damping is greatest for the SO followed by the LEG, SB, and SBB. The three configurations with directed lubrication provide damping that decreases with speed; the SO configuration has a small initial decrease but is approximately constant over most of

the speed range. Typically, the SO provides greater damping in both the loaded, and unloaded, directions.

Figure 44 shows predicted and measured values for C_{xx} as a function of load. The trends are similar to those for C_{yy}. Figure 44a shows C_{xx} for a surface speed of 38 m/s. As a function of load, there are no major differences between the trends or values of the measured damping for the four different configurations. Figure 44b shows C_{xx} for a surface speed of 53 m/s. Of the four configurations, the SBB provides the lowest damping while the SO provides the most. The SBB is lower by a factor of 0.8 (compared to the SO). The difference in damping between the SO and the SBB continues to increase for surface speeds of 69 m/s and 85 m/s (while the values for the LEG and SB typically fall between the two). Figure 44c (C_{xx} at 69 m/s) shows measured damping for the SBB that is lower than the SO damping by a factor of 0.8 to 0.6. For a surface speed of 85 m/s (Figure 44d), the damping from the SBB is lower than the SO damping by up to 45% at the low load condition (0.7 MPa).

As with the direct stiffness, XL_TPJB also predicts isotropic direct damping ($C_{xx} = C_{yy}$); however, measurements for C_{xx} typically have a better correlation with predicted values than C_{yy}. Like C_{yy}, predicted values for C_{xx} correlate best with measurements at low loads and low speeds, and the correlation is best for the SBB and worst for the SO. Ratios of predicted to measured C_{xx} range from 1.1 to 0.6 for the SO, 1.1 to 0.7 for the LEG, 1.1 to 0.9 for the SBB, and 1.1 to 0.8 for the SB.

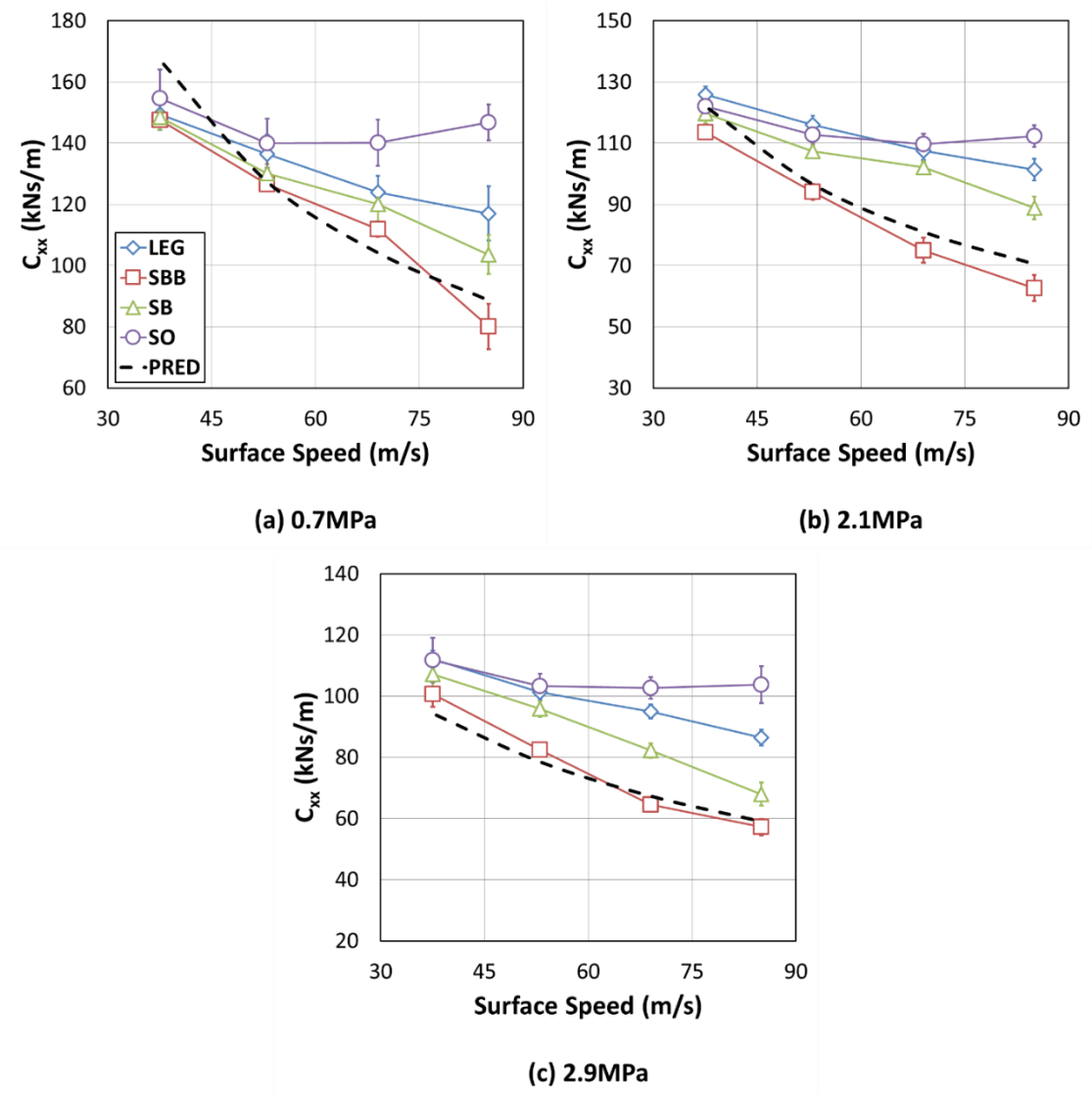

Figure 43: C_{xx} - Measured and Predicted Direct Damping in the Direction Perpendicular to Load as a Function of Speed for (a) 0.7, (b) 2.1, and (c) 2.9 MPa

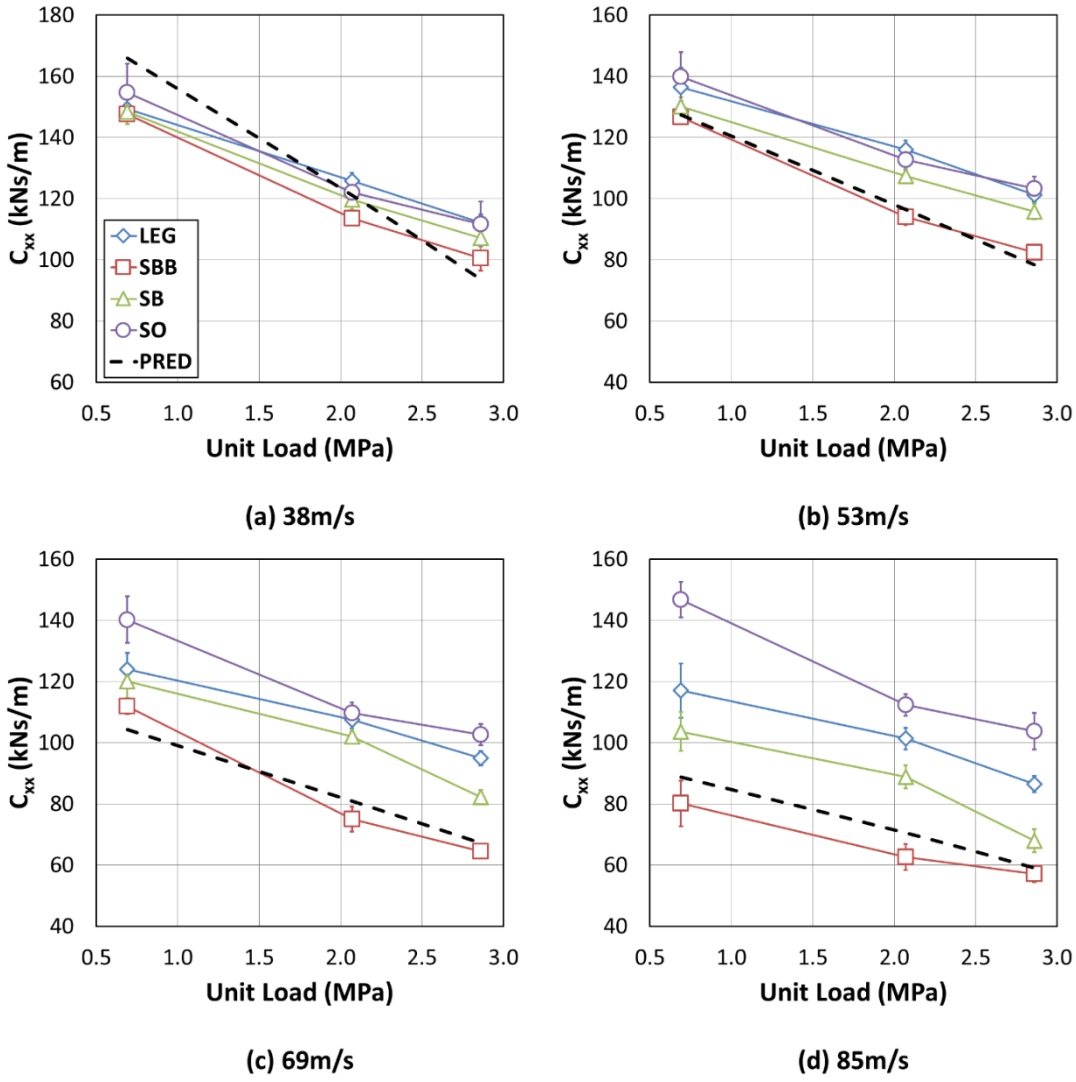

Figure 44: C_{xx} - Measured and Predicted Direct Damping in the Direction Perpendicular to Load as a Function of Load for Speeds of (a) 38, (b) 53, (c) 69, and (d) 85 m/s

Figure 45 shows the measured C_{xx} from Harris [6]. Damping decreases with speed (Figure 45a), and is approximately constant with load (Figure 45b) except at 21 m/s. For the SBB configuration in this study, C_{xx} does decrease with speed (Figure 43); however, C_{xx} also decreases with load (Figure 44) contrary to the results from Harris in Figure 45b (approximately constant damping with load).

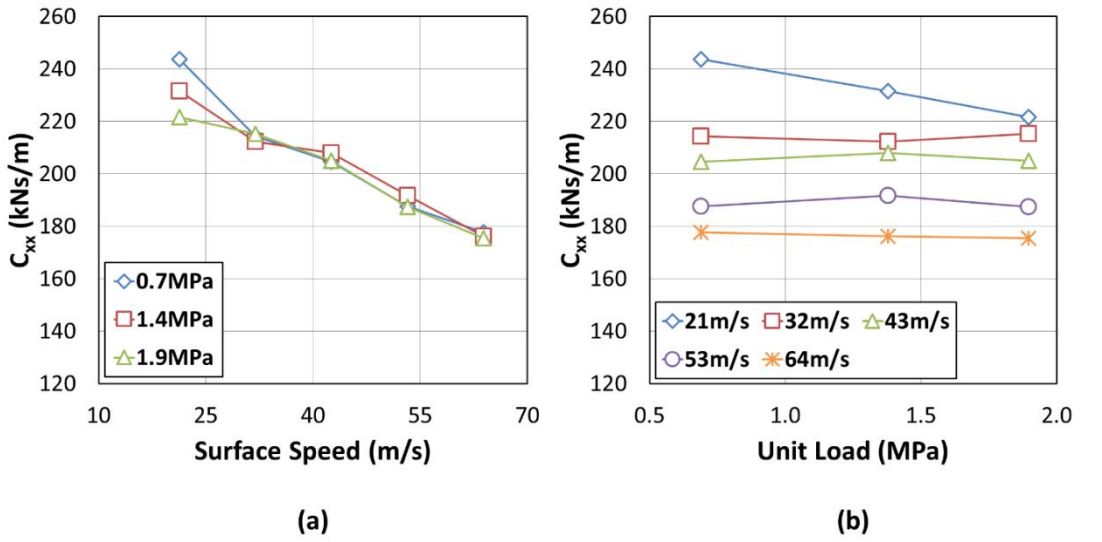

Figure 45: C_{xx} - Direct Damping in the Direction Perpendicular to Load from Harris [6] as (a) a Function of Speed and (b) a Function of Load

Figure 46 independently shows C_{yy} as a function of speed for each of the four configurations to highlight the difference in trends. Figure 46a shows C_{yy} for the SO; the only configuration that is tested with end seals (flooded). Figure 46bcd all show C_{yy} for evacuated configurations with directed lubrication. The damping has an initial decrease for the flooded SO but is approximately constant at high speeds; the damping for the LEG, SBB, and SB all continue to decrease over the entire speed range. Of the configurations with directed lubrication, the damping for the SBB has the greatest decrease and the lowest damping while the LEG decreases the least and provides the maximum amount of damping (for methods with directed lubrication). The trends are the same for C_{xx}, although the difference between feed types is not as severe.

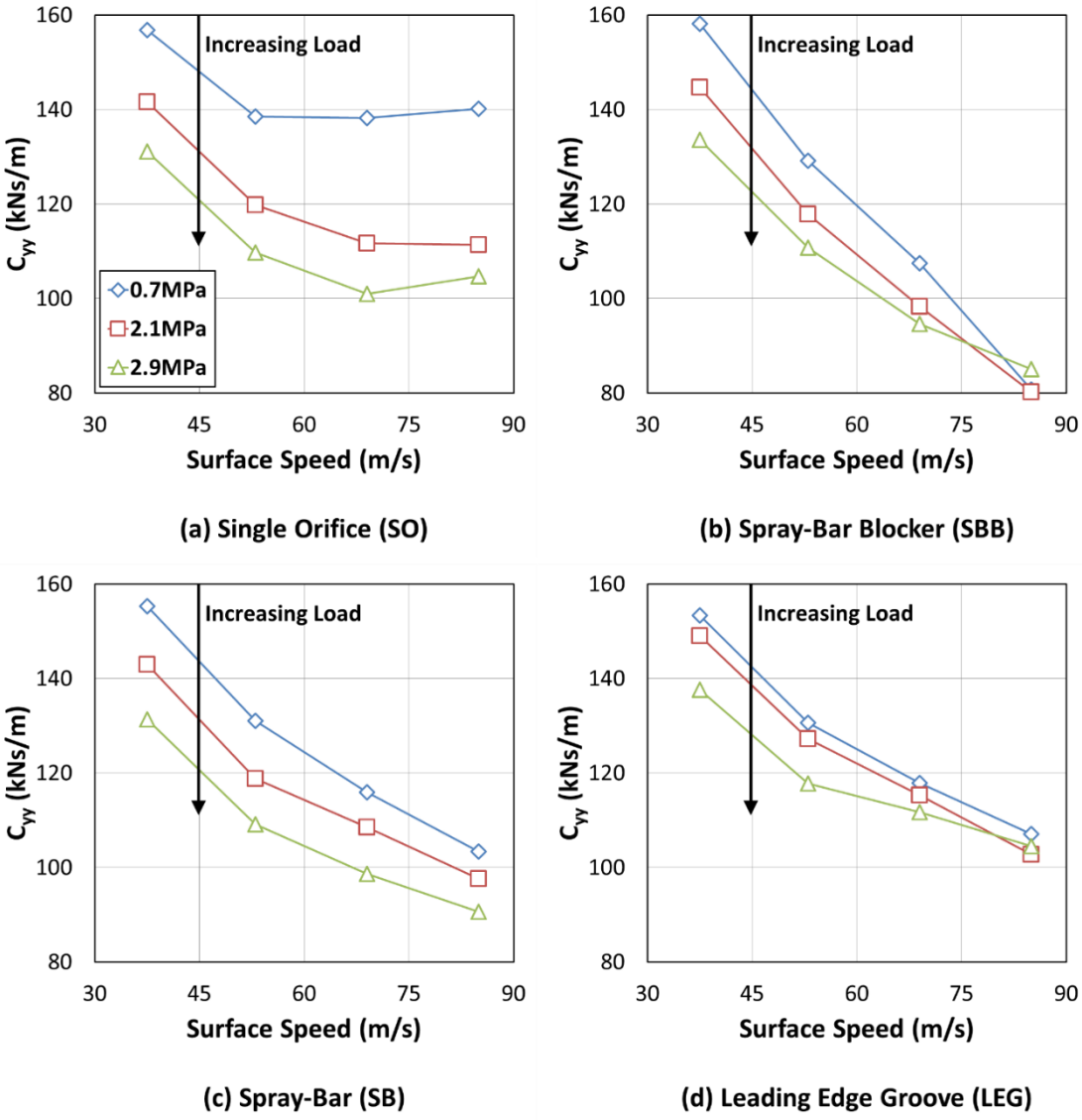

Figure 46: C_{yy} - Direct Damping Trends for the (a) SO, (b) SBB, (c) SB, and (d) LEG.

Whirl Frequency Ratio

Table 11 shows the WFR calculated from measured data using Eq. (29); Lund's method, which neglects virtual mass terms. Virtual mass terms were neglected in WFR calculations due to high uncertainties in the measured cross-coupled virtual mass values. A null WFR is desired and typical for most TPJBs; a finite WFR indicates the possibility

of rotordynamic instability. At the lightest load (0.7 MPa), the WFR is finite for all speeds and lowest (most stable) for the flooded SO. At 2.1 MPa, the WFR is null for the flooded SO but finite for the LEG, SB, and SBB at surface speeds of 69 and 85 m/s. At the highest unit load (2.9 MPa) the WFR is null for all configurations and test speeds. Harris [6] presented WFR = 0 for all test conditions, contrary to what is presented here, even though he measured a similar level of direct stiffness orthotropy.

Ertas and Vance [38] state that rotordynamic instability "is dictated by two types of forces: (i) direct damping and cross-coupled or cross-axis stiffness." They continue by noting that the direct damping has a positive impact on stability while the cross-coupled stiffness terms (K_{xy}, K_{yx}) "must be of opposite signs in order to be destabilizing." Each test condition that produced a finite WFR also had cross-coupled stiffness terms with opposing signs. Harris measured same-sign cross-coupled stiffness for all cases. A lack of direct stiffness orthotropy may also be a contributing factor to the magnitude of the WFR. Smith [37] stated that increasing direct stiffness orthotropy could increase the OSI, and the results presented in this thesis follow his observation. The level of orthotropy increases from K_{xx}/K_{yy} = 1.0 at 0.7 MPa to K_{xx}/K_{yy} = 0.9 at 2.1 MPa, and the increase in orthotropy is accompanied by a decrease in the WFR (increase in OSI) as Smith predicted.

There is not a noticeable trend between WFR and the magnitude of the attitude angles. Each case resulting in a finite WFR had an attitude angle greater than 9°, with the LEG and SB having the largest. However, a high attitude angle did not always correspond with higher WFR. Comparing the three methods of directed lubrication, the SBB always has the lowest attitude angle, but has the largest WFR at 0.7 MPa and the lowest WFR at 2.1 MPa.

Table 11: Calculated Whirl Frequency Ratio from Measured Data

Load (MPa)	Surface Speed (m/s)	LEG	SBB	SB	SO
0.7	38	0.27	0.31	0.29	0.24
	53	0.27	0.36	0.31	0.23
	69	0.33	0.40	0.33	0.22
	85	0.32	0.39	0.34	0.19
2.1	38	Null	Null	Null	Null
	53	Null	Null	Null	Null
	69	0.17	0.12	0.13	Null
	85	0.25	0.18	0.30	Null
2.9	38	Null	Null	Null	Null
	53	Null	Null	Null	Null
	69	Null	Null	Null	Null
	85	Null	Null	Null	Null

Direct Virtual Mass: M_{yy} & M_{xx}

Figure 47 shows measured and predicted values for virtual mass in the loaded direction, M_{yy}, as a function of speed. The predictions are the same order of magnitude as measured values; however, predicted values are typically positive (except at 38 m/s), and measured values are always negative. All measured values of M_{yy} are negative, indicating that the real part of the impedance values increase with excitation frequency. Harris [6] also measured negative virtual mass terms along with Kulhanek [7], Delgado et al. [8], Tschoepe [9], and Dmochowski et al. [39]. Harris only measured negative M_{yy} for surface speeds of 21 and 32 m/s; whereas M_{yy} is negative for the entire speed range in this study. Delgado et al. [8] state that a negative virtual mass term has no physical meaning and is just a value used to capture the frequency dependence of the impedance values (real part). Harris measured values from -40 to 15 kg, and predicted all positive values for M_{yy}. His measured pivot stiffness was 350 MN/m. Figure 47 shows M_{yy} terms from -46 to -14 kg, and predicted values that are typically positive above a surface speed

of 38 m/s. The bearing tested in this thesis has a measured pivot stiffness of 412 MN/m. The pivot stiffness and measurement process are discussed on pages 34-35 and shown in Figure 16.

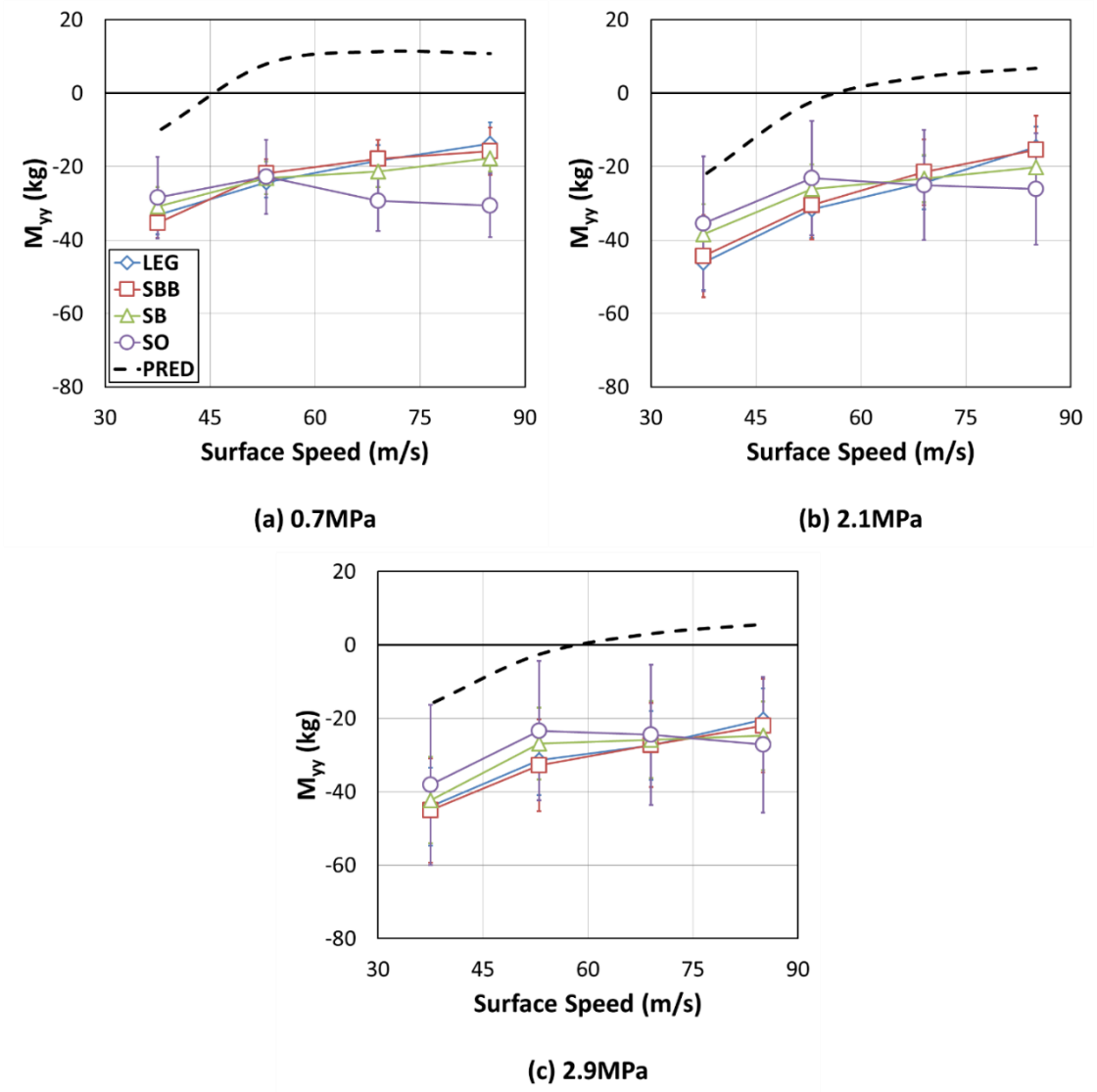

Figure 47: M_{yy} - Measured and Predicted Direct Virtual Mass in the Loaded Direction as a Function of Speed for (a) 0.7, (b) 2.1, and (c) 2.9 MPa

Figure 48 shows measured values for the virtual mass in the direction perpendicular to load, M_{xx}, as a function of speed. As with M_{yy}, all measured values of M_{xx} are negative; Harris only measured negative M_{xx} values for a surface speed of 21 m/s.

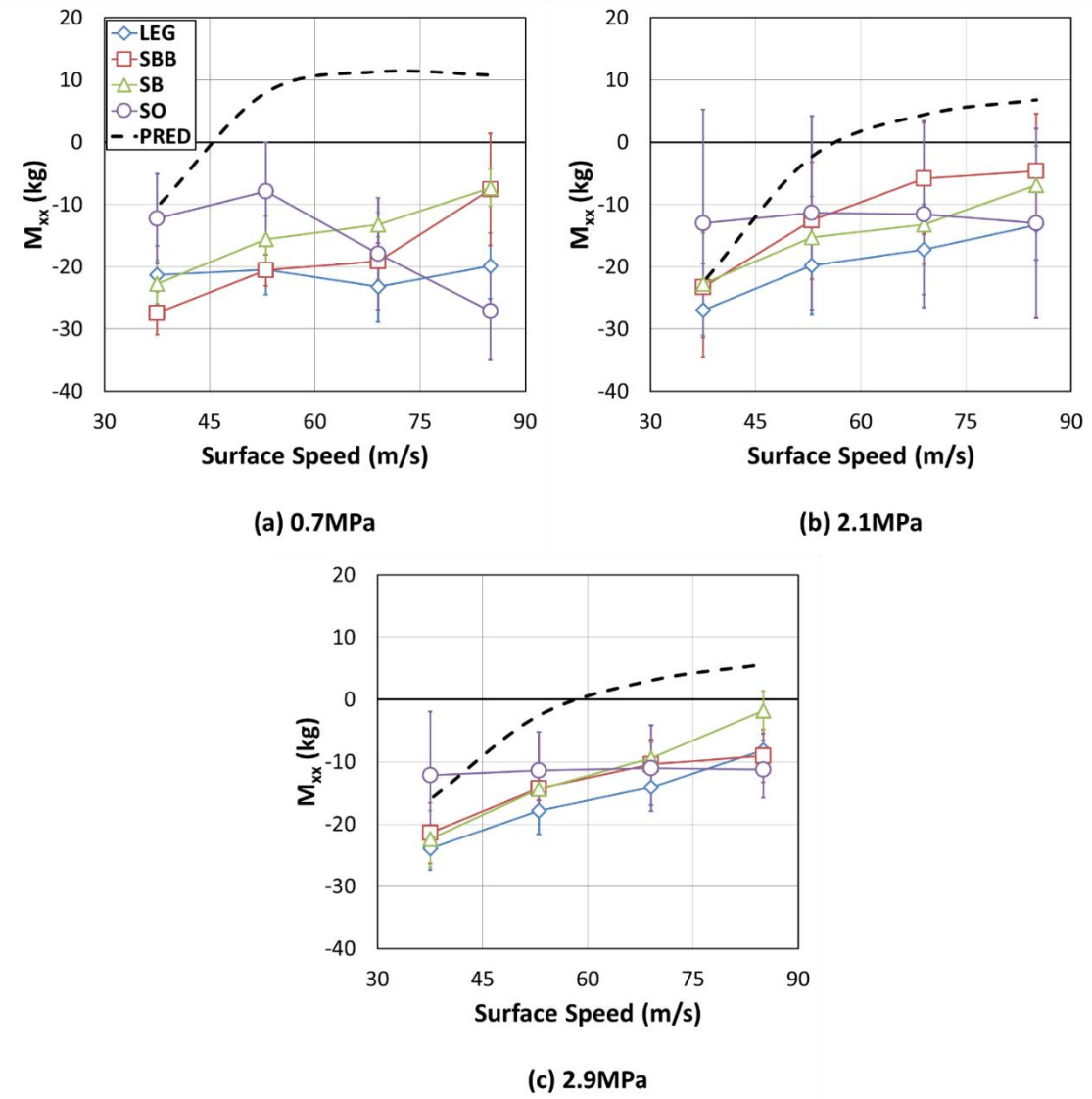

Figure 48: M_{xx} - Measured and Predicted Direct Virtual Mass in the Direction Perpendicular to Load as a Function of Speed for (a) 0.7, (b) 2.1, and (c) 2.9 MPa Pivot Stiffness

Figure 48 shows that, at high loads (2.1 and 2.9 MPa), M_{xx} is approximately constant (-12 kg) with speed for the SO configuration but becomes less negative (positive slope) with speed for the three configurations with directed lubrication. The magnitude of M_{xx} is typically lower than the magnitude of M_{yy}.

Childs [40] uses the model in Figure 49, and the following derivation, to account for negative virtual mass terms. The model represents the pivot-stiffness (k_1) in series with the stiffness and damping from the fluid film (k_2, c).

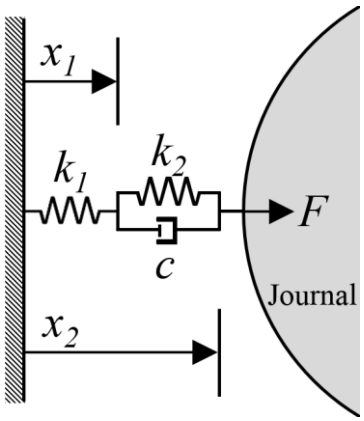

Figure 49: Pivot Stiffness in Series with Fluid Film Stiffness and Damping

In the time domain and frequency domain the equilibrium equations are:

$$f(t) = -k_2(x_2 - x_1) - c(\dot{x}_2 - \dot{x}_1) = -k_1 x_1$$
$$F(s) = -(k_2 + sc)X(s) + (k_2 + sc)X_1(s) = -k_1 X_1(s)$$
$$\therefore \frac{F(s)}{X_1(s)} = -\frac{k_1(k_2 + sc)}{(k_2 + k_1) + sc}$$

and substituting $j\Omega$ for s gives the following transfer function

$$\frac{F(j\Omega)}{X_1(j\Omega)} = -\frac{k_1\left[k_2 + c(j\Omega)\right]}{\left[(k_2+k_1) + c(j\Omega)\right]} = -\frac{\left[k_2k_1(k_2+k_1) + k_1c^2\Omega^2\right] + ck_1^2(j\Omega)}{(k_2+k_1)^2 + c^2\Omega^2}$$

then using a Taylor series expansion gives the following expression with effective stiffness, K_{eff}, and effective damping, C_{eff}.

$$\frac{F(j\Omega)}{X_1(j\Omega)} = \\ -\left[k_2\left(\frac{k_1}{k_2+k_1}\right) + \frac{c^2k_1^2\Omega^2}{(k_2+k_1)^3} + \ldots\right] - c\left[\left(\frac{k_1}{k_2+k_1}\right)^2 - \frac{c^2k_1^2\Omega^2}{(k_2+k_1)^4} + \ldots\right](j\Omega) \qquad (31)$$

$$= -K_{eff}(\Omega) - C_{eff}(\Omega)(j\Omega)$$

At low frequencies, Eq. (31) predicts that the fluid film stiffness (k_2) will be reduced by the factor $k_1/(k_2+k_1)$, and the damping from the fluid film (c) is reduced by the factor $[k_1/(k_2+k_1)]^2$ [40]. As excitation frequency (Ω) increases, K_{eff} will increase and C_{eff} will decrease. An increase in K_{eff} with excitation frequency indicates a positive slope, which is captured by a negative virtual mass term (negative virtual mass indicates a positive slope for the real part of the impedance, refer to Eq.17).

Static Stiffness: K_{STATIC}

The static stiffness is approximated by dividing the measured change in static load by the measured change in eccentricity (in the direction of load). Figure 50 shows static stiffness and direct stiffness in the direction of load (K_{yy} measured during dynamic testing) for the evacuated configuration with the LEG. Figure 50a shows static and dynamic stiffness for the LEG configuration at a surface speed of 38 m/s. For loads of 0.7, 2.1, and 2.9 MPa, the static stiffness is 1.28, 0.75, and 1.14 times the dynamic stiffness (respectively); or an average of 1.06 times the dynamic stiffness. An average

factor is used to compare the rest of the static and dynamic stiffness values. As speed increases the correlation between static and dynamic stiffness tends to decrease; in order of increasing surface speed (38, 53, 69, 85 m/s) the static stiffness is an average of 1.06, 1.06, 1.17, and 1.29 times the dynamic stiffness (for the LEG).

Figure 51 shows the static and dynamic stiffness for the evacuated configuration with the SBB. As with the LEG, the correlation between static and dynamic stiffness decreases with speed. In order of increasing speed, the static stiffness is an average of 1.03, 1.06, 1.18, and 1.43 times the dynamic stiffness.

Figure 52 shows the static and dynamic stiffness for the SB configuration; the static stiffness is an average of 0.94, 1.09, 1.24, and 1.31 times the dynamic stiffness (as speed increases).

Figure 53 shows the static and dynamic stiffness for the flooded SO configuration; the static stiffness is an average of 0.95, 1.07, 1.08, and 1.22 times the dynamic values. All configurations (on average) have approximately the same (reasonable) correlation between static and dynamic stiffness values. The dynamic stiffness is likely the more accurate value since the measurement occurs at one load condition, which diminishes the affect that thermal expansion has on the eddy current probes. The static stiffness requires the journal displacement at different loads, and changing the load changes the thermal expansion of the eddy current probes.

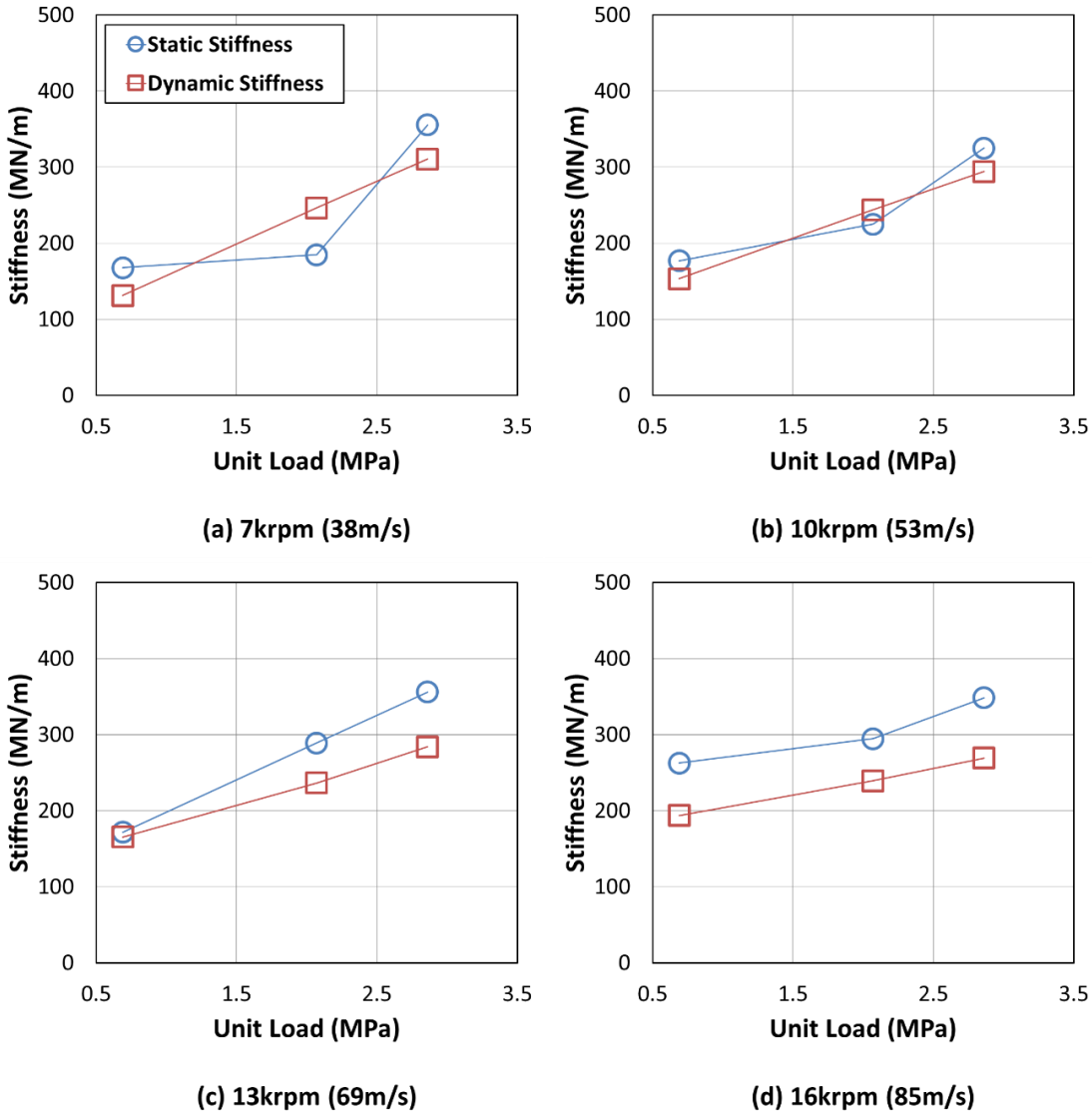

Figure 50: LEG - Comparison of Static and Dynamic Stiffness for the Evacuated Leading Edge Groove Configuration

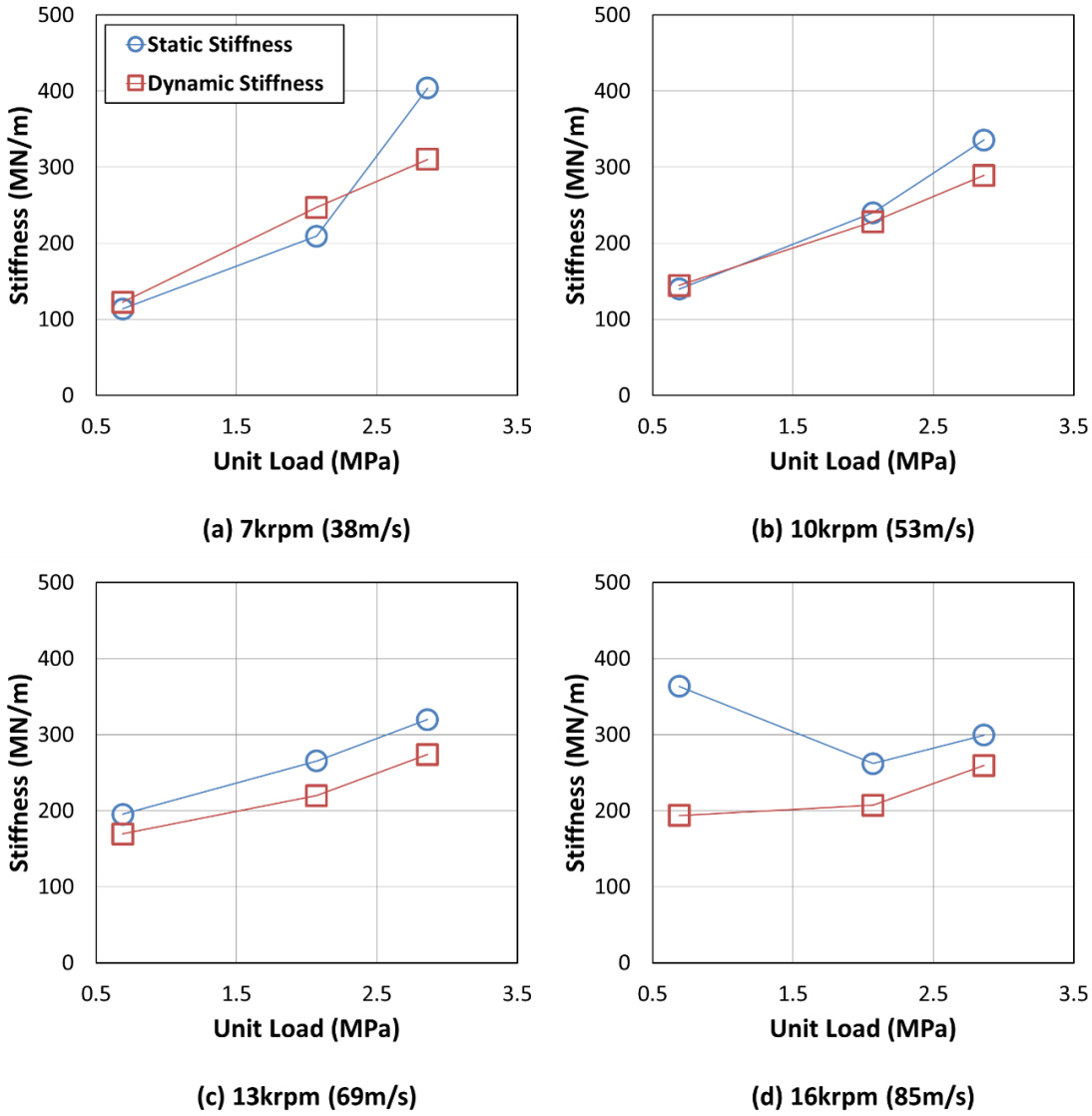

Figure 51: SBB - Comparison of Static and Dynamic Stiffness for the Evacuated Spray-Bar Blocker Configuration

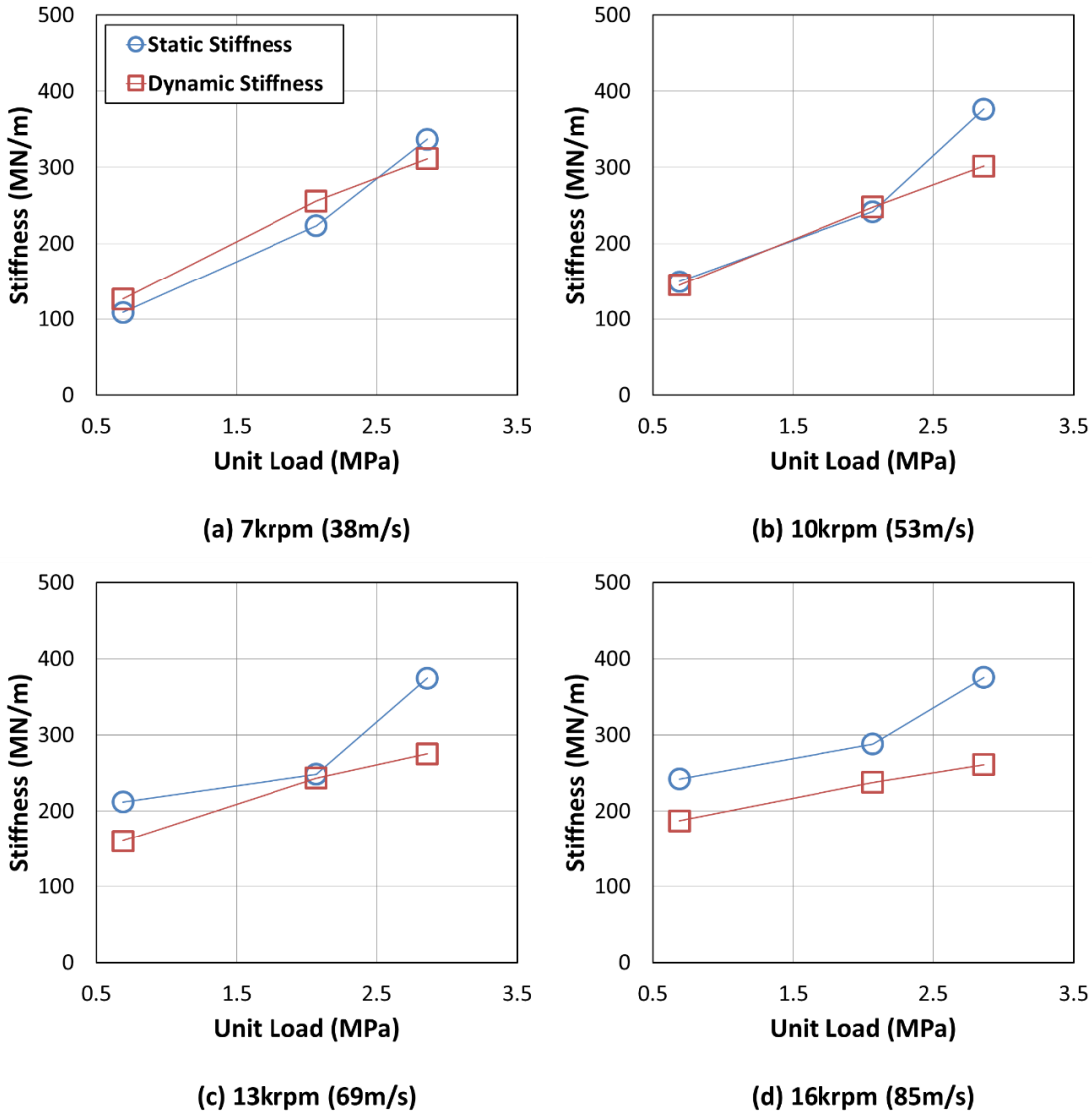

Figure 52: SB - Comparison of Static and Dynamic Stiffness for the Evacuated Spray-Bar Configuration

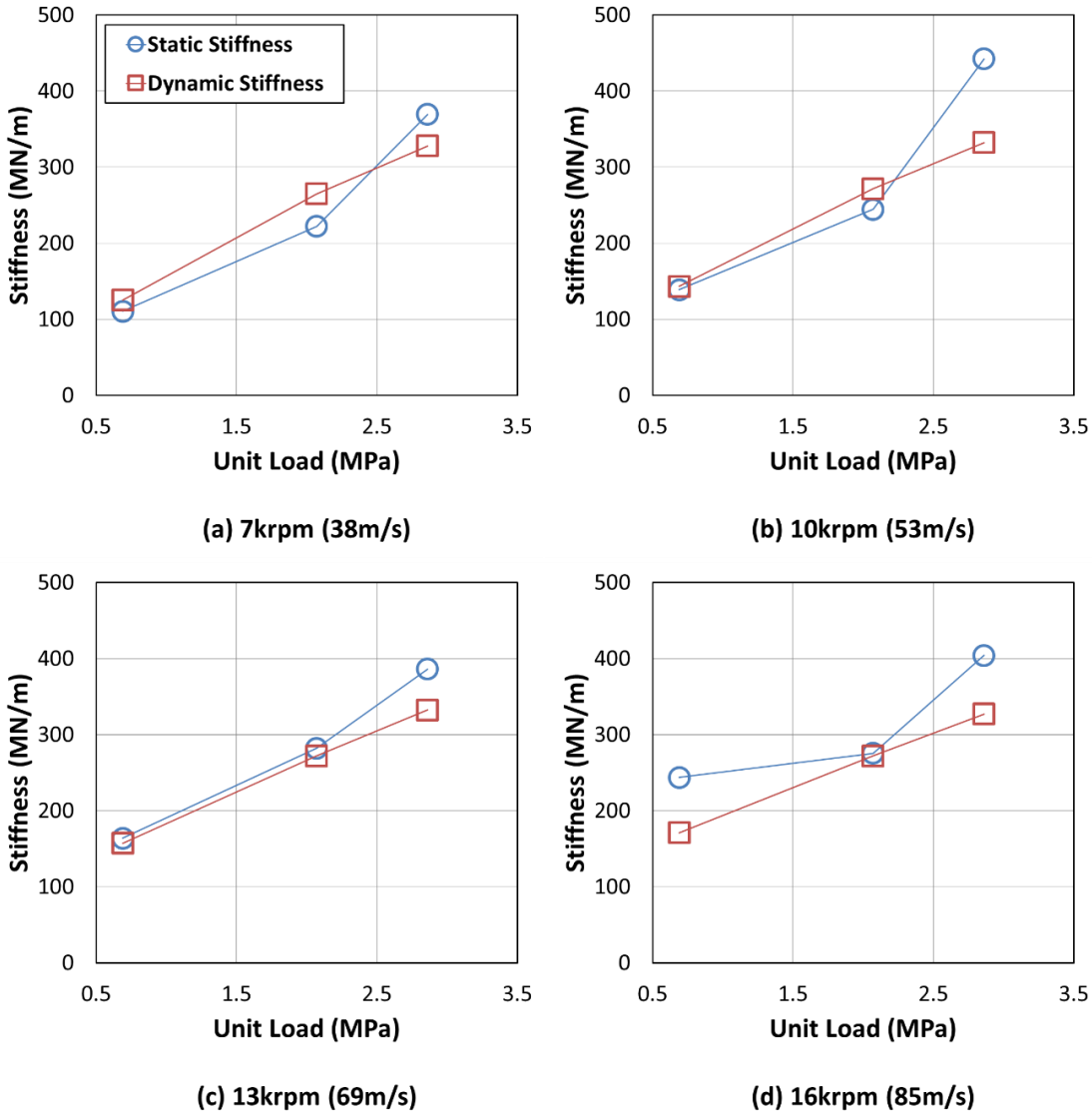

Figure 53: SO - Comparison of Static and Dynamic Stiffness for the Conventional Flooded Single Orifice Configuration

CONCLUSIONS

Static, dynamic, and thermal characteristics (measured and predicted) were presented for a 4-pad, spherical-seat, tilting-pad journal bearing (TPJB) with 0.5 pivot offset, 0.6 L/D, and 0.3 preload in the load between pivot (LBP) orientation. One bearing was tested four separate times with the following four different lubrication configurations: (1) flooded single-orifice (SO) at the bearing shell, (2) evacuated leading edge groove (LEG), (3) evacuated spray-bar blocker (SBB), and (4) evacuated spray-bar (SB). The same set of pads was used for every test. Each method of lubrication was added as an assembly to the bearing. Test conditions included changes in surface speeds and unit loads up to 85 m/s and 2.9 MPa, respectively. Predictions were made using XL_TPJB [27], a computer code developed at the Texas A&M Turbomachinery Lab (which utilizes a thermohydrodynamic analysis). The predictions were made using a thermal mixing coefficient of 0.8, and including fluid inertia effects and measured pivot stiffness (412 MN/m). XL_TPJB was not designed to model different methods of lubrication such as the leading edge groove (LEG), spray-bar blocker (SBB), or spray-bar (SB).

Static and Thermal Results

Cold Clearance

Harris [6] previously tested a spherical seat bearing at the Texas A&M Turbomachinery Laboratory; however, his measured clearance showed that the intended shape of the bearing was significantly distorted, likely crushed by the split housing stator. For this study, care was taken to preserve the intended shape of the bearing. All four measured clearances were approximately symmetric and equal, indicating no significant distortion of the intended bearing shape. The hot clearance of the bearing was also measured.

Hot Clearance

Hot clearance measurements were made for each of the four bearing configurations at the highest load (2.9 MPa) for each of the four speeds tested (a total of sixteen hot clearance measurements). These measurements serve as an approximation of the operational clearance of the bearing. Typically, the hot bearing clearance was inversely proportional to the max bearing temperature. The SO configuration had the highest max bearing temperature and the smallest measured hot clearance. The maximum difference between measured hot and cold clearances was recorded for the flooded SO configuration; the hot clearance (77 μm radial) is lower than the cold clearance (95 μm radial) by a factor of 0.81 (a 19% decrease).

Hot Bearing Center: New Methodology

To determine eccentricities and attitude angles, the measured rotor coordinates must be related to the hot bearing center (operational center). Defining the hot bearing center is difficult due to thermal expansion of the bearing, shaft, and eddy current probes, which also changes for every speed/load combination. Previously (for this rig), the operational bearing center was defined as the rotor position with zero applied load (F_s = 0). Wygant [35] takes issue with this approach and uses another method, stating, "The hot center cannot be found by applying a net load of zero on the housing. It is impossible to completely cancel out the gravity load and run at a zero load condition." For this work, a new method for determining the hot bearing center was introduced: after testing, the rig is shut down quickly, the hot clearance is measured and then used as the reference frame for the measured rotor coordinates. This method eliminates the gravity load of previous concern but also introduces a new (as yet unaddressed) concern over the level of difference between the actual operational clearance of the bearing and the measured hot clearance caused by the changing level of thermal expansion between operation and shutdown. An example was presented on page 46 from previous data for a rocker-back pad. The new method resulted in more negative *y*-eccentricities and more positive *x*-

eccentricities, which in turn yielded more positive attitude angles. Predictions were not shown. Further investigation is needed.

Eccentricity

As predicted, the *y*-eccentricity increased as load increased, and decreased as speed increased. For a fixed speed and load combination the *y*-eccentricity was approximately constant across all four bearing configurations. The *x*-eccentricity was slightly different across the four bearing configurations. Typically the SBB had the lowest *x*-eccentricity followed closely by the SO; the SB and LEG tended to have the largest *x*-eccentricities. The predicted *y*-eccentricity was greater than measured by a factor of 0.9 to 2.3 and the predicted x-eccentricity was approximately zero while measured values were finite.

Attitude Angle

Similar to previous spherical-seat bearing tests [6] [10] [12], a significant attitude angle was measured for all configurations (LEG, SBB, SB, SO) at most test cases. Wygant attributes the measured attitude angle to pad-pivot friction impeding the tilt motion of the pads. A significant attitude angle indicates the presence of cross-coupled stiffness, which is typically alleviated by the tilt motion of the pads in a TPJB. Typically, the LEG had the largest measured attitude angles (29° max) followed by the SB (24° max), SO (14° max), and SBB (12° max). Using the same rig, Tschoepe [9] measured attitude angles that were always below 10° (except at one point) for a rocker-back bearing. Here, the measured attitude angles were likely due to impeded tilt motion of the pads caused by friction between the pad and spherical pivot. Predicted attitude angles were approximately zero (XL_TPJB assumes unimpeded radial and axial tilt motion of the pads).

Bearing Temperatures

Pad temperatures (babbitt layer) were measured at the leading edge, 75% location (API 670 [36]), and trailing edge of the loaded pads along with lubricant temperatures

(exposed thermocouples) at the leading and trailing edges. Pad temperatures at the 75% location were also measured for the unloaded pads. Maximum temperatures always occurred at the loaded pads. The temperature rise (instead of temperature) was presented to minimize differences caused by small deviations (±0.5 °C) in the inlet temperature between tests. Typically, the maximum measured temperatures occurred at the 2nd loaded pad in the direction of shaft rotation (Pad C from Figure 29) at 75% of the pad length from the leading edge (Thermocouples 11, 12 from Figure 29). Contrary to measurements, predicted max temperatures were always at the trailing edge. All methods of directed lubrication offered some temperature relief (compared to the flooded SO configuration) with the LEG offering the greatest reduction in max temperature (up to 13.9 °C) followed by the SB (up to 12.8 °C) and then the SBB (up to 10.2 °C). The SBB and SB actually increased pad temperatures at the leading and trailing edge when compared to the SO configuration; however, the temperature at the 75% location (typical location of the max temperature) was still reduced. The temperature at the trailing edge of the loaded pads was significantly higher for the SBB than the other three configurations; the SBB attempts to "scrape" away the hot oil and in doing so seems to "back-up" the hot oil onto the upstream pad increasing trailing edge temperatures. Predicted temperatures are typically higher than measured at the leading and trailing edge but cooler at the 75% location. The predicted max bearing temperature was consistently lower (cooler) than measured, and the two differed by up to 14.3 °C; a significant discrepancy. An axial temperature difference of up to 9.6 °C was measured indicating that the film thickness changes along the axial length of the pad, likely due to impeded motion of the tilt pad.

Dynamic Results

Measured accelerations, forces, and displacements were used to calculate frequency-dependent impedance values. A least-squares linear regression was then used to fit the measured impedance values to a KCM model to determine frequency independent rotordynamic coefficients. The KCM model was a good fit for all rotordynamic

coefficients except C_{yx} and M_{xy}, indicating possible frequency dependence of these terms. Due to the poor fit of C_{yx} and M_{xy}, the cross-coupled damping and cross-coupled virtual mass terms were not presented in the body of this thesis but are given in Appendix B. In general, the direct stiffness is isotropic ($K_{yy} \approx K_{xx}$) at 0.7 MPa (light load) but becomes increasingly orthotropic ($K_{yy} > K_{xx}$) as the load is increased; at 2.1 and 2.9 MPa loads K_{xx} is less than K_{yy} by average factors of 0.9 and 0.8 respectively. This trend in stiffness isotropy/orthotropy is approximately the same for all four bearing configurations.

Direct Stiffness: K_{yy} and K_{xx}

At 0.7 MPa, K_{yy} and K_{xx} increased with speed and were approximately equal across all four bearing configurations. At heavier unit loads of 2.1 and 2.9 MPa, K_{yy} and K_{xx} were approximately constant with increasing speed (K_{xx} increased slightly) for the flooded SO but typically decreased with increasing speed for the LEG, SBB, and SB.

The SO provided the greatest direct stiffness (K_{yy} and K_{xx}) at high loads (2.1 and 2.9 MPa) and the SBB provided the least. Compared to the SO; the LEG (18%), SBB (25%), and SB (20%) can reduce the direct stiffness (K_{yy} and K_{xx} have similar reductions). These reductions typically occurred at the high-speed/high-load condition (2.9 MPa at 85 m/s).

Harris [6], who also used spray-bar blockers, always measured K_{yy} that increased with speed; however, his evacuated configuration used end seals with enlarged clearances (unlike the pad retainers used here). Other distinct differences between Harris and this study are: bearing crush (large for Harris), different L/D ratios, by-pass cooling, leading-edge chamfers, and different lubricants (VG32 vs. VG46).

Predicted values for K_{yy} and K_{xx} correlated very well with measurements for all four configurations, especially at the low load condition (0.7 MPa). Typically, the ratio of predicted to measured K_{yy} ranges from 0.9 - 1.2 for all configurations. For K_{xx}, the ratios range from 1.0 – 1.2 for the SO, LEG, and SB; and 1.0 – 1.4 for the SBB. The predicted trends for the direct stiffness most closely match the measured trends for the SO.

Cross-Coupled Stiffness: K_{xy} and K_{yx}

Significant cross-coupled stiffness values were measured for each bearing configuration at most test conditions. The magnitude of the cross-coupled terms was 20-50% of the direct terms. Harris [6] measured cross-coupled stiffness terms with magnitudes 15-35% of the direct terms. Typically, at low loads and/or high speeds the cross-coupled stiffness terms had opposite signs; which is destabilizing for forward whirl. Significant attitude angles were measured at most conditions regardless of whether the cross-coupled stiffness terms had opposing signs or not. K_{yx} was always negative regardless of speed or load; K_{xy} became less negative (transitions to positive values) as speed was increased but became more negative (transitions from positive values) as load was increased. Essentially, increasing speed can promote instability and increasing load can help stabilize the system. The low-load/high-speed condition (0.7 MPa at 85 m/s) had the largest magnitude destabilizing cross-coupled stiffness terms. Wygant et al. [11] also measured cross-coupled stiffness terms with opposite signs, while cross-coupled stiffness terms from Harris always had the same sign (negative).

Direct Damping: C_{yy} and C_{xx}

For all speeds, C_{yy} and C_{xx} decreased linearly (approximately) with increasing load for all four configurations. For all loads, C_{yy} and C_{xx} decreased with speed for the LEG, SBB, and SB. As a function of speed, the SO had an initial decrease but reached a constant value at higher speeds. At the low surface speed of 38 m/s, C_{yy} and C_{xx} were approximately equal across the four configurations for any unit load. However, as speed increases, the difference in direct damping between the four configurations became significant. The difference in direct damping between the four configurations was greatest at the high speed/low load condition (85 m/s at 0.7 MPa). At this condition the LEG, SBB, and SB provided 24%, 45%, and 29% less damping, respectively, than the SO. The reduction in damping was similar for both C_{yy} and C_{xx}. Typically, the SO provided the most direct damping, and the SBB provided the least. Of the three configurations with directed-lubrication, the LEG provided the greatest direct damping.

Predictions for direct damping did not correlate as well with measurements as the predictions for direct stiffness. Typically, the predictions for C_{xx} correlated better with measurements than the predictions for C_{yy}, and the correlation was better at low loads and low speeds. Most predicted damping values were lower than measured. The ratio of predicted to measured values for the direct damping ranged from 0.6 – 1.1 for the SO and LEG, and 0.7 – 1.1 for the SBB and SB. In comparison, Harris [6] presented ratios for direct damping that ranged from 0.8 – 1.7. Overall, the direct damping predictions in this study most closely correlated with measurements for the SBB.

Whirl Frequency Ratio

A finite WFR was calculated for all four bearing configurations at certain test conditions. TPJBs are typically expected to have a null WFR while fixed-arc bearings are expected to have finite WFRs. Harris [6] presented WFR = 0 for all test conditions; however, he also had same-sign cross-coupled stiffness terms. All test conditions that had finite WFRs in this study also had opposing-sign cross-coupled stiffness terms. Typically, the finite WFRs also corresponded with the level of direct stiffness orthotropy. For all conditions with a 0.7 MPa load, the support stiffness was isotropic (for all four configurations), and the WFR was finite. At 2.9 MPa, K_{xx}/K_{yy} = 0.8, and the WFR was zero (for all four configurations). The WFRs ranged from 0.19 ~ 0.24 for the SO, 0.17 ~ 0.33 for the LEG, 0.12 ~ 0.40 for the SBB, and 0.13 ~ 0.34 for the SB. The flooded SO had the best stability characteristics with WFR ≈ 0 for 8 of 12 test cases compared to 6 of 12 for each of the evacuated configurations. A finite WFR provides further evidence that the tilt motion of the pad is likely to be impeded, resulting in a finite WFR that is more typical of a fixed arc bearing than a TPJB.

Virtual Mass: M_{yy} & M_{xx}

All measured direct virtual mass coefficients were negative with values ranging from -46 to -2 kg; the magnitudes were similar to those measured by Harris [6] except that he also measured positive direct virtual mass terms (+29 to -39 kg). When Harris tested, the

accelerometers were rotated 180° about the bearing centerline in Figure 10. It is possible that this difference in the test rig setup may have contributed to the difference in test results. A negative virtual mass term indicates that the real part of the impedance value increases with excitation frequency; a trend supported by modeling the stiffness and damping from the fluid film in series with the pad and pivot stiffness.

Comparison of Static and Dynamic Stiffness

The static stiffness was compared to the measured dynamic stiffness to check the magnitude and credibility of dynamic results. For all bearing configurations and test conditions, the order of magnitude was the same, and most cases correlated reasonably well. As speed increased the correlation between static and dynamic stiffness tended to decrease. On average the static stiffness was 1.06 to 1.29 times the dynamic stiffness for the LEG, 1.03 to 1.43 for the SBB, 0.94 to 1.31 for the SB, and 0.95 to 1.22 for the SO. The dynamic stiffness is the more reliable value since its determination relies on measurements of relative displacement at one load and speed, which is less affected by thermal expansion of the eddy current probes than static measurements. Static stiffness requires comparing the journal displacement at different loads; however, changing the load changes the thermal expansion of the eddy current probes. This leads to an undetermined (possibly significant) level of error. Also, the dynamic measurement is the local stiffness at a given eccentricity and the static measurement is not.

REFERENCES

[1] Lund, J.W., 1964, "Spring and Damping Coefficients for the Tilting-Pad Journal Bearing," ASLE Transactions, **7**(3), pp. 342-352.

[2] Nicholas, J.C., 2003, "Lund's Tilting Pad Journal Bearing Pad Assembly Method," ASME Journal of Vibration and Acoustics, **125**(4), pp. 448-454.

[3] Rodriguez, L.E., 2004, "Experimental Frequency-Dependent Rotordynamic Coefficients for a Load-On-Pad, High-Speed, Flexible-Pivot Tilting-Pad Bearing," M.S. Thesis, Texas A&M University, College Station, Texas.

[4] Dmochowski, W., 2006, "Dynamic Properties of Tilting-Pad Journal Bearings: Experimental and Theoretical Investigation of Frequency Effects Due to Pivot Flexibility," ASME Turbo Expo 2006, Paper GT2006-90280, May 8-11, Barcelona, Spain.

[5] Carter, C.R., 2007, "Measured and Predicted Rotordynamic Coefficients and Static Performance of a Rocker-Pivot, Tilt Pad Bearing in Load-On-Pad and Load-Between-Pad Configurations," M.S. Thesis, Texas A&M University, College Station, Texas.

[6] Harris, J.M., 2008, "Static Characteristics and Rotordynamic Coefficients of a Four-Pad Tilting-Pad Journal Bearing with Ball-In-Socket Pivots in Load-Between-Pad Configuration," M.S. Thesis, Texas A&M University, College Station, Texas.

[7] Kulhanek, C.D., 2010, "Dynamic and Static Characteristics of a Rocker-Pivot, Tilting-Pad Bearing with 50% and 60% Offsets," M.S. Thesis, Texas A&M University, College Station, Texas.

[8] Delgado, A., Ertas, B., Drexel M., Naldi, L., and Vannini, G., 2010, "Identification and Prediction of Force Coefficients in a Five-Pad and Four-Pad Tilting Pad Bearing for Load-On-Pad and Load-Between-Pad Configurations," Proceedings of ASME Turbo Expo 2010, Glasgow, UK, Paper GT2010-23802.

[9] Tschoepe, D.P., 2012, "Measurements Versus Predictions for the Static and Dynamic Characteristics of a Four-Pad, Rocker-Pivot, Tilting-Pad Journal Bearing," M.S. Thesis, Texas A&M University, College Station, Texas.

[10] Wygant, K.D., Flack, R.D., and Barrett, L.E., 1999, "Influence of Pad Pivot Friction on Tilting-Pad Journal Bearing Measurements – Part I: Steady Operating Position," STLE Tribology Transactions, **42**(1), pp. 210-215.

[11] Wygant, K.D., Flack, R.D., and Barrett, L.E., 1999, "Influence of Pad Pivot Friction on Tilting-Pad Journal Bearing Measurements – Part II: Dynamic Coefficients," STLE Tribology Transactions, **42**(1), pp. 250-256.

[12] Pettinato, B., and De Choudhury, P., 1999, "Test Results of Key and Spherical Pivot Five-Shoe Tilt Pad Journal Bearings – Part I: Performance Measurements," STLE Tribology Transactions, **42**(3), pp. 541-547.

[13] Pettinato, B., and De Choudhury, P., 1999, "Test Results of Key and Spherical Pivot Five-Shoe Tilt Pad Journal Bearings – Part II: Dynamic Measurements," STLE Tribology Transactions, **42**(3), pp. 675-680.

[14] San Andrés, L., 2010, Modern Lubrication Theory, "Static Load Performance of Plain Journal Bearings," Notes 4, Texas A&M University Digital Libraries, http://repository.tamu.edu/handle/1969.1/93197 [9/9/2013].

[15] Nicholas, J.C., 1994, "Tilting Pad Bearing Design," Proceedings of the 23rd Turbomachinery Symposium, Turbomachinery Laboratory, Texas A&M University, College Station, Texas, pp. 179-194.

[16] Nicholas, J.C., 1998, "Pad Bearing Assembly with Fluid Spray and Blocker Bar," US Patent No. 5,738,447, Rotating Machinery Technology, Inc., Wellsville, New York.

[17] Sasaki, T., Morii, S., Takenaga, H., and Tsutsumi, M., 1987, "New Technology on High Performance and Reliability of Mechanical Drive Steam Turbines," Proceedings of the 20th Turbomachinery Symposium, Turbomachinery Laboratory, Texas A&M University, College Station, Texas, pp. 145-154

[18] Tanaka, M., 1991, "Thermohydrodynamic Performance of a Tilting Pad Journal Bearing with Spot Lubrication," ASME Journal of Tribology, **113**, pp. 615-619.

[19] Nicholas, J.C., 2003, "Tilting Pad Journal Bearings with Spray-Bar Blockers and By-Pass Cooling for High Speed, High Load Applications," Proceedings of the 32nd Turbomachinery Symposium, Turbomachinery Laboratory, Texas A&M University, College Station, Texas, pp. 179-194.

[20] DeCamillo, S., Brockwell, K., 2001, "A Study of Parameters That Affect Pivoted Shoe Journal Bearing Performance in High Speed Machinery," Proceedings of the 30th Turbomachinery Symposium, Turbomachinery Laboratory, Texas A&M University, College Station, Texas, pp. 9-22.

[21] Nicholas, J.C., 2002, "Bearing Assembly with By-Pass Cooling," US Patent No. 6,485,182, Rotating Machinery Technology, Inc., Wellsville, New York.

[22] Dmochowski, W., Brockwell, K., DeCamillo, S., and Mikula, A., 1993, "A Study of the Thermal Characteristics of the Leading Edge Groove and Conventional Tilting Pad Journal Bearing," ASME Journal of Tribology, **115**, pp. 219-226.

[23] Brockwell, K., Dmochowski, W., and DeCamillo, S., 1994, "Analysis and Testing of the LEG Tilting Pad Journal Bearing – A New Design for Increasing Load Capacity, Reducing Operating Temperatures and Conserving Energy," Proceedings of the 23rd Turbomachinery Symposium, Turbomachinery Laboratory, Texas A&M University, College Station, Texas, pp. 43-56.

[24] Harangozo, A.V., Stolarski, T.A., and Gozdawa, R.J., 1991, "The Effect of Different Lubrication Methods on the Performance of a Tilting-Pad Journal Bearing," STLE Tribology Transactions, **34**(4), pp. 529-536.

[25] Dmochowski, W.M., and Blair, B., 2006, "Effect of Oil Evacuation on the Static and Dynamic Properties of Tilting Pad Journal Bearings," STLE Tribology Transactions, **49**, pp. 536-544.

[26] Rouvas C., Murphy, B.T., and Hale, R.K., 1992, "Bearing Parameter Identification Using Power Spectral Density Method," Proceedings of the 5th

International Conference on Vibrations in Rotating Machinery, Bath, England, pp. 297-303.

[27] San Andrés, L., and Tao, Y., 2013, "The Role of Pivot Stiffness on the Dynamic Force Coefficients of Tilting Pad Journal Bearings," ASME, J. Eng. Gas Turbines Power, **135**, 112505.

[28] Kaul, A., 1999, "Design and Development of a Test Setup for the Experimental Determination of the Rotordynamic and Leakage Characteristics of Annular Bushing Oil Seals," M.S. Thesis, Texas A&M University, College Station, Texas.

[29] Glienicke, J., 1966, 'Experimental Investigation of Stiffness and Damping Coefficients of Turbine Bearings and Their Application to Instability Predictions," Proceedings of the International Mech. E., **181**(3B), pp. 116-129.

[30] Beckwith, T.G., Marangoni, R.D., and Lienhard, J.H., 1995, "Mechanical Measurements: Fifth Edition," Addison-Wesley Publishing Company Inc., Reading, Massachusetts, pp. 857-859.

[31] Vance, J., Zeidan, F., and Murphy, B., 2010, "Machinery Vibration and Rotordynamics," John Wiley & Sons Inc., Hoboken, New Jersey, pp. 91, 278.

[32] San Andres, L., 2006, "Hydrodynamic Fluid Film Bearings and Their Effect on the Stability of Rotating Machinery," Design and Analysis of High Speed Pumps, pp. 10-1 – 10-36.

[33] Lund, J., 1965, "The Stability of an Elastic Rotor in Journal Bearings with Flexible Damped Supports," ASME Journal of Applied Mechanics, **87**, pp. 911-920.

[34] Kirk, R.G., and Reedy, S.W., 1988, "Evaluation of Pivot Stiffness for Typical Tilting-Pad Journal Bearing Designs," ASME Journal of Vibration, Acoustics, and Reliability in Design, **110**, pp. 165-171.

[35] Wygant, K.D., 2001, "The Influence of Negative Preload and Non-Synchronous Excitations on the Performance of Tilting Pad Journal Bearings," PhD Thesis, University of Virginia, Charlottesville, Virginia.

[36] American Petroleum Institute Standard 670, “Machinery Protection Systems,” Published by the American Petroleum Institute, Washington D.C., 4th Edition (2000).

[37] Smith, D.M., 1933, “The Motion of a Rotor Carried by a Flexible Shaft in Flexible Bearings,” Proceedings of the Royal Society of London, 92-119.

[38] Ertas, B., Vance, J., 2007, “The Influence of Same-Sign Cross-Coupled Stiffness on Rotordynamics,” Transactions of the ASME, **129,** pp. 24-31.

[39] Dmochowski, W., 2007, “Dynamic Properties of Tilting-Pad Journal Bearings: Experimental and Theoretical Investigation of Frequency Effects Due to Pivot Flexibility,” J. Eng. Gas Turbines Power, **12(**3), pp. 865-870.

[40] Childs, D.W., 2013, “Turbomachinery Rotordynamics with Case Studies,” Minter Spring Publishing, Wellborn, Texas, 247-248.

APPENDIX A

CLEARANCE MEASUREMENTS (COLD AND HOT)

Table A.1: Cold Clearance Measurement

Feed Type	Circular Clearance Estimate (µm)	X-Corner Point (µm)	Y-Corner Point (µm)	X-Pivot Point (µm)	Y-Pivot Point (µm)
Leading Edge Groove	96	136.36	2.36	67.85	-67.08
		-0.65	-136.53	-67.72	-68.95
		-134.80	-1.37	-67.56	66.79
		-0.32	134.95	68.02	68.65
Spray Bar Blocker (Scraper)	96	137.87	3.94	67.61	-66.72
		-2.64	-137.38	-69.23	-70.57
		-135.82	-3.77	-66.64	65.75
		2.53	135.27	70.20	69.61
Spray Bar	94	134.09	1.31	67.04	-66.07
		-0.02	-133.45	-66.39	-66.64
		-132.77	0.17	-67.05	66.08
		-1.33	131.99	66.38	66.65
Single Orifice	95	135.35	2.21	67.30	-66.46
		-0.75	-135.14	-66.82	-68.03
		-132.89	-0.92	-67.12	66.28
		-1.34	133.48	67.01	67.84

Table A.2: Hot Clearance Measurements for LEG and SBB

Feed Type	Prior Speed (rpm)	Prior Static Load (MPa)	Circular Clearance Estimate (µm)	X-Corner Point (µm)	Y-Corner Point (µm)	X-Pivot Point (µm)	Y-Pivot Point (µm)
Leading Edge Groove	7000	2.9	87	125.44	3.18	61.20	-60.85
				-3.05	-124.88	-63.05	-63.67
				-123.06	-2.45	-60.38	60.03
				2.31	122.51	63.87	62.84
	10000	2.9	86	122.24	2.22	60.09	-59.87
				-2.06	-121.95	-61.05	-61.75
				-120.05	-1.55	-59.60	59.38
				0.84	120.30	61.54	61.26
	13000	2.9	85	120.82	2.59	59.54	-59.11
				-1.75	-120.82	-60.37	-60.87
				-118.99	-0.92	-59.09	58.67
				0.81	118.26	60.81	60.42
	16000	2.9	85	122.18	2.72	60.04	-59.37
				-2.10	-121.46	-61.00	-61.66
				-119.90	-1.87	-59.47	58.81
				0.95	119.48	61.56	61.10
Spray Bar Blocker (Scraper)	7000	2.9	84	120.87	4.94	58.37	-58.00
				-4.14	-120.93	-61.17	-62.97
				-118.21	-5.00	-56.93	56.57
				4.35	118.14	62.61	61.54
	10000	2.9	82	118.03	4.61	57.04	-56.68
				-3.95	-117.97	-59.60	-61.16
				-115.26	-4.35	-55.75	55.40
				3.75	115.15	60.89	59.88
	13000	2.9	82	117.92	4.55	57.12	-56.49
				-3.69	-117.52	-59.47	-60.86
				-115.24	-4.19	-55.89	55.27
				3.46	114.72	60.69	59.63
	16000	2.9	82	117.21	3.69	57.15	-56.51
				-2.91	-116.71	-58.78	-60.06
				-114.66	-3.41	-56.23	55.59
				2.20	114.59	59.71	59.14

Table A.3: Hot Clearance Measurements for SB and SO

Feed Type	Prior Speed (rpm)	Prior Static Load (MPa)	Circular Clearance Estimate (µm)	X-Corner Point (µm)	Y-Corner Point (µm)	X-Pivot Point (µm)	Y-Pivot Point (µm)
Spray Bar	7000	2.9	84	119.71	0.75	59.41	-59.37
				-0.89	-119.50	-59.57	-59.74
				-118.25	0.02	-59.32	59.28
				-0.39	118.55	59.66	59.65
	10000	2.9	82	117.40	0.37	58.46	-58.27
				-0.48	-116.91	-58.26	-58.22
				-116.04	0.46	-58.50	58.31
				-0.97	116.16	58.22	58.26
	13000	2.9	81	115.57	0.33	57.69	-57.39
				-0.18	-115.11	-57.17	-57.33
				-114.15	0.44	-57.79	57.49
				-1.42	114.53	57.07	57.43
	16000	2.9	81	115.66	0.81	57.42	-57.45
				-0.81	-115.70	-57.51	-57.73
				-114.20	0.25	-57.36	57.39
				-0.52	114.53	57.57	57.67
Single Orifice	7000	2.9	83	118.62	0.84	59.30	-58.75
				-0.02	-118.33	-58.40	-58.75
				-116.78	0.84	-59.45	58.90
				-2.13	116.96	58.25	58.90
	10000	2.9	80	114.37	1.63	57.06	-56.49
				-0.25	-114.61	-56.57	-57.13
				-112.89	0.34	-57.04	56.46
				-1.18	112.59	56.60	57.11
	13000	2.9	78	110.98	0.99	55.70	-55.23
				0.42	-111.45	-54.92	-55.46
				-110.25	0.54	-55.79	55.32
				-1.34	110.11	54.82	55.55
	16000	2.9	77	108.91	1.25	54.51	-54.29
				0.11	-109.84	-54.04	-54.56
				-108.18	0.72	-54.54	54.33
				-0.90	107.94	54.00	54.59

APPENDIX B

ROTORDYNAMIC COEFFICIENTS AND DYNAMIC TEST CONDITIONS

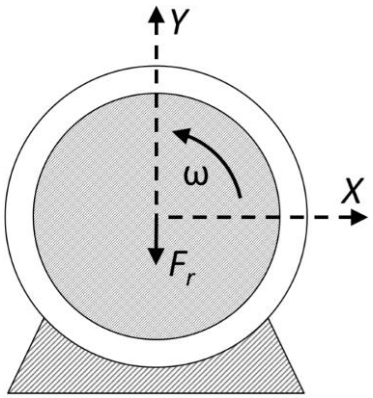

Figure B.1: Bearing Fixed Coordinate System for Coefficients in Appendix B

Table B.1: Measured and Predicted Rotordynamic Stiffness Coefficients for the SO

Feed Type	Speed (rpm)	Load (MPa)	Flow Rate (LPM)	Inlet (°C)	K_{xx} (MN/m)	K_{xy} (MN/m)	K_{yx} (MN/m)	K_{yy} (MN/m)
Single Orifice Between Pads	7069	0.69	38.3	48.9	124.5 ± 7.6	18.8 ± 8.2	-40.3 ± 14.2	125.4 ± 11.7
	10012	0.69	38.4	49.0	146.6 ± 8.7	21.7 ± 5.7	-51.0 ± 10.6	143.3 ± 11.1
	13000	0.69	38.1	49.3	160.6 ± 9.9	32.5 ± 5.4	-51.9 ± 7.6	157.3 ± 9.1
	16094	0.69	38.0	48.8	174.8 ± 8.7	37.8 ± 5.2	-54.6 ± 15.4	171.1 ± 9.6
	7053	2.06	38.4	48.7	220.3 ± 7.6	-10.3 ± 5.2	-53.6 ± 9.2	264.9 ± 19.3
	10109	2.07	38.4	48.6	233.4 ± 5.3	-14.8 ± 4.7	-60.4 ± 8.1	271.4 ± 17.2
	13110	2.07	38.3	48.6	239.1 ± 5.5	-8.4 ± 5.4	-58.2 ± 7.3	272.0 ± 16.6
	16061	2.07	38.2	48.4	246.2 ± 5.5	-1.0 ± 5.8	-62.1 ± 7.2	272.1 ± 16.8
	7176	2.87	38.2	48.6	260.7 ± 10.7	-22.5 ± 5.6	-59.1 ± 8.2	327.9 ± 23.0
	10064	2.87	38.4	48.4	269.1 ± 6.8	-29.0 ± 4.6	-62.9 ± 8.4	332.1 ± 20.9
	13075	2.87	38.2	48.8	274.7 ± 7.6	-25.4 ± 5.2	-62.6 ± 7.9	332.6 ± 21.1
	16084	2.86	38.2	49.0	279.8 ± 5.2	-16.7 ± 5.2	-66.8 ± 6.6	327.2 ± 20.4
Predicted	7069	0.69	11.5	48.9	146.07	-0.25	0.02	146.07
	10012	0.69	15.0	48.9	165.76	-0.07	0.14	165.76
	13000	0.69	18.7	48.9	182.20	0.03	0.17	182.20
	16094	0.69	22.8	48.9	196.34	0.09	0.19	196.34
	7053	2.06	12.7	48.9	249.16	-1.12	-0.87	249.16
	10109	2.07	15.8	48.9	251.07	0.42	0.66	251.07
	13110	2.07	19.0	48.9	254.36	1.44	1.66	254.34
	16061	2.07	22.7	48.9	257.90	2.06	2.25	257.87
	7176	2.87	13.3	48.9	290.11	-1.43	-1.20	290.11
	10064	2.87	16.1	48.9	287.88	0.77	1.03	287.88
	13075	2.87	19.1	48.9	288.16	2.65	2.94	288.15
	16084	2.86	23.1	49.0	289.82	4.10	4.38	289.80

Table B.2: Measured Rotordynamic Stiffness Coefficients for the LEG, SBB, & SB

Feed Type	Speed (rpm)	Load (MPa)	Flow Rate (LPM)	Inlet (°C)	K_{xx} (MN/m)	K_{xy} (MN/m)	K_{yx} (MN/m)	K_{yy} (MN/m)
Leading Edge Groove	6949	0.69	42.2	48.7	129.7 ± 4.9	13.7 ± 5.7	-58.8 ± 5.8	131.2 ± 5.6
	10036	0.69	42.1	49.3	150.0 ± 4.4	20.6 ± 4.4	-68.1 ± 4.7	153.4 ± 4.6
	13028	0.69	41.7	49.0	160.6 ± 6.2	36.6 ± 4.8	-78.3 ± 5.7	165.3 ± 4.7
	16056	0.69	42.0	48.6	187.6 ± 5.9	36.3 ± 8.0	-93.6 ± 3.9	193.8 ± 6.5
	7046	2.07	42.7	48.6	209.6 ± 3.3	-18.0 ± 4.4	-74.4 ± 2.6	246.5 ± 7.9
	10032	2.07	42.3	49.0	213.8 ± 4.2	-11.5 ± 4.3	-84.7 ± 2.1	243.9 ± 8.7
	13004	2.07	41.7	48.6	212.7 ± 3.5	4.8 ± 3.5	-90.8 ± 4.4	236.4 ± 8.0
	15991	2.07	42.1	48.5	219.6 ± 4.7	13.1 ± 4.4	-101.1 ± 3.9	239.4 ± 6.2
	6970	2.86	42.4	49.2	248.6 ± 3.7	-34.3 ± 3.1	-79.2 ± 3.6	310.6 ± 11.1
	10056	2.86	42.0	49.4	248.7 ± 4.2	-30.4 ± 4.3	-87.4 ± 3.5	294.3 ± 10.5
	13013	2.86	41.9	49.1	245.9 ± 3.2	-20.8 ± 3.8	-96.8 ± 4.4	284.0 ± 10.4
	15999	2.87	41.9	48.4	242.3 ± 2.9	-9.1 ± 3.1	-103.5 ± 3.8	269.1 ± 9.4
Spray Bar Blocker (Scraper)	6964	0.69	42.0	48.9	121.7 ± 3.6	19.6 ± 6.5	-58.3 ± 6.3	122.5 ± 4.3
	10027	0.69	42.3	48.8	144.6 ± 2.8	28.8 ± 5.2	-74.8 ± 5.2	144.5 ± 4.2
	12972	0.69	41.9	48.5	163.3 ± 3.3	40.5 ± 4.0	-83.0 ± 3.8	169.6 ± 5.8
	16053	0.69	42.1	49.0	189.3 ± 9.9	26.7 ± 6.9	-91.3 ± 10.8	193.8 ± 7.2
	6970	2.07	42.0	48.9	215.1 ± 2.4	-20.8 ± 5.5	-72.8 ± 6.2	247.1 ± 11.8
	10034	2.07	42.2	48.7	206.4 ± 1.9	-6.8 ± 4.3	-70.3 ± 6.5	228.1 ± 10.4
	13051	2.07	41.9	49.0	195.7 ± 3.0	1.5 ± 1.9	-70.3 ± 5.1	219.9 ± 9.9
	16042	2.07	41.9	49.2	184.8 ± 4.7	6.4 ± 2.0	-64.4 ± 7.4	207.1 ± 10.2
	6974	2.86	41.7	49.2	254.2 ± 5.2	-34.0 ± 3.3	-73.1 ± 5.7	310.4 ± 15.0
	10034	2.86	42.2	48.8	240.2 ± 2.1	-22.3 ± 3.1	-70.4 ± 5.1	289.3 ± 13.8
	13061	2.87	41.8	49.3	231.0 ± 4.3	-16.0 ± 2.6	-70.2 ± 5.6	273.8 ± 12.7
	16045	2.86	42.0	49.4	221.1 ± 4.7	-7.8 ± 2.4	-70.3 ± 5.3	259.4 ± 14.1
Spray Bar (No Scraper)	7044	0.69	42.2	49.3	123.5 ± 4.0	19.1 ± 6.3	-52.4 ± 6.1	126.3 ± 5.6
	10050	0.69	41.8	48.9	143.8 ± 4.1	28.1 ± 4.9	-64.1 ± 4.2	144.7 ± 4.9
	12989	0.69	42.1	49.3	161.4 ± 2.2	39.4 ± 5.0	-71.7 ± 3.4	160.0 ± 4.7
	15992	0.69	42.0	48.7	187.6 ± 3.3	43.1 ± 5.3	-78.9 ± 3.6	187.2 ± 4.0
	7003	2.07	42.2	48.9	213.7 ± 3.3	-18.5 ± 4.0	-71.2 ± 6.6	256.0 ± 8.7
	9998	2.07	41.9	48.5	217.3 ± 4.2	-13.9 ± 4.4	-77.8 ± 6.6	248.1 ± 7.3
	13024	2.07	42.1	49.2	220.9 ± 3.2	2.4 ± 4.3	-86.3 ± 4.5	243.4 ± 7.1
	16000	2.07	42.3	49.0	221.4 ± 3.4	23.9 ± 4.0	-82.1 ± 4.5	237.8 ± 6.9
	7009	2.86	42.3	49.2	250.0 ± 4.8	-32.3 ± 3.3	-74.7 ± 6.9	311.6 ± 12.4
	9983	2.87	41.9	48.7	248.4 ± 4.2	-32.3 ± 4.2	-79.5 ± 7.2	301.7 ± 10.8
	13008	2.86	42.0	49.2	236.0 ± 2.9	-12.6 ± 3.3	-69.7 ± 6.7	275.3 ± 11.6
	16045	2.86	41.9	49.1	233.1 ± 3.5	-1.1 ± 2.8	-72.9 ± 4.7	261.0 ± 10.3

Table B.3: Measured & Predicted Rotordynamic Damping Coefficients for the SO

Feed Type	Speed (rpm)	Load (MPa)	Flow Rate (LPM)	Inlet (°C)	C_{xx} (kN-s/m)	C_{xy} (kN-s/m)	C_{yx} (kN-s/m)	C_{yy} (kN-s/m)
Single Orifice Between Pads	7069	0.69	38.3	48.9	154.7 ± 9.3	-18.1 ± 7.8	1.9 ± 12.0	156.8 ± 8.5
	10012	0.69	38.4	49.0	139.9 ± 8.0	-19.9 ± 9.4	4.8 ± 7.6	138.5 ± 8.7
	13000	0.69	38.1	49.3	140.2 ± 7.6	-29.6 ± 7.2	7.7 ± 9.8	138.2 ± 9.2
	16094	0.69	38.0	48.8	146.8 ± 5.8	-36.3 ± 4.5	5.9 ± 11.9	140.2 ± 8.4
	7053	2.06	38.4	48.7	122.1 ± 4.5	-24.9 ± 2.6	-1.4 ± 8.9	141.7 ± 9.9
	10109	2.07	38.4	48.6	112.8 ± 3.2	-17.5 ± 3.2	-7.4 ± 8.5	119.9 ± 9.8
	13110	2.07	38.3	48.6	109.7 ± 3.4	-18.1 ± 4.9	-7.7 ± 9.3	111.7 ± 9.7
	16061	2.07	38.2	48.4	112.3 ± 3.5	-23.2 ± 5.1	-7.9 ± 8.6	111.4 ± 9.9
	7176	2.87	38.2	48.6	111.7 ± 7.3	-27.1 ± 3.5	-8.4 ± 12.0	131.2 ± 10.5
	10064	2.87	38.4	48.4	103.3 ± 3.9	-16.3 ± 2.6	-11.6 ± 8.7	109.8 ± 10.5
	13075	2.87	38.2	48.8	102.6 ± 3.5	-14.9 ± 3.2	-12.4 ± 9.1	101.0 ± 9.8
	16084	2.86	38.2	49.0	103.7 ± 6.0	-21.2 ± 4.5	-11.4 ± 10.6	104.7 ± 10.1
Predicted	7069	0.69	11.5	48.9	165.93	0.81	-0.51	165.93
	10012	0.69	15.0	48.9	127.45	0.57	-0.67	127.45
	13000	0.69	18.7	48.9	104.24	0.42	-0.68	104.25
	16094	0.69	22.8	48.9	88.72	0.32	-0.65	88.72
	7053	2.06	12.7	48.9	121.16	1.56	0.37	121.16
	10109	2.07	15.8	48.9	96.52	0.22	-1.12	96.53
	13110	2.07	19.0	48.9	80.93	-0.42	-1.81	80.95
	16061	2.07	22.7	48.9	70.47	-0.78	-2.12	70.53
	7176	2.87	13.3	48.9	93.73	1.82	0.70	93.73
	10064	2.87	16.1	48.9	78.47	-0.04	-1.40	78.48
	13075	2.87	19.1	48.9	67.28	-1.07	-2.65	67.32
	16084	2.86	23.1	49.0	59.01	-1.67	-3.34	59.13

Table B.4: Measured Rotordynamic Damping Coefficients for the LEG, SBB, & SB

Feed Type	Speed (rpm)	Load (MPa)	Flow Rate (LPM)	Inlet (°C)	C_{xx} (kN-s/m)	C_{xy} (kN-s/m)	C_{yx} (kN-s/m)	C_{yy} (kN-s/m)
Leading Edge Groove	6949	0.69	42.2	48.7	149.4 ± 5.0	-38.9 ± 7.2	6.6 ± 6.8	153.4 ± 3.5
	10036	0.69	42.1	49.3	136.5 ± 6.3	-40.6 ± 4.7	16.1 ± 4.9	130.7 ± 2.9
	13028	0.69	41.7	49.0	124.0 ± 5.4	-46.3 ± 4.0	24.3 ± 3.6	117.8 ± 4.2
	16056	0.69	42.0	48.6	117.0 ± 8.8	-47.6 ± 3.1	27.0 ± 7.6	107.1 ± 3.7
	7046	2.07	42.7	48.6	125.8 ± 2.7	-41.9 ± 5.1	-0.6 ± 3.9	149.0 ± 7.2
	10032	2.07	42.3	49.0	116.1 ± 2.9	-42.6 ± 6.1	5.9 ± 3.2	127.3 ± 5.1
	13004	2.07	41.7	48.6	107.5 ± 2.9	-49.3 ± 5.0	11.4 ± 4.9	115.3 ± 4.8
	15991	2.07	42.1	48.5	101.3 ± 3.5	-51.9 ± 3.4	16.3 ± 4.2	102.8 ± 5.1
	6970	2.86	42.4	49.2	112.1 ± 2.7	-41.6 ± 3.3	-6.0 ± 3.4	137.6 ± 5.8
	10056	2.86	42.0	49.4	101.3 ± 2.3	-41.6 ± 4.9	-4.1 ± 3.7	117.8 ± 5.1
	13013	2.86	41.9	49.1	94.9 ± 2.3	-47.2 ± 4.4	1.3 ± 5.0	111.7 ± 5.4
	15999	2.87	41.9	48.4	86.5 ± 2.6	-50.7 ± 2.8	7.1 ± 5.6	104.6 ± 5.3
Spray Bar Blocker (Scraper)	6964	0.69	42.0	48.9	147.6 ± 2.4	-37.5 ± 9.5	6.9 ± 7.1	158.2 ± 5.1
	10027	0.69	42.3	48.8	126.6 ± 1.3	-43.9 ± 8.7	14.8 ± 4.1	129.2 ± 4.6
	12972	0.69	41.9	48.5	111.9 ± 2.5	-48.5 ± 5.8	22.2 ± 3.4	107.5 ± 5.6
	16053	0.69	42.1	49.0	80.1 ± 7.4	-42.5 ± 6.8	24.9 ± 8.8	80.8 ± 8.3
	6970	2.07	42.0	48.9	113.5 ± 2.3	-41.8 ± 5.1	-9.9 ± 5.0	144.7 ± 4.7
	10034	2.07	42.2	48.7	94.1 ± 2.6	-39.7 ± 7.2	-3.0 ± 3.6	117.9 ± 4.3
	13051	2.07	41.9	49.0	75.0 ± 4.1	-35.7 ± 3.7	4.5 ± 3.7	98.3 ± 4.3
	16042	2.07	41.9	49.2	62.6 ± 4.2	-27.8 ± 2.5	12.7 ± 5.5	80.3 ± 4.4
	6974	2.86	41.7	49.2	100.6 ± 4.2	-42.3 ± 2.8	-15.9 ± 5.5	133.6 ± 5.1
	10034	2.86	42.2	48.8	82.4 ± 1.4	-35.6 ± 4.5	-8.3 ± 3.4	110.8 ± 4.1
	13061	2.87	41.8	49.3	64.6 ± 2.4	-32.0 ± 3.2	-4.7 ± 4.0	94.7 ± 3.9
	16045	2.86	42.0	49.4	57.2 ± 2.7	-29.3 ± 2.9	2.4 ± 7.5	85.1 ± 4.1
Spray Bar (No Scraper)	7044	0.69	42.2	49.3	148.5 ± 4.1	-30.1 ± 8.3	8.7 ± 5.7	155.3 ± 4.1
	10050	0.69	41.8	48.9	130.1 ± 3.1	-32.9 ± 7.8	15.7 ± 4.0	131.1 ± 3.6
	12989	0.69	42.1	49.3	120.0 ± 5.5	-37.7 ± 5.9	25.1 ± 4.8	116.0 ± 4.1
	15992	0.69	42.0	48.7	103.6 ± 6.4	-38.4 ± 3.1	22.6 ± 5.9	103.3 ± 5.3
	7003	2.07	42.2	48.9	119.7 ± 3.3	-35.3 ± 2.6	-1.4 ± 5.1	143.0 ± 5.9
	9998	2.07	41.9	48.5	107.3 ± 2.1	-31.1 ± 5.6	1.7 ± 4.9	118.8 ± 5.3
	13024	2.07	42.1	49.2	102.1 ± 1.9	-39.6 ± 5.9	8.9 ± 3.0	108.5 ± 5.3
	16000	2.07	42.3	49.0	88.8 ± 3.7	-44.3 ± 3.6	15.7 ± 4.6	97.7 ± 5.8
	7009	2.86	42.3	49.2	107.1 ± 4.0	-36.7 ± 1.6	-7.4 ± 5.7	131.3 ± 6.6
	9983	2.87	41.9	48.7	95.8 ± 2.6	-30.3 ± 3.7	-6.3 ± 5.0	109.2 ± 6.2
	13008	2.86	42.0	49.2	82.2 ± 2.4	-35.3 ± 4.0	-3.1 ± 4.9	98.7 ± 5.9
	16045	2.86	41.9	49.1	68.0 ± 3.8	-33.4 ± 2.7	7.4 ± 5.0	90.7 ± 5.9

Table B.5: Measured & Predicted Virtual Mass Coefficients for the SO

Feed Type	Speed (rpm)	Load (MPa)	Flow Rate (LPM)	Inlet (°C)	M_{xx} (kg)	M_{xy} (kg)	M_{yx} (kg)	M_{yy} (kg)
Single Orifice Between Pads	7069	0.69	38.3	48.9	-12.3 ± 7.2	-8.7 ± 7.8	-14.2 ± 13.4	-28.5 ± 11.1
	10012	0.69	38.4	49.0	-7.9 ± 7.9	-1.0 ± 5.1	-14.3 ± 9.6	-22.8 ± 10.1
	13000	0.69	38.1	49.3	-17.9 ± 9.0	0.8 ± 4.8	-16.0 ± 6.9	-29.3 ± 8.2
	16094	0.69	38.0	48.8	-27.1 ± 7.8	-3.3 ± 4.7	-8.5 ± 14.0	-30.5 ± 8.7
	7053	2.06	38.4	48.7	-13.0 ± 7.2	-13.4 ± 5.0	-14.2 ± 8.7	-35.5 ± 18.3
	10109	2.07	38.4	48.6	-11.3 ± 4.8	-12.3 ± 4.2	-7.0 ± 7.3	-23.1 ± 15.6
	13110	2.07	38.3	48.6	-11.6 ± 5.0	-8.4 ± 4.9	-5.5 ± 6.6	-25.0 ± 15.0
	16061	2.07	38.2	48.4	-13.0 ± 5.0	-5.3 ± 5.2	-5.7 ± 6.5	-26.1 ± 15.2
	7176	2.87	38.2	48.6	-12.1 ± 10.2	-12.9 ± 5.3	-10.3 ± 7.8	-38.1 ± 21.8
	10064	2.87	38.4	48.4	-11.4 ± 6.2	-16.8 ± 4.2	-5.7 ± 7.6	-23.4 ± 19.0
	13075	2.87	38.2	48.8	-11.0 ± 6.9	-13.2 ± 4.7	-4.9 ± 7.2	-24.4 ± 19.1
	16084	2.86	38.2	49.0	-11.2 ± 4.7	-7.6 ± 4.7	-5.7 ± 6.0	-27.1 ± 18.5
Predicted	7069	0.69	11.5	48.9	-9.77	0.72	-0.91	-9.77
	10012	0.69	15.0	48.9	7.96	1.32	-1.26	7.96
	13000	0.69	18.7	48.9	11.31	1.66	-1.55	11.31
	16094	0.69	22.8	48.9	10.78	1.87	-1.72	10.78
	7053	2.06	12.7	48.9	-21.82	0.18	-1.24	-21.82
	10109	2.07	15.8	48.9	-2.31	1.33	-0.99	-2.31
	13110	2.07	19.0	48.9	4.44	1.85	-1.21	4.42
	16061	2.07	22.7	48.9	6.81	2.24	-1.41	6.80
	7176	2.87	13.3	48.9	-15.62	0.02	-1.42	-15.62
	10064	2.87	16.1	48.9	-2.55	1.38	-0.82	-2.55
	13075	2.87	19.1	48.9	3.10	1.94	-0.98	3.08
	16084	2.86	23.1	49.0	5.67	2.35	-1.25	5.64

Table B.6: Measured Virtual Mass Coefficients for the LEG, SBB, and SB

Feed Type	Speed (rpm)	Load (MPa)	Flow Rate (LPM)	Inlet (°C)	M_{xx} (kg)	M_{xy} (kg)	M_{yx} (kg)	M_{yy} (kg)
Leading Edge Groove	6949	0.69	42.2	48.7	-21.3 ± 4.7	-0.7 ± 5.4	-20.2 ± 5.5	-33.1 ± 5.4
	10036	0.69	42.1	49.3	-20.5 ± 4.0	-3.2 ± 4.0	-24.4 ± 4.3	-24.2 ± 4.2
	13028	0.69	41.7	49.0	-23.2 ± 5.7	-6.8 ± 4.4	-32.8 ± 5.2	-18.3 ± 4.2
	16056	0.69	42.0	48.6	-19.9 ± 5.3	-9.5 ± 7.3	-27.6 ± 3.5	-13.8 ± 5.9
	7046	2.07	42.7	48.6	-27.0 ± 3.1	-2.6 ± 4.2	-20.5 ± 2.5	-46.1 ± 7.5
	10032	2.07	42.3	49.0	-19.8 ± 3.8	-0.2 ± 3.9	-21.1 ± 1.9	-31.6 ± 7.9
	13004	2.07	41.7	48.6	-17.2 ± 3.2	1.9 ± 3.2	-24.2 ± 4.0	-24.4 ± 7.2
	15991	2.07	42.1	48.5	-13.3 ± 4.2	0.0 ± 4.0	-21.6 ± 3.6	-14.6 ± 5.6
	6970	2.86	42.4	49.2	-23.9 ± 3.5	-4.1 ± 3.0	-19.4 ± 3.4	-44.0 ± 10.6
	10056	2.86	42.0	49.4	-17.9 ± 3.8	-1.7 ± 3.9	-17.7 ± 3.2	-31.4 ± 9.5
	13013	2.86	41.9	49.1	-14.1 ± 2.9	2.2 ± 3.5	-18.4 ± 3.9	-27.4 ± 9.4
	15999	2.87	41.9	48.4	-8.1 ± 2.6	0.7 ± 2.8	-18.7 ± 3.4	-20.3 ± 8.5
Spray Bar Blocker (Scraper)	6964	0.69	42.0	48.9	-27.5 ± 3.4	2.0 ± 6.2	-28.0 ± 6.0	-35.3 ± 4.1
	10027	0.69	42.3	48.8	-20.6 ± 2.5	6.9 ± 4.7	-29.1 ± 4.7	-21.8 ± 3.8
	12972	0.69	41.9	48.5	-19.2 ± 3.0	4.8 ± 3.7	-29.9 ± 3.5	-17.9 ± 5.2
	16053	0.69	42.1	49.0	-7.6 ± 9.0	3.6 ± 6.3	-33.3 ± 9.8	-15.8 ± 6.5
	6970	2.07	42.0	48.9	-23.3 ± 2.3	-2.6 ± 5.2	-23.1 ± 5.9	-44.3 ± 11.2
	10034	2.07	42.2	48.7	-12.6 ± 1.7	5.2 ± 3.9	-21.3 ± 5.8	-30.5 ± 9.4
	13051	2.07	41.9	49.0	-5.8 ± 2.7	3.1 ± 1.7	-22.7 ± 4.6	-21.5 ± 8.9
	16042	2.07	41.9	49.2	-4.7 ± 4.3	-1.0 ± 1.8	-18.4 ± 6.7	-15.4 ± 9.3
	6974	2.86	41.7	49.2	-21.4 ± 4.9	-4.3 ± 3.1	-16.7 ± 5.4	-45.0 ± 14.2
	10034	2.86	42.2	48.8	-14.3 ± 1.9	0.8 ± 2.8	-16.1 ± 4.6	-32.8 ± 12.5
	13061	2.87	41.8	49.3	-10.4 ± 3.9	-0.1 ± 2.4	-16.9 ± 5.1	-27.3 ± 11.5
	16045	2.86	42.0	49.4	-9.0 ± 4.3	-0.6 ± 2.2	-17.9 ± 4.8	-22.0 ± 12.8
Spray Bar (No Scraper)	7044	0.69	42.2	49.3	-22.8 ± 3.8	-3.9 ± 6.0	-20.4 ± 5.8	-30.9 ± 5.3
	10050	0.69	41.8	48.9	-15.6 ± 3.7	0.1 ± 4.5	-24.8 ± 3.8	-23.1 ± 4.5
	12989	0.69	42.1	49.3	-13.3 ± 2.0	-2.2 ± 4.5	-27.6 ± 3.0	-21.3 ± 4.2
	15992	0.69	42.0	48.7	-7.3 ± 3.0	-7.7 ± 4.8	-19.6 ± 3.2	-17.8 ± 3.6
	7003	2.07	42.2	48.9	-22.8 ± 3.2	-7.9 ± 3.8	-20.4 ± 6.3	-38.5 ± 8.2
	9998	2.07	41.9	48.5	-15.3 ± 3.8	-4.1 ± 3.9	-19.8 ± 5.9	-26.0 ± 6.6
	13024	2.07	42.1	49.2	-13.2 ± 2.9	3.1 ± 3.9	-23.8 ± 4.1	-23.3 ± 6.5
	16000	2.07	42.3	49.0	-6.9 ± 3.1	3.5 ± 3.6	-19.9 ± 4.1	-20.2 ± 6.3
	7009	2.86	42.3	49.2	-22.4 ± 4.5	-7.8 ± 3.1	-16.6 ± 6.5	-42.3 ± 11.8
	9983	2.87	41.9	48.7	-14.4 ± 3.8	-7.4 ± 3.8	-14.3 ± 6.5	-26.9 ± 9.7
	13008	2.86	42.0	49.2	-9.4 ± 2.6	0.1 ± 3.0	-14.8 ± 6.1	-25.8 ± 10.5
	16045	2.86	41.9	49.1	-1.8 ± 3.2	0.6 ± 2.5	-14.8 ± 4.2	-24.7 ± 9.3

APPENDIX C

MEASURED AND PREDICTED STATIC TEST CONDITIONS

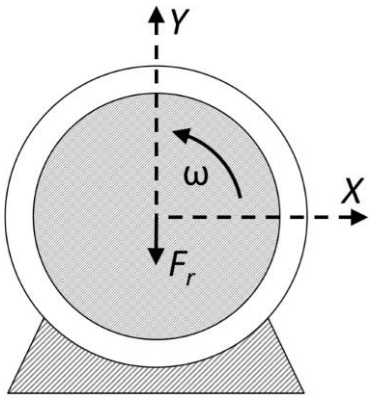

Figure C.1: Bearing Fixed Coordinate System for Data in Appendix C

Table C.1: XL_TPJB Predicted Eccentricities and Maximum Temperature Rise

Feed Type	Input Speed (rpm)	Input Load (MPa)	Output Flow Rate (LPM)	Input Inlet Temperature (°C)	Output Max Temperature Rise (°C)	Output e_x (μm)	Output e_y (μm)
Static Predictions	7069	0.69	11.5	48.9	22.76	0.25	-36.52
	10012	0.69	15.0	49.0	26.45	-0.11	-31.85
	13000	0.69	18.7	49.3	29.77	-0.41	-28.92
	16094	0.69	22.8	48.8	32.61	-0.65	-26.86
	7053	2.06	12.7	48.7	35.74	0.68	-83.94
	10109	2.07	15.8	48.6	39.44	-0.46	-78.47
	13110	2.07	19.0	48.6	43.44	-1.51	-74.51
	16061	2.07	22.7	48.4	46.53	-2.37	-71.32
	7176	2.87	13.3	48.6	42.62	0.81	-103.80
	10064	2.87	16.1	48.4	46.12	-0.63	-98.64
	13075	2.87	19.1	48.8	50.98	-2.20	-94.87
	16084	2.86	23.1	49.0	55.12	-3.67	-92.07

Table C.2: XL_TPJB Temperature Predictions

Feed Type	Input Speed (rpm)	Input Load (MPa)	Input Inlet Temperature (°C)	1st Loaded Pad: Leading Edge (°C)	1st Loaded Pad: 75% Pad Arc (°C)	1st Loaded Pad: Trailing Edge (°C)	2nd Loaded Pad: Leading Edge (°C)	2nd Loaded Pad: 75% Pad Arc (°C)	2nd Loaded Pad: Trailing Edge (°C)
Temperature Predictions	7069	0.69	48.9	11.77	19.3	22.4	12.17	19.67	22.76
	10012	0.69	49.0	14.72	23.1	26.5	14.54	22.93	26.29
	13000	0.69	49.3	17.08	26.2	29.8	16.43	25.63	29.21
	16094	0.69	48.8	19.03	28.8	32.6	18.02	27.95	31.74
	7053	2.06	48.7	15.21	29.1	34.4	16.58	30.44	35.74
	10109	2.07	48.6	19.75	34.1	39.4	18.75	33.13	38.52
	13110	2.07	48.6	23.40	38.0	43.4	20.32	35.16	40.64
	16061	2.07	48.4	26.19	41.0	46.5	21.46	36.73	42.29
	7176	2.87	48.6	16.67	34.5	40.9	18.51	36.28	42.62
	10064	2.87	48.4	21.83	39.7	46.1	20.27	38.22	44.64
	13075	2.87	48.8	26.57	44.5	51.0	21.52	39.77	46.24
	16084	2.86	49.0	30.56	48.7	55.1	22.35	40.98	47.50

Table C.3: Measured Operating Conditions for Static and Thermal Testing

Feed Type	Speed (rpm)	Load (MPa)	Flow Rate (LPM)	Inlet (°C)	Pressure Drop (bar)	Rotor X (µm)	Rotor Y (µm)
Leading Edge Groove	7086 ± 2	0.69 ± 4.4E-5	42.24 ± 0.04	48.93 ± 0.01	8.83 ± 1.2E-2	-35.83 ± 0.03	16.18 ± 0.02
	6985 ± 1	2.07 ± 2.8E-5	42.2 ± 0.03	48.96 ± 0.00	9.05 ± 7.6E-3	-32.49 ± 0.03	-30.11 ± 0.02
	7056 ± 2	2.87 ± 1.0E-4	42.54 ± 0.00	49.22 ± 0.11	9.29 ± 3.2E-3	-30.97 ± 0.02	-43.87 ± 0.02
	10018 ± 2	0.69 ± 3.2E-5	42.01 ± 0.07	49.12 ± 0.02	9.68 ± 2.0E-2	-44.35 ± 0.05	19.94 ± 0.06
	10061 ± 3	2.07 ± 3.9E-5	41.9 ± 0.01	49.23 ± 0.02	9.51 ± 6.7E-3	-38.1 ± 0.05	-18.02 ± 0.06
	10003 ± 1	2.87 ± 3.3E-5	41.79 ± 0.01	49.17 ± 0.01	9.6 ± 5.2E-3	-34.92 ± 0.05	-33.06 ± 0.04
	13016 ± 2	0.69 ± 2.6E-5	41.75 ± 0.01	49.3 ± 0.02	10.57 ± 1.2E-2	-53.21 ± 0.07	20.59 ± 0.05
	12992 ± 2	2.07 ± 4.1E-5	42.05 ± 0.00	48.94 ± 0.02	10.46 ± 6.2E-3	-42.05 ± 0.04	-8.99 ± 0.05
	12989 ± 7	2.86 ± 3.3E-4	41.82 ± 0.01	49.16 ± 0.01	10.38 ± 6.4E-3	-37.34 ± 0.05	-22.74 ± 0.06
	16077 ± 5	0.69 ± 4.2E-5	42.13 ± 0.05	48.9 ± 0.02	10.51 ± 1.6E-2	-53.39 ± 0.03	28.88 ± 0.04
	16005 ± 3	2.07 ± 4.9E-5	41.94 ± 0.01	49.41 ± 0.02	10.45 ± 8.7E-3	-42.71 ± 0.04	-0.14 ± 0.06
	16056 ± 3	2.86 ± 3.3E-4	41.94 ± 0.06	48.39 ± 0.01	10.63 ± 1.7E-2	-38.81 ± 0.03	-14.18 ± 0.05
Spray Bar Blocker (Scraper)	7025 ± 2	0.69 ± 4.7E-5	42.16 ± 0.00	48.68 ± 0.01	1.79 ± 2.1E-3	-39.16 ± 0.02	1.72 ± 0.02
	6992 ± 1	2.07 ± 3.1E-5	42.2 ± 0.03	48.92 ± 0.02	1.77 ± 2.2E-3	-33.77 ± 0.04	-39.14 ± 0.02
	6973 ± 3	2.87 ± 2.1E-4	42.28 ± 0.01	48.91 ± 0.01	1.79 ± 1.9E-3	-31.81 ± 0.02	-51.25 ± 0.05
	10004 ± 1	0.69 ± 1.2E-4	41.9 ± 0.00	48.74 ± 0.01	1.81 ± 2.0E-3	-43.9 ± 0.04	9.35 ± 0.02
	10019 ± 1	2.07 ± 4.5E-5	41.86 ± 0.00	48.73 ± 0.01	1.83 ± 2.1E-3	-37.43 ± 0.02	-26.23 ± 0.02
	10042 ± 3	2.87 ± 6.1E-5	41.86 ± 0.00	49.14 ± 0.00	1.84 ± 1.9E-3	-35.08 ± 0.04	-40.8 ± 0.02
	13031 ± 1	0.69 ± 4.2E-5	42.09 ± 0.00	48.68 ± 0.02	1.83 ± 2.1E-3	-48.73 ± 0.04	18.18 ± 0.03
	13050 ± 1	2.07 ± 3.0E-5	42.05 ± 0.01	48.72 ± 0.01	1.85 ± 2.1E-3	-41.66 ± 0.03	-14.01 ± 0.02
	13057 ± 1	2.86 ± 4.6E-5	42.05 ± 0.00	49.05 ± 0.03	1.85 ± 2.0E-3	-38.49 ± 0.02	-29.32 ± 0.02
	16054 ± 2	0.69 ± 2.7E-5	41.9 ± 0.00	48.54 ± 0.01	1.94 ± 2.0E-3	-53.77 ± 0.03	25.85 ± 0.04
	16003 ± 1	2.07 ± 3.5E-5	42.16 ± 0.00	49.16 ± 0.00	1.95 ± 2.0E-3	-44.47 ± 0.03	-6.78 ± 0.03
	16045 ± 2	2.87 ± 2.6E-5	42.39 ± 0.01	49.24 ± 0.01	1.95 ± 1.9E-3	-39.78 ± 0.02	-23.11 ± 0.02
Spray Bar (No Scraper)	7016 ± 1	0.7 ± 2.4E-5	42.2 ± 0.00	49.11 ± 0.01	1.69 ± 2.2E-3	-36.41 ± 0.02	-6.34 ± 0.02
	6924 ± 1	2.07 ± 3.9E-5	41.98 ± 0.00	49.36 ± 0.02	1.73 ± 2.0E-3	-32.5 ± 0.02	-44.61 ± 0.03
	7007 ± 2	2.87 ± 2.8E-5	41.98 ± 0.00	48.99 ± 0.01	1.77 ± 2.1E-3	-28.98 ± 0.03	-59.14 ± 0.02
	10000 ± 1	0.69 ± 2.4E-5	42.24 ± 0.01	48.46 ± 0.01	1.7 ± 2.1E-3	-39.56 ± 0.02	1.94 ± 0.01
	10006 ± 3	2.07 ± 4.5E-5	42.16 ± 0.02	48.63 ± 0.02	1.76 ± 2.3E-3	-31.98 ± 0.04	-33.36 ± 0.05
	10056 ± 2	2.87 ± 4.6E-5	42.16 ± 0.01	49.11 ± 0.01	1.79 ± 2.4E-3	-30.17 ± 0.02	-46.35 ± 0.02
	12965 ± 3	0.69 ± 3.4E-5	41.98 ± 0.00	49.33 ± 0.02	1.75 ± 1.8E-3	-46.29 ± 0.05	11.67 ± 0.03
	13032 ± 1	2.07 ± 5.3E-5	42.01 ± 0.00	48.91 ± 0.01	1.81 ± 2.1E-3	-36.24 ± 0.03	-22.74 ± 0.03
	13040 ± 1	2.87 ± 4.7E-5	41.79 ± 0.00	49.33 ± 0.01	1.84 ± 1.9E-3	-34.59 ± 0.02	-35.8 ± 0.03
	16030 ± 3	0.69 ± 2.5E-5	42.32 ± 0.01	49.09 ± 0.01	1.78 ± 2.0E-3	-48.84 ± 0.03	17.32 ± 0.03
	15985 ± 3	2.07 ± 2.4E-5	42.28 ± 0.03	48.98 ± 0.01	1.85 ± 2.6E-3	-37.15 ± 0.03	-12.34 ± 0.04
	15996 ± 2	2.87 ± 2.2E-4	41.94 ± 0.00	49.02 ± 0.02	1.89 ± 1.9E-3	-35.28 ± 0.03	-25.37 ± 0.02
Single Orifice Between Pads	7051 ± 2	0.69 ± 6.5E-5	38.3 ± 0.06	48.93 ± 0.01	2.2 ± 4.9E-3	-70.41 ± 0.02	17.67 ± 0.02
	7011 ± 3	2.07 ± 2.3E-5	38.3 ± 0.01	48.72 ± 0.01	2.2 ± 9.5E-4	-62.05 ± 0.01	-20.79 ± 0.01
	7033 ± 1	2.87 ± 2.8E-5	38.38 ± 0.01	48.56 ± 0.01	2.22 ± 1.1E-3	-59.39 ± 0.04	-34.03 ± 0.06
	10045 ± 2	0.69 ± 4.1E-5	38.42 ± 0.01	49.04 ± 0.00	2.22 ± 7.6E-4	-72.08 ± 0.02	28.05 ± 0.01
	10015 ± 1	2.07 ± 2.6E-5	38.42 ± 0.05	48.61 ± 0.00	2.24 ± 4.0E-3	-63.84 ± 0.02	-6.92 ± 0.01
	10032 ± 2	2.87 ± 3.0E-5	38.46 ± 0.00	48.42 ± 0.01	2.26 ± 1.1E-3	-60.62 ± 0.02	-17.98 ± 0.04
	13031 ± 1	0.7 ± 7.1E-5	38.15 ± 0.01	49.26 ± 0.02	2.29 ± 1.1E-3	-76.52 ± 0.04	33.62 ± 0.02
	13059 ± 2	2.07 ± 2.6E-5	38.19 ± 0.01	48.64 ± 0.01	2.31 ± 9.2E-4	-68.17 ± 0.06	3.32 ± 0.04
	13044 ± 9	2.87 ± 3.9E-4	38.11 ± 0.06	48.84 ± 0.01	2.33 ± 5.1E-3	-66.11 ± 0.04	-9.35 ± 0.04
	16052 ± 2	0.69 ± 3.1E-5	38.08 ± 0.01	48.78 ± 0.01	2.42 ± 1.1E-3	-91.61 ± 0.05	42.77 ± 0.03
	16088 ± 2	2.07 ± 3.0E-5	38.15 ± 0.01	48.42 ± 0.01	2.47 ± 1.1E-3	-78.4 ± 0.05	11.74 ± 0.03
	15973 ± 2	2.87 ± 8.2E-5	38.19 ± 0.00	49.02 ± 0.01	2.49 ± 5.6E-4	-75.81 ± 0.08	-0.37 ± 0.03

Table C.4: Measured Maximum Pad, Ambient, Stator, and Outlet Temperatures

Feed Type	Speed (rpm)	Load (MPa)	Max Pad (°C)	Ambient (°C)	Stator (°C)	DE Outlet (°C)	NDE Outlet (°C)
Leading Edge Groove	7086 ± 2	0.69 ± 4.4E-5	70.28 ± 0.03	20.59 ± 0.01	51.26 ± 0.05	51.52 ± 0.01	53.98 ± 0.01
	6985 ± 1	2.07 ± 2.8E-5	85.50 ± 0.04	20.99 ± 0.03	51.92 ± 0.42	52.06 ± 0.02	54.14 ± 0.01
	7056 ± 2	2.87 ± 1.0E-4	91.64 ± 0.02	20.16 ± 0.02	52.53 ± 0.06	52.44 ± 0.02	54.38 ± 0.02
	10018 ± 2	0.69 ± 3.2E-5	75.72 ± 0.03	20.70 ± 0.02	53.56 ± 0.05	55.49 ± 0.01	57.23 ± 0.01
	10061 ± 3	2.07 ± 3.9E-5	90.95 ± 0.04	20.98 ± 0.01	54.01 ± 0.11	55.31 ± 0.01	58.03 ± 0.01
	10003 ± 1	2.87 ± 3.3E-5	98.39 ± 0.02	21.83 ± 0.02	54.70 ± 0.07	55.21 ± 0.01	58.06 ± 0.02
	13016 ± 2	0.69 ± 2.6E-5	81.16 ± 0.03	17.08 ± 0.02	55.91 ± 0.07	59.51 ± 0.02	62.02 ± 0.02
	12992 ± 2	2.07 ± 4.1E-5	94.98 ± 0.02	14.75 ± 0.02	55.98 ± 0.05	58.68 ± 0.02	61.72 ± 0.01
	12989 ± 7	2.86 ± 3.3E-4	104.96 ± 0.04	14.63 ± 0.02	56.64 ± 0.10	59.04 ± 0.03	62.27 ± 0.03
	16077 ± 5	0.69 ± 4.2E-5	87.56 ± 0.05	26.93 ± 0.01	60.59 ± 0.10	63.40 ± 0.02	67.04 ± 0.02
	16005 ± 3	2.07 ± 4.9E-5	99.01 ± 0.03	27.18 ± 0.01	60.56 ± 0.08	63.65 ± 0.01	67.67 ± 0.01
	16056 ± 3	2.86 ± 3.3E-4	105.47 ± 0.03	27.21 ± 0.02	59.88 ± 0.26	62.74 ± 0.01	66.84 ± 0.02
Spray Bar Blocker (Scraper)	7025 ± 2	0.69 ± 4.7E-5	72.79 ± 0.03	24.79 ± 0.01	50.58 ± 0.07	51.67 ± 0.02	53.90 ± 0.04
	6992 ± 1	2.07 ± 3.1E-5	88.13 ± 0.02	26.46 ± 0.01	50.81 ± 0.12	52.18 ± 0.01	52.13 ± 0.01
	6973 ± 3	2.87 ± 2.1E-4	93.75 ± 0.02	26.77 ± 0.01	51.69 ± 0.09	52.30 ± 0.01	52.55 ± 0.01
	10004 ± 1	0.69 ± 1.2E-4	80.83 ± 0.05	26.26 ± 0.02	52.35 ± 0.07	53.63 ± 0.01	54.18 ± 0.01
	10019 ± 1	2.07 ± 4.5E-5	94.90 ± 0.04	26.10 ± 0.02	53.43 ± 0.09	53.67 ± 0.02	55.09 ± 0.01
	10042 ± 3	2.87 ± 6.1E-5	101.74 ± 0.06	26.63 ± 0.01	54.17 ± 0.08	54.18 ± 0.02	55.65 ± 0.02
	13031 ± 1	0.69 ± 4.2E-5	87.26 ± 0.03	24.78 ± 0.02	54.19 ± 0.13	56.64 ± 0.01	56.60 ± 0.02
	13050 ± 1	2.07 ± 3.0E-5	98.20 ± 0.03	25.49 ± 0.02	55.24 ± 0.07	56.20 ± 0.01	56.90 ± 0.01
	13057 ± 1	2.86 ± 4.6E-5	106.56 ± 0.03	25.38 ± 0.02	55.93 ± 0.05	56.85 ± 0.01	57.53 ± 0.02
	16054 ± 2	0.69 ± 2.7E-5	90.52 ± 0.03	24.04 ± 0.01	56.29 ± 0.06	59.18 ± 0.01	59.42 ± 0.01
	16003 ± 1	2.07 ± 3.5E-5	102.46 ± 0.04	23.20 ± 0.01	57.30 ± 0.11	59.26 ± 0.01	59.50 ± 0.02
	16045 ± 2	2.87 ± 2.6E-5	109.88 ± 0.02	23.68 ± 0.01	58.11 ± 0.04	59.87 ± 0.01	60.11 ± 0.01
Spray Bar (No Scraper)	7016 ± 1	0.7 ± 2.4E-5	73.16 ± 0.02	27.61 ± 0.02	51.84 ± 0.15	51.55 ± 0.01	52.39 ± 0.01
	6924 ± 1	2.07 ± 3.9E-5	86.92 ± 0.02	27.64 ± 0.01	51.85 ± 0.06	51.76 ± 0.01	52.68 ± 0.01
	7007 ± 2	2.87 ± 2.8E-5	92.77 ± 0.02	27.69 ± 0.01	52.63 ± 0.08	51.51 ± 0.02	52.63 ± 0.01
	10000 ± 1	0.69 ± 2.4E-5	79.27 ± 0.02	27.49 ± 0.01	53.06 ± 0.04	53.40 ± 0.01	54.60 ± 0.01
	10006 ± 3	2.07 ± 4.5E-5	95.12 ± 0.05	27.65 ± 0.02	53.64 ± 0.07	54.14 ± 0.03	55.62 ± 0.02
	10056 ± 2	2.87 ± 4.6E-5	102.00 ± 0.02	27.71 ± 0.01	54.29 ± 0.04	54.66 ± 0.02	56.18 ± 0.02
	12965 ± 3	0.69 ± 3.4E-5	84.66 ± 0.03	27.32 ± 0.01	55.72 ± 0.12	57.78 ± 0.02	58.81 ± 0.02
	13032 ± 1	2.07 ± 5.3E-5	99.24 ± 0.04	27.39 ± 0.01	56.00 ± 0.12	57.07 ± 0.02	58.53 ± 0.02
	13040 ± 1	2.87 ± 4.7E-5	106.75 ± 0.02	27.63 ± 0.01	56.53 ± 0.09	57.93 ± 0.02	59.49 ± 0.02
	16030 ± 3	0.69 ± 2.5E-5	90.86 ± 0.02	22.63 ± 0.02	57.36 ± 0.05	62.18 ± 0.01	63.16 ± 0.01
	15985 ± 3	2.07 ± 2.4E-5	99.76 ± 0.03	22.38 ± 0.02	57.72 ± 0.05	61.37 ± 0.02	62.28 ± 0.02
	15996 ± 2	2.87 ± 2.2E-4	107.66 ± 0.03	22.65 ± 0.03	58.14 ± 0.14	61.00 ± 0.02	62.23 ± 0.02
Single Orifice Between Pads	7051 ± 2	0.69 ± 6.5E-5	73.10 ± 0.05	22.64 ± 0.01	51.76 ± 0.13	56.70 ± 0.03	52.52 ± 0.01
	7011 ± 3	2.07 ± 2.3E-5	86.06 ± 0.03	22.56 ± 0.01	51.87 ± 0.06	56.81 ± 0.02	52.79 ± 0.01
	7033 ± 1	2.87 ± 2.8E-5	91.35 ± 0.04	21.87 ± 0.02	52.11 ± 0.06	56.99 ± 0.07	53.01 ± 0.08
	10045 ± 2	0.69 ± 4.1E-5	81.93 ± 0.03	25.00 ± 0.01	55.10 ± 0.06	63.42 ± 0.02	55.50 ± 0.02
	10015 ± 1	2.07 ± 2.6E-5	97.49 ± 0.02	25.12 ± 0.01	55.21 ± 0.07	62.92 ± 0.02	56.00 ± 0.01
	10032 ± 2	2.87 ± 3.0E-5	104.04 ± 0.03	24.93 ± 0.01	55.43 ± 0.11	63.54 ± 0.01	56.28 ± 0.02
	13031 ± 1	0.7 ± 7.1E-5	88.84 ± 0.03	24.66 ± 0.01	57.73 ± 0.07	71.75 ± 0.02	59.41 ± 0.03
	13059 ± 2	2.07 ± 2.6E-5	106.41 ± 0.07	24.05 ± 0.01	58.14 ± 0.13	71.02 ± 0.03	59.98 ± 0.02
	13044 ± 9	2.87 ± 3.9E-4	112.64 ± 0.02	24.43 ± 0.01	58.72 ± 0.04	72.03 ± 0.02	60.51 ± 0.02
	16052 ± 2	0.69 ± 3.1E-5	93.75 ± 0.06	23.11 ± 0.01	62.84 ± 0.09	80.06 ± 0.06	63.53 ± 0.02
	16088 ± 2	2.07 ± 3.0E-5	111.94 ± 0.02	22.61 ± 0.02	62.87 ± 0.05	81.14 ± 0.06	64.80 ± 0.03
	15973 ± 2	2.87 ± 8.2E-5	118.50 ± 0.04	23.01 ± 0.02	63.86 ± 0.08	82.23 ± 0.05	65.65 ± 0.01

Table C.5: Measured Temperatures for Pad B (Refer to Figure 13)

Feed Type	Speed (rpm)	Load (MPa)	TC3 (°C)	TC4 (°C)	TC5 (°C)	TC6 (°C)	TC7 (°C)	TC8 (°C)
Leading Edge Groove	7086 ± 2	0.69 ± 4.4E-5	51.94 ± 0.03	53.48 ± 0.02	62.89 ± 0.02	62.21 ± 0.03	61.97 ± 0.02	53.95 ± 0.01
	6985 ± 1	2.07 ± 2.8E-5	51.93 ± 0.04	54.13 ± 0.03	74.42 ± 0.03	73.12 ± 0.03	71.16 ± 0.03	54.08 ± 0.02
	7056 ± 2	2.87 ± 1.0E-4	52.45 ± 0.02	55.33 ± 0.02	83.01 ± 0.02	81.42 ± 0.02	77.03 ± 0.02	54.27 ± 0.01
	10018 ± 2	0.69 ± 3.2E-5	52.59 ± 0.03	55.45 ± 0.02	70.15 ± 0.02	67.22 ± 0.02	68.13 ± 0.03	55.92 ± 0.02
	10061 ± 3	2.07 ± 3.9E-5	52.72 ± 0.04	56.34 ± 0.04	83.28 ± 0.03	78.06 ± 0.03	77.60 ± 0.04	55.54 ± 0.02
	10003 ± 1	2.87 ± 3.3E-5	53.46 ± 0.02	58.12 ± 0.02	91.49 ± 0.02	85.85 ± 0.02	83.00 ± 0.02	55.31 ± 0.01
	13016 ± 2	0.69 ± 2.6E-5	53.49 ± 0.03	58.27 ± 0.03	76.37 ± 0.03	75.68 ± 0.03	74.45 ± 0.03	58.67 ± 0.02
	12992 ± 2	2.07 ± 4.1E-5	53.68 ± 0.02	59.10 ± 0.01	86.51 ± 0.01	84.62 ± 0.01	82.19 ± 0.01	57.73 ± 0.02
	12989 ± 7	2.86 ± 3.3E-4	54.83 ± 0.05	61.36 ± 0.04	94.04 ± 0.03	91.64 ± 0.03	87.27 ± 0.04	57.04 ± 0.04
	16077 ± 5	0.69 ± 4.2E-5	55.25 ± 0.05	61.72 ± 0.04	82.96 ± 0.04	79.56 ± 0.04	80.12 ± 0.04	63.47 ± 0.07
	16005 ± 3	2.07 ± 4.9E-5	57.32 ± 0.04	64.13 ± 0.03	92.61 ± 0.02	86.65 ± 0.03	86.60 ± 0.03	61.30 ± 0.02
	16056 ± 3	2.86 ± 3.3E-4	57.20 ± 0.04	65.11 ± 0.02	98.94 ± 0.02	92.08 ± 0.02	90.44 ± 0.02	59.32 ± 0.01
Spray Bar Blocker (Scraper)	7025 ± 2	0.69 ± 4.7E-5	52.86 ± 0.02	57.69 ± 0.02	71.95 ± 0.01	68.91 ± 0.01	71.20 ± 0.02	61.15 ± 0.16
	6992 ± 1	2.07 ± 3.1E-5	53.86 ± 0.02	60.04 ± 0.02	85.80 ± 0.02	80.12 ± 0.02	83.40 ± 0.02	67.24 ± 0.14
	6973 ± 3	2.87 ± 2.1E-4	54.36 ± 0.02	61.77 ± 0.02	93.52 ± 0.02	87.79 ± 0.02	90.05 ± 0.02	68.70 ± 0.16
	10004 ± 1	0.69 ± 1.2E-4	53.98 ± 0.03	61.37 ± 0.03	79.63 ± 0.03	76.08 ± 0.03	80.19 ± 0.03	67.70 ± 0.08
	10019 ± 1	2.07 ± 4.5E-5	54.81 ± 0.03	63.66 ± 0.03	91.67 ± 0.02	85.80 ± 0.03	90.47 ± 0.03	67.12 ± 0.17
	10042 ± 3	2.87 ± 6.1E-5	55.74 ± 0.05	65.51 ± 0.03	100.02 ± 0.03	93.69 ± 0.03	97.08 ± 0.05	66.75 ± 0.19
	13031 ± 1	0.69 ± 4.2E-5	55.21 ± 0.04	65.00 ± 0.04	87.26 ± 0.03	81.17 ± 0.03	86.35 ± 0.04	69.39 ± 0.11
	13050 ± 1	2.07 ± 3.0E-5	56.14 ± 0.03	66.83 ± 0.02	97.90 ± 0.02	90.02 ± 0.02	95.81 ± 0.03	71.36 ± 0.13
	13057 ± 1	2.86 ± 4.6E-5	56.89 ± 0.03	68.30 ± 0.02	106.46 ± 0.02	96.82 ± 0.02	102.28 ± 0.02	71.99 ± 0.20
	16054 ± 2	0.69 ± 2.7E-5	55.76 ± 0.03	67.61 ± 0.02	90.45 ± 0.02	86.81 ± 0.02	89.85 ± 0.02	72.54 ± 0.12
	16003 ± 1	2.07 ± 3.5E-5	57.07 ± 0.04	69.46 ± 0.03	101.56 ± 0.02	96.04 ± 0.03	100.17 ± 0.03	79.49 ± 0.17
	16045 ± 2	2.87 ± 2.6E-5	57.46 ± 0.02	70.15 ± 0.02	108.79 ± 0.02	101.72 ± 0.02	105.70 ± 0.02	80.99 ± 0.20
Spray Bar (No Scraper)	7016 ± 1	0.7 ± 2.4E-5	53.80 ± 0.02	57.41 ± 0.02	73.10 ± 0.02	67.67 ± 0.02	70.47 ± 0.02	53.27 ± 0.01
	6924 ± 1	2.07 ± 3.9E-5	54.95 ± 0.02	59.68 ± 0.01	86.53 ± 0.02	78.71 ± 0.02	81.11 ± 0.02	53.89 ± 0.02
	7007 ± 2	2.87 ± 2.8E-5	54.99 ± 0.03	60.99 ± 0.02	92.77 ± 0.02	85.60 ± 0.02	85.48 ± 0.02	53.66 ± 0.02
	10000 ± 1	0.69 ± 2.4E-5	55.28 ± 0.02	59.67 ± 0.02	78.88 ± 0.01	73.99 ± 0.01	76.50 ± 0.02	54.67 ± 0.02
	10006 ± 3	2.07 ± 4.5E-5	57.01 ± 0.05	61.68 ± 0.04	91.91 ± 0.03	83.95 ± 0.04	86.80 ± 0.04	55.80 ± 0.06
	10056 ± 2	2.87 ± 4.6E-5	58.18 ± 0.04	63.26 ± 0.01	100.22 ± 0.01	91.99 ± 0.01	92.98 ± 0.01	56.82 ± 0.05
	12965 ± 3	0.69 ± 3.4E-5	59.83 ± 0.05	62.69 ± 0.03	84.66 ± 0.03	80.24 ± 0.02	82.22 ± 0.03	56.62 ± 0.04
	13032 ± 1	2.07 ± 5.3E-5	61.15 ± 0.04	64.20 ± 0.03	94.78 ± 0.03	89.13 ± 0.03	91.20 ± 0.04	57.29 ± 0.05
	13040 ± 1	2.87 ± 4.7E-5	61.90 ± 0.02	65.56 ± 0.02	102.13 ± 0.01	95.95 ± 0.01	97.38 ± 0.02	58.38 ± 0.08
	16030 ± 3	0.69 ± 2.5E-5	62.26 ± 0.03	65.69 ± 0.02	90.86 ± 0.02	85.33 ± 0.02	86.98 ± 0.03	57.28 ± 0.03
	15985 ± 3	2.07 ± 2.4E-5	63.57 ± 0.03	67.09 ± 0.02	98.86 ± 0.02	91.40 ± 0.02	93.96 ± 0.02	59.85 ± 0.06
	15996 ± 2	2.87 ± 2.2E-4	63.84 ± 0.02	68.40 ± 0.02	105.27 ± 0.02	96.98 ± 0.02	99.49 ± 0.02	61.03 ± 0.06
Single Orifice Between Pads	7051 ± 2	0.69 ± 6.5E-5	54.13 ± 0.04	56.64 ± 0.04	70.38 ± 0.04	72.66 ± 0.03	66.92 ± 0.04	51.98 ± 0.01
	7011 ± 3	2.07 ± 2.3E-5	55.92 ± 0.03	59.22 ± 0.02	83.23 ± 0.02	85.19 ± 0.02	76.22 ± 0.02	52.09 ± 0.01
	7033 ± 1	2.87 ± 2.8E-5	56.96 ± 0.10	61.27 ± 0.06	90.62 ± 0.04	91.35 ± 0.04	79.40 ± 0.05	52.14 ± 0.11
	10045 ± 2	0.69 ± 4.1E-5	54.63 ± 0.03	57.55 ± 0.03	74.80 ± 0.03	81.05 ± 0.03	72.54 ± 0.03	53.06 ± 0.02
	10015 ± 1	2.07 ± 2.6E-5	57.16 ± 0.03	61.18 ± 0.02	91.49 ± 0.02	96.06 ± 0.02	83.74 ± 0.02	53.13 ± 0.02
	10032 ± 2	2.87 ± 3.0E-5	58.17 ± 0.04	63.12 ± 0.03	100.67 ± 0.03	104.04 ± 0.03	87.92 ± 0.04	53.07 ± 0.01
	13031 ± 1	0.7 ± 7.1E-5	56.12 ± 0.04	59.67 ± 0.02	82.56 ± 0.03	88.52 ± 0.02	79.16 ± 0.03	54.65 ± 0.02
	13059 ± 2	2.07 ± 2.6E-5	58.65 ± 0.09	63.47 ± 0.05	100.43 ± 0.06	103.12 ± 0.07	90.70 ± 0.06	54.40 ± 0.03
	13044 ± 9	2.87 ± 3.9E-4	60.37 ± 0.03	65.98 ± 0.02	111.38 ± 0.02	112.64 ± 0.02	95.54 ± 0.02	54.80 ± 0.02
	16052 ± 2	0.69 ± 3.1E-5	57.35 ± 0.06	61.62 ± 0.06	89.13 ± 0.05	92.78 ± 0.06	83.96 ± 0.07	56.19 ± 0.03
	16088 ± 2	2.07 ± 3.0E-5	60.39 ± 0.03	66.19 ± 0.03	108.21 ± 0.01	107.96 ± 0.01	96.55 ± 0.02	56.07 ± 0.03
	15973 ± 2	2.87 ± 8.2E-5	62.53 ± 0.04	68.75 ± 0.03	118.49 ± 0.03	117.50 ± 0.03	101.64 ± 0.03	56.62 ± 0.02

Table C.6: Measured Temperatures for Pad C (Refer to Figure 13)

Feed Type	Speed (rpm)	Load (MPa)	TC9 (°C)	TC10 (°C)	TC11 (°C)	TC12 (°C)	TC13 (°C)	TC14 (°C)
Leading Edge Groove	7086 ± 2	0.69 ± 4.4E-5	51.89 ± 0.05	54.10 ± 0.04	67.94 ± 0.03	70.28 ± 0.03	67.00 ± 0.04	54.06 ± 0.01
	6985 ± 1	2.07 ± 2.8E-5	52.21 ± 0.06	55.51 ± 0.05	81.93 ± 0.04	85.50 ± 0.04	78.50 ± 0.05	53.55 ± 0.02
	7056 ± 2	2.87 ± 1.0E-4	52.78 ± 0.03	56.64 ± 0.02	89.54 ± 0.02	91.64 ± 0.02	83.12 ± 0.03	53.73 ± 0.04
	10018 ± 2	0.69 ± 3.2E-5	52.60 ± 0.04	55.69 ± 0.03	73.75 ± 0.03	75.72 ± 0.03	73.20 ± 0.03	55.97 ± 0.02
	10061 ± 3	2.07 ± 3.9E-5	52.86 ± 0.08	56.80 ± 0.06	88.65 ± 0.05	90.95 ± 0.04	84.96 ± 0.06	54.93 ± 0.02
	10003 ± 1	2.87 ± 3.3E-5	53.10 ± 0.04	57.54 ± 0.04	97.46 ± 0.02	98.39 ± 0.02	89.87 ± 0.03	54.71 ± 0.01
	13016 ± 2	0.69 ± 2.6E-5	53.27 ± 0.04	57.75 ± 0.04	78.53 ± 0.03	81.16 ± 0.03	78.79 ± 0.04	58.36 ± 0.05
	12992 ± 2	2.07 ± 4.1E-5	53.22 ± 0.02	58.03 ± 0.02	91.05 ± 0.02	94.98 ± 0.02	89.10 ± 0.02	56.58 ± 0.02
	12989 ± 7	2.86 ± 3.3E-4	53.45 ± 0.06	58.73 ± 0.05	102.15 ± 0.04	104.96 ± 0.04	95.77 ± 0.05	56.19 ± 0.04
	16077 ± 5	0.69 ± 4.2E-5	53.79 ± 0.07	60.06 ± 0.05	84.59 ± 0.05	87.56 ± 0.05	85.07 ± 0.06	62.61 ± 0.07
	16005 ± 3	2.07 ± 4.9E-5	54.11 ± 0.06	60.40 ± 0.03	95.42 ± 0.04	99.01 ± 0.03	93.55 ± 0.04	60.01 ± 0.03
	16056 ± 3	2.86 ± 3.3E-4	53.16 ± 0.04	59.64 ± 0.04	102.40 ± 0.03	105.47 ± 0.03	98.02 ± 0.04	57.48 ± 0.04
Spray Bar Blocker (Scraper)	7025 ± 2	0.69 ± 4.7E-5	52.42 ± 0.04	56.83 ± 0.03	72.40 ± 0.02	72.49 ± 0.02	72.79 ± 0.03	59.21 ± 0.10
	6992 ± 1	2.07 ± 3.1E-5	52.99 ± 0.04	58.71 ± 0.03	88.13 ± 0.02	87.55 ± 0.02	86.15 ± 0.03	58.48 ± 0.09
	6973 ± 3	2.87 ± 2.1E-4	53.07 ± 0.03	59.57 ± 0.03	93.75 ± 0.02	93.11 ± 0.03	89.78 ± 0.03	58.75 ± 0.09
	10004 ± 1	0.69 ± 1.2E-4	53.60 ± 0.06	60.57 ± 0.05	80.26 ± 0.04	79.84 ± 0.04	80.83 ± 0.05	62.60 ± 0.08
	10019 ± 1	2.07 ± 4.5E-5	53.72 ± 0.07	61.71 ± 0.05	94.90 ± 0.04	94.00 ± 0.04	93.63 ± 0.05	63.83 ± 0.10
	10042 ± 3	2.87 ± 6.1E-5	54.36 ± 0.08	62.83 ± 0.07	101.74 ± 0.06	101.14 ± 0.06	98.52 ± 0.07	64.17 ± 0.10
	13031 ± 1	0.69 ± 4.2E-5	54.58 ± 0.07	63.43 ± 0.07	85.80 ± 0.05	85.82 ± 0.05	86.20 ± 0.06	63.22 ± 0.15
	13050 ± 1	2.07 ± 3.0E-5	54.44 ± 0.05	64.07 ± 0.04	98.09 ± 0.03	98.20 ± 0.03	97.46 ± 0.05	66.89 ± 0.14
	13057 ± 1	2.86 ± 4.6E-5	54.94 ± 0.04	65.02 ± 0.04	106.47 ± 0.03	106.56 ± 0.03	104.05 ± 0.03	68.21 ± 0.15
	16054 ± 2	0.69 ± 2.7E-5	56.03 ± 0.05	67.12 ± 0.03	88.63 ± 0.03	90.52 ± 0.03	89.55 ± 0.03	67.07 ± 0.10
	16003 ± 1	2.07 ± 3.5E-5	56.54 ± 0.06	68.05 ± 0.04	102.46 ± 0.04	102.42 ± 0.04	100.52 ± 0.05	70.40 ± 0.17
	16045 ± 2	2.87 ± 2.6E-5	56.78 ± 0.02	68.34 ± 0.03	109.54 ± 0.02	109.88 ± 0.02	106.78 ± 0.03	72.55 ± 0.17
Spray Bar (No Scraper)	7016 ± 1	0.7 ± 2.4E-5	53.10 ± 0.04	56.72 ± 0.03	72.51 ± 0.02	73.16 ± 0.02	72.39 ± 0.03	53.35 ± 0.03
	6924 ± 1	2.07 ± 3.9E-5	53.63 ± 0.03	58.47 ± 0.02	86.88 ± 0.02	86.92 ± 0.02	84.00 ± 0.02	54.00 ± 0.03
	7007 ± 2	2.87 ± 2.8E-5	53.39 ± 0.04	58.97 ± 0.03	91.60 ± 0.03	91.28 ± 0.02	86.42 ± 0.03	53.75 ± 0.03
	10000 ± 1	0.69 ± 2.4E-5	53.85 ± 0.03	58.63 ± 0.03	78.42 ± 0.02	79.27 ± 0.02	78.48 ± 0.02	55.03 ± 0.06
	10006 ± 3	2.07 ± 4.5E-5	54.18 ± 0.08	60.23 ± 0.05	94.60 ± 0.05	95.12 ± 0.05	91.29 ± 0.05	56.48 ± 0.10
	10056 ± 2	2.87 ± 4.6E-5	54.68 ± 0.03	61.39 ± 0.02	101.18 ± 0.02	102.00 ± 0.02	94.93 ± 0.02	56.56 ± 0.08
	12965 ± 3	0.69 ± 3.4E-5	56.24 ± 0.06	61.11 ± 0.04	83.39 ± 0.04	83.95 ± 0.04	83.35 ± 0.04	57.07 ± 0.07
	13032 ± 1	2.07 ± 5.3E-5	55.75 ± 0.06	62.14 ± 0.05	98.65 ± 0.04	99.24 ± 0.04	96.47 ± 0.05	58.16 ± 0.12
	13040 ± 1	2.87 ± 4.7E-5	56.45 ± 0.04	63.33 ± 0.03	106.23 ± 0.02	106.75 ± 0.02	101.16 ± 0.02	58.57 ± 0.10
	16030 ± 3	0.69 ± 2.5E-5	59.99 ± 0.07	64.26 ± 0.05	88.84 ± 0.05	88.80 ± 0.04	88.11 ± 0.04	57.12 ± 0.03
	15985 ± 3	2.07 ± 2.4E-5	58.53 ± 0.06	64.66 ± 0.03	99.76 ± 0.03	99.54 ± 0.03	98.00 ± 0.03	58.40 ± 0.10
	15996 ± 2	2.87 ± 2.2E-4	58.37 ± 0.04	66.01 ± 0.03	107.66 ± 0.03	107.11 ± 0.02	103.79 ± 0.03	59.26 ± 0.11
Single Orifice Between Pads	7051 ± 2	0.69 ± 6.5E-5	52.61 ± 0.08	54.98 ± 0.06	71.40 ± 0.06	73.10 ± 0.05	68.29 ± 0.07	52.01 ± 0.01
	7011 ± 3	2.07 ± 2.3E-5	53.11 ± 0.04	56.80 ± 0.04	86.06 ± 0.03	86.06 ± 0.03	78.23 ± 0.03	52.11 ± 0.01
	7033 ± 1	2.87 ± 2.8E-5	53.25 ± 0.11	57.54 ± 0.06	90.57 ± 0.04	89.63 ± 0.04	80.09 ± 0.05	52.08 ± 0.12
	10045 ± 2	0.69 ± 4.1E-5	53.74 ± 0.06	56.31 ± 0.04	77.54 ± 0.04	81.93 ± 0.03	75.32 ± 0.04	53.56 ± 0.03
	10015 ± 1	2.07 ± 2.6E-5	54.39 ± 0.04	58.10 ± 0.03	96.12 ± 0.02	97.49 ± 0.02	87.05 ± 0.03	53.75 ± 0.02
	10032 ± 2	2.87 ± 3.0E-5	54.22 ± 0.07	58.35 ± 0.06	101.75 ± 0.05	102.21 ± 0.05	89.43 ± 0.06	53.71 ± 0.02
	13031 ± 1	0.7 ± 7.1E-5	55.39 ± 0.05	58.33 ± 0.04	81.64 ± 0.03	88.84 ± 0.03	81.31 ± 0.04	56.04 ± 0.02
	13059 ± 2	2.07 ± 2.6E-5	55.62 ± 0.11	59.43 ± 0.11	102.85 ± 0.07	106.41 ± 0.07	94.87 ± 0.10	56.43 ± 0.03
	13044 ± 9	2.87 ± 3.9E-4	56.14 ± 0.03	59.94 ± 0.03	110.41 ± 0.03	112.40 ± 0.02	97.88 ± 0.03	57.13 ± 0.02
	16052 ± 2	0.69 ± 3.1E-5	58.14 ± 0.11	61.45 ± 0.09	86.53 ± 0.07	93.75 ± 0.06	86.22 ± 0.08	58.37 ± 0.03
	16088 ± 2	2.07 ± 3.0E-5	57.54 ± 0.04	62.28 ± 0.04	109.59 ± 0.02	111.94 ± 0.02	101.04 ± 0.02	59.81 ± 0.04
	15973 ± 2	2.87 ± 8.2E-5	58.26 ± 0.06	62.71 ± 0.05	117.31 ± 0.04	118.50 ± 0.04	104.39 ± 0.04	60.94 ± 0.03

Table C.7: Measured Temperatures for Pads A and D (Refer to Figure 13)

Feed Type	Speed (rpm)	Load (MPa)	TC1 (°C)	TC2 (°C)	TC15 (°C)	TC16 (°C)
Leading Edge Groove	7086 ± 2	0.69 ± 4.4E-5	62.12 ± 0.04	60.57 ± 0.03	59.51 ± 0.03	59.21 ± 0.04
	6985 ± 1	2.07 ± 2.8E-5	59.01 ± 0.06	58.15 ± 0.04	57.64 ± 0.04	57.56 ± 0.06
	7056 ± 2	2.87 ± 1.0E-4	58.79 ± 0.02	58.13 ± 0.03	57.75 ± 0.03	57.67 ± 0.03
	10018 ± 2	0.69 ± 3.2E-5	66.55 ± 0.03	66.77 ± 0.03	64.61 ± 0.02	64.59 ± 0.03
	10061 ± 3	2.07 ± 3.9E-5	63.70 ± 0.05	63.71 ± 0.06	61.97 ± 0.04	62.18 ± 0.06
	10003 ± 1	2.87 ± 3.3E-5	62.86 ± 0.03	62.41 ± 0.03	61.28 ± 0.03	61.49 ± 0.03
	13016 ± 2	0.69 ± 2.6E-5	71.81 ± 0.03	70.64 ± 0.04	71.68 ± 0.03	70.67 ± 0.04
	12992 ± 2	2.07 ± 4.1E-5	69.07 ± 0.01	69.16 ± 0.02	68.24 ± 0.01	67.31 ± 0.01
	12989 ± 7	2.86 ± 3.3E-4	68.04 ± 0.05	68.09 ± 0.05	67.09 ± 0.04	66.28 ± 0.05
	16077 ± 5	0.69 ± 4.2E-5	81.09 ± 0.06	78.02 ± 0.05	76.82 ± 0.05	75.74 ± 0.06
	16005 ± 3	2.07 ± 4.9E-5	78.00 ± 0.03	76.22 ± 0.04	73.98 ± 0.04	72.95 ± 0.03
	16056 ± 3	2.86 ± 3.3E-4	74.19 ± 0.03	74.29 ± 0.03	73.38 ± 0.03	72.32 ± 0.03
Spray Bar Blocker (Scraper)	7025 ± 2	0.69 ± 4.7E-5	62.56 ± 0.03	60.51 ± 0.03	64.63 ± 0.02	62.23 ± 0.03
	6992 ± 1	2.07 ± 3.1E-5	59.43 ± 0.03	58.32 ± 0.03	61.46 ± 0.02	60.14 ± 0.03
	6973 ± 3	2.87 ± 2.1E-4	59.59 ± 0.03	58.62 ± 0.03	61.08 ± 0.03	59.88 ± 0.03
	10004 ± 1	0.69 ± 1.2E-4	69.59 ± 0.04	67.58 ± 0.05	73.97 ± 0.05	68.85 ± 0.06
	10019 ± 1	2.07 ± 4.5E-5	64.64 ± 0.04	63.60 ± 0.05	69.72 ± 0.03	66.43 ± 0.05
	10042 ± 3	2.87 ± 6.1E-5	64.96 ± 0.06	63.86 ± 0.06	67.50 ± 0.06	66.57 ± 0.06
	13031 ± 1	0.69 ± 4.2E-5	76.73 ± 0.06	74.71 ± 0.05	78.41 ± 0.05	76.28 ± 0.05
	13050 ± 1	2.07 ± 3.0E-5	70.81 ± 0.05	70.68 ± 0.04	73.15 ± 0.04	74.25 ± 0.04
	13057 ± 1	2.86 ± 4.6E-5	71.12 ± 0.03	70.96 ± 0.03	72.38 ± 0.03	72.95 ± 0.04
	16054 ± 2	0.69 ± 2.7E-5	84.74 ± 0.04	83.94 ± 0.03	83.57 ± 0.03	84.87 ± 0.03
	16003 ± 1	2.07 ± 3.5E-5	79.07 ± 0.05	78.48 ± 0.05	78.70 ± 0.05	80.45 ± 0.05
	16045 ± 2	2.87 ± 2.6E-5	78.46 ± 0.02	77.71 ± 0.02	77.73 ± 0.02	78.50 ± 0.02
Spray Bar (No Scraper)	7016 ± 1	0.7 ± 2.4E-5	62.75 ± 0.03	61.17 ± 0.03	61.70 ± 0.02	61.06 ± 0.03
	6924 ± 1	2.07 ± 3.9E-5	59.73 ± 0.02	58.92 ± 0.02	59.61 ± 0.02	59.44 ± 0.02
	7007 ± 2	2.87 ± 2.8E-5	58.50 ± 0.03	57.93 ± 0.04	58.78 ± 0.04	58.55 ± 0.04
	10000 ± 1	0.69 ± 2.4E-5	68.78 ± 0.02	66.52 ± 0.02	67.45 ± 0.02	66.27 ± 0.02
	10006 ± 3	2.07 ± 4.5E-5	64.32 ± 0.06	63.20 ± 0.06	64.12 ± 0.05	63.75 ± 0.05
	10056 ± 2	2.87 ± 4.6E-5	63.38 ± 0.02	62.53 ± 0.02	63.86 ± 0.02	63.38 ± 0.02
	12965 ± 3	0.69 ± 3.4E-5	75.28 ± 0.04	73.85 ± 0.04	72.48 ± 0.04	74.15 ± 0.04
	13032 ± 1	2.07 ± 5.3E-5	69.87 ± 0.06	68.83 ± 0.05	69.36 ± 0.04	70.18 ± 0.05
	13040 ± 1	2.87 ± 4.7E-5	68.36 ± 0.03	67.58 ± 0.02	68.75 ± 0.02	69.58 ± 0.02
	16030 ± 3	0.69 ± 2.5E-5	83.59 ± 0.04	81.98 ± 0.03	79.50 ± 0.03	82.62 ± 0.04
	15985 ± 3	2.07 ± 2.4E-5	77.28 ± 0.03	75.93 ± 0.04	76.10 ± 0.03	78.33 ± 0.03
	15996 ± 2	2.87 ± 2.2E-4	74.71 ± 0.04	73.60 ± 0.03	75.41 ± 0.03	76.33 ± 0.03
Single Orifice Between Pads	7051 ± 2	0.69 ± 6.5E-5	58.88 ± 0.07	58.57 ± 0.06	59.82 ± 0.06	58.57 ± 0.06
	7011 ± 3	2.07 ± 2.3E-5	57.62 ± 0.04	57.57 ± 0.04	57.22 ± 0.03	56.85 ± 0.03
	7033 ± 1	2.87 ± 2.8E-5	57.29 ± 0.04	57.22 ± 0.04	57.02 ± 0.03	56.76 ± 0.03
	10045 ± 2	0.69 ± 4.1E-5	63.30 ± 0.04	63.06 ± 0.04	64.19 ± 0.04	62.32 ± 0.04
	10015 ± 1	2.07 ± 2.6E-5	62.00 ± 0.03	62.19 ± 0.02	60.95 ± 0.03	60.42 ± 0.03
	10032 ± 2	2.87 ± 3.0E-5	61.78 ± 0.06	62.00 ± 0.05	60.69 ± 0.04	60.24 ± 0.05
	13031 ± 1	0.7 ± 7.1E-5	68.89 ± 0.03	68.17 ± 0.04	68.67 ± 0.03	67.52 ± 0.04
	13059 ± 2	2.07 ± 2.6E-5	67.53 ± 0.11	67.57 ± 0.08	65.16 ± 0.07	64.82 ± 0.10
	13044 ± 9	2.87 ± 3.9E-4	67.87 ± 0.03	67.96 ± 0.03	65.23 ± 0.03	65.02 ± 0.03
	16052 ± 2	0.69 ± 3.1E-5	74.42 ± 0.10	72.89 ± 0.10	73.84 ± 0.09	71.93 ± 0.11
	16088 ± 2	2.07 ± 3.0E-5	73.38 ± 0.03	73.06 ± 0.03	70.31 ± 0.03	69.36 ± 0.04
	15973 ± 2	2.87 ± 8.2E-5	73.90 ± 0.05	73.83 ± 0.04	71.02 ± 0.05	70.11 ± 0.04

APPENDIX D

XL_TPJB INPUTS

Table D.1: XL_TPJB Inputs

Shaft Speed (rpm)	Load (N)	Supply Pressure (bar)
7069	-4289	2.20
7053	-12782	2.20
7176	-17796	2.22
10012	-4280	2.22
10109	-12829	2.24
10064	-17754	2.26
13000	-4272	2.29
13110	-12815	2.31
13075	-17751	2.33
16094	-4259	2.42
16061	-12806	2.47
16084	-17739	2.49

APPENDIX E

TEMPERATURE PROFILES FOR 0.7 AND 2.9 MPA UNIT LOADS

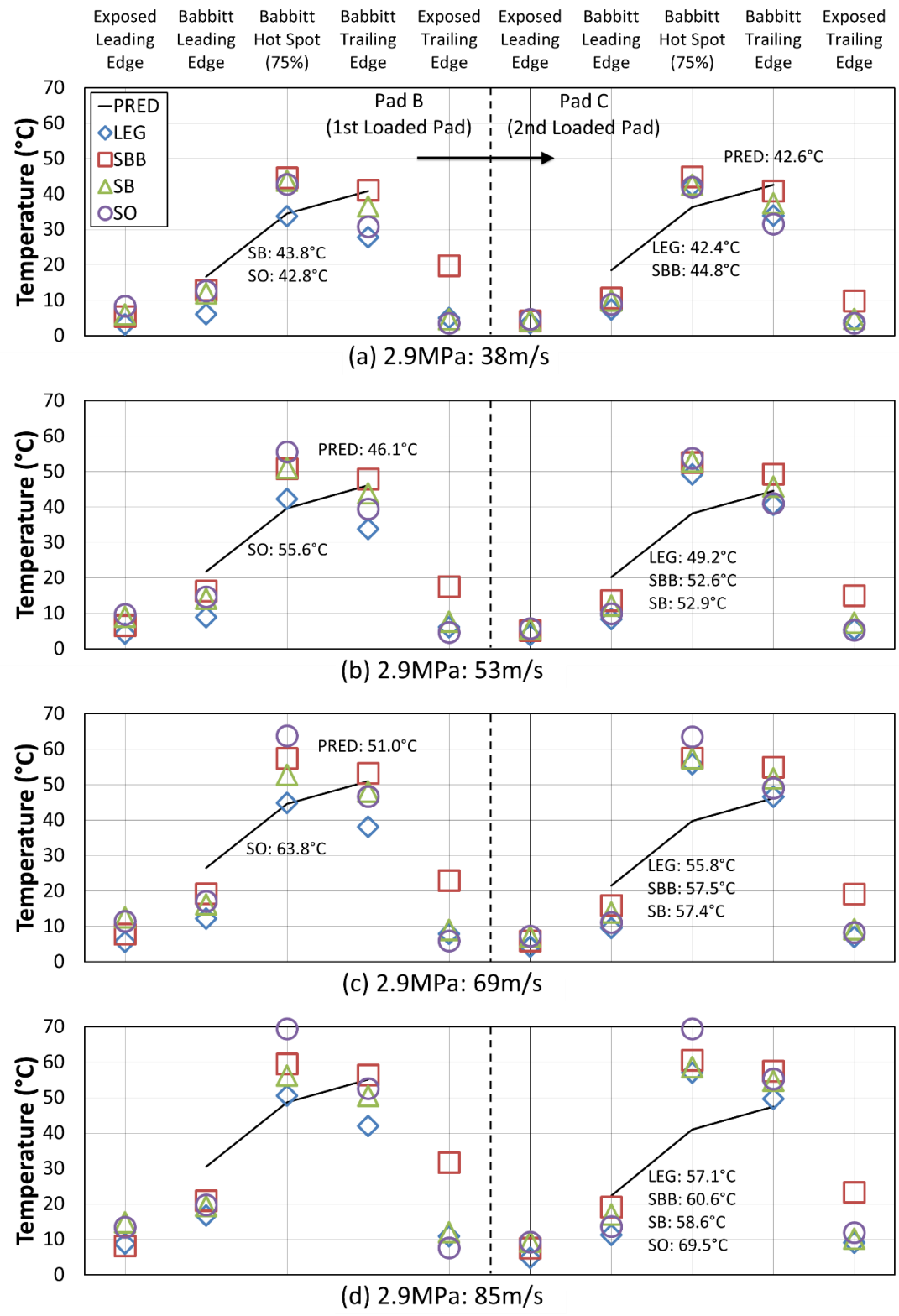

Figure E.1: Temperature Profiles for Loaded Pads with Unit Load of 2.9MPa

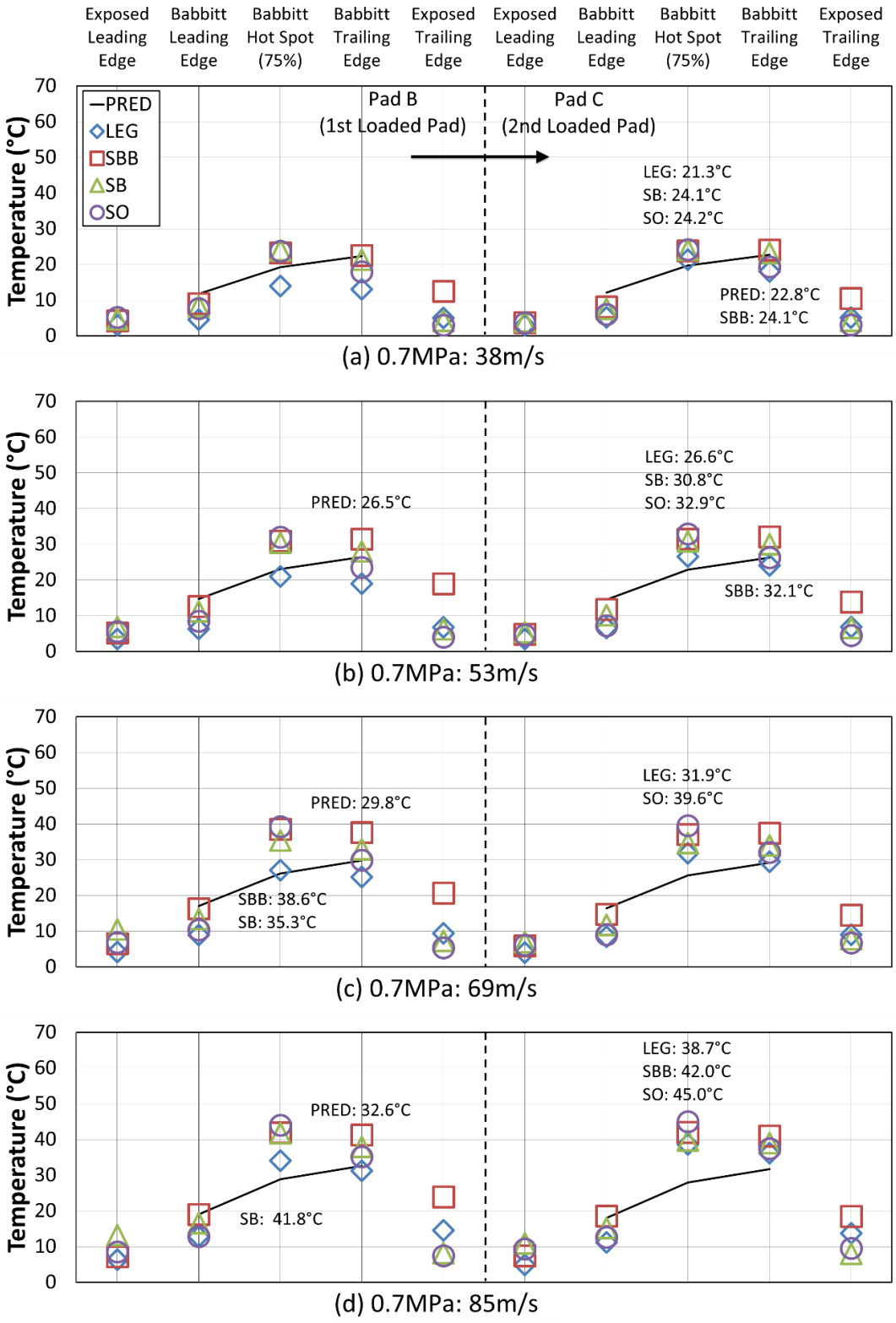

Figure E.2: Temperature Profiles for Loaded Pads with Unit Load of 0.7MPa

APPENDIX F

IMPEDANCE VALUES WITH 95% CONFIDENCE INTERVALS

Table F.1: SO - Impedance Values at 38 m/s and 0.7 MPa

Freq.	Re(H_{xx})	Re(H_{xy})	Re(H_{yx})	Re(H_{yy})	Im(H_{xx})	Im(H_{xy})	Im(H_{yx})	Im(H_{yy})
Hz	MN/m	MN/m	MN/m	MN/m	MN/m	MN/m	MN/m	MN/m
9.8	118.7 ± 0.2	24.7 ± 0.3	-45.6 ± 0.3	123.1 ± 0.7	11.0 ± 0.2	-2.9 ± 0.3	7.5 ± 0.2	13.1 ± 0.7
19.5	119.3 ± 0.1	25.0 ± 0.1	-44.0 ± 0.1	120.9 ± 0.5	20.1 ± 0.2	-4.8 ± 0.1	4.9 ± 0.1	19.1 ± 0.5
29.3	119.8 ± 0.2	22.5 ± 0.2	-44.1 ± 0.1	128.9 ± 0.2	29.6 ± 0.1	-7.5 ± 0.2	4.1 ± 0.1	28.5 ± 0.5
39.1	121.5 ± 0.1	24.8 ± 0.1	-41.9 ± 0.1	122.3 ± 0.2	39.2 ± 0.1	-10.8 ± 0.2	1.6 ± 0.1	40.5 ± 0.5
48.8	122.7 ± 0.1	23.7 ± 0.2	-42.2 ± 0.1	123.9 ± 0.3	47.8 ± 0.1	-15.6 ± 0.2	2.1 ± 0.1	54.4 ± 0.4
58.6	123.3 ± 0.1	22.1 ± 0.2	-40.3 ± 0.1	126.3 ± 0.3	57.1 ± 0.1	-15.7 ± 0.2	1.2 ± 0.2	61.5 ± 0.6
68.4	125.5 ± 0.1	20.0 ± 0.3	-40.5 ± 0.1	127.5 ± 0.2	67.9 ± 0.1	-13.0 ± 0.2	5.1 ± 0.1	77.1 ± 0.4
78.1	126.2 ± 0.1	23.9 ± 0.3	-34.5 ± 0.1	128.5 ± 0.5	74.0 ± 0.2	-17.3 ± 0.2	-1.8 ± 0.1	84.7 ± 0.4
87.9	129.8 ± 0.1	19.6 ± 0.2	-35.5 ± 0.1	142.5 ± 0.4	80.9 ± 0.1	-16.4 ± 0.2	4.7 ± 0.1	75.7 ± 0.6
97.7	131.1 ± 0.2	20.9 ± 0.2	-41.3 ± 0.1	139.2 ± 0.2	93.6 ± 0.1	-23.7 ± 0.1	1.1 ± 0.2	104.2 ± 0.7
107.4	133.0 ± 0.1	19.2 ± 0.2	-37.8 ± 0.2	144.2 ± 0.4	101.4 ± 0.1	-23.5 ± 0.3	2.5 ± 0.1	110.5 ± 0.6
117.2	134.5 ± 1.2	18.0 ± 1.5	-36.1 ± 2.9	145.2 ± 2.3	108.4 ± 2.4	-25.6 ± 2.1	0.4 ± 1.0	120.7 ± 2.0
127.0	136.5 ± 0.5	18.3 ± 0.4	-31.4 ± 0.3	147.6 ± 0.3	117.2 ± 0.2	-24.0 ± 0.1	-6.1 ± 0.4	123.8 ± 0.5
136.7	139.6 ± 0.2	19.1 ± 0.1	-22.6 ± 0.2	154.1 ± 0.3	128.6 ± 0.1	-24.1 ± 0.1	10.4 ± 0.2	131.4 ± 0.3
146.5	141.2 ± 0.1	19.1 ± 0.2	-22.9 ± 0.1	156.1 ± 0.2	138.1 ± 0.1	-22.5 ± 0.2	6.9 ± 0.1	141.8 ± 0.4
156.3	141.5 ± 0.1	23.7 ± 0.2	-19.1 ± 0.1	153.5 ± 0.3	146.8 ± 0.1	-20.1 ± 0.1	-0.1 ± 0.1	148.5 ± 0.3
166.0	141.9 ± 0.1	20.8 ± 0.2	-22.1 ± 0.1	157.9 ± 0.2	154.9 ± 0.1	-23.9 ± 0.1	-0.5 ± 0.1	165.3 ± 0.3
175.8	146.6 ± 0.1	22.2 ± 0.2	-13.8 ± 0.2	164.8 ± 0.2	165.8 ± 0.2	-21.7 ± 0.2	7.8 ± 0.1	170.8 ± 0.4
185.5	140.4 ± 0.2	25.5 ± 0.2	-26.5 ± 0.3	161.5 ± 0.2	174.2 ± 0.2	-19.9 ± 0.3	-13.7 ± 0.3	188.0 ± 0.4
195.3	152.7 ± 1.2	23.9 ± 0.3	17.3 ± 2.0	159.8 ± 0.3	161.7 ± 0.8	-18.4 ± 0.2	-44.8 ± 0.9	185.6 ± 0.6
205.1	147.4 ± 0.2	33.9 ± 0.1	-16.1 ± 0.1	164.7 ± 0.3	200.8 ± 0.2	-17.7 ± 0.3	11.0 ± 0.2	205.0 ± 0.4
214.8	142.5 ± 0.1	48.4 ± 0.2	-14.8 ± 0.1	152.5 ± 0.3	220.3 ± 0.2	-15.8 ± 0.3	10.4 ± 0.3	213.7 ± 0.5
224.6	147.1 ± 0.1	48.1 ± 0.1	-18.3 ± 0.3	205.8 ± 0.3	232.7 ± 0.3	-9.0 ± 0.5	12.8 ± 0.5	195.3 ± 0.8
234.4	149.8 ± 1.2	47.3 ± 1.4	-20.3 ± 0.8	178.8 ± 1.4	262.5 ± 2.3	-23.5 ± 2.9	34.2 ± 2.9	262.9 ± 4.1
244.1	137.4 ± 0.2	41.7 ± 0.3	-33.7 ± 0.4	192.9 ± 0.8	262.6 ± 0.4	-17.8 ± 0.8	20.4 ± 0.4	260.8 ± 1.7

Table F.2: SO - Impedance Values at 38 m/s and 2.1 MPa

Freq.	Re(H_{xx})	Re(H_{xy})	Re(H_{yx})	Re(H_{yy})	Im(H_{xx})	Im(H_{xy})	Im(H_{yx})	Im(H_{yy})
Hz	MN/m	MN/m	MN/m	MN/m	MN/m	MN/m	MN/m	MN/m
9.8	214.8 ± 0.6	-10.5 ± 0.5	-52.7 ± 0.3	269.0 ± 0.2	7.7 ± 0.6	-2.1 ± 0.6	13.5 ± 0.4	10.6 ± 0.6
19.5	215.7 ± 0.2	-8.9 ± 0.3	-52.7 ± 0.2	264.8 ± 0.3	16.9 ± 0.3	-2.1 ± 0.4	5.9 ± 0.1	12.4 ± 0.4
29.3	216.5 ± 0.2	-14.8 ± 0.4	-51.0 ± 0.1	279.6 ± 0.4	24.6 ± 0.3	-3.8 ± 0.3	0.2 ± 0.2	19.8 ± 0.5
39.1	217.0 ± 0.2	-9.8 ± 0.3	-48.0 ± 0.2	266.8 ± 0.4	32.9 ± 0.2	-6.5 ± 0.2	-3.8 ± 0.1	31.2 ± 0.4
48.8	219.6 ± 0.2	-10.2 ± 0.2	-48.5 ± 0.2	268.7 ± 0.3	39.1 ± 0.1	-10.0 ± 0.3	-4.3 ± 0.2	44.3 ± 0.4
58.6	221.2 ± 0.1	-9.3 ± 0.2	-47.2 ± 0.1	267.6 ± 0.4	46.3 ± 0.2	-8.8 ± 0.1	-4.9 ± 0.1	49.9 ± 0.5
68.4	223.1 ± 0.1	-11.3 ± 0.4	-50.7 ± 0.2	271.8 ± 0.3	54.7 ± 0.2	-9.5 ± 0.2	-8.8 ± 0.1	53.0 ± 0.3
78.1	224.3 ± 0.2	-3.4 ± 0.4	-47.0 ± 0.2	276.5 ± 0.3	64.6 ± 0.2	-6.9 ± 0.1	-5.6 ± 0.2	68.1 ± 0.4
87.9	227.0 ± 0.3	-7.9 ± 0.4	-49.5 ± 0.3	282.3 ± 0.4	65.6 ± 0.2	-5.8 ± 0.2	-2.7 ± 0.4	56.4 ± 0.7
97.7	228.5 ± 0.1	-4.9 ± 0.3	-57.6 ± 0.2	279.0 ± 0.5	79.3 ± 0.3	-15.6 ± 0.3	-12.1 ± 0.4	87.3 ± 0.4
107.4	229.9 ± 0.2	-3.8 ± 0.3	-56.2 ± 0.3	280.5 ± 0.6	85.2 ± 0.3	-15.5 ± 0.4	-10.1 ± 0.3	92.7 ± 0.6
117.2	229.2 ± 68.1	35.7 ± 45.4	-136.3 ± 49	276.7 ± 38.0	19.0 ± 24.7	-10.7 ± 37.6	20.2 ± 70.4	56.9 ± 58.7
127.0	231.6 ± 0.3	0.2 ± 0.5	-52.6 ± 0.5	282.9 ± 0.6	100.0 ± 0.3	-18.2 ± 0.4	-14.6 ± 0.3	106.1 ± 0.7
136.7	234.2 ± 0.1	0.9 ± 0.1	-41.1 ± 0.1	286.1 ± 0.3	100.6 ± 0.2	-20.2 ± 0.2	1.4 ± 0.1	115.9 ± 0.4
146.5	235.5 ± 0.1	2.4 ± 0.2	-41.6 ± 0.1	289.4 ± 0.3	109.0 ± 0.1	-21.2 ± 0.2	-2.2 ± 0.2	127.4 ± 0.4
156.3	236.0 ± 0.1	7.4 ± 0.2	-39.5 ± 0.2	300.1 ± 0.2	118.1 ± 0.1	-24.1 ± 0.1	-9.6 ± 0.1	137.3 ± 0.4
166.0	238.2 ± 0.1	3.4 ± 0.2	-43.4 ± 0.1	297.8 ± 0.3	125.9 ± 0.1	-29.7 ± 0.1	-8.8 ± 0.1	153.6 ± 0.5
175.8	247.2 ± 0.3	3.0 ± 0.3	-35.6 ± 0.4	301.8 ± 0.3	123.2 ± 0.4	-28.6 ± 0.2	11.9 ± 0.3	153.9 ± 0.5
185.5	242.1 ± 0.2	8.5 ± 0.2	-44.0 ± 0.5	303.5 ± 0.4	143.8 ± 0.3	-32.0 ± 0.1	-12.2 ± 0.1	178.7 ± 0.8
195.3	220.9 ± 0.7	10.7 ± 0.2	-10.0 ± 1.6	305.9 ± 0.5	145.1 ± 0.6	-26.8 ± 0.2	-14.3 ± 2.1	174.2 ± 0.5
205.1	242.7 ± 0.3	11.0 ± 0.3	-29.6 ± 0.3	315.1 ± 0.4	150.6 ± 0.2	-34.4 ± 0.2	8.8 ± 0.3	193.1 ± 0.4
214.8	240.4 ± 0.1	25.4 ± 0.2	-24.6 ± 0.3	303.8 ± 0.3	165.6 ± 0.3	-36.6 ± 0.3	6.1 ± 0.4	201.0 ± 0.4
224.6	246.6 ± 0.3	17.0 ± 0.3	-35.5 ± 0.7	392.2 ± 0.8	176.7 ± 0.3	-36.1 ± 0.3	13.7 ± 0.6	172.0 ± 0.8
234.4	243.9 ± 106	26.2 ± 29.5	-151.9 ± 182	326.6 ± 52.8	310.3 ± 139	-18.6 ± 36.7	127.4 ± 157	275.7 ± 36.9
244.1	248.7 ± 0.7	10.7 ± 0.9	-17.4 ± 0.7	349.3 ± 0.9	198.0 ± 0.4	-38.1 ± 0.6	7.0 ± 0.5	236.3 ± 0.8

Table F.3: SO - Impedance Values at 38 m/s and 2.9 MPa

Freq.	Re(H_{xx})	Re(H_{xy})	Re(H_{yx})	Re(H_{yy})	Im(H_{xx})	Im(H_{xy})	Im(H_{yx})	Im(H_{yy})
Hz	MN/m	MN/m	MN/m	MN/m	MN/m	MN/m	MN/m	MN/m
9.8	255.0 ± 0.3	-24.0 ± 0.3	-56.5 ± 0.4	331.9 ± 0.6	8.8 ± 0.2	-1.3 ± 0.5	11.9 ± 0.3	10.3 ± 0.8
19.5	255.2 ± 0.1	-21.1 ± 0.1	-56.1 ± 0.2	325.6 ± 0.4	16.6 ± 0.3	-0.9 ± 0.3	2.6 ± 0.2	10.3 ± 0.6
29.3	256.6 ± 0.1	-26.9 ± 0.2	-54.8 ± 0.2	344.6 ± 0.4	22.7 ± 0.2	-3.2 ± 0.2	-3.3 ± 0.2	18.9 ± 0.6
39.1	255.8 ± 0.1	-21.7 ± 0.3	-51.1 ± 0.1	331.4 ± 0.2	30.4 ± 0.1	-5.9 ± 0.1	-7.8 ± 0.1	28.6 ± 0.4
48.8	259.8 ± 0.1	-21.6 ± 0.1	-52.0 ± 0.1	333.4 ± 0.3	36.0 ± 0.2	-9.6 ± 0.2	-7.8 ± 0.2	39.6 ± 0.4
58.6	262.7 ± 0.2	-21.1 ± 0.4	-53.1 ± 0.1	332.1 ± 0.4	42.6 ± 0.2	-7.9 ± 0.1	-7.9 ± 0.1	44.5 ± 0.4
68.4	263.5 ± 0.1	-22.2 ± 0.2	-55.1 ± 0.2	336.4 ± 0.5	51.3 ± 0.2	-9.6 ± 0.3	-11.4 ± 0.1	47.6 ± 0.5
78.1	262.3 ± 0.1	-22.8 ± 0.3	-60.1 ± 0.2	329.3 ± 0.4	63.8 ± 0.1	-3.8 ± 0.2	-7.7 ± 0.2	70.2 ± 0.5
87.9	269.0 ± 0.2	-20.0 ± 0.2	-57.3 ± 0.3	348.1 ± 0.3	59.6 ± 0.3	-6.3 ± 0.1	-9.5 ± 0.1	52.0 ± 0.6
97.7	268.3 ± 0.3	-16.7 ± 0.2	-60.5 ± 0.3	343.5 ± 0.5	74.2 ± 0.2	-15.6 ± 0.3	-17.0 ± 0.3	78.8 ± 0.6
107.4	269.9 ± 0.2	-15.3 ± 0.2	-61.3 ± 0.2	343.8 ± 0.8	79.5 ± 0.3	-16.8 ± 0.6	-17.1 ± 0.4	85.7 ± 0.7
117.2	271.5 ± 0.7	-14.1 ± 2.1	-61.3 ± 1.1	347.7 ± 3.0	85.1 ± 1.1	-19.5 ± 1.8	-18.8 ± 1.2	94.8 ± 2.5
127.0	272.7 ± 0.2	-11.6 ± 0.4	-60.8 ± 0.9	346.8 ± 0.9	91.2 ± 0.6	-19.7 ± 0.8	-19.3 ± 0.3	98.4 ± 0.8
136.7	276.1 ± 0.2	-10.5 ± 0.2	-51.3 ± 0.2	349.5 ± 0.3	91.6 ± 0.4	-21.6 ± 0.2	-5.0 ± 0.2	106.8 ± 0.5
146.5	275.4 ± 0.1	-9.6 ± 0.2	-52.8 ± 0.1	355.6 ± 0.3	98.3 ± 0.2	-22.9 ± 0.2	-8.5 ± 0.1	117.3 ± 0.4
156.3	274.9 ± 0.1	-4.9 ± 0.1	-50.2 ± 0.1	374.6 ± 0.4	107.2 ± 0.2	-31.1 ± 0.2	-17.0 ± 0.1	140.6 ± 0.6
166.0	278.3 ± 0.1	-10.2 ± 0.1	-53.5 ± 0.2	366.5 ± 0.2	113.5 ± 0.2	-32.1 ± 0.1	-14.3 ± 0.1	141.9 ± 0.4
175.8	291.1 ± 0.3	-10.1 ± 0.2	-53.7 ± 0.2	368.4 ± 0.2	110.3 ± 0.2	-31.1 ± 0.3	6.7 ± 0.2	141.8 ± 0.3
185.5	285.6 ± 0.3	-3.8 ± 0.1	-55.3 ± 0.3	368.8 ± 0.4	130.3 ± 0.2	-35.6 ± 0.3	-16.4 ± 0.2	166.5 ± 0.5
195.3	250.4 ± 1.7	2.5 ± 0.2	-35.9 ± 1.2	368.8 ± 0.4	163.2 ± 0.7	-31.1 ± 0.3	-45.1 ± 1.5	163.5 ± 0.6
205.1	280.5 ± 0.1	-1.9 ± 0.2	-38.5 ± 0.1	380.2 ± 0.4	132.8 ± 0.3	-37.1 ± 0.2	2.3 ± 0.1	176.6 ± 0.5
214.8	279.0 ± 0.2	11.6 ± 0.3	-32.9 ± 0.2	367.2 ± 0.5	146.1 ± 0.4	-39.2 ± 0.2	0.0 ± 0.2	187.5 ± 0.5
224.6	287.0 ± 0.3	0.2 ± 0.3	-47.0 ± 0.4	470.6 ± 0.6	155.7 ± 0.3	-40.6 ± 0.2	9.3 ± 0.5	152.1 ± 0.5
234.4	289.5 ± 1.0	-1.1 ± 1.2	-43.2 ± 1.1	406.2 ± 2.0	168.4 ± 0.6	-45.9 ± 0.8	-6.0 ± 1.1	225.7 ± 0.8
244.1	286.9 ± 1.0	-3.2 ± 1.0	-23.3 ± 1.0	413.7 ± 1.5	174.4 ± 0.6	-39.2 ± 0.5	0.4 ± 1.3	215.9 ± 0.9

Table F.4: SO - Impedance Values at 53 m/s and 0.7 MPa

Freq.	Re(H_{xx})	Re(H_{xy})	Re(H_{yx})	Re(H_{yy})	Im(H_{xx})	Im(H_{xy})	Im(H_{yx})	Im(H_{yy})
Hz	MN/m	MN/m	MN/m	MN/m	MN/m	MN/m	MN/m	MN/m
9.8	138.5 ± 0.2	25.0 ± 0.3	-51.4 ± 0.2	138.5 ± 0.5	11.1 ± 0.2	-2.7 ± 0.4	5.0 ± 0.4	11.4 ± 0.5
19.5	138.9 ± 0.1	26.6 ± 0.2	-49.5 ± 0.1	135.5 ± 0.4	19.0 ± 0.1	-4.4 ± 0.2	3.8 ± 0.2	16.5 ± 0.5
29.3	140.1 ± 0.2	22.9 ± 0.1	-50.0 ± 0.2	147.4 ± 0.3	27.2 ± 0.2	-7.5 ± 0.3	2.8 ± 0.2	24.6 ± 0.6
39.1	141.7 ± 0.2	26.5 ± 0.1	-47.8 ± 0.1	138.7 ± 0.2	35.9 ± 0.2	-11.9 ± 0.3	2.0 ± 0.2	35.9 ± 0.5
48.8	143.0 ± 0.2	24.3 ± 0.3	-48.3 ± 0.2	138.8 ± 0.4	45.2 ± 0.2	-16.7 ± 0.4	0.9 ± 0.2	48.5 ± 0.4
58.6	144.1 ± 0.2	23.4 ± 0.2	-48.1 ± 0.1	139.4 ± 0.2	53.9 ± 0.2	-18.6 ± 0.2	-2.0 ± 0.2	56.7 ± 0.5
68.4	146.3 ± 0.1	23.1 ± 0.2	-47.1 ± 0.1	144.6 ± 0.5	62.8 ± 0.3	-14.0 ± 0.1	2.1 ± 0.2	69.5 ± 0.4
78.1	146.8 ± 0.2	25.8 ± 0.1	-42.5 ± 0.3	140.5 ± 0.3	69.6 ± 0.2	-19.1 ± 0.2	-6.1 ± 0.2	73.4 ± 0.4
87.9	149.3 ± 0.3	20.1 ± 0.3	-42.9 ± 0.3	156.0 ± 0.3	75.5 ± 0.2	-17.7 ± 0.2	0.6 ± 0.4	67.6 ± 0.4
97.7	154.0 ± 0.3	21.0 ± 0.2	-50.9 ± 0.1	152.6 ± 0.3	85.6 ± 0.3	-25.6 ± 0.2	-2.6 ± 0.2	96.3 ± 0.6
107.4	154.7 ± 0.1	19.4 ± 0.3	-48.8 ± 0.1	157.8 ± 0.2	91.7 ± 0.1	-25.2 ± 0.2	0.0 ± 0.2	101.4 ± 0.5
117.2	156.4 ± 0.1	19.4 ± 0.2	-46.8 ± 0.1	159.9 ± 0.2	98.9 ± 0.1	-27.0 ± 0.1	-2.4 ± 0.1	110.7 ± 0.3
127.0	157.3 ± 0.1	18.3 ± 0.2	-47.6 ± 0.4	161.8 ± 0.2	103.3 ± 0.1	-27.0 ± 0.1	-5.9 ± 0.2	114.0 ± 0.3
136.7	159.3 ± 0.2	19.2 ± 0.1	-38.3 ± 0.2	169.3 ± 0.2	116.0 ± 0.2	-27.5 ± 0.1	9.0 ± 0.0	120.5 ± 0.3
146.5	160.6 ± 0.1	18.8 ± 0.2	-39.1 ± 0.2	171.8 ± 0.2	123.7 ± 0.1	-27.0 ± 0.1	5.9 ± 0.2	129.8 ± 0.4
156.3	161.3 ± 0.2	22.8 ± 0.2	-33.8 ± 0.2	169.5 ± 0.2	131.0 ± 0.1	-26.6 ± 0.1	1.4 ± 0.2	134.1 ± 0.3
166.0	162.4 ± 1.1	16.4 ± 0.6	-36.9 ± 1.0	178.4 ± 0.6	137.6 ± 1.1	-30.6 ± 0.7	5.1 ± 1.3	147.2 ± 1.1
175.8	164.0 ± 0.6	16.9 ± 0.2	-27.4 ± 0.5	178.2 ± 0.2	147.8 ± 0.1	-27.0 ± 0.2	8.9 ± 0.7	147.4 ± 0.5
185.5	160.6 ± 0.4	17.0 ± 0.1	-36.7 ± 0.4	181.2 ± 0.3	152.7 ± 0.3	-27.4 ± 0.2	-3.3 ± 0.5	165.7 ± 0.5
195.3	152.2 ± 1.0	17.0 ± 0.4	-58.6 ± 1.5	179.2 ± 1.0	154.3 ± 2.5	-22.8 ± 0.2	-22.2 ± 6.4	168.0 ± 0.6
205.1	165.2 ± 0.2	19.8 ± 0.2	-20.9 ± 0.3	180.1 ± 0.4	176.9 ± 0.1	-21.9 ± 0.1	13.8 ± 0.1	171.7 ± 0.4
214.8	160.2 ± 0.2	31.7 ± 0.1	-16.0 ± 0.3	162.9 ± 0.3	191.0 ± 0.2	-17.8 ± 0.1	11.6 ± 0.3	180.3 ± 0.5
224.6	162.0 ± 0.2	31.8 ± 0.2	-17.7 ± 0.3	206.1 ± 0.2	200.1 ± 0.1	-8.5 ± 0.1	9.1 ± 0.3	161.6 ± 0.6
234.4	163.9 ± 0.3	28.1 ± 0.3	-3.4 ± 0.5	179.7 ± 0.4	232.4 ± 0.9	-18.3 ± 0.1	24.8 ± 0.6	221.2 ± 0.4
244.1	145.0 ± 0.2	26.5 ± 0.3	-29.3 ± 0.2	188.7 ± 0.3	235.4 ± 0.4	-7.3 ± 0.1	17.1 ± 0.2	220.0 ± 0.6

Table F.5: SO - Impedance Values at 53 m/s and 2.1 MPa

Freq.	Re(H_{xx})	Re(H_{xy})	Re(H_{yx})	Re(H_{yy})	Im(H_{xx})	Im(H_{xy})	Im(H_{yx})	Im(H_{yy})
Hz	MN/m	MN/m	MN/m	MN/m	MN/m	MN/m	MN/m	MN/m
9.8	226.4 ± 0.6	-10.6 ± 0.2	-59.6 ± 0.5	270.0 ± 0.9	8.2 ± 0.6	-2.2 ± 0.5	8.9 ± 0.5	9.0 ± 0.9
19.5	227.7 ± 0.1	-8.5 ± 0.3	-57.7 ± 0.3	264.5 ± 0.5	16.7 ± 0.3	-2.9 ± 0.3	3.9 ± 0.2	9.0 ± 0.8
29.3	229.4 ± 0.2	-15.9 ± 0.2	-58.2 ± 0.1	284.1 ± 0.3	24.3 ± 0.2	-5.8 ± 0.2	-1.3 ± 0.1	17.6 ± 0.5
39.1	230.0 ± 0.4	-10.7 ± 0.3	-54.2 ± 0.1	269.4 ± 0.3	31.5 ± 0.3	-8.9 ± 0.2	-4.5 ± 0.4	28.5 ± 0.6
48.8	232.8 ± 0.4	-12.6 ± 0.1	-56.2 ± 0.3	271.3 ± 0.3	38.4 ± 0.2	-13.3 ± 0.3	-5.4 ± 0.2	39.7 ± 0.6
58.6	233.5 ± 0.3	-12.1 ± 0.3	-55.4 ± 0.2	268.9 ± 0.4	45.7 ± 0.4	-12.4 ± 0.7	-6.6 ± 0.1	44.5 ± 0.4
68.4	235.6 ± 0.1	-14.3 ± 0.1	-57.9 ± 0.2	271.7 ± 0.3	52.4 ± 0.2	-12.2 ± 0.2	-11.2 ± 0.2	46.0 ± 0.3
78.1	237.4 ± 0.2	-8.4 ± 0.1	-53.6 ± 0.3	276.0 ± 0.4	61.4 ± 0.1	-9.8 ± 0.1	-11.4 ± 0.2	59.9 ± 0.6
87.9	239.4 ± 0.4	-14.6 ± 0.3	-54.3 ± 0.4	283.9 ± 0.6	62.0 ± 0.4	-8.3 ± 0.1	-9.0 ± 0.2	49.9 ± 0.4
97.7	241.4 ± 0.3	-12.8 ± 0.1	-63.1 ± 0.3	280.7 ± 0.3	74.8 ± 0.3	-16.3 ± 0.1	-18.2 ± 0.4	78.8 ± 0.4
107.4	243.5 ± 0.2	-12.5 ± 0.2	-64.3 ± 0.2	282.0 ± 0.2	79.3 ± 0.2	-15.6 ± 0.2	-17.6 ± 0.2	84.0 ± 0.4
117.2	244.6 ± 0.1	-11.4 ± 0.1	-64.5 ± 0.1	286.4 ± 0.2	85.2 ± 0.1	-16.2 ± 0.2	-20.2 ± 0.2	92.6 ± 0.4
127.0	245.2 ± 0.3	-9.0 ± 0.2	-65.1 ± 0.6	285.5 ± 0.3	91.3 ± 0.2	-15.9 ± 0.1	-22.8 ± 0.3	94.9 ± 0.4
136.7	245.0 ± 0.1	-7.1 ± 0.2	-55.0 ± 0.3	287.5 ± 0.3	94.0 ± 0.3	-15.8 ± 0.0	-9.2 ± 0.3	101.8 ± 0.5
146.5	246.9 ± 0.2	-7.0 ± 0.3	-58.6 ± 0.2	299.2 ± 0.2	101.9 ± 0.2	-16.7 ± 0.2	-10.6 ± 0.3	112.6 ± 0.5
156.3	246.7 ± 0.4	0.4 ± 0.3	-55.4 ± 0.4	298.9 ± 0.3	109.4 ± 0.2	-17.9 ± 0.3	-15.6 ± 0.6	116.9 ± 0.6
166.0	249.0 ± 1.2	-5.6 ± 1.1	-61.2 ± 1.9	300.5 ± 1.7	116.0 ± 1.8	-21.0 ± 1.4	-14.3 ± 1.9	127.7 ± 1.7
175.8	250.9 ± 1.6	-3.3 ± 0.6	-51.4 ± 0.8	300.7 ± 1.1	117.8 ± 0.8	-19.6 ± 0.6	-0.6 ± 1.6	126.8 ± 1.1
185.5	251.4 ± 0.5	0.8 ± 0.5	-60.1 ± 1.2	299.8 ± 0.6	133.4 ± 0.8	-22.0 ± 0.5	-16.3 ± 0.4	147.2 ± 0.6
195.3	240.7 ± 1.4	2.7 ± 0.4	-32.2 ± 1.3	300.4 ± 0.4	134.4 ± 0.7	-18.8 ± 0.2	-14.4 ± 1.8	141.4 ± 0.7
205.1	252.8 ± 0.3	5.0 ± 0.3	-46.9 ± 0.3	302.4 ± 0.7	139.8 ± 0.3	-21.7 ± 0.3	1.8 ± 0.4	156.6 ± 0.4
214.8	249.9 ± 0.2	18.3 ± 0.3	-41.5 ± 0.2	289.7 ± 0.2	151.7 ± 0.4	-21.1 ± 0.2	0.9 ± 0.5	163.0 ± 0.4
224.6	255.8 ± 0.4	13.1 ± 0.3	-51.2 ± 0.3	371.3 ± 0.4	160.3 ± 0.3	-20.7 ± 0.1	6.9 ± 0.4	130.3 ± 0.4
234.4	259.2 ± 0.3	11.7 ± 0.4	-49.7 ± 0.4	306.5 ± 0.5	166.5 ± 0.5	-24.8 ± 0.2	0.2 ± 0.3	201.0 ± 0.5
244.1	255.9 ± 0.1	11.8 ± 0.2	-37.3 ± 0.2	316.2 ± 0.5	176.2 ± 0.5	-20.3 ± 0.2	-4.1 ± 0.5	196.5 ± 0.5

Table F.6: SO - Impedance Values at 53 m/s and 2.9 MPa

Freq.	Re(H_{xx})	Re(H_{xy})	Re(H_{yx})	Re(H_{yy})	Im(H_{xx})	Im(H_{xy})	Im(H_{yx})	Im(H_{yy})
Hz	MN/m	MN/m	MN/m	MN/m	MN/m	MN/m	MN/m	MN/m
9.8	263.1 ± 0.4	-26.1 ± 0.5	-60.8 ± 0.5	332.3 ± 0.4	7.8 ± 0.3	-2.9 ± 0.5	11.0 ± 0.4	9.4 ± 0.7
19.5	264.3 ± 0.1	-23.6 ± 0.4	-60.3 ± 0.2	326.7 ± 0.2	15.7 ± 0.3	-2.1 ± 0.4	2.3 ± 0.1	9.1 ± 0.4
29.3	265.3 ± 0.2	-31.1 ± 0.3	-59.9 ± 0.3	345.9 ± 0.3	22.5 ± 0.1	-4.3 ± 0.4	-3.6 ± 0.2	17.4 ± 0.6
39.1	265.6 ± 0.2	-25.6 ± 0.2	-56.6 ± 0.2	332.4 ± 0.4	29.2 ± 0.3	-5.6 ± 0.2	-7.0 ± 0.1	24.7 ± 0.4
48.8	268.3 ± 0.2	-27.1 ± 0.2	-57.4 ± 0.1	334.8 ± 0.2	36.3 ± 0.2	-9.6 ± 0.4	-7.8 ± 0.1	34.6 ± 0.5
58.6	270.2 ± 0.2	-26.3 ± 0.4	-58.2 ± 0.1	331.9 ± 0.4	42.2 ± 0.3	-9.2 ± 0.3	-9.0 ± 0.2	39.1 ± 0.4
68.4	271.4 ± 0.2	-27.6 ± 0.4	-60.3 ± 0.2	335.6 ± 0.2	48.5 ± 0.2	-7.9 ± 0.2	-11.4 ± 0.2	38.2 ± 0.5
78.1	269.9 ± 0.2	-26.7 ± 0.2	-63.2 ± 0.2	331.6 ± 0.3	59.8 ± 0.1	-0.9 ± 0.1	-10.2 ± 0.2	62.1 ± 0.5
87.9	276.4 ± 0.3	-26.7 ± 0.2	-60.2 ± 0.2	347.0 ± 0.4	58.0 ± 0.3	-4.8 ± 0.1	-13.1 ± 0.2	43.3 ± 0.5
97.7	276.2 ± 0.2	-23.9 ± 0.3	-63.3 ± 0.3	342.1 ± 0.3	69.7 ± 0.4	-12.2 ± 0.3	-20.7 ± 0.3	68.5 ± 0.4
107.4	277.9 ± 0.1	-23.8 ± 0.2	-65.4 ± 0.0	342.8 ± 0.2	74.5 ± 0.1	-11.7 ± 0.2	-21.0 ± 0.1	73.7 ± 0.5
117.2	279.8 ± 0.2	-22.3 ± 0.3	-66.3 ± 0.1	346.6 ± 0.3	79.7 ± 0.1	-12.9 ± 0.2	-23.3 ± 0.1	82.3 ± 0.5
127.0	280.8 ± 0.2	-19.1 ± 0.2	-67.1 ± 0.3	345.2 ± 0.3	85.5 ± 0.2	-12.0 ± 0.2	-25.7 ± 0.1	83.7 ± 0.4
136.7	282.0 ± 0.2	-16.7 ± 0.2	-59.4 ± 0.1	346.6 ± 0.3	87.2 ± 0.2	-11.9 ± 0.1	-13.5 ± 0.3	89.8 ± 0.4
146.5	282.2 ± 0.1	-14.7 ± 0.1	-62.0 ± 0.2	351.0 ± 0.3	93.7 ± 0.1	-12.0 ± 0.0	-14.1 ± 0.1	97.5 ± 0.5
156.3	282.2 ± 0.3	-8.4 ± 0.4	-58.8 ± 0.3	361.3 ± 0.4	100.7 ± 0.3	-14.6 ± 0.3	-19.2 ± 0.2	104.5 ± 0.7
166.0	285.4 ± 1.6	-15.4 ± 2.7	-64.3 ± 1.6	360.7 ± 2.0	107.2 ± 1.1	-19.2 ± 0.8	-18.5 ± 1.8	115.0 ± 3.3
175.8	289.3 ± 1.4	-10.8 ± 0.9	-58.4 ± 1.6	358.4 ± 0.4	104.8 ± 1.3	-16.0 ± 0.2	-0.5 ± 0.8	113.5 ± 0.9
185.5	291.1 ± 0.5	-5.5 ± 0.4	-65.4 ± 1.1	356.9 ± 0.3	125.4 ± 1.0	-20.5 ± 0.2	-20.5 ± 1.0	134.1 ± 0.7
195.3	268.4 ± 1.2	-2.7 ± 0.4	-36.3 ± 0.9	357.8 ± 0.3	121.9 ± 0.9	-17.3 ± 0.3	-20.8 ± 1.6	129.8 ± 0.7
205.1	288.3 ± 0.1	-0.9 ± 0.2	-51.3 ± 0.3	360.4 ± 0.3	126.6 ± 0.1	-20.4 ± 0.3	-3.7 ± 0.2	140.9 ± 0.4
214.8	285.8 ± 0.1	14.1 ± 0.2	-44.4 ± 0.3	343.3 ± 0.3	138.0 ± 0.3	-21.7 ± 0.2	-4.6 ± 0.3	153.4 ± 0.4
224.6	293.5 ± 0.3	4.3 ± 0.2	-58.9 ± 0.3	446.4 ± 0.3	145.8 ± 0.2	-25.9 ± 0.1	1.7 ± 0.5	120.1 ± 0.4
234.4	295.2 ± 0.5	4.6 ± 0.3	-57.5 ± 0.3	375.1 ± 0.4	152.5 ± 0.4	-29.7 ± 0.4	-12.6 ± 0.2	195.0 ± 0.4
244.1	291.5 ± 0.5	5.8 ± 0.2	-39.2 ± 0.5	376.6 ± 0.2	159.1 ± 0.2	-22.5 ± 0.1	-8.3 ± 0.4	183.5 ± 0.6

Table F.7: SO - Impedance Values at 69 m/s and 0.7 MPa

Freq.	Re(H_{xx})	Re(H_{xy})	Re(H_{yx})	Re(H_{yy})	Im(H_{xx})	Im(H_{xy})	Im(H_{yx})	Im(H_{yy})
Hz	MN/m	MN/m	MN/m	MN/m	MN/m	MN/m	MN/m	MN/m
9.8	150.1 ± 0.8	32.8 ± 0.7	-47.8 ± 0.3	157.3 ± 0.6	9.0 ± 0.8	-2.9 ± 0.4	7.3 ± 0.5	11.8 ± 0.7
19.5	151.4 ± 0.2	35.2 ± 0.4	-46.7 ± 0.2	153.6 ± 0.7	19.8 ± 0.4	-4.6 ± 0.4	3.7 ± 0.3	16.6 ± 0.4
29.3	153.4 ± 0.2	30.2 ± 0.4	-49.1 ± 0.3	165.7 ± 0.4	29.9 ± 0.4	-7.6 ± 0.4	1.0 ± 0.2	23.3 ± 0.5
39.1	155.1 ± 0.3	35.6 ± 0.2	-46.5 ± 0.2	156.7 ± 0.3	39.9 ± 0.2	-11.4 ± 0.2	-2.1 ± 0.1	34.2 ± 0.4
48.8	157.3 ± 0.2	34.8 ± 0.2	-47.1 ± 0.2	156.5 ± 0.3	48.2 ± 0.3	-16.9 ± 0.3	-1.9 ± 0.1	46.0 ± 0.4
58.6	158.4 ± 0.4	32.7 ± 0.2	-46.5 ± 0.3	157.8 ± 0.6	56.9 ± 0.6	-18.6 ± 0.5	-5.0 ± 0.2	52.9 ± 0.7
68.4	162.9 ± 0.1	32.7 ± 0.3	-46.9 ± 0.1	160.9 ± 0.4	66.2 ± 0.2	-14.5 ± 0.3	0.3 ± 0.4	67.7 ± 0.6
78.1	163.6 ± 0.5	36.5 ± 0.3	-42.9 ± 0.2	154.4 ± 0.5	72.2 ± 0.2	-20.1 ± 0.4	-7.2 ± 0.1	71.5 ± 0.5
87.9	167.3 ± 0.5	29.6 ± 0.4	-47.6 ± 0.4	171.6 ± 0.5	79.8 ± 0.4	-19.7 ± 0.3	0.0 ± 0.3	65.7 ± 0.5
97.7	169.3 ± 0.3	31.3 ± 0.4	-51.1 ± 0.1	167.9 ± 0.2	90.9 ± 0.2	-28.4 ± 0.1	-2.6 ± 0.4	94.8 ± 0.7
107.4	173.3 ± 0.2	31.5 ± 0.3	-49.6 ± 0.3	169.7 ± 0.2	99.1 ± 0.4	-28.4 ± 0.1	-2.0 ± 0.2	100.7 ± 0.8
117.2	177.8 ± 0.2	30.8 ± 0.4	-48.6 ± 0.3	174.8 ± 0.6	105.0 ± 0.1	-31.0 ± 0.2	-2.3 ± 0.2	109.9 ± 0.4
127.0	180.3 ± 0.3	30.0 ± 0.2	-48.5 ± 0.2	176.4 ± 0.3	107.3 ± 0.4	-33.1 ± 0.2	-2.6 ± 0.2	115.5 ± 0.5
136.7	182.7 ± 0.3	31.1 ± 0.2	-42.2 ± 0.3	183.4 ± 0.4	122.9 ± 0.3	-32.7 ± 0.2	2.7 ± 0.4	122.8 ± 0.4
146.5	184.2 ± 0.2	30.1 ± 0.2	-41.5 ± 0.3	186.8 ± 0.3	128.3 ± 0.1	-33.7 ± 0.2	4.0 ± 0.1	132.5 ± 0.6
156.3	185.8 ± 0.2	35.6 ± 0.2	-37.2 ± 0.2	183.6 ± 0.2	135.1 ± 0.1	-34.2 ± 0.3	-0.1 ± 0.2	138.2 ± 0.4
166.0	187.2 ± 0.3	26.0 ± 0.3	-41.2 ± 0.3	197.7 ± 0.2	139.5 ± 0.5	-37.3 ± 0.2	6.2 ± 0.1	149.4 ± 0.4
175.8	190.1 ± 0.3	28.9 ± 0.2	-32.1 ± 0.3	198.1 ± 0.3	151.7 ± 0.4	-37.1 ± 0.2	7.9 ± 0.4	151.0 ± 0.6
185.5	186.5 ± 0.7	27.7 ± 0.3	-44.5 ± 0.3	200.2 ± 0.6	154.9 ± 0.4	-38.4 ± 0.3	1.5 ± 0.4	174.1 ± 0.6
195.3	198.4 ± 1.5	23.5 ± 0.3	-29.0 ± 0.9	199.5 ± 0.7	142.2 ± 0.5	-38.4 ± 0.3	-21.9 ± 2.4	168.6 ± 0.4
205.1	193.1 ± 0.2	29.4 ± 0.4	-26.2 ± 0.4	204.5 ± 0.5	176.5 ± 0.4	-35.0 ± 0.5	19.4 ± 0.4	173.5 ± 0.5
214.8	187.3 ± 1.5	43.2 ± 0.9	-17.5 ± 1.8	192.3 ± 3.3	191.8 ± 2.0	-33.3 ± 3.4	21.9 ± 1.6	179.1 ± 1.2
224.6	191.2 ± 0.6	39.0 ± 0.4	-16.5 ± 0.4	235.7 ± 0.6	199.7 ± 0.3	-24.9 ± 0.6	16.3 ± 0.6	156.0 ± 0.7
234.4	198.4 ± 0.3	30.0 ± 0.5	-0.7 ± 0.6	213.9 ± 0.5	219.9 ± 0.9	-38.5 ± 0.6	34.9 ± 0.5	216.9 ± 0.7
244.1	182.4 ± 0.3	27.8 ± 0.2	-18.7 ± 0.4	221.3 ± 0.5	229.8 ± 0.4	-25.3 ± 0.6	30.8 ± 0.3	212.4 ± 0.5

Table F.8: SO - Impedance Values at 69 m/s and 2.1 MPa

Freq.	Re(H_{xx})	Re(H_{xy})	Re(H_{yx})	Re(H_{yy})	Im(H_{xx})	Im(H_{xy})	Im(H_{yx})	Im(H_{yy})
Hz	MN/m	MN/m	MN/m	MN/m	MN/m	MN/m	MN/m	MN/m
9.8	232.1 ± 0.9	-3.8 ± 0.7	-58.4 ± 0.5	271.9 ± 1.0	6.8 ± 1.0	-2.8 ± 0.5	12.0 ± 0.7	8.5 ± 1.0
19.5	233.3 ± 0.2	-1.6 ± 0.5	-57.4 ± 0.1	266.9 ± 0.5	16.4 ± 0.6	-2.8 ± 0.5	4.8 ± 0.3	9.4 ± 1.0
29.3	234.7 ± 0.5	-8.5 ± 0.3	-56.1 ± 0.4	284.3 ± 0.3	23.5 ± 0.5	-7.0 ± 0.5	-1.1 ± 0.1	17.1 ± 0.9
39.1	235.3 ± 0.9	-3.5 ± 0.1	-53.9 ± 0.3	272.0 ± 0.4	31.0 ± 0.2	-9.8 ± 0.4	-4.9 ± 0.2	26.6 ± 0.8
48.8	237.3 ± 0.4	-6.0 ± 0.3	-55.1 ± 0.2	273.2 ± 0.4	37.4 ± 0.1	-15.1 ± 0.2	-6.3 ± 0.6	37.1 ± 0.6
58.6	238.8 ± 0.7	-5.1 ± 0.4	-52.7 ± 0.2	270.3 ± 0.6	44.2 ± 0.3	-15.3 ± 0.2	-5.9 ± 0.3	41.7 ± 0.4
68.4	240.7 ± 0.2	-8.2 ± 0.1	-55.5 ± 0.1	273.4 ± 0.5	51.5 ± 0.3	-14.5 ± 0.3	-10.6 ± 0.2	43.9 ± 0.6
78.1	243.2 ± 0.4	-1.9 ± 0.4	-50.7 ± 0.2	276.8 ± 0.4	60.1 ± 0.4	-13.7 ± 0.4	-9.2 ± 0.2	56.6 ± 0.5
87.9	244.6 ± 0.2	-9.0 ± 0.3	-54.3 ± 0.1	284.1 ± 0.4	61.9 ± 0.1	-11.7 ± 0.4	-7.5 ± 0.2	46.7 ± 0.6
97.7	247.4 ± 0.3	-8.1 ± 0.2	-61.6 ± 0.1	280.6 ± 0.4	74.6 ± 0.3	-19.6 ± 0.2	-19.4 ± 0.3	73.9 ± 0.6
107.4	249.0 ± 0.1	-8.3 ± 0.3	-61.4 ± 0.2	282.0 ± 0.4	79.3 ± 0.2	-19.7 ± 0.2	-18.5 ± 0.3	80.3 ± 0.5
117.2	250.8 ± 0.3	-8.4 ± 0.1	-60.8 ± 0.3	286.2 ± 0.6	84.6 ± 0.3	-19.9 ± 0.2	-21.3 ± 0.3	88.6 ± 0.4
127.0	251.2 ± 0.4	-6.2 ± 0.1	-60.2 ± 0.3	285.6 ± 0.2	90.0 ± 0.2	-18.8 ± 0.2	-24.0 ± 0.2	90.4 ± 0.4
136.7	251.4 ± 0.2	-5.0 ± 0.1	-52.7 ± 0.2	288.3 ± 0.3	93.2 ± 0.1	-18.5 ± 0.2	-11.5 ± 0.2	98.4 ± 0.4
146.5	252.8 ± 0.2	-5.8 ± 0.2	-55.3 ± 0.3	298.6 ± 0.5	99.8 ± 0.1	-18.6 ± 0.1	-13.8 ± 0.2	107.2 ± 0.5
156.3	253.0 ± 0.2	1.9 ± 0.2	-53.1 ± 0.1	298.2 ± 0.2	107.1 ± 0.2	-19.2 ± 0.2	-19.8 ± 0.2	112.9 ± 0.4
166.0	255.7 ± 0.1	-4.1 ± 0.1	-60.2 ± 0.1	301.3 ± 0.3	113.5 ± 0.3	-22.3 ± 0.2	-17.5 ± 0.1	123.5 ± 0.5
175.8	260.0 ± 0.5	-3.8 ± 0.2	-54.1 ± 0.4	305.0 ± 0.5	113.0 ± 0.4	-19.8 ± 0.2	-1.0 ± 0.2	121.6 ± 0.4
185.5	258.4 ± 0.5	1.4 ± 0.2	-60.7 ± 0.2	304.3 ± 0.5	127.0 ± 0.2	-22.8 ± 0.3	-18.1 ± 0.5	139.6 ± 0.5
195.3	250.3 ± 0.7	3.0 ± 0.3	-34.2 ± 2.1	306.2 ± 0.6	131.4 ± 1.5	-19.1 ± 0.4	-9.3 ± 0.8	132.2 ± 0.5
205.1	257.9 ± 0.4	4.5 ± 0.4	-49.5 ± 0.4	309.4 ± 1.0	135.4 ± 0.2	-20.3 ± 0.5	0.9 ± 0.5	144.1 ± 0.8
214.8	255.1 ± 0.6	18.2 ± 1.0	-44.7 ± 0.8	296.0 ± 2.5	147.2 ± 1.0	-20.1 ± 2.1	0.6 ± 1.3	149.6 ± 1.7
224.6	259.9 ± 0.4	12.6 ± 0.5	-51.4 ± 1.0	375.2 ± 1.4	155.1 ± 0.9	-19.4 ± 0.7	7.0 ± 0.5	116.1 ± 0.9
234.4	264.2 ± 0.4	11.3 ± 0.3	-50.5 ± 0.6	310.7 ± 0.7	161.9 ± 0.7	-23.4 ± 0.4	0.0 ± 0.3	184.7 ± 0.7
244.1	261.3 ± 0.1	10.1 ± 0.3	-35.9 ± 0.5	319.1 ± 0.5	170.2 ± 0.4	-17.1 ± 0.3	-1.0 ± 0.5	176.8 ± 0.7

Table F.9: SO - Impedance Values at 69 m/s and 2.9 MPa

Freq.	Re(H_{xx})	Re(H_{xy})	Re(H_{yx})	Re(H_{yy})	Im(H_{xx})	Im(H_{xy})	Im(H_{yx})	Im(H_{yy})
Hz	MN/m	MN/m	MN/m	MN/m	MN/m	MN/m	MN/m	MN/m
9.8	269.1 ± 1.0	-20.8 ± 1.0	-61.0 ± 0.2	332.3 ± 0.8	6.3 ± 0.6	-3.0 ± 1.2	13.8 ± 0.5	9.6 ± 0.9
19.5	269.4 ± 0.2	-19.0 ± 0.6	-62.1 ± 0.2	327.1 ± 0.4	15.3 ± 0.3	-3.1 ± 0.7	4.3 ± 0.2	9.1 ± 0.7
29.3	271.2 ± 0.2	-26.3 ± 0.2	-60.9 ± 0.1	346.8 ± 0.3	21.7 ± 0.3	-5.5 ± 0.8	-3.0 ± 0.2	17.3 ± 0.6
39.1	270.0 ± 0.4	-20.7 ± 0.2	-57.2 ± 0.3	333.3 ± 0.4	29.5 ± 0.5	-7.8 ± 0.6	-7.1 ± 0.3	23.6 ± 0.6
48.8	273.1 ± 0.3	-23.0 ± 0.2	-57.7 ± 0.3	335.8 ± 0.5	35.1 ± 0.2	-11.9 ± 0.3	-7.5 ± 0.4	33.2 ± 0.5
58.6	275.4 ± 0.4	-21.9 ± 0.4	-57.5 ± 0.2	333.4 ± 0.7	40.5 ± 0.3	-11.3 ± 0.5	-7.2 ± 0.4	37.2 ± 0.5
68.4	276.1 ± 0.5	-23.2 ± 0.3	-59.2 ± 0.1	335.5 ± 0.8	47.3 ± 0.3	-9.7 ± 0.2	-10.3 ± 0.2	36.4 ± 0.5
78.1	276.0 ± 0.3	-23.0 ± 0.6	-62.2 ± 0.3	332.2 ± 0.4	59.1 ± 0.2	-3.4 ± 0.3	-6.7 ± 0.1	59.9 ± 0.5
87.9	283.3 ± 0.2	-24.4 ± 0.3	-60.8 ± 0.3	348.4 ± 0.4	57.9 ± 0.4	-8.2 ± 0.3	-11.8 ± 0.3	40.6 ± 0.7
97.7	281.8 ± 0.2	-22.4 ± 0.3	-62.5 ± 0.1	342.5 ± 0.4	70.0 ± 0.2	-15.2 ± 0.4	-20.7 ± 0.3	65.1 ± 0.5
107.4	284.3 ± 0.1	-22.7 ± 0.2	-64.4 ± 0.1	343.1 ± 0.3	74.2 ± 0.3	-14.0 ± 0.3	-21.3 ± 0.2	70.0 ± 0.4
117.2	285.8 ± 0.1	-22.3 ± 0.2	-65.1 ± 0.1	347.3 ± 0.4	79.3 ± 0.1	-15.3 ± 0.3	-23.8 ± 0.2	78.0 ± 0.4
127.0	287.0 ± 0.3	-20.0 ± 0.2	-65.1 ± 0.3	345.2 ± 0.3	84.7 ± 0.1	-14.5 ± 0.3	-25.6 ± 0.1	79.7 ± 0.4
136.7	287.3 ± 0.3	-17.9 ± 0.2	-57.0 ± 0.2	346.7 ± 0.2	87.0 ± 0.3	-14.0 ± 0.2	-14.9 ± 0.1	86.2 ± 0.4
146.5	287.1 ± 0.2	-16.1 ± 0.2	-60.2 ± 0.1	350.4 ± 0.3	92.6 ± 0.2	-12.6 ± 0.2	-16.5 ± 0.1	93.0 ± 0.5
156.3	287.3 ± 0.1	-10.0 ± 0.1	-58.0 ± 0.2	360.2 ± 0.3	99.8 ± 0.2	-15.1 ± 0.1	-22.6 ± 0.1	99.7 ± 0.5
166.0	291.0 ± 0.1	-16.4 ± 0.2	-63.7 ± 0.1	361.1 ± 0.3	105.6 ± 0.1	-17.3 ± 0.2	-20.9 ± 0.1	108.6 ± 0.5
175.8	296.5 ± 0.4	-13.8 ± 0.2	-63.8 ± 0.3	361.6 ± 0.5	105.1 ± 0.2	-14.3 ± 0.3	-3.0 ± 0.4	108.0 ± 0.3
185.5	296.3 ± 0.3	-9.2 ± 0.3	-66.7 ± 0.2	362.0 ± 0.5	120.9 ± 0.1	-18.8 ± 0.3	-21.4 ± 0.3	126.2 ± 0.8
195.3	270.9 ± 1.4	-5.1 ± 0.3	-39.1 ± 1.7	362.3 ± 0.6	125.3 ± 1.1	-14.8 ± 0.4	-26.6 ± 1.7	121.5 ± 0.6
205.1	292.4 ± 0.5	-3.5 ± 0.6	-53.7 ± 0.4	365.2 ± 0.9	125.6 ± 0.4	-17.0 ± 0.6	-4.9 ± 0.5	129.9 ± 1.0
214.8	290.9 ± 0.7	12.3 ± 2.2	-46.8 ± 1.3	348.4 ± 2.7	137.6 ± 1.1	-18.2 ± 2.2	-5.2 ± 1.4	138.5 ± 3.0
224.6	298.0 ± 0.8	1.6 ± 0.8	-61.8 ± 1.2	450.7 ± 1.3	144.1 ± 0.7	-20.6 ± 1.1	2.2 ± 0.8	103.2 ± 1.2
234.4	300.4 ± 0.2	2.2 ± 0.6	-56.6 ± 0.8	374.2 ± 0.6	152.4 ± 0.4	-23.0 ± 0.6	-12.2 ± 0.5	174.8 ± 0.8
244.1	297.2 ± 0.4	3.3 ± 0.3	-39.4 ± 0.5	376.3 ± 0.5	157.3 ± 0.3	-15.7 ± 0.4	-8.1 ± 0.5	161.6 ± 0.7

Table F.10: SO - Impedance Values at 85 m/s and 0.7 MPa

Freq.	Re(H_{xx})	Re(H_{xy})	Re(H_{yx})	Re(H_{yy})	Im(H_{xx})	Im(H_{xy})	Im(H_{yx})	Im(H_{yy})
Hz	MN/m	MN/m	MN/m	MN/m	MN/m	MN/m	MN/m	MN/m
9.8	163.7 ± 0.5	36.8 ± 1.1	-47.9 ± 0.5	173.8 ± 0.5	20.0 ± 0.5	-0.4 ± 0.5	-3.0 ± 0.4	8.7 ± 0.5
19.5	165.1 ± 0.4	35.1 ± 0.7	-47.8 ± 0.2	174.0 ± 0.6	28.4 ± 0.2	-1.8 ± 0.4	-4.8 ± 0.3	13.4 ± 1.0
29.3	166.0 ± 0.4	40.1 ± 0.6	-47.9 ± 0.2	176.2 ± 0.3	35.1 ± 0.2	-7.5 ± 0.6	-5.1 ± 0.3	24.1 ± 0.5
39.1	171.1 ± 0.3	36.5 ± 0.4	-48.5 ± 0.2	176.4 ± 0.5	42.6 ± 0.2	-7.1 ± 0.5	-5.3 ± 0.1	30.6 ± 0.7
48.8	173.7 ± 0.3	38.5 ± 0.8	-49.4 ± 0.3	174.8 ± 0.7	54.2 ± 0.3	-14.2 ± 0.7	-7.8 ± 0.3	42.5 ± 0.7
58.6	175.4 ± 0.5	39.4 ± 0.7	-49.5 ± 0.6	173.7 ± 1.1	58.8 ± 0.5	-13.3 ± 0.6	-8.7 ± 0.4	45.3 ± 0.9
68.4	182.3 ± 0.4	39.1 ± 0.5	-52.6 ± 0.4	179.8 ± 0.6	70.8 ± 0.3	-16.8 ± 0.5	-3.8 ± 0.5	67.0 ± 0.7
78.1	182.4 ± 0.6	40.8 ± 0.3	-47.6 ± 0.7	175.4 ± 0.9	75.2 ± 0.8	-20.0 ± 1.1	-8.0 ± 0.4	65.3 ± 0.9
87.9	181.9 ± 0.4	38.5 ± 0.7	-51.4 ± 0.6	183.8 ± 0.6	89.5 ± 0.9	-18.7 ± 0.7	-12.3 ± 0.6	59.5 ± 0.5
97.7	192.8 ± 0.4	38.9 ± 0.2	-61.8 ± 0.4	181.7 ± 0.6	92.1 ± 0.5	-29.8 ± 0.5	-2.4 ± 0.4	90.6 ± 0.7
107.4	193.8 ± 0.3	39.1 ± 0.1	-57.7 ± 0.4	182.9 ± 0.6	102.6 ± 0.2	-30.5 ± 0.4	-5.3 ± 0.2	96.6 ± 0.8
117.2	196.5 ± 0.2	38.5 ± 0.3	-55.8 ± 0.3	185.8 ± 0.7	110.2 ± 0.2	-32.3 ± 0.3	-6.6 ± 0.4	104.8 ± 0.7
127.0	195.4 ± 0.4	40.4 ± 0.5	-52.4 ± 0.8	183.6 ± 1.0	120.0 ± 0.3	-32.5 ± 0.5	-15.6 ± 0.5	109.6 ± 0.5
136.7	201.5 ± 0.3	40.1 ± 0.4	-47.8 ± 0.5	193.8 ± 0.7	127.7 ± 0.4	-36.8 ± 0.5	1.2 ± 0.4	120.9 ± 0.6
146.5	204.9 ± 0.4	39.6 ± 0.3	-49.5 ± 0.2	198.5 ± 0.5	135.3 ± 0.2	-37.0 ± 0.3	0.8 ± 0.5	129.9 ± 0.5
156.3	209.0 ± 0.5	48.5 ± 0.2	-44.7 ± 0.4	191.2 ± 0.3	142.8 ± 0.2	-39.5 ± 0.4	-2.9 ± 0.3	138.9 ± 0.4
166.0	212.4 ± 0.6	37.8 ± 0.3	-50.6 ± 0.2	207.5 ± 0.3	147.5 ± 0.2	-46.2 ± 0.6	0.6 ± 0.5	150.9 ± 1.1
175.8	215.9 ± 0.4	35.6 ± 0.5	-43.1 ± 0.7	211.8 ± 0.6	157.0 ± 0.9	-43.9 ± 0.4	4.6 ± 0.3	151.1 ± 1.0
185.5	216.8 ± 0.6	41.0 ± 0.3	-57.2 ± 0.6	208.9 ± 0.8	161.3 ± 0.5	-46.2 ± 0.9	1.5 ± 0.4	174.8 ± 0.7
195.3	210.8 ± 2.1	39.8 ± 1.2	-87.5 ± 1.6	212.5 ± 1.0	172.9 ± 1.9	-43.1 ± 0.6	-18.5 ± 1.2	179.8 ± 1.1
205.1	217.3 ± 0.3	41.7 ± 0.6	-34.8 ± 0.2	218.0 ± 0.3	182.9 ± 0.4	-44.5 ± 0.8	13.3 ± 0.4	178.4 ± 1.1
214.8	220.2 ± 0.4	53.2 ± 0.6	-28.2 ± 0.3	207.2 ± 0.8	198.2 ± 0.3	-45.3 ± 0.6	17.3 ± 0.5	187.2 ± 0.7
224.6	226.6 ± 0.5	54.1 ± 0.1	-29.5 ± 0.5	257.5 ± 0.8	201.4 ± 0.3	-42.4 ± 0.5	20.1 ± 0.5	166.0 ± 0.8
234.4	233.6 ± 0.6	41.4 ± 0.4	-14.1 ± 0.4	237.7 ± 0.4	222.1 ± 0.6	-51.7 ± 0.6	35.4 ± 0.3	223.1 ± 1.1
244.1	225.2 ± 0.5	38.9 ± 0.3	-31.1 ± 0.5	246.3 ± 1.1	233.3 ± 0.8	-42.2 ± 1.1	39.6 ± 0.7	221.6 ± 0.9

Table F.11: SO - Impedance Values at 85 m/s and 2.1 MPa

Freq.	Re(H_{xx})	Re(H_{xy})	Re(H_{yx})	Re(H_{yy})	Im(H_{xx})	Im(H_{xy})	Im(H_{yx})	Im(H_{yy})
Hz	MN/m	MN/m	MN/m	MN/m	MN/m	MN/m	MN/m	MN/m
9.8	241.2 ± 0.4	1.9 ± 0.4	-62.3 ± 0.7	274.6 ± 0.5	9.6 ± 0.6	-2.3 ± 0.4	10.9 ± 0.4	10.1 ± 0.5
19.5	240.9 ± 0.3	5.8 ± 0.7	-62.8 ± 0.3	268.8 ± 0.4	17.8 ± 0.3	-2.9 ± 0.3	4.4 ± 0.5	10.7 ± 1.1
29.3	242.5 ± 0.5	-1.8 ± 0.2	-61.7 ± 0.4	285.8 ± 0.4	23.9 ± 0.5	-6.4 ± 0.8	-1.7 ± 0.4	16.6 ± 0.8
39.1	242.4 ± 0.4	4.7 ± 0.2	-58.4 ± 0.3	272.9 ± 0.6	31.4 ± 0.4	-11.5 ± 0.6	-5.4 ± 0.3	25.4 ± 0.9
48.8	245.3 ± 0.2	1.1 ± 0.6	-59.1 ± 0.5	274.5 ± 0.5	36.8 ± 0.4	-16.6 ± 0.5	-7.1 ± 0.4	37.0 ± 0.6
58.6	245.6 ± 0.1	3.3 ± 0.4	-56.3 ± 0.3	270.8 ± 0.6	44.2 ± 0.5	-16.0 ± 0.8	-5.2 ± 0.2	41.4 ± 0.5
68.4	246.8 ± 0.4	-1.3 ± 0.5	-59.8 ± 0.4	275.9 ± 1.2	50.8 ± 0.3	-15.7 ± 0.5	-9.4 ± 0.2	40.4 ± 0.6
78.1	250.5 ± 0.2	5.2 ± 0.3	-55.6 ± 0.3	276.7 ± 0.6	60.6 ± 0.4	-15.1 ± 0.4	-7.4 ± 0.3	54.9 ± 1.0
87.9	253.2 ± 0.4	-2.6 ± 0.8	-58.2 ± 1.2	284.8 ± 0.6	64.1 ± 0.5	-15.8 ± 0.4	-6.7 ± 0.4	44.3 ± 0.8
97.7	254.1 ± 0.2	-1.4 ± 0.4	-66.2 ± 0.7	280.6 ± 1.0	75.9 ± 0.3	-23.1 ± 0.5	-17.0 ± 0.2	73.4 ± 0.4
107.4	256.3 ± 0.5	-2.1 ± 0.4	-65.4 ± 0.5	282.2 ± 0.8	81.0 ± 0.2	-23.7 ± 0.5	-16.6 ± 0.6	79.3 ± 0.8
117.2	257.7 ± 0.3	-2.1 ± 0.3	-64.1 ± 0.4	284.2 ± 0.7	86.9 ± 0.3	-24.3 ± 0.2	-19.5 ± 0.2	87.0 ± 0.5
127.0	258.4 ± 0.1	-1.1 ± 0.4	-63.7 ± 0.4	284.3 ± 0.2	92.8 ± 0.5	-23.2 ± 0.2	-22.5 ± 0.1	89.9 ± 0.6
136.7	259.5 ± 0.2	-0.6 ± 0.2	-54.6 ± 0.1	287.9 ± 0.3	95.1 ± 0.3	-23.3 ± 0.4	-8.3 ± 0.1	97.1 ± 0.5
146.5	260.6 ± 0.4	-0.8 ± 0.3	-57.5 ± 0.2	296.9 ± 0.4	102.1 ± 0.2	-23.6 ± 0.2	-11.8 ± 0.1	105.1 ± 0.5
156.3	261.5 ± 0.3	5.8 ± 0.3	-56.3 ± 0.2	298.9 ± 0.2	109.9 ± 0.2	-25.2 ± 0.2	-18.6 ± 0.2	112.3 ± 0.4
166.0	264.5 ± 0.1	-0.9 ± 0.2	-63.4 ± 0.2	302.9 ± 0.3	116.5 ± 0.2	-29.5 ± 0.1	-17.1 ± 0.1	127.3 ± 0.6
175.8	269.2 ± 0.3	-0.8 ± 0.5	-54.8 ± 0.6	305.0 ± 0.6	114.6 ± 0.3	-24.7 ± 0.4	-0.2 ± 0.3	121.8 ± 0.8
185.5	268.5 ± 0.4	1.8 ± 0.5	-65.0 ± 0.7	306.7 ± 0.5	130.1 ± 0.5	-29.0 ± 0.3	-18.0 ± 0.5	140.9 ± 0.9
195.3	256.7 ± 2.0	7.3 ± 0.5	-37.7 ± 2.5	305.7 ± 1.1	142.0 ± 1.1	-23.3 ± 0.7	-19.3 ± 2.4	132.8 ± 0.6
205.1	267.2 ± 0.2	6.4 ± 0.4	-52.8 ± 0.2	310.7 ± 0.8	138.2 ± 0.2	-27.0 ± 0.6	1.6 ± 0.3	145.7 ± 0.5
214.8	265.6 ± 0.3	21.1 ± 0.3	-46.8 ± 0.2	295.3 ± 0.5	150.3 ± 0.4	-28.1 ± 0.2	-1.4 ± 0.3	150.9 ± 0.8
224.6	270.8 ± 0.1	14.0 ± 0.4	-55.9 ± 0.5	378.4 ± 0.3	156.9 ± 0.1	-26.5 ± 0.3	5.5 ± 0.6	115.3 ± 0.5
234.4	276.2 ± 0.5	12.1 ± 0.2	-55.1 ± 0.5	316.9 ± 0.8	166.1 ± 0.5	-30.4 ± 0.5	-1.1 ± 0.4	183.4 ± 1.2
244.1	271.1 ± 0.9	10.1 ± 0.3	-42.3 ± 0.6	324.6 ± 0.6	171.6 ± 0.6	-23.8 ± 0.2	-1.2 ± 0.5	174.6 ± 0.7

Table F.12: SO - Impedance Values at 85 m/s and 2.9 MPa

Freq.	Re(H_{xx})	Re(H_{xy})	Re(H_{yx})	Re(H_{yy})	Im(H_{xx})	Im(H_{xy})	Im(H_{yx})	Im(H_{yy})
Hz	MN/m	MN/m	MN/m	MN/m	MN/m	MN/m	MN/m	MN/m
9.8	274.8 ± 1.1	-12.6 ± 0.6	-68.5 ± 0.4	329.7 ± 1.1	5.4 ± 0.8	-2.9 ± 0.6	14.7 ± 0.8	7.6 ± 1.2
19.5	275.5 ± 0.3	-10.4 ± 0.8	-69.0 ± 0.5	324.3 ± 0.8	14.8 ± 0.5	-1.9 ± 0.4	3.8 ± 0.4	8.5 ± 1.0
29.3	277.1 ± 0.5	-17.7 ± 0.5	-66.1 ± 0.5	340.1 ± 0.6	20.5 ± 0.6	-6.5 ± 0.9	-2.6 ± 0.5	16.2 ± 1.0
39.1	275.8 ± 0.5	-12.4 ± 0.5	-62.0 ± 0.5	327.7 ± 0.8	28.5 ± 0.3	-9.7 ± 0.2	-6.5 ± 0.3	25.2 ± 0.7
48.8	278.7 ± 0.6	-14.1 ± 0.7	-60.4 ± 0.4	330.2 ± 0.6	33.5 ± 0.2	-14.6 ± 0.6	-5.8 ± 0.2	34.0 ± 1.2
58.6	279.7 ± 0.4	-12.6 ± 0.6	-60.7 ± 0.3	326.4 ± 0.4	39.3 ± 0.2	-14.1 ± 0.7	-4.3 ± 0.4	36.9 ± 0.6
68.4	280.8 ± 0.4	-15.1 ± 0.3	-62.8 ± 0.3	330.4 ± 0.6	46.9 ± 0.2	-14.4 ± 0.4	-7.8 ± 0.3	37.5 ± 1.0
78.1	280.7 ± 0.7	-12.7 ± 0.3	-66.5 ± 0.5	330.4 ± 0.9	60.0 ± 0.7	-8.2 ± 0.6	-1.7 ± 0.4	60.7 ± 0.8
87.9	286.3 ± 0.3	-17.1 ± 0.4	-63.5 ± 0.5	342.4 ± 0.6	55.9 ± 0.7	-13.6 ± 0.4	-7.6 ± 0.4	41.7 ± 0.7
97.7	286.5 ± 0.2	-15.7 ± 0.4	-67.2 ± 0.1	337.1 ± 0.6	69.3 ± 0.3	-21.7 ± 0.4	-16.6 ± 0.2	67.3 ± 1.0
107.4	288.3 ± 0.2	-16.0 ± 0.1	-67.8 ± 0.1	336.8 ± 0.5	74.0 ± 0.2	-21.0 ± 0.2	-17.3 ± 0.4	72.6 ± 0.8
117.2	290.1 ± 0.2	-15.8 ± 0.2	-67.4 ± 0.3	340.7 ± 0.5	78.8 ± 0.4	-22.7 ± 0.2	-20.1 ± 0.2	80.4 ± 0.9
127.0	291.3 ± 0.1	-14.9 ± 0.4	-67.9 ± 0.3	340.0 ± 0.3	84.7 ± 0.3	-21.7 ± 0.2	-22.7 ± 0.4	82.9 ± 0.5
136.7	292.1 ± 0.2	-14.3 ± 0.3	-58.3 ± 0.3	342.0 ± 0.4	86.4 ± 0.2	-21.7 ± 0.3	-9.1 ± 0.3	89.0 ± 0.5
146.5	291.0 ± 0.1	-13.9 ± 0.4	-60.6 ± 0.2	348.4 ± 0.4	92.1 ± 0.2	-20.5 ± 0.2	-12.3 ± 0.2	96.4 ± 0.3
156.3	291.5 ± 0.2	-10.0 ± 0.3	-60.4 ± 0.3	367.9 ± 0.2	100.5 ± 0.1	-25.6 ± 0.1	-21.6 ± 0.2	110.5 ± 0.5
166.0	294.6 ± 0.3	-15.0 ± 0.3	-64.8 ± 0.2	359.2 ± 0.5	105.3 ± 0.2	-25.1 ± 0.2	-19.1 ± 0.1	114.3 ± 0.5
175.8	302.5 ± 0.5	-13.2 ± 0.2	-64.1 ± 0.5	358.3 ± 0.7	103.8 ± 0.4	-22.4 ± 0.3	2.5 ± 0.3	112.5 ± 0.7
185.5	301.7 ± 0.2	-8.9 ± 0.2	-67.1 ± 0.8	358.1 ± 1.0	119.2 ± 0.3	-25.8 ± 0.4	-19.2 ± 0.3	131.1 ± 0.6
195.3	292.6 ± 2.0	-3.5 ± 0.4	-60.6 ± 1.9	358.4 ± 0.6	152.9 ± 2.6	-23.6 ± 0.3	-48.9 ± 2.6	128.6 ± 0.6
205.1	295.6 ± 0.5	-3.8 ± 0.3	-53.2 ± 0.3	363.9 ± 0.4	125.5 ± 0.1	-23.8 ± 0.3	-2.8 ± 0.4	136.1 ± 0.5
214.8	294.6 ± 0.4	9.8 ± 0.5	-47.9 ± 0.2	347.4 ± 0.4	136.4 ± 0.6	-25.6 ± 0.3	-5.6 ± 0.4	144.3 ± 0.6
224.6	301.8 ± 0.5	-0.3 ± 0.5	-62.1 ± 0.3	446.6 ± 0.4	143.1 ± 0.3	-25.7 ± 0.6	4.4 ± 0.5	105.4 ± 0.6
234.4	303.4 ± 0.4	0.3 ± 0.3	-61.1 ± 0.5	377.6 ± 0.5	152.8 ± 0.2	-28.9 ± 0.4	-11.8 ± 0.7	177.8 ± 0.7
244.1	301.0 ± 0.3	0.5 ± 0.4	-40.2 ± 0.2	379.3 ± 0.9	156.4 ± 0.3	-20.8 ± 0.3	-5.4 ± 0.7	162.6 ± 1.1

Table F.13: LEG - Impedance Values at 38 m/s and 0.7 MPa

Freq.	Re(H_{xx})	Re(H_{xy})	Re(H_{yx})	Re(H_{yy})	Im(H_{xx})	Im(H_{xy})	Im(H_{yx})	Im(H_{yy})
Hz	MN/m	MN/m	MN/m	MN/m	MN/m	MN/m	MN/m	MN/m
9.8	127.5 ± 1.0	17.5 ± 0.7	-59.8 ± 1.3	129.1 ± 1.0	7.4 ± 1.6	-4.2 ± 0.7	0.0 ± 1.2	12.4 ± 0.5
19.5	128.1 ± 0.4	15.3 ± 0.7	-59.1 ± 0.3	128.6 ± 0.7	16.0 ± 0.3	-5.5 ± 0.7	2.4 ± 0.5	20.0 ± 0.7
29.3	128.1 ± 0.7	16.4 ± 0.6	-59.3 ± 0.7	130.2 ± 0.8	26.7 ± 0.4	-9.4 ± 0.7	0.5 ± 0.5	27.9 ± 1.1
39.1	128.5 ± 0.8	18.7 ± 1.0	-59.7 ± 0.5	130.2 ± 0.5	36.3 ± 1.0	-14.1 ± 0.4	1.2 ± 0.5	37.0 ± 0.4
48.8	130.4 ± 0.3	15.6 ± 0.5	-58.7 ± 0.7	133.5 ± 0.7	43.8 ± 0.7	-18.7 ± 0.7	1.3 ± 0.5	47.2 ± 1.2
58.6	130.4 ± 0.4	15.8 ± 0.7	-58.6 ± 0.4	132.4 ± 0.8	54.8 ± 1.0	-20.6 ± 0.9	1.4 ± 0.4	56.1 ± 0.3
68.4	131.3 ± 0.8	15.1 ± 0.7	-57.9 ± 0.5	141.4 ± 0.9	64.2 ± 1.0	-21.9 ± 0.5	6.0 ± 0.7	69.4 ± 0.4
78.1	131.9 ± 0.3	17.4 ± 0.5	-52.0 ± 0.3	136.2 ± 0.8	74.4 ± 0.5	-27.4 ± 0.6	1.1 ± 1.2	77.8 ± 0.8
87.9	135.3 ± 0.7	13.3 ± 0.4	-55.8 ± 1.4	144.0 ± 0.9	81.3 ± 1.0	-32.7 ± 0.6	2.8 ± 1.5	81.2 ± 1.1
97.7	140.0 ± 0.7	14.1 ± 0.5	-53.4 ± 1.0	147.3 ± 0.9	90.7 ± 0.7	-33.4 ± 0.5	4.4 ± 1.2	94.7 ± 0.6
107.4	141.7 ± 0.3	10.5 ± 0.8	-48.7 ± 0.3	147.2 ± 0.9	98.9 ± 0.6	-35.5 ± 0.8	4.0 ± 0.5	106.2 ± 0.8
117.2	143.1 ± 2.2	6.9 ± 5.2	-48.8 ± 2.3	157.2 ± 7.7	105.5 ± 3.2	-32.6 ± 7.0	5.3 ± 2.7	114.1 ± 3.4
127.0	145.5 ± 0.3	10.5 ± 0.5	-45.1 ± 1.2	155.0 ± 0.3	116.7 ± 0.7	-38.9 ± 0.5	0.4 ± 0.9	121.8 ± 1.0
136.7	148.9 ± 0.3	8.8 ± 0.4	-38.3 ± 0.6	159.7 ± 0.5	124.5 ± 0.3	-40.8 ± 0.3	6.8 ± 0.5	130.8 ± 0.3
146.5	152.4 ± 0.2	10.2 ± 0.4	-38.0 ± 0.6	162.6 ± 0.5	133.9 ± 0.6	-42.4 ± 0.2	5.4 ± 0.4	139.7 ± 0.2
156.3	154.7 ± 0.3	11.9 ± 0.3	-33.9 ± 0.5	161.0 ± 0.4	142.0 ± 0.5	-41.3 ± 0.3	2.8 ± 0.6	148.4 ± 0.5
166.0	158.0 ± 0.4	6.6 ± 0.4	-35.7 ± 0.3	167.3 ± 0.5	150.5 ± 0.8	-45.9 ± 0.5	3.2 ± 0.4	159.0 ± 0.5
175.8	160.1 ± 0.4	9.3 ± 0.2	-29.6 ± 0.8	173.2 ± 0.6	158.7 ± 0.8	-43.8 ± 0.3	4.9 ± 0.4	166.6 ± 0.3
185.5	162.2 ± 1.2	10.8 ± 0.3	-38.2 ± 0.8	181.1 ± 0.9	172.2 ± 0.5	-47.0 ± 0.6	0.4 ± 1.3	183.6 ± 0.6
195.3	154.1 ± 1.7	14.5 ± 0.6	-20.7 ± 1.5	176.1 ± 1.2	179.7 ± 1.5	-43.1 ± 0.5	-11.4 ± 2.4	191.0 ± 1.1
205.1	166.7 ± 0.4	12.4 ± 0.5	-22.6 ± 0.7	185.8 ± 1.0	189.5 ± 0.3	-46.5 ± 0.6	10.6 ± 0.7	199.5 ± 0.9
214.8	168.3 ± 0.6	17.1 ± 1.2	-20.9 ± 0.4	185.7 ± 0.8	203.1 ± 0.5	-46.3 ± 0.6	11.9 ± 0.2	210.3 ± 0.8
224.6	172.9 ± 0.6	25.9 ± 1.2	-16.6 ± 0.7	208.0 ± 1.2	215.7 ± 1.4	-38.4 ± 1.1	12.4 ± 1.3	204.4 ± 1.9
234.4	176.9 ± 5.4	10.4 ± 9.8	-14.2 ± 5.4	189.0 ± 9.8	225.6 ± 3.6	-39.6 ± 13.2	18.2 ± 4.1	239.2 ± 15.6
244.1	171.5 ± 0.7	20.4 ± 1.8	-23.9 ± 2.8	201.0 ± 1.6	249.0 ± 2.7	-47.1 ± 1.7	33.5 ± 1.7	240.1 ± 2.0

Table F.14: LEG - Impedance Values at 38 m/s and 2.1 MPa

Freq.	Re(H_{xx})	Re(H_{xy})	Re(H_{yx})	Re(H_{yy})	Im(H_{xx})	Im(H_{xy})	Im(H_{yx})	Im(H_{yy})
Hz	MN/m	MN/m	MN/m	MN/m	MN/m	MN/m	MN/m	MN/m
9.8	204.6 ± 0.3	-12.4 ± 0.7	-72.0 ± 0.9	243.3 ± 0.3	13.1 ± 1.1	-6.5 ± 0.6	-1.4 ± 1.3	16.3 ± 0.9
19.5	206.5 ± 0.2	-14.2 ± 0.3	-72.3 ± 0.7	241.5 ± 0.7	16.7 ± 0.3	-7.6 ± 0.4	-0.6 ± 0.6	19.2 ± 0.4
29.3	208.5 ± 1.2	-17.2 ± 0.3	-75.5 ± 1.0	250.9 ± 1.0	26.4 ± 1.2	-10.9 ± 0.8	-2.9 ± 0.5	26.8 ± 1.1
39.1	210.0 ± 0.8	-14.2 ± 1.0	-72.7 ± 0.7	246.5 ± 0.5	34.1 ± 0.5	-14.7 ± 0.5	-3.9 ± 1.1	37.9 ± 0.6
48.8	212.1 ± 0.5	-17.9 ± 0.9	-71.2 ± 0.8	252.6 ± 0.9	42.5 ± 1.2	-19.7 ± 0.7	-0.6 ± 1.6	52.3 ± 0.5
58.6	212.5 ± 0.4	-15.7 ± 0.3	-69.1 ± 0.7	250.5 ± 0.7	48.9 ± 0.8	-20.8 ± 0.8	-1.0 ± 0.4	56.7 ± 0.5
68.4	212.8 ± 0.5	-18.4 ± 0.2	-70.5 ± 0.6	254.6 ± 0.9	56.2 ± 1.0	-23.2 ± 0.9	-3.0 ± 0.9	61.4 ± 0.4
78.1	214.7 ± 0.3	-15.6 ± 0.4	-70.1 ± 0.4	258.8 ± 0.5	64.7 ± 0.5	-21.1 ± 0.8	3.0 ± 0.4	81.9 ± 1.0
87.9	218.9 ± 0.4	-18.4 ± 0.4	-68.9 ± 0.2	263.9 ± 0.8	71.2 ± 0.3	-30.9 ± 0.6	1.8 ± 0.3	78.5 ± 0.7
97.7	223.3 ± 0.4	-17.9 ± 0.6	-71.2 ± 0.6	269.2 ± 0.9	79.6 ± 0.8	-32.2 ± 0.7	-0.4 ± 0.6	94.7 ± 0.3
107.4	224.8 ± 0.8	-19.2 ± 0.3	-68.6 ± 0.6	268.6 ± 0.4	86.9 ± 0.7	-33.9 ± 0.7	-3.4 ± 0.4	106.4 ± 0.8
117.2	230.3 ± 6.9	-20.8 ± 2.0	-63.1 ± 1.1	271.5 ± 3.8	97.0 ± 3.3	-43.0 ± 5.4	-9.9 ± 6.8	116.5 ± 3.4
127.0	228.9 ± 0.3	-19.3 ± 0.8	-62.2 ± 0.2	279.1 ± 0.7	100.5 ± 0.7	-37.6 ± 0.4	-3.8 ± 0.7	121.0 ± 0.5
136.7	233.4 ± 0.2	-19.6 ± 0.3	-56.8 ± 0.3	281.6 ± 0.5	107.6 ± 0.3	-40.5 ± 0.2	0.6 ± 0.5	130.1 ± 0.4
146.5	235.4 ± 0.2	-18.2 ± 0.5	-55.0 ± 0.3	285.1 ± 0.4	114.6 ± 0.3	-41.9 ± 0.2	-3.6 ± 0.3	139.0 ± 0.4
156.3	238.1 ± 0.2	-18.0 ± 0.3	-53.3 ± 0.4	292.9 ± 0.3	121.8 ± 0.4	-43.0 ± 0.3	-5.7 ± 0.4	148.3 ± 0.4
166.0	241.5 ± 0.3	-22.2 ± 0.3	-55.3 ± 0.4	297.3 ± 0.4	128.8 ± 0.2	-46.6 ± 0.4	-4.7 ± 0.3	159.5 ± 0.3
175.8	244.1 ± 0.3	-18.3 ± 0.4	-49.9 ± 0.2	300.4 ± 0.5	136.5 ± 0.3	-47.2 ± 0.4	-2.2 ± 0.4	165.7 ± 0.4
185.5	246.8 ± 0.1	-17.4 ± 0.2	-46.9 ± 0.3	306.2 ± 0.6	144.2 ± 0.4	-48.1 ± 0.6	-5.2 ± 0.4	183.2 ± 0.9
195.3	250.2 ± 0.7	-14.7 ± 0.4	-45.3 ± 0.3	310.4 ± 0.7	151.7 ± 0.3	-48.1 ± 0.6	-4.3 ± 0.5	185.8 ± 1.1
205.1	252.5 ± 0.2	-12.3 ± 0.2	-38.4 ± 0.4	320.2 ± 0.8	159.8 ± 0.4	-50.0 ± 0.4	3.4 ± 0.2	199.7 ± 0.9
214.8	257.9 ± 0.5	-11.3 ± 0.6	-35.6 ± 0.7	323.5 ± 1.3	168.9 ± 0.3	-52.4 ± 1.0	-0.4 ± 0.5	207.2 ± 0.5
224.6	260.8 ± 0.6	-5.5 ± 0.8	-34.4 ± 0.8	360.3 ± 0.8	177.4 ± 1.2	-45.0 ± 0.8	-0.5 ± 0.9	193.1 ± 0.8
234.4	266.7 ± 1.0	-13.1 ± 8.5	-36.5 ± 2.1	356.6 ± 12.4	188.1 ± 3.6	-52.0 ± 6.1	10.0 ± 3.8	232.7 ± 5.9
244.1	270.1 ± 0.3	-9.6 ± 1.3	-25.4 ± 1.1	347.3 ± 1.8	198.9 ± 0.8	-63.5 ± 2.3	12.3 ± 0.8	207.9 ± 2.3

Table F.15: LEG - Impedance Values at 38 m/s and 2.9 MPa

Freq.	Re(H_{xx})	Re(H_{xy})	Re(H_{yx})	Re(H_{yy})	Im(H_{xx})	Im(H_{xy})	Im(H_{yx})	Im(H_{yy})
Hz	MN/m	MN/m	MN/m	MN/m	MN/m	MN/m	MN/m	MN/m
9.8	241.6 ± 0.8	-29.9 ± 0.6	-74.1 ± 1.7	306.9 ± 1.9	14.1 ± 0.4	-5.6 ± 0.6	0.2 ± 2.9	13.2 ± 2.2
19.5	244.6 ± 0.7	-30.7 ± 0.7	-75.7 ± 0.3	307.1 ± 0.6	17.4 ± 0.6	-5.4 ± 0.8	-0.3 ± 1.2	15.5 ± 0.7
29.3	247.3 ± 0.5	-34.6 ± 0.6	-77.8 ± 0.7	319.7 ± 0.5	25.0 ± 0.4	-9.3 ± 0.5	-3.4 ± 0.9	22.6 ± 0.5
39.1	250.0 ± 0.4	-31.8 ± 0.4	-77.6 ± 0.5	314.4 ± 0.7	29.5 ± 0.3	-12.5 ± 0.8	-3.5 ± 0.5	32.8 ± 0.6
48.8	250.4 ± 1.0	-33.3 ± 0.3	-74.7 ± 1.0	316.3 ± 1.1	36.6 ± 0.6	-16.7 ± 0.3	-5.2 ± 0.9	44.5 ± 0.7
58.6	252.1 ± 0.5	-33.2 ± 0.4	-74.2 ± 0.5	315.1 ± 1.1	42.3 ± 0.8	-19.2 ± 0.7	-5.0 ± 1.6	49.6 ± 1.1
68.4	251.9 ± 0.5	-33.6 ± 0.8	-74.8 ± 0.6	317.9 ± 1.2	50.3 ± 0.4	-21.2 ± 0.8	-7.1 ± 0.8	57.0 ± 0.5
78.1	252.6 ± 0.4	-36.8 ± 0.9	-75.3 ± 0.8	313.8 ± 1.0	56.5 ± 0.3	-20.1 ± 0.2	-6.2 ± 0.5	71.7 ± 0.5
87.9	258.4 ± 0.4	-33.7 ± 0.3	-75.0 ± 0.3	329.1 ± 0.9	63.5 ± 0.2	-27.9 ± 0.7	-3.5 ± 0.3	71.5 ± 0.7
97.7	261.1 ± 0.8	-32.2 ± 0.3	-77.1 ± 1.4	331.6 ± 0.4	71.9 ± 0.6	-29.7 ± 0.8	-6.6 ± 0.6	86.3 ± 0.7
107.4	264.0 ± 0.7	-33.9 ± 0.7	-74.1 ± 1.0	330.8 ± 1.0	78.7 ± 1.2	-30.9 ± 0.6	-8.3 ± 0.7	95.1 ± 0.5
117.2	268.3 ± 8.0	-49.6 ± 22.4	-64.0 ± 7.9	288.4 ± 40.7	94.9 ± 12.1	-102.7 ± 63	-17.5 ± 10.3	145.5 ± 43.7
127.0	266.5 ± 0.5	-32.9 ± 0.5	-69.7 ± 0.2	340.2 ± 0.5	90.6 ± 0.3	-36.2 ± 0.3	-8.3 ± 0.4	110.3 ± 0.5
136.7	269.2 ± 0.3	-32.0 ± 0.2	-63.8 ± 0.3	341.8 ± 0.2	95.5 ± 0.2	-38.3 ± 0.3	-4.8 ± 0.1	116.9 ± 0.3
146.5	270.9 ± 0.2	-31.8 ± 0.3	-62.7 ± 0.3	347.4 ± 0.5	102.0 ± 0.1	-40.9 ± 0.3	-8.0 ± 0.2	127.6 ± 0.4
156.3	273.4 ± 0.3	-32.3 ± 0.4	-61.6 ± 0.2	359.4 ± 0.6	109.0 ± 0.2	-43.6 ± 0.3	-10.7 ± 0.3	138.4 ± 0.3
166.0	277.1 ± 0.1	-35.9 ± 0.3	-63.1 ± 0.3	357.6 ± 0.4	114.8 ± 0.3	-46.0 ± 0.2	-9.2 ± 0.3	146.6 ± 0.6
175.8	279.3 ± 0.2	-31.8 ± 0.3	-57.6 ± 0.2	360.7 ± 0.3	120.9 ± 0.4	-47.1 ± 0.4	-6.0 ± 0.4	153.1 ± 0.5
185.5	281.7 ± 0.3	-29.4 ± 0.3	-53.6 ± 0.6	365.5 ± 0.8	128.2 ± 0.3	-48.4 ± 0.5	-9.1 ± 0.7	169.4 ± 0.7
195.3	285.0 ± 0.2	-27.2 ± 0.6	-52.2 ± 0.4	370.3 ± 0.9	136.2 ± 0.2	-50.1 ± 0.4	-8.0 ± 0.4	172.2 ± 1.1
205.1	286.4 ± 0.4	-27.5 ± 0.7	-44.9 ± 0.4	380.6 ± 0.5	142.5 ± 0.4	-50.6 ± 0.3	-2.6 ± 0.7	179.8 ± 1.0
214.8	291.0 ± 0.6	-25.5 ± 0.4	-40.6 ± 0.4	381.5 ± 1.0	150.2 ± 0.4	-56.0 ± 0.6	-6.7 ± 0.6	192.9 ± 1.1
224.6	294.7 ± 1.4	-22.8 ± 1.1	-39.1 ± 1.9	429.9 ± 1.8	158.4 ± 1.6	-50.6 ± 1.6	-6.6 ± 1.2	171.4 ± 1.5
234.4	307.0 ± 9.8	-165.7 ± 154	-9.3 ± 29.6	104.0 ± 278	144.3 ± 21.5	114.0 ± 144	-12.2 ± 11.2	212.2 ± 55.8
244.1	301.2 ± 0.5	-22.3 ± 1.2	-31.2 ± 1.0	403.4 ± 1.8	176.1 ± 0.7	-58.1 ± 1.6	0.3 ± 0.7	208.8 ± 1.3

Table F.16: LEG - Impedance Values at 53 m/s and 0.7 MPa

Freq.	Re(H_{xx})	Re(H_{xy})	Re(H_{yx})	Re(H_{yy})	Im(H_{xx})	Im(H_{xy})	Im(H_{yx})	Im(H_{yy})
Hz	MN/m	MN/m	MN/m	MN/m	MN/m	MN/m	MN/m	MN/m
9.8	147.5 ± 2.6	23.5 ± 2.4	-68.7 ± 2.2	150.5 ± 2.0	5.0 ± 3.4	-4.0 ± 0.9	-0.6 ± 2.0	10.1 ± 0.8
19.5	148.9 ± 2.3	22.2 ± 0.9	-65.9 ± 1.1	151.4 ± 0.5	15.1 ± 2.5	-6.4 ± 1.0	0.7 ± 3.0	13.9 ± 2.3
29.3	145.9 ± 2.0	22.1 ± 0.6	-66.6 ± 2.7	156.3 ± 0.8	17.4 ± 2.7	-7.7 ± 1.5	4.0 ± 3.3	24.3 ± 1.2
39.1	150.7 ± 2.5	23.5 ± 1.1	-70.4 ± 2.3	151.9 ± 1.1	34.2 ± 1.2	-10.5 ± 1.2	3.1 ± 2.6	32.2 ± 1.6
48.8	151.4 ± 1.2	23.2 ± 1.1	-66.1 ± 1.1	156.3 ± 2.2	36.6 ± 1.6	-14.8 ± 1.4	0.4 ± 1.1	39.0 ± 1.3
58.6	153.7 ± 1.5	23.3 ± 1.6	-66.5 ± 4.4	155.7 ± 1.1	47.9 ± 0.5	-19.8 ± 0.5	2.1 ± 2.1	48.2 ± 1.3
68.4	152.4 ± 0.9	19.4 ± 0.7	-69.1 ± 1.0	157.9 ± 0.9	54.7 ± 0.5	-19.7 ± 0.9	6.5 ± 0.8	59.2 ± 0.4
78.1	153.9 ± 1.4	25.1 ± 0.6	-57.9 ± 0.8	156.6 ± 1.2	62.7 ± 1.4	-23.6 ± 0.8	5.4 ± 1.1	67.0 ± 0.7
87.9	154.7 ± 0.3	20.8 ± 0.8	-61.0 ± 0.5	164.4 ± 0.5	71.3 ± 0.3	-29.9 ± 0.4	9.7 ± 1.0	66.1 ± 0.5
97.7	159.1 ± 0.8	22.4 ± 0.6	-60.1 ± 0.6	165.8 ± 0.6	78.8 ± 1.0	-32.4 ± 0.5	9.5 ± 1.2	79.8 ± 0.4
107.4	160.3 ± 0.5	21.4 ± 0.6	-55.4 ± 0.6	165.4 ± 0.6	87.3 ± 0.8	-33.4 ± 0.2	10.3 ± 0.6	87.9 ± 0.5
117.2	163.1 ± 0.5	20.8 ± 0.1	-54.5 ± 0.4	168.3 ± 0.3	96.4 ± 0.3	-36.6 ± 0.6	9.5 ± 0.2	94.3 ± 0.5
127.0	163.5 ± 0.5	20.9 ± 0.4	-52.5 ± 0.2	169.5 ± 0.6	103.3 ± 0.6	-38.7 ± 0.4	8.9 ± 0.4	101.8 ± 0.4
136.7	167.9 ± 0.3	19.9 ± 0.4	-47.7 ± 0.4	173.2 ± 0.5	110.0 ± 0.8	-40.7 ± 0.4	12.8 ± 0.5	110.0 ± 0.4
146.5	171.2 ± 0.5	20.9 ± 0.5	-46.4 ± 0.5	174.9 ± 0.8	119.1 ± 0.3	-42.9 ± 0.4	11.4 ± 0.4	119.1 ± 0.8
156.3	172.5 ± 0.4	23.2 ± 0.3	-41.1 ± 0.6	172.6 ± 0.6	126.7 ± 0.5	-42.7 ± 0.4	11.0 ± 0.5	127.8 ± 0.3
166.0	175.0 ± 1.5	16.8 ± 2.7	-41.2 ± 3.1	177.8 ± 2.3	136.6 ± 3.8	-46.8 ± 1.9	12.2 ± 1.6	135.1 ± 2.2
175.8	176.0 ± 0.3	19.9 ± 1.1	-37.8 ± 0.9	182.1 ± 0.8	144.4 ± 0.7	-47.2 ± 0.6	13.0 ± 0.2	146.1 ± 0.8
185.5	181.0 ± 1.1	20.1 ± 0.9	-34.2 ± 1.1	188.2 ± 0.8	157.3 ± 0.3	-48.9 ± 0.6	12.7 ± 0.7	156.1 ± 0.5
195.3	179.7 ± 1.6	25.2 ± 0.7	-34.4 ± 0.8	188.2 ± 0.8	164.7 ± 1.1	-46.8 ± 0.5	18.9 ± 1.2	163.0 ± 0.2
205.1	182.8 ± 0.7	23.8 ± 0.8	-28.3 ± 0.5	194.9 ± 0.5	173.6 ± 0.3	-48.3 ± 0.6	20.0 ± 0.4	170.7 ± 0.7
214.8	183.6 ± 0.2	26.8 ± 0.8	-25.6 ± 0.5	193.9 ± 0.9	189.0 ± 0.5	-50.9 ± 0.3	23.7 ± 0.4	178.6 ± 0.9
224.6	200.1 ± 1.2	36.4 ± 0.6	-6.8 ± 1.2	214.3 ± 1.3	197.2 ± 0.8	-47.5 ± 0.9	16.1 ± 1.8	174.3 ± 0.4
234.4	192.6 ± 0.4	27.9 ± 0.4	-19.5 ± 0.4	202.9 ± 0.7	213.8 ± 0.3	-55.0 ± 0.6	35.3 ± 0.2	197.0 ± 0.4
244.1	189.3 ± 0.5	32.4 ± 0.4	-17.1 ± 1.0	204.6 ± 0.9	231.1 ± 0.5	-52.0 ± 1.0	43.1 ± 0.6	201.2 ± 0.8

Table F.17: LEG - Impedance Values at 53 m/s and 2.1 MPa

Freq.	Re(H_{xx})	Re(H_{xy})	Re(H_{yx})	Re(H_{yy})	Im(H_{xx})	Im(H_{xy})	Im(H_{yx})	Im(H_{yy})
Hz	MN/m	MN/m	MN/m	MN/m	MN/m	MN/m	MN/m	MN/m
9.8	211.2 ± 2.1	-10.4 ± 3.2	-82.2 ± 1.1	240.1 ± 2.9	14.2 ± 3.6	-11.8 ± 1.8	-0.3 ± 1.7	11.8 ± 2.2
19.5	212.9 ± 1.0	-7.8 ± 0.9	-81.2 ± 1.8	239.7 ± 1.0	16.1 ± 2.9	-4.1 ± 1.5	1.1 ± 3.5	19.4 ± 1.4
29.3	209.5 ± 3.1	-9.5 ± 0.9	-83.8 ± 4.2	246.4 ± 0.9	23.3 ± 3.1	-10.5 ± 2.5	-5.6 ± 3.7	24.4 ± 1.7
39.1	216.4 ± 0.8	-9.1 ± 0.8	-85.0 ± 0.7	245.2 ± 1.2	30.2 ± 1.6	-15.8 ± 1.2	4.1 ± 2.1	32.4 ± 1.6
48.8	210.0 ± 2.3	-9.4 ± 1.5	-83.3 ± 4.8	249.5 ± 1.7	40.6 ± 3.4	-20.9 ± 1.4	3.1 ± 3.7	41.4 ± 1.1
58.6	211.2 ± 1.3	-6.9 ± 0.9	-80.4 ± 2.6	243.2 ± 2.0	45.1 ± 2.7	-21.1 ± 0.4	0.8 ± 3.0	49.6 ± 1.9
68.4	215.1 ± 0.9	-8.8 ± 2.1	-83.2 ± 0.6	248.9 ± 1.2	52.6 ± 1.0	-26.5 ± 0.6	-1.8 ± 1.5	54.8 ± 2.8
78.1	217.5 ± 3.0	-7.5 ± 0.7	-79.2 ± 1.6	253.5 ± 0.6	60.1 ± 0.6	-22.9 ± 0.9	5.4 ± 1.6	69.2 ± 1.4
87.9	220.6 ± 0.7	-12.3 ± 1.0	-77.8 ± 0.7	254.3 ± 1.2	65.2 ± 0.4	-33.7 ± 0.7	3.4 ± 0.6	66.6 ± 0.3
97.7	227.4 ± 1.9	-12.4 ± 0.6	-79.6 ± 1.5	257.5 ± 0.6	73.8 ± 1.4	-35.1 ± 1.2	5.4 ± 1.1	79.6 ± 1.2
107.4	225.4 ± 0.3	-13.8 ± 0.8	-76.5 ± 0.5	258.9 ± 1.0	80.2 ± 0.4	-35.9 ± 0.9	3.9 ± 0.7	89.4 ± 0.8
117.2	227.7 ± 0.7	-14.6 ± 0.5	-74.5 ± 0.4	264.4 ± 1.1	84.8 ± 0.4	-39.5 ± 0.5	2.5 ± 1.1	95.1 ± 0.6
127.0	227.7 ± 0.4	-14.7 ± 0.5	-71.2 ± 0.8	265.1 ± 0.5	91.7 ± 0.6	-39.9 ± 0.3	1.2 ± 0.4	101.2 ± 0.5
136.7	232.1 ± 1.1	-15.2 ± 0.3	-67.9 ± 1.1	268.7 ± 0.6	97.9 ± 0.3	-42.8 ± 0.3	4.7 ± 0.7	109.3 ± 0.4
146.5	233.4 ± 0.5	-15.7 ± 0.4	-65.5 ± 0.6	275.2 ± 0.5	104.2 ± 0.4	-43.8 ± 0.6	2.8 ± 0.3	117.1 ± 0.5
156.3	236.3 ± 0.2	-13.6 ± 0.3	-64.7 ± 0.9	275.4 ± 0.9	112.1 ± 0.7	-44.8 ± 0.3	1.3 ± 1.0	126.0 ± 0.3
166.0	238.2 ± 1.7	-17.2 ± 1.9	-63.7 ± 0.8	274.6 ± 3.0	117.3 ± 0.9	-49.9 ± 3.1	3.9 ± 2.0	133.6 ± 1.6
175.8	240.7 ± 0.3	-16.7 ± 0.8	-60.0 ± 0.5	282.0 ± 1.2	124.1 ± 0.6	-47.4 ± 0.9	4.4 ± 0.7	140.5 ± 0.6
185.5	244.0 ± 0.4	-14.3 ± 0.5	-56.5 ± 0.6	285.7 ± 1.0	132.3 ± 0.7	-50.0 ± 0.8	3.4 ± 1.8	156.1 ± 0.8
195.3	245.1 ± 0.9	-11.2 ± 0.3	-51.9 ± 0.7	286.2 ± 0.7	137.9 ± 1.3	-51.2 ± 0.6	3.3 ± 3.6	159.4 ± 1.5
205.1	244.3 ± 0.3	-11.1 ± 0.5	-47.3 ± 0.5	295.7 ± 0.9	147.7 ± 0.7	-52.7 ± 1.2	8.7 ± 0.7	172.0 ± 0.7
214.8	247.7 ± 0.3	-10.2 ± 0.5	-44.2 ± 0.4	295.5 ± 0.9	156.6 ± 0.8	-52.8 ± 0.7	8.7 ± 0.8	172.3 ± 1.0
224.6	250.8 ± 1.3	-6.0 ± 0.6	-43.6 ± 1.0	334.3 ± 0.7	165.7 ± 0.4	-47.7 ± 1.1	6.8 ± 1.2	157.0 ± 1.2
234.4	254.9 ± 0.4	-8.6 ± 0.6	-41.1 ± 0.7	304.5 ± 0.4	174.2 ± 0.5	-53.8 ± 0.7	15.9 ± 0.5	188.3 ± 1.1
244.1	256.4 ± 0.8	-6.3 ± 1.0	-34.0 ± 0.9	308.5 ± 1.5	184.2 ± 0.7	-54.7 ± 1.1	18.2 ± 0.6	192.9 ± 1.6

Table F.18: LEG - Impedance Values at 53 m/s and 2.9 MPa

Freq.	Re(H_{xx})	Re(H_{xy})	Re(H_{yx})	Re(H_{yy})	Im(H_{xx})	Im(H_{xy})	Im(H_{yx})	Im(H_{yy})
Hz	MN/m	MN/m	MN/m	MN/m	MN/m	MN/m	MN/m	MN/m
9.8	239.3 ± 1.7	-23.8 ± 0.9	-85.2 ± 1.7	292.5 ± 1.3	8.0 ± 1.6	-7.5 ± 1.3	2.4 ± 1.6	11.9 ± 2.4
19.5	247.2 ± 1.3	-25.3 ± 1.8	-82.9 ± 0.8	289.2 ± 1.6	13.7 ± 0.6	-6.6 ± 0.8	-1.2 ± 0.6	14.2 ± 0.9
29.3	246.0 ± 2.5	-29.2 ± 1.2	-86.7 ± 2.0	299.9 ± 0.9	21.8 ± 0.9	-10.7 ± 1.1	-3.5 ± 2.5	19.7 ± 0.8
39.1	247.8 ± 0.8	-27.3 ± 0.9	-84.6 ± 0.9	297.8 ± 1.4	24.8 ± 0.7	-13.8 ± 0.5	-2.1 ± 1.6	27.4 ± 2.3
48.8	249.9 ± 1.8	-27.4 ± 0.7	-83.9 ± 1.5	299.5 ± 0.8	37.2 ± 2.3	-19.5 ± 1.3	-1.2 ± 1.9	35.0 ± 2.2
58.6	250.1 ± 1.0	-28.4 ± 0.8	-84.3 ± 1.0	297.0 ± 0.9	35.6 ± 1.1	-19.8 ± 1.3	-7.0 ± 1.5	44.9 ± 1.6
68.4	250.3 ± 1.1	-29.9 ± 0.7	-85.6 ± 1.0	301.7 ± 1.0	45.7 ± 0.9	-23.5 ± 1.0	-4.0 ± 1.0	45.7 ± 0.8
78.1	250.8 ± 0.8	-31.9 ± 0.5	-83.8 ± 0.9	291.7 ± 0.7	52.6 ± 0.6	-25.5 ± 0.6	-7.0 ± 0.6	64.7 ± 1.1
87.9	256.2 ± 0.7	-30.7 ± 1.0	-81.3 ± 1.2	306.1 ± 1.0	56.7 ± 0.4	-32.5 ± 0.4	-3.0 ± 1.0	60.5 ± 0.8
97.7	260.2 ± 0.5	-30.2 ± 1.2	-84.2 ± 0.7	310.0 ± 1.0	65.5 ± 1.0	-32.8 ± 0.8	-5.2 ± 1.4	73.6 ± 1.1
107.4	261.8 ± 1.0	-32.6 ± 0.7	-81.9 ± 0.4	309.7 ± 0.9	68.8 ± 0.5	-34.0 ± 0.7	-5.2 ± 1.0	81.5 ± 0.7
117.2	262.0 ± 0.2	-32.7 ± 0.5	-79.8 ± 0.5	314.6 ± 0.6	75.5 ± 0.5	-37.6 ± 0.5	-7.9 ± 0.5	89.6 ± 0.6
127.0	263.1 ± 0.5	-32.7 ± 0.2	-79.0 ± 0.5	316.4 ± 0.8	79.4 ± 0.7	-37.6 ± 0.6	-8.8 ± 0.6	93.1 ± 0.6
136.7	264.7 ± 0.6	-31.7 ± 0.3	-71.4 ± 0.4	316.9 ± 0.5	85.3 ± 0.2	-39.9 ± 0.3	-5.0 ± 0.3	99.7 ± 0.6
146.5	266.4 ± 0.2	-31.5 ± 0.3	-71.7 ± 0.4	320.9 ± 0.5	91.1 ± 0.3	-42.8 ± 0.5	-7.6 ± 0.3	109.5 ± 0.3
156.3	267.4 ± 0.7	-30.4 ± 0.3	-69.0 ± 0.6	325.1 ± 0.6	97.3 ± 0.5	-42.8 ± 0.5	-8.7 ± 0.8	114.6 ± 0.7
166.0	270.2 ± 2.4	-35.1 ± 1.6	-73.6 ± 1.9	327.4 ± 1.1	102.3 ± 2.5	-46.0 ± 1.9	-5.7 ± 2.5	123.2 ± 1.6
175.8	272.5 ± 0.9	-33.2 ± 1.0	-67.3 ± 0.3	330.1 ± 0.8	108.2 ± 0.2	-47.3 ± 0.7	-3.6 ± 0.8	130.7 ± 1.5
185.5	272.5 ± 0.8	-31.1 ± 0.5	-62.7 ± 1.1	334.7 ± 0.5	114.8 ± 1.1	-47.9 ± 0.3	-5.3 ± 1.0	145.1 ± 0.8
195.3	278.3 ± 1.7	-27.2 ± 0.6	-65.7 ± 2.1	336.3 ± 0.9	124.2 ± 0.4	-49.0 ± 0.4	-10.2 ± 1.1	145.9 ± 0.8
205.1	276.1 ± 0.3	-27.6 ± 0.5	-55.5 ± 0.5	345.3 ± 1.1	128.2 ± 0.5	-49.2 ± 0.6	-1.2 ± 0.4	154.5 ± 0.8
214.8	279.6 ± 0.4	-25.6 ± 0.5	-51.2 ± 0.5	343.5 ± 0.4	137.6 ± 0.5	-53.2 ± 0.5	-4.5 ± 0.3	163.1 ± 0.8
224.6	282.9 ± 0.7	-22.1 ± 0.7	-51.8 ± 2.2	390.0 ± 0.8	144.6 ± 0.5	-49.0 ± 0.5	-4.8 ± 0.9	144.7 ± 1.0
234.4	286.9 ± 0.5	-26.0 ± 1.2	-51.4 ± 1.0	358.8 ± 0.8	152.5 ± 0.4	-57.6 ± 0.4	2.5 ± 0.9	181.0 ± 0.4
244.1	286.2 ± 0.7	-20.9 ± 1.3	-41.6 ± 0.3	355.0 ± 0.6	158.8 ± 1.0	-54.6 ± 0.6	3.2 ± 1.3	179.1 ± 0.7

Table F.19: LEG - Impedance Values at 69 m/s and 0.7 MPa

Freq.	Re(H_{xx})	Re(H_{xy})	Re(H_{yx})	Re(H_{yy})	Im(H_{xx})	Im(H_{xy})	Im(H_{yx})	Im(H_{yy})
Hz	MN/m	MN/m	MN/m	MN/m	MN/m	MN/m	MN/m	MN/m
9.8	159.1 ± 2.8	37.1 ± 2.3	-74.9 ± 2.5	163.1 ± 2.1	10.8 ± 2.9	-4.1 ± 2.3	0.0 ± 1.9	7.2 ± 0.7
19.5	163.1 ± 3.8	36.5 ± 2.2	-76.3 ± 2.8	166.2 ± 2.0	13.3 ± 2.5	-4.2 ± 3.1	3.8 ± 2.4	11.7 ± 1.5
29.3	161.3 ± 1.8	37.9 ± 1.4	-75.9 ± 2.0	165.6 ± 2.1	20.0 ± 1.9	-8.5 ± 1.8	7.3 ± 2.0	20.6 ± 2.8
39.1	162.8 ± 1.6	38.3 ± 2.0	-77.5 ± 2.7	163.6 ± 1.2	30.6 ± 2.1	-11.8 ± 1.8	-0.3 ± 3.7	27.2 ± 1.9
48.8	167.6 ± 1.5	34.5 ± 1.5	-78.9 ± 2.7	169.1 ± 2.8	32.1 ± 2.2	-15.8 ± 1.9	7.8 ± 1.0	38.0 ± 0.7
58.6	162.6 ± 2.3	40.2 ± 1.6	-74.7 ± 2.5	168.0 ± 2.2	42.8 ± 0.8	-17.9 ± 1.1	4.8 ± 1.6	42.9 ± 2.1
68.4	161.5 ± 2.0	36.5 ± 1.2	-74.3 ± 1.0	167.1 ± 0.9	48.2 ± 0.6	-19.3 ± 0.9	11.0 ± 1.7	53.6 ± 1.7
78.1	164.6 ± 0.9	42.2 ± 0.8	-64.5 ± 1.6	164.1 ± 0.7	55.5 ± 2.0	-25.6 ± 1.6	9.8 ± 0.9	56.5 ± 1.5
87.9	169.5 ± 1.2	39.0 ± 1.1	-72.7 ± 2.0	169.9 ± 1.2	61.7 ± 2.2	-32.6 ± 0.9	11.4 ± 1.3	59.8 ± 1.1
97.7	169.0 ± 0.9	40.4 ± 0.7	-66.6 ± 1.5	175.9 ± 1.1	72.5 ± 0.8	-32.0 ± 1.4	13.8 ± 0.3	70.6 ± 0.5
107.4	169.9 ± 0.6	37.7 ± 0.5	-64.6 ± 0.7	175.4 ± 0.8	78.2 ± 0.4	-34.0 ± 0.5	15.5 ± 0.7	79.5 ± 0.5
117.2	172.3 ± 0.5	39.3 ± 0.9	-61.2 ± 0.6	177.7 ± 0.6	86.0 ± 0.3	-37.6 ± 0.7	15.6 ± 0.6	82.9 ± 0.9
127.0	174.2 ± 0.4	40.5 ± 0.8	-58.6 ± 0.6	180.3 ± 0.4	93.6 ± 1.5	-40.2 ± 0.3	19.2 ± 0.8	90.4 ± 0.4
136.7	177.1 ± 0.8	40.4 ± 0.5	-51.9 ± 0.8	182.6 ± 0.4	101.8 ± 0.5	-43.2 ± 0.4	21.5 ± 0.7	97.4 ± 0.5
146.5	180.3 ± 1.0	42.0 ± 0.3	-48.5 ± 0.2	182.4 ± 0.3	108.6 ± 0.4	-46.4 ± 0.4	20.9 ± 0.5	104.1 ± 0.3
156.3	181.7 ± 1.1	46.5 ± 0.3	-45.4 ± 0.5	174.3 ± 0.3	117.2 ± 0.3	-46.9 ± 0.5	19.6 ± 0.4	112.7 ± 0.4
166.0	182.9 ± 1.0	37.3 ± 0.5	-43.8 ± 0.3	186.7 ± 0.6	122.7 ± 1.0	-51.5 ± 0.3	23.3 ± 0.6	119.5 ± 0.4
175.8	186.4 ± 0.6	41.9 ± 0.5	-40.0 ± 1.2	190.1 ± 0.6	135.7 ± 0.8	-52.7 ± 0.3	26.3 ± 1.4	128.7 ± 0.9
185.5	190.6 ± 0.8	40.5 ± 1.0	-39.7 ± 1.1	194.5 ± 1.3	137.5 ± 2.3	-55.7 ± 0.7	26.4 ± 3.5	141.1 ± 0.7
195.3	207.6 ± 8.3	50.4 ± 1.2	-22.9 ± 5.2	191.5 ± 1.7	163.0 ± 4.3	-58.8 ± 2.4	21.5 ± 5.4	141.4 ± 1.5
205.1	206.5 ± 0.8	48.0 ± 0.4	-15.8 ± 0.6	199.8 ± 0.6	167.0 ± 0.4	-60.6 ± 0.8	37.5 ± 1.1	150.0 ± 0.7
214.8	207.8 ± 0.7	47.1 ± 0.6	-13.7 ± 1.3	191.9 ± 2.5	163.6 ± 0.5	-65.1 ± 1.1	28.2 ± 2.9	160.2 ± 1.2
224.6	200.7 ± 0.9	63.1 ± 0.5	-15.9 ± 1.2	196.7 ± 1.3	182.4 ± 1.2	-49.8 ± 0.9	34.9 ± 0.4	158.7 ± 0.6
234.4	197.1 ± 0.8	48.0 ± 0.8	-20.2 ± 1.8	209.6 ± 1.8	193.4 ± 1.3	-61.6 ± 0.5	45.1 ± 0.7	186.0 ± 1.0
244.1	221.6 ± 1.8	50.6 ± 0.9	4.9 ± 1.7	207.5 ± 0.9	197.9 ± 1.6	-66.9 ± 1.0	44.6 ± 1.8	192.3 ± 1.1

Table F.20: LEG - Impedance Values at 69 m/s and 2.1 MPa

Freq.	Re(H_{xx})	Re(H_{xy})	Re(H_{yx})	Re(H_{yy})	Im(H_{xx})	Im(H_{xy})	Im(H_{yx})	Im(H_{yy})
Hz	MN/m	MN/m	MN/m	MN/m	MN/m	MN/m	MN/m	MN/m
9.8	209.5 ± 4.9	6.2 ± 3.1	-88.3 ± 3.8	233.4 ± 1.1	2.0 ± 2.6	0.6 ± 2.2	-2.7 ± 2.8	13.6 ± 1.0
19.5	209.5 ± 1.7	6.3 ± 4.4	-86.7 ± 1.9	231.3 ± 4.4	14.7 ± 2.1	-4.5 ± 1.8	4.2 ± 1.7	13.5 ± 0.9
29.3	213.4 ± 3.7	1.4 ± 2.4	-88.5 ± 5.4	239.7 ± 3.7	18.0 ± 2.1	-8.0 ± 2.1	-1.4 ± 3.2	19.7 ± 5.1
39.1	210.3 ± 1.4	8.4 ± 2.3	-89.8 ± 3.3	235.1 ± 1.1	25.3 ± 0.9	-13.8 ± 0.9	-1.7 ± 2.4	31.4 ± 2.4
48.8	209.6 ± 4.4	5.2 ± 1.7	-91.5 ± 2.6	242.7 ± 2.3	36.4 ± 1.2	-19.0 ± 2.0	3.9 ± 3.1	39.9 ± 1.9
58.6	214.9 ± 2.0	8.4 ± 1.3	-86.7 ± 2.0	241.2 ± 2.3	42.0 ± 1.0	-24.1 ± 3.4	5.1 ± 2.7	41.3 ± 2.9
68.4	215.0 ± 1.7	3.3 ± 1.0	-85.3 ± 2.3	239.2 ± 2.4	45.2 ± 0.5	-24.1 ± 1.3	3.2 ± 0.8	46.9 ± 1.7
78.1	214.7 ± 1.9	7.6 ± 1.1	-90.0 ± 1.4	242.3 ± 1.0	51.2 ± 0.9	-24.4 ± 1.6	6.0 ± 1.6	62.3 ± 1.5
87.9	218.3 ± 2.4	4.6 ± 0.7	-79.3 ± 2.5	246.8 ± 0.4	54.9 ± 1.4	-35.5 ± 1.1	9.6 ± 1.4	57.4 ± 1.5
97.7	221.8 ± 1.1	6.2 ± 0.8	-84.9 ± 2.2	249.3 ± 1.2	69.9 ± 0.9	-37.4 ± 0.7	4.6 ± 0.6	68.6 ± 0.9
107.4	222.9 ± 1.2	2.4 ± 0.2	-82.0 ± 1.1	248.1 ± 0.6	74.2 ± 0.6	-39.0 ± 0.7	6.6 ± 0.4	78.0 ± 0.7
117.2	224.9 ± 0.8	2.7 ± 0.5	-81.7 ± 1.2	252.0 ± 0.5	78.9 ± 0.8	-42.6 ± 0.5	4.8 ± 1.0	84.4 ± 0.7
127.0	226.9 ± 0.9	2.3 ± 0.5	-78.9 ± 0.6	251.6 ± 0.7	87.5 ± 0.8	-45.5 ± 0.6	1.3 ± 0.9	90.8 ± 0.5
136.7	229.9 ± 0.5	1.4 ± 0.4	-69.4 ± 0.3	254.0 ± 0.7	89.8 ± 0.6	-47.9 ± 0.4	11.0 ± 1.2	97.5 ± 0.8
146.5	231.0 ± 0.7	1.6 ± 0.4	-68.8 ± 0.9	256.4 ± 0.4	96.6 ± 0.7	-50.2 ± 0.5	10.7 ± 0.3	104.5 ± 0.7
156.3	232.2 ± 0.4	2.2 ± 0.4	-65.6 ± 0.7	262.3 ± 0.6	104.3 ± 0.2	-53.7 ± 0.4	6.8 ± 0.7	113.8 ± 0.5
166.0	234.8 ± 0.7	-4.8 ± 0.4	-68.6 ± 0.9	262.9 ± 0.4	109.1 ± 0.5	-56.3 ± 0.4	7.7 ± 0.6	121.7 ± 0.5
175.8	234.2 ± 0.7	-1.1 ± 1.1	-59.1 ± 1.3	265.2 ± 1.3	114.2 ± 0.5	-55.8 ± 0.4	13.4 ± 0.8	127.4 ± 0.5
185.5	236.9 ± 2.1	0.1 ± 1.0	-62.1 ± 1.6	267.9 ± 0.8	122.3 ± 1.2	-59.9 ± 1.1	9.2 ± 1.4	142.0 ± 0.8
195.3	238.4 ± 3.3	3.8 ± 1.6	-44.7 ± 4.9	263.1 ± 1.3	129.2 ± 2.7	-58.2 ± 1.3	-2.6 ± 2.3	142.6 ± 1.2
205.1	240.3 ± 0.6	0.9 ± 0.8	-49.6 ± 1.1	277.2 ± 1.5	136.5 ± 0.5	-60.4 ± 1.1	19.1 ± 0.8	153.2 ± 0.4
214.8	242.8 ± 1.9	2.0 ± 1.2	-46.5 ± 2.4	273.3 ± 2.4	145.6 ± 3.0	-64.8 ± 2.3	19.6 ± 1.9	160.3 ± 1.2
224.6	246.5 ± 1.3	4.3 ± 0.4	-41.9 ± 0.5	309.7 ± 0.5	154.0 ± 0.9	-58.5 ± 0.8	17.7 ± 1.0	143.2 ± 0.9
234.4	250.2 ± 2.0	0.4 ± 0.7	-41.6 ± 1.3	286.1 ± 0.5	160.4 ± 1.4	-65.7 ± 1.0	28.5 ± 0.9	173.1 ± 0.7
244.1	247.7 ± 1.2	4.8 ± 0.4	-34.7 ± 1.9	287.3 ± 0.5	173.6 ± 1.3	-65.1 ± 0.4	24.8 ± 1.1	179.1 ± 0.6

Table F.21: LEG - Impedance Values at 69 m/s and 2.9 MPa

Freq.	Re(H_{xx})	Re(H_{xy})	Re(H_{yx})	Re(H_{yy})	Im(H_{xx})	Im(H_{xy})	Im(H_{yx})	Im(H_{yy})
Hz	MN/m	MN/m	MN/m	MN/m	MN/m	MN/m	MN/m	MN/m
9.8	243.7 ± 1.5	-17.0 ± 3.2	-93.6 ± 1.4	278.9 ± 3.2	9.7 ± 1.1	-8.3 ± 2.1	4.2 ± 1.3	11.6 ± 1.3
19.5	243.7 ± 1.3	-16.5 ± 1.3	-92.1 ± 1.1	275.8 ± 1.0	9.0 ± 1.3	-4.3 ± 1.7	2.9 ± 0.9	12.3 ± 0.9
29.3	246.0 ± 2.3	-22.5 ± 1.4	-96.4 ± 1.1	290.4 ± 1.7	19.0 ± 2.7	-12.4 ± 0.7	-3.2 ± 3.4	22.6 ± 1.6
39.1	244.0 ± 1.2	-16.2 ± 1.9	-92.2 ± 1.7	284.8 ± 2.1	23.4 ± 2.7	-13.9 ± 1.4	2.7 ± 2.4	23.7 ± 0.9
48.8	245.1 ± 2.0	-18.0 ± 0.7	-95.7 ± 2.5	291.0 ± 2.8	29.3 ± 1.9	-21.4 ± 1.3	1.2 ± 2.1	33.0 ± 1.3
58.6	245.8 ± 1.5	-17.7 ± 1.7	-94.4 ± 1.6	286.3 ± 1.3	33.8 ± 1.2	-22.1 ± 1.2	-0.9 ± 1.0	44.3 ± 1.6
68.4	249.6 ± 1.2	-23.6 ± 0.9	-97.5 ± 1.2	293.3 ± 1.0	39.2 ± 1.4	-25.1 ± 0.6	-1.6 ± 1.5	43.5 ± 1.6
78.1	247.4 ± 1.0	-23.9 ± 1.3	-94.6 ± 1.7	284.9 ± 1.6	43.9 ± 1.5	-25.2 ± 0.3	-2.9 ± 2.6	58.3 ± 1.6
87.9	250.9 ± 1.8	-22.0 ± 0.6	-87.0 ± 1.0	293.5 ± 0.8	51.7 ± 2.0	-32.6 ± 1.2	-1.2 ± 2.5	55.5 ± 0.7
97.7	252.0 ± 0.8	-21.1 ± 0.8	-90.5 ± 2.0	298.0 ± 1.2	62.2 ± 0.8	-36.1 ± 0.9	-1.7 ± 1.7	69.4 ± 1.2
107.4	255.6 ± 0.7	-22.7 ± 0.6	-91.9 ± 0.6	295.1 ± 0.6	67.1 ± 1.1	-37.7 ± 1.0	-3.2 ± 0.9	77.2 ± 1.1
117.2	256.7 ± 0.5	-25.4 ± 0.6	-91.9 ± 0.8	302.5 ± 0.7	70.3 ± 0.3	-40.9 ± 0.8	-4.7 ± 0.7	84.5 ± 0.6
127.0	257.6 ± 0.6	-24.3 ± 0.4	-87.8 ± 1.5	302.6 ± 0.9	74.3 ± 1.2	-41.8 ± 0.4	-3.2 ± 1.0	87.5 ± 0.7
136.7	258.2 ± 0.3	-24.3 ± 0.4	-80.7 ± 1.3	303.2 ± 0.4	80.6 ± 1.4	-44.4 ± 0.3	2.0 ± 1.7	94.4 ± 0.5
146.5	261.0 ± 1.0	-25.6 ± 0.4	-82.2 ± 1.2	307.7 ± 0.3	84.9 ± 0.5	-47.3 ± 0.4	1.0 ± 0.6	101.5 ± 0.5
156.3	262.7 ± 0.5	-26.0 ± 0.3	-80.3 ± 0.4	317.0 ± 0.4	91.4 ± 0.3	-50.5 ± 0.5	-2.1 ± 0.6	111.3 ± 0.6
166.0	264.4 ± 0.3	-30.0 ± 0.4	-82.5 ± 1.1	314.8 ± 0.5	96.5 ± 0.6	-52.1 ± 0.3	-2.7 ± 0.6	118.7 ± 0.7
175.8	264.4 ± 1.1	-26.3 ± 0.8	-72.9 ± 1.4	315.8 ± 0.8	99.8 ± 0.5	-52.4 ± 0.5	6.1 ± 0.8	122.2 ± 1.0
185.5	262.6 ± 2.3	-23.9 ± 0.7	-72.0 ± 3.2	317.7 ± 1.3	107.5 ± 1.3	-53.6 ± 0.8	-2.2 ± 2.6	137.8 ± 1.4
195.3	261.7 ± 6.3	-21.5 ± 0.8	-62.2 ± 7.1	314.7 ± 1.6	116.1 ± 3.7	-56.1 ± 1.7	-16.3 ± 6.0	140.2 ± 2.0
205.1	269.8 ± 0.6	-25.1 ± 1.2	-64.6 ± 1.2	328.1 ± 1.6	121.5 ± 0.7	-58.8 ± 0.8	7.3 ± 0.7	147.5 ± 1.4
214.8	268.5 ± 2.3	-22.9 ± 1.0	-59.8 ± 2.5	325.9 ± 2.1	128.8 ± 4.5	-61.7 ± 2.7	7.8 ± 2.2	155.9 ± 1.0
224.6	274.7 ± 1.0	-23.1 ± 0.8	-60.3 ± 1.4	369.1 ± 0.9	137.7 ± 1.6	-57.7 ± 1.2	5.0 ± 1.3	134.3 ± 0.9
234.4	278.1 ± 0.6	-25.6 ± 0.7	-63.1 ± 2.6	341.7 ± 1.1	142.6 ± 1.9	-65.6 ± 0.8	12.1 ± 0.6	172.2 ± 1.6
244.1	277.2 ± 1.1	-22.0 ± 0.9	-51.4 ± 2.0	336.2 ± 1.4	150.4 ± 0.6	-63.1 ± 0.3	7.9 ± 2.3	170.2 ± 0.6

Table F.22: LEG - Impedance Values at 85 m/s and 0.7 MPa

Freq.	Re(H_{xx})	Re(H_{xy})	Re(H_{yx})	Re(H_{yy})	Im(H_{xx})	Im(H_{xy})	Im(H_{yx})	Im(H_{yy})
Hz	MN/m	MN/m	MN/m	MN/m	MN/m	MN/m	MN/m	MN/m
9.8	188.4 ± 3.0	36.8 ± 2.5	-90.0 ± 0.9	190.6 ± 1.6	8.7 ± 3.5	-9.1 ± 3.5	1.1 ± 2.9	8.5 ± 3.6
19.5	189.7 ± 1.4	35.2 ± 1.4	-90.3 ± 1.9	190.1 ± 0.9	11.6 ± 1.4	-2.4 ± 1.1	0.6 ± 2.0	13.2 ± 2.6
29.3	187.5 ± 1.4	39.2 ± 3.2	-91.6 ± 1.8	196.8 ± 1.6	21.2 ± 1.6	-11.1 ± 1.5	4.2 ± 0.5	17.8 ± 0.6
39.1	190.7 ± 2.0	37.4 ± 2.1	-94.1 ± 1.6	194.2 ± 2.7	27.0 ± 1.0	-12.2 ± 1.1	-0.5 ± 0.9	23.2 ± 1.3
48.8	192.0 ± 0.7	37.8 ± 1.0	-91.9 ± 0.8	195.5 ± 1.7	33.9 ± 0.8	-14.1 ± 1.1	5.2 ± 1.2	31.8 ± 1.3
58.6	189.9 ± 0.9	38.9 ± 0.5	-90.3 ± 0.4	193.8 ± 0.8	38.3 ± 0.7	-18.8 ± 1.6	4.2 ± 0.9	36.2 ± 1.2
68.4	194.6 ± 0.8	40.5 ± 1.2	-87.2 ± 0.8	200.4 ± 1.1	48.3 ± 1.0	-19.8 ± 1.0	11.4 ± 0.5	46.2 ± 0.7
78.1	191.7 ± 0.9	42.6 ± 0.8	-81.9 ± 0.7	190.3 ± 0.9	51.9 ± 1.0	-25.1 ± 0.4	3.0 ± 0.9	55.0 ± 1.3
87.9	193.4 ± 0.6	37.9 ± 0.5	-85.9 ± 0.7	198.8 ± 1.2	56.6 ± 0.8	-30.5 ± 0.4	12.5 ± 1.4	53.8 ± 1.0
97.7	195.7 ± 0.7	41.6 ± 0.6	-84.4 ± 0.4	202.7 ± 0.4	64.0 ± 0.5	-32.1 ± 1.0	13.8 ± 0.3	60.9 ± 0.5
107.4	195.4 ± 0.3	37.4 ± 0.1	-82.0 ± 0.4	202.7 ± 0.9	70.7 ± 0.3	-33.9 ± 0.3	14.2 ± 0.5	69.8 ± 0.7
117.2	196.3 ± 0.5	39.6 ± 0.5	-80.5 ± 0.4	204.0 ± 0.5	78.1 ± 0.3	-37.4 ± 0.7	14.9 ± 0.3	73.3 ± 0.3
127.0	199.6 ± 0.3	43.6 ± 0.3	-78.8 ± 0.3	204.9 ± 0.3	92.9 ± 0.8	-38.1 ± 0.6	16.2 ± 0.6	79.7 ± 0.3
136.7	205.4 ± 0.5	42.7 ± 0.4	-72.8 ± 0.4	208.5 ± 0.3	92.1 ± 0.3	-44.4 ± 0.3	20.4 ± 0.3	86.4 ± 0.4
146.5	205.9 ± 0.3	44.1 ± 0.3	-69.5 ± 0.2	206.9 ± 0.5	98.4 ± 0.6	-47.6 ± 0.3	20.6 ± 0.3	91.8 ± 0.2
156.3	208.1 ± 0.3	51.7 ± 0.4	-65.4 ± 0.2	194.4 ± 0.4	106.1 ± 0.4	-49.9 ± 0.4	19.8 ± 0.3	102.9 ± 0.7
166.0	209.2 ± 0.2	37.3 ± 0.3	-67.0 ± 0.4	209.6 ± 0.4	108.6 ± 0.3	-55.7 ± 0.4	20.6 ± 0.3	108.0 ± 0.7
175.8	204.8 ± 0.6	40.0 ± 0.2	-62.4 ± 0.6	212.7 ± 0.4	114.8 ± 0.4	-54.9 ± 0.7	22.0 ± 0.3	117.5 ± 0.4
185.5	209.4 ± 0.4	42.5 ± 0.5	-61.6 ± 0.4	217.8 ± 0.6	129.2 ± 0.6	-55.9 ± 0.5	27.4 ± 0.6	125.7 ± 0.3
195.3	214.7 ± 1.0	45.4 ± 0.9	-56.7 ± 1.2	213.3 ± 0.8	136.4 ± 1.0	-57.5 ± 0.7	23.9 ± 0.6	131.5 ± 0.7
205.1	205.7 ± 0.8	49.4 ± 0.5	-50.7 ± 0.4	218.4 ± 0.7	154.4 ± 0.7	-55.2 ± 0.5	36.1 ± 0.3	138.8 ± 0.5
214.8	225.6 ± 0.3	56.6 ± 0.6	-41.8 ± 0.6	216.4 ± 0.3	173.2 ± 0.7	-62.3 ± 0.3	39.0 ± 0.5	147.4 ± 0.6
224.6	232.6 ± 0.7	79.0 ± 0.7	-32.4 ± 0.8	208.1 ± 0.7	175.3 ± 0.4	-62.1 ± 0.5	35.7 ± 0.2	159.9 ± 0.6
234.4	241.0 ± 0.6	50.9 ± 0.5	-28.5 ± 0.4	232.4 ± 0.4	184.8 ± 0.5	-69.9 ± 0.7	55.3 ± 0.8	162.5 ± 0.8
244.1	236.4 ± 0.4	56.5 ± 0.6	-28.9 ± 1.2	227.0 ± 0.5	206.6 ± 1.7	-67.5 ± 1.0	70.8 ± 0.3	171.4 ± 0.5

Table F.23: LEG - Impedance Values at 85 m/s and 2.1 MPa

Freq.	Re(H_{xx})	Re(H_{xy})	Re(H_{yx})	Re(H_{yy})	Im(H_{xx})	Im(H_{xy})	Im(H_{yx})	Im(H_{yy})
Hz	MN/m	MN/m	MN/m	MN/m	MN/m	MN/m	MN/m	MN/m
9.8	218.8 ± 1.3	11.0 ± 2.9	-99.5 ± 1.1	231.8 ± 2.7	2.1 ± 2.8	-1.3 ± 3.0	-3.8 ± 2.6	9.5 ± 3.6
19.5	223.3 ± 1.4	15.6 ± 1.1	-93.4 ± 0.6	232.4 ± 1.1	16.3 ± 3.6	-9.6 ± 2.7	5.7 ± 3.2	7.2 ± 2.4
29.3	218.7 ± 1.1	10.8 ± 1.6	-101.5 ± 1.0	243.8 ± 2.2	16.8 ± 2.5	-7.8 ± 1.7	1.0 ± 3.0	20.3 ± 3.5
39.1	220.7 ± 1.8	14.8 ± 2.4	-98.7 ± 3.2	238.8 ± 2.5	22.6 ± 2.1	-15.7 ± 0.4	-0.5 ± 2.5	21.0 ± 2.2
48.8	225.8 ± 2.1	14.1 ± 2.4	-96.4 ± 3.4	241.1 ± 4.3	35.7 ± 0.7	-18.8 ± 1.7	1.1 ± 1.5	35.7 ± 2.6
58.6	218.1 ± 1.6	16.9 ± 2.2	-99.8 ± 1.3	242.3 ± 2.8	34.3 ± 1.2	-17.7 ± 0.7	1.7 ± 1.5	36.2 ± 1.5
68.4	223.0 ± 1.0	11.8 ± 1.3	-100.3 ± 1.5	243.3 ± 2.2	41.7 ± 0.9	-24.0 ± 0.3	6.7 ± 2.6	38.7 ± 2.1
78.1	218.5 ± 1.8	17.1 ± 1.2	-96.7 ± 1.4	246.6 ± 1.1	45.9 ± 0.9	-20.9 ± 0.4	7.0 ± 2.2	56.0 ± 1.2
87.9	220.6 ± 1.4	12.7 ± 0.7	-92.1 ± 1.0	245.9 ± 1.0	52.6 ± 0.9	-31.9 ± 0.5	10.7 ± 2.4	48.3 ± 0.8
97.7	226.7 ± 1.6	14.2 ± 0.7	-95.0 ± 1.3	248.6 ± 1.2	60.4 ± 1.0	-36.9 ± 1.1	6.4 ± 0.6	62.0 ± 0.9
107.4	225.3 ± 0.7	10.8 ± 0.6	-94.8 ± 0.9	247.9 ± 0.5	64.9 ± 0.8	-38.1 ± 0.7	8.6 ± 0.7	69.7 ± 0.8
117.2	226.1 ± 0.4	13.1 ± 0.5	-93.2 ± 0.5	250.5 ± 0.5	74.0 ± 0.5	-42.6 ± 0.5	9.2 ± 0.5	71.5 ± 0.9
127.0	228.2 ± 0.9	12.1 ± 0.6	-92.0 ± 0.6	249.9 ± 0.6	81.6 ± 1.2	-43.3 ± 0.4	8.1 ± 0.3	77.9 ± 0.5
136.7	232.9 ± 0.6	14.2 ± 0.4	-82.3 ± 0.7	250.6 ± 0.3	83.0 ± 0.5	-48.4 ± 0.5	13.9 ± 0.6	84.0 ± 0.3
146.5	233.4 ± 0.6	13.5 ± 0.3	-81.4 ± 0.3	249.1 ± 0.7	89.5 ± 0.9	-51.3 ± 0.5	13.6 ± 0.4	91.2 ± 0.4
156.3	232.8 ± 0.5	12.9 ± 0.5	-79.7 ± 0.7	255.1 ± 0.5	96.6 ± 0.7	-54.7 ± 0.4	12.0 ± 0.6	98.6 ± 0.3
166.0	236.7 ± 1.0	6.6 ± 0.7	-81.7 ± 0.6	257.0 ± 0.6	103.1 ± 0.9	-59.8 ± 0.4	14.4 ± 0.8	107.8 ± 0.3
175.8	237.3 ± 1.5	5.5 ± 1.0	-73.6 ± 1.4	257.0 ± 0.8	104.3 ± 1.1	-58.5 ± 0.8	17.9 ± 0.6	111.3 ± 1.3
185.5	237.4 ± 0.7	10.1 ± 0.4	-73.6 ± 1.0	256.4 ± 1.1	116.2 ± 1.3	-60.8 ± 0.4	13.8 ± 1.0	126.1 ± 0.5
195.3	229.7 ± 2.8	16.3 ± 1.0	-66.6 ± 1.2	255.5 ± 1.0	127.2 ± 3.7	-59.1 ± 1.0	10.5 ± 1.3	126.7 ± 0.8
205.1	237.9 ± 0.5	10.5 ± 0.4	-62.8 ± 0.6	262.9 ± 0.9	129.1 ± 0.5	-65.3 ± 0.5	25.7 ± 0.9	137.6 ± 0.6
214.8	241.1 ± 0.7	16.3 ± 1.1	-58.4 ± 0.9	260.1 ± 0.9	145.2 ± 1.1	-69.1 ± 0.4	24.9 ± 0.9	144.6 ± 0.5
224.6	249.0 ± 0.7	21.7 ± 0.5	-54.6 ± 0.6	283.5 ± 1.1	148.1 ± 0.2	-65.2 ± 0.4	23.5 ± 0.6	129.0 ± 0.5
234.4	256.9 ± 1.1	10.7 ± 1.1	-59.1 ± 2.6	273.8 ± 1.1	151.4 ± 2.5	-76.5 ± 1.0	35.7 ± 1.9	160.1 ± 1.0
244.1	248.8 ± 1.3	13.1 ± 0.9	-50.4 ± 1.0	266.5 ± 0.7	160.7 ± 1.3	-73.5 ± 1.0	32.7 ± 1.2	164.1 ± 1.0

Table F.24: LEG - Impedance Values at 85 m/s and 2.1 MPa

Freq.	Re(H_{xx})	Re(H_{xy})	Re(H_{yx})	Re(H_{yy})	Im(H_{xx})	Im(H_{xy})	Im(H_{yx})	Im(H_{yy})
Hz	MN/m	MN/m	MN/m	MN/m	MN/m	MN/m	MN/m	MN/m
9.8	240.7 ± 0.9	-7.4 ± 1.1	-100.4 ± 1.9	267.3 ± 2.5	3.3 ± 1.5	-5.1 ± 0.9	0.5 ± 2.6	6.8 ± 1.8
19.5	241.1 ± 1.4	-5.3 ± 1.8	-99.3 ± 0.7	266.9 ± 2.2	8.4 ± 1.3	-5.7 ± 1.4	-1.5 ± 2.2	9.1 ± 3.2
29.3	242.7 ± 0.5	-12.3 ± 1.0	-99.1 ± 3.1	273.0 ± 1.2	16.8 ± 0.8	-9.3 ± 0.6	-0.9 ± 1.8	20.1 ± 0.3
39.1	240.4 ± 1.6	-6.2 ± 0.9	-101.9 ± 3.4	270.2 ± 1.6	23.6 ± 1.4	-14.0 ± 1.2	0.7 ± 1.5	27.9 ± 1.7
48.8	243.5 ± 1.3	-10.4 ± 0.5	-101.4 ± 1.2	270.3 ± 1.4	27.2 ± 1.8	-19.0 ± 1.1	-3.5 ± 1.5	35.3 ± 2.0
58.6	242.5 ± 0.7	-7.1 ± 1.5	-103.3 ± 1.6	272.0 ± 1.5	28.8 ± 0.9	-20.9 ± 0.7	0.4 ± 1.5	38.3 ± 1.2
68.4	242.8 ± 0.9	-9.1 ± 1.0	-99.9 ± 1.3	272.2 ± 1.7	34.1 ± 0.9	-22.9 ± 0.8	1.1 ± 2.9	42.9 ± 1.7
78.1	243.7 ± 0.6	-11.2 ± 0.7	-97.9 ± 1.7	264.7 ± 1.4	41.1 ± 0.9	-23.6 ± 1.4	-2.5 ± 0.9	56.8 ± 0.6
87.9	244.7 ± 0.7	-10.7 ± 0.6	-98.2 ± 0.7	279.2 ± 0.9	43.4 ± 2.3	-31.1 ± 0.4	3.2 ± 1.7	54.0 ± 1.3
97.7	247.5 ± 0.7	-8.3 ± 0.5	-99.6 ± 1.5	280.5 ± 0.7	54.4 ± 0.8	-34.5 ± 0.4	3.2 ± 1.3	62.7 ± 0.6
107.4	247.8 ± 0.8	-10.5 ± 0.4	-97.4 ± 0.3	279.6 ± 0.9	58.6 ± 0.5	-36.3 ± 0.3	1.9 ± 0.6	71.9 ± 0.3
117.2	249.0 ± 0.8	-10.0 ± 0.8	-97.1 ± 0.7	283.4 ± 0.4	62.7 ± 0.3	-40.9 ± 0.3	1.7 ± 1.0	76.1 ± 0.6
127.0	249.1 ± 0.8	-10.2 ± 0.3	-95.8 ± 0.4	282.5 ± 0.7	66.0 ± 0.7	-42.7 ± 0.5	-0.8 ± 0.5	81.3 ± 0.5
136.7	249.4 ± 0.5	-8.9 ± 0.2	-86.5 ± 0.5	283.3 ± 0.6	71.3 ± 0.5	-45.7 ± 0.6	8.0 ± 0.2	87.1 ± 0.4
146.5	250.9 ± 0.9	-9.6 ± 0.3	-86.6 ± 0.6	284.3 ± 0.3	76.9 ± 0.4	-49.0 ± 0.3	5.4 ± 0.4	93.4 ± 0.3
156.3	251.3 ± 0.3	-10.3 ± 0.1	-85.5 ± 0.5	296.3 ± 0.4	84.0 ± 0.2	-54.4 ± 0.4	4.1 ± 0.4	103.8 ± 0.5
166.0	253.0 ± 0.5	-15.4 ± 0.4	-88.9 ± 0.7	293.8 ± 0.5	89.1 ± 0.8	-56.7 ± 0.4	4.4 ± 0.4	111.4 ± 0.7
175.8	253.1 ± 0.9	-13.7 ± 0.8	-80.6 ± 0.8	294.2 ± 0.4	87.8 ± 1.4	-56.2 ± 0.4	14.3 ± 1.2	113.1 ± 0.7
185.5	252.9 ± 1.7	-9.6 ± 1.0	-81.1 ± 1.3	294.1 ± 0.9	100.0 ± 0.8	-61.2 ± 0.8	4.0 ± 2.0	128.8 ± 1.2
195.3	246.5 ± 2.7	-7.9 ± 0.9	-75.3 ± 4.5	289.4 ± 0.6	107.4 ± 2.4	-58.4 ± 0.7	-11.2 ± 3.2	129.3 ± 1.5
205.1	255.8 ± 0.3	-11.2 ± 0.6	-68.7 ± 0.5	299.8 ± 0.7	112.3 ± 0.3	-65.1 ± 0.4	13.8 ± 0.5	138.8 ± 1.1
214.8	256.6 ± 0.9	-8.0 ± 1.1	-64.6 ± 0.7	295.5 ± 1.1	119.2 ± 0.5	-69.1 ± 0.7	12.9 ± 0.6	148.3 ± 0.9
224.6	258.9 ± 0.7	-6.1 ± 0.5	-64.4 ± 0.4	334.9 ± 0.8	124.5 ± 0.7	-64.0 ± 1.0	14.5 ± 1.0	124.2 ± 0.9
234.4	263.4 ± 1.3	-14.1 ± 0.9	-66.6 ± 1.7	318.4 ± 1.1	131.2 ± 1.3	-73.1 ± 1.2	25.3 ± 2.1	159.9 ± 1.1
244.1	259.4 ± 1.4	-9.2 ± 0.6	-57.9 ± 1.3	304.0 ± 1.1	138.0 ± 0.9	-71.8 ± 1.0	15.4 ± 1.7	164.0 ± 0.7

Table F.25: SBB - Impedance Values at 38 m/s and 0.7 MPa

Freq.	Re(H_{xx})	Re(H_{xy})	Re(H_{yx})	Re(H_{yy})	Im(H_{xx})	Im(H_{xy})	Im(H_{yx})	Im(H_{yy})
Hz	MN/m	MN/m	MN/m	MN/m	MN/m	MN/m	MN/m	MN/m
9.8	120.1 ± 0.3	22.3 ± 0.7	-61.9 ± 0.4	120.9 ± 0.6	9.0 ± 0.3	-4.5 ± 0.6	3.2 ± 0.5	11.0 ± 1.2
19.5	120.0 ± 0.8	22.4 ± 0.8	-61.9 ± 0.6	121.2 ± 0.7	18.8 ± 0.4	-6.9 ± 0.3	4.2 ± 0.4	20.6 ± 0.8
29.3	120.2 ± 0.5	21.6 ± 0.8	-62.1 ± 0.5	125.6 ± 1.2	27.9 ± 0.3	-10.2 ± 0.5	4.9 ± 0.4	28.2 ± 1.0
39.1	120.8 ± 0.3	25.4 ± 0.8	-61.2 ± 0.4	124.5 ± 0.5	36.7 ± 0.4	-16.1 ± 0.6	4.4 ± 0.4	38.2 ± 1.3
48.8	122.4 ± 0.6	21.7 ± 0.7	-59.6 ± 0.4	125.0 ± 0.8	46.4 ± 0.9	-20.0 ± 1.1	5.8 ± 0.6	48.6 ± 1.1
58.6	123.3 ± 0.3	21.3 ± 0.6	-57.8 ± 0.3	125.9 ± 0.8	56.3 ± 0.3	-21.7 ± 0.6	7.0 ± 0.3	58.6 ± 1.0
68.4	125.1 ± 0.3	21.9 ± 0.4	-54.7 ± 0.3	129.5 ± 0.6	66.6 ± 0.4	-23.0 ± 0.6	11.1 ± 0.7	67.9 ± 0.9
78.1	126.7 ± 0.5	23.4 ± 0.5	-47.3 ± 0.5	127.1 ± 0.9	74.6 ± 0.6	-28.3 ± 0.5	8.0 ± 0.3	73.6 ± 0.8
87.9	130.5 ± 0.6	18.8 ± 0.4	-46.1 ± 0.4	134.5 ± 0.9	82.2 ± 0.9	-34.0 ± 0.4	8.8 ± 0.7	78.1 ± 1.1
97.7	133.7 ± 0.7	18.3 ± 0.6	-49.2 ± 0.5	138.7 ± 0.7	92.3 ± 0.3	-34.6 ± 0.4	10.4 ± 0.4	98.1 ± 0.7
107.4	135.3 ± 0.2	16.0 ± 0.6	-45.1 ± 0.2	140.5 ± 0.5	101.5 ± 0.4	-37.6 ± 0.3	9.4 ± 0.3	104.3 ± 0.9
117.2	138.6 ± 1.5	12.0 ± 2.9	-41.2 ± 1.8	143.1 ± 4.4	111.0 ± 2.1	-42.5 ± 4.9	7.0 ± 0.9	117.1 ± 2.9
127.0	140.3 ± 0.5	13.3 ± 0.3	-38.2 ± 0.2	145.3 ± 0.5	117.8 ± 0.4	-40.5 ± 0.3	2.6 ± 0.1	123.7 ± 0.7
136.7	147.0 ± 0.4	12.0 ± 0.3	-28.4 ± 0.2	152.9 ± 0.5	126.1 ± 0.2	-42.0 ± 0.2	12.8 ± 0.3	130.7 ± 0.8
146.5	149.3 ± 0.2	11.9 ± 0.3	-27.6 ± 0.1	156.1 ± 0.5	134.6 ± 0.2	-41.9 ± 0.2	9.4 ± 0.1	140.1 ± 0.8
156.3	151.0 ± 0.2	14.7 ± 0.3	-24.8 ± 0.2	148.1 ± 0.6	142.7 ± 0.3	-40.4 ± 0.3	4.8 ± 0.1	149.2 ± 0.7
166.0	154.7 ± 0.1	10.4 ± 0.3	-26.3 ± 0.3	161.8 ± 0.6	150.9 ± 0.1	-45.6 ± 0.3	2.7 ± 0.3	162.3 ± 0.8
175.8	159.3 ± 0.2	10.9 ± 0.3	-18.3 ± 0.5	168.9 ± 0.4	157.7 ± 0.3	-44.4 ± 0.3	8.3 ± 0.3	168.7 ± 0.9
185.5	160.8 ± 0.5	12.6 ± 0.6	-25.6 ± 0.4	173.2 ± 0.7	170.0 ± 0.3	-45.0 ± 0.7	1.7 ± 0.6	190.0 ± 1.1
195.3	163.0 ± 1.2	15.0 ± 0.6	-13.7 ± 1.1	170.9 ± 0.7	181.3 ± 1.7	-42.3 ± 0.5	-18.4 ± 1.3	193.0 ± 0.8
205.1	166.8 ± 0.3	15.5 ± 0.8	-10.3 ± 0.4	182.7 ± 0.7	188.2 ± 0.4	-43.5 ± 0.4	12.8 ± 0.5	207.0 ± 1.2
214.8	169.9 ± 0.4	18.7 ± 0.7	-9.0 ± 0.6	182.9 ± 1.1	199.0 ± 0.4	-41.6 ± 0.5	11.0 ± 0.5	212.2 ± 1.4
224.6	174.2 ± 1.4	29.2 ± 0.9	-3.7 ± 1.4	197.5 ± 1.0	209.2 ± 0.3	-26.9 ± 1.2	11.0 ± 0.5	240.4 ± 2.0
234.4	176.4 ± 3.3	20.9 ± 13.0	-15.2 ± 8.8	196.2 ± 10.8	220.5 ± 10.3	-40.5 ± 12.8	10.0 ± 9.8	251.5 ± 19.7
244.1	180.6 ± 1.4	18.6 ± 1.4	-2.3 ± 2.1	203.4 ± 1.7	233.3 ± 0.9	-45.5 ± 1.4	17.5 ± 0.7	245.0 ± 2.9

Table F.26: SBB - Impedance Values at 38 m/s and 2.1 MPa

Freq.	Re(H_{xx})	Re(H_{xy})	Re(H_{yx})	Re(H_{yy})	Im(H_{xx})	Im(H_{xy})	Im(H_{yx})	Im(H_{yy})
Hz	MN/m	MN/m	MN/m	MN/m	MN/m	MN/m	MN/m	MN/m
9.8	212.2 ± 0.9	-13.4 ± 0.6	-75.8 ± 1.3	248.6 ± 1.3	3.5 ± 0.8	-2.9 ± 1.1	1.1 ± 1.5	12.1 ± 1.5
19.5	216.0 ± 1.5	-14.3 ± 0.7	-69.5 ± 0.7	245.7 ± 1.3	14.4 ± 0.6	-7.6 ± 0.8	2.5 ± 0.3	14.8 ± 1.3
29.3	214.2 ± 0.5	-20.9 ± 0.9	-75.4 ± 0.8	260.8 ± 0.7	20.4 ± 0.6	-8.8 ± 0.3	2.2 ± 1.3	22.6 ± 1.3
39.1	214.2 ± 0.4	-15.9 ± 0.5	-71.3 ± 1.0	250.5 ± 0.7	31.7 ± 0.4	-17.2 ± 0.3	0.4 ± 1.0	34.3 ± 1.4
48.8	217.3 ± 1.1	-20.7 ± 1.0	-71.5 ± 1.2	251.0 ± 1.1	38.1 ± 1.0	-21.0 ± 1.2	-0.3 ± 0.5	44.7 ± 0.8
58.6	218.6 ± 0.6	-19.2 ± 0.4	-68.7 ± 0.3	248.6 ± 0.7	40.8 ± 0.3	-23.3 ± 0.6	-4.7 ± 0.9	52.0 ± 1.2
68.4	218.4 ± 0.8	-20.9 ± 0.4	-69.5 ± 0.7	253.9 ± 0.7	47.7 ± 0.8	-23.4 ± 0.8	-4.6 ± 0.8	55.8 ± 1.4
78.1	220.9 ± 0.4	-17.7 ± 0.8	-62.4 ± 0.4	256.3 ± 1.0	58.7 ± 0.7	-24.1 ± 0.5	-2.5 ± 0.3	72.6 ± 0.9
87.9	225.1 ± 2.0	-22.9 ± 0.5	-63.7 ± 1.1	261.7 ± 0.9	60.9 ± 1.1	-29.6 ± 0.5	-7.5 ± 1.4	70.0 ± 0.8
97.7	224.2 ± 0.4	-22.1 ± 0.4	-67.8 ± 0.9	266.1 ± 0.7	72.6 ± 0.9	-32.5 ± 0.4	-5.6 ± 0.4	90.5 ± 1.2
107.4	227.8 ± 0.5	-24.5 ± 0.4	-65.6 ± 0.6	268.1 ± 0.6	78.5 ± 0.8	-34.8 ± 0.7	-6.7 ± 0.6	97.4 ± 0.9
117.2	223.8 ± 6.6	-20.0 ± 2.9	-66.4 ± 6.5	276.3 ± 4.8	79.3 ± 5.7	-32.4 ± 6.6	-1.7 ± 3.6	102.8 ± 5.0
127.0	231.6 ± 0.7	-23.7 ± 0.4	-62.0 ± 0.6	274.3 ± 0.5	89.8 ± 0.6	-37.6 ± 0.3	-13.8 ± 1.0	114.9 ± 0.9
136.7	234.3 ± 0.4	-22.7 ± 0.3	-50.6 ± 0.4	278.3 ± 0.6	96.7 ± 0.5	-38.7 ± 0.2	-4.0 ± 0.4	120.0 ± 0.8
146.5	236.7 ± 0.2	-23.1 ± 0.2	-50.8 ± 0.4	289.0 ± 0.4	103.2 ± 0.1	-41.3 ± 0.2	-6.0 ± 0.2	130.6 ± 0.7
156.3	237.6 ± 0.2	-19.1 ± 0.3	-47.2 ± 0.3	283.8 ± 0.6	110.9 ± 0.3	-41.7 ± 0.3	-9.4 ± 0.3	139.2 ± 0.7
166.0	240.7 ± 0.2	-24.0 ± 0.3	-50.8 ± 0.3	293.9 ± 0.6	117.7 ± 0.3	-46.9 ± 0.3	-13.5 ± 0.3	152.5 ± 0.7
175.8	245.4 ± 0.5	-22.6 ± 0.4	-43.0 ± 0.6	298.8 ± 0.6	119.1 ± 0.7	-45.5 ± 0.2	-7.3 ± 0.6	155.4 ± 0.9
185.5	247.3 ± 0.7	-18.6 ± 0.5	-51.4 ± 0.7	303.7 ± 0.7	135.2 ± 0.6	-50.2 ± 0.6	-18.8 ± 1.0	180.2 ± 0.9
195.3	245.4 ± 2.3	-15.3 ± 0.7	-23.8 ± 1.9	299.9 ± 0.8	141.6 ± 1.5	-46.9 ± 0.6	-29.3 ± 2.6	176.9 ± 1.0
205.1	252.6 ± 0.5	-14.7 ± 0.6	-34.0 ± 0.5	319.5 ± 0.5	144.9 ± 0.3	-51.2 ± 0.6	-7.9 ± 0.5	193.3 ± 0.9
214.8	256.1 ± 0.4	-10.7 ± 0.4	-31.7 ± 0.9	321.1 ± 0.5	152.3 ± 0.5	-51.4 ± 0.2	-10.0 ± 0.6	198.2 ± 1.1
224.6	261.9 ± 1.5	-7.9 ± 1.1	-28.6 ± 1.9	369.3 ± 1.2	160.3 ± 0.7	-47.2 ± 0.3	-10.6 ± 1.2	209.3 ± 1.3
234.4	252.5 ± 16.5	-6.3 ± 7.1	-54.7 ± 30.7	345.9 ± 10.7	176.8 ± 19.4	-56.0 ± 5.5	-24.1 ± 17.1	236.1 ± 6.4
244.1	271.0 ± 2.2	-15.6 ± 1.0	-21.8 ± 2.5	343.3 ± 1.2	175.8 ± 1.6	-61.0 ± 0.5	-9.5 ± 1.9	214.7 ± 0.9

Table F.27: SBB - Impedance Values at 38 m/s and 2.9 MPa

Freq.	Re(H_{xx})	Re(H_{xy})	Re(H_{yx})	Re(H_{yy})	Im(H_{xx})	Im(H_{xy})	Im(H_{yx})	Im(H_{yy})
Hz	MN/m	MN/m	MN/m	MN/m	MN/m	MN/m	MN/m	MN/m
9.8	253.1 ± 0.7	-32.6 ± 0.6	-67.7 ± 1.3	310.1 ± 1.3	7.6 ± 1.2	-2.1 ± 1.3	-0.2 ± 1.1	15.8 ± 1.2
19.5	253.0 ± 0.7	-29.9 ± 0.7	-67.2 ± 0.9	304.4 ± 0.6	13.9 ± 0.6	-3.6 ± 0.5	0.6 ± 0.5	13.2 ± 0.7
29.3	253.1 ± 0.6	-35.9 ± 0.4	-71.9 ± 0.4	325.3 ± 0.4	20.8 ± 0.3	-8.7 ± 0.6	-3.5 ± 0.6	21.0 ± 0.8
39.1	250.0 ± 0.6	-30.6 ± 0.5	-69.1 ± 0.7	315.0 ± 0.7	29.2 ± 0.8	-14.2 ± 0.7	-3.7 ± 0.7	31.5 ± 1.2
48.8	254.1 ± 1.3	-33.4 ± 0.8	-69.8 ± 0.8	317.3 ± 1.1	35.7 ± 1.2	-17.3 ± 0.5	-5.9 ± 0.7	39.5 ± 1.2
58.6	256.3 ± 0.7	-32.0 ± 0.8	-68.9 ± 0.7	315.1 ± 0.8	40.1 ± 1.2	-19.8 ± 1.1	-9.8 ± 0.6	48.2 ± 1.1
68.4	256.9 ± 0.9	-33.0 ± 1.3	-70.4 ± 0.9	319.5 ± 1.3	45.9 ± 0.9	-19.6 ± 0.3	-11.6 ± 0.7	49.1 ± 1.1
78.1	258.3 ± 1.3	-33.9 ± 0.9	-71.6 ± 0.4	317.4 ± 0.6	55.5 ± 0.5	-20.9 ± 0.7	-8.4 ± 0.4	67.4 ± 1.3
87.9	265.2 ± 1.2	-34.1 ± 0.4	-66.9 ± 0.4	328.4 ± 0.7	54.3 ± 1.8	-25.8 ± 0.6	-12.2 ± 0.8	62.9 ± 1.2
97.7	264.6 ± 0.4	-33.6 ± 0.8	-70.5 ± 0.1	330.7 ± 0.6	66.6 ± 0.7	-29.3 ± 0.4	-15.5 ± 0.4	81.4 ± 0.8
107.4	267.5 ± 0.7	-33.6 ± 0.6	-70.6 ± 0.3	330.3 ± 0.5	71.8 ± 0.5	-31.8 ± 0.6	-16.1 ± 0.3	88.0 ± 1.1
117.2	267.9 ± 7.1	-36.0 ± 4.0	-72.6 ± 2.3	333.3 ± 2.9	73.3 ± 4.7	-40.5 ± 5.4	-14.5 ± 7.4	101.9 ± 5.8
127.0	271.6 ± 0.5	-32.7 ± 0.5	-70.6 ± 0.9	336.5 ± 0.5	83.4 ± 0.8	-36.5 ± 0.2	-20.4 ± 0.9	104.5 ± 0.8
136.7	273.9 ± 0.3	-31.9 ± 0.4	-59.2 ± 0.4	340.3 ± 0.5	85.6 ± 0.8	-37.6 ± 0.3	-12.8 ± 0.4	109.8 ± 0.6
146.5	275.3 ± 0.2	-30.8 ± 0.2	-59.6 ± 0.3	346.1 ± 0.5	90.8 ± 0.2	-39.5 ± 0.2	-13.7 ± 0.3	118.9 ± 0.7
156.3	275.4 ± 0.1	-30.1 ± 0.2	-58.2 ± 0.2	353.9 ± 0.5	97.7 ± 0.3	-43.5 ± 0.3	-16.7 ± 0.3	129.7 ± 0.7
166.0	278.4 ± 0.6	-34.6 ± 0.2	-61.6 ± 0.4	358.3 ± 0.5	103.9 ± 0.3	-47.1 ± 0.3	-19.5 ± 0.4	139.0 ± 1.0
175.8	282.8 ± 0.6	-32.4 ± 0.3	-52.3 ± 0.3	360.8 ± 0.5	101.2 ± 0.7	-46.8 ± 0.3	-12.8 ± 0.5	143.8 ± 0.8
185.5	287.1 ± 1.1	-27.8 ± 0.3	-59.5 ± 0.9	364.7 ± 0.7	122.6 ± 0.4	-51.8 ± 0.3	-23.1 ± 0.5	169.1 ± 1.0
195.3	273.2 ± 2.5	-22.8 ± 0.5	-40.2 ± 2.3	363.0 ± 0.9	131.7 ± 3.1	-49.7 ± 0.8	-35.2 ± 2.4	164.9 ± 0.9
205.1	288.4 ± 0.6	-25.6 ± 0.4	-42.7 ± 0.4	380.3 ± 0.7	124.7 ± 0.3	-52.9 ± 0.2	-13.9 ± 0.5	178.4 ± 0.9
214.8	292.0 ± 0.3	-21.8 ± 0.7	-40.0 ± 0.4	384.5 ± 0.5	132.0 ± 0.8	-56.0 ± 0.4	-15.5 ± 0.7	185.7 ± 1.0
224.6	299.5 ± 1.4	-24.6 ± 0.9	-40.0 ± 2.6	444.5 ± 0.8	140.8 ± 1.4	-52.3 ± 0.5	-12.5 ± 1.1	188.1 ± 1.6
234.4	306.7 ± 8.5	-27.0 ± 5.7	-48.0 ± 33.1	407.1 ± 7.7	155.0 ± 24.2	-62.4 ± 4.2	-13.2 ± 13.0	213.5 ± 6.6
244.1	304.4 ± 1.4	-26.2 ± 0.9	-30.9 ± 4.0	406.3 ± 1.1	151.8 ± 1.9	-61.4 ± 0.5	-17.4 ± 0.9	202.3 ± 1.6

Table F.28: SBB - Impedance Values at 53 m/s and 0.7 MPa

Freq.	Re(H_{xx})	Re(H_{xy})	Re(H_{yx})	Re(H_{yy})	Im(H_{xx})	Im(H_{xy})	Im(H_{yx})	Im(H_{yy})
Hz	MN/m	MN/m	MN/m	MN/m	MN/m	MN/m	MN/m	MN/m
9.8	145.0 ± 0.7	28.7 ± 0.5	-74.8 ± 1.0	142.2 ± 0.9	9.2 ± 0.7	-2.1 ± 1.1	3.0 ± 1.6	8.7 ± 1.1
19.5	145.5 ± 0.3	31.0 ± 0.8	-75.3 ± 0.4	141.7 ± 1.2	16.2 ± 0.7	-7.4 ± 1.0	5.0 ± 0.6	14.9 ± 1.3
29.3	144.1 ± 0.4	29.6 ± 0.5	-77.7 ± 0.3	149.5 ± 0.9	22.1 ± 1.1	-10.3 ± 0.6	4.8 ± 0.7	22.1 ± 1.4
39.1	145.3 ± 1.2	32.1 ± 0.8	-75.6 ± 0.9	146.0 ± 1.2	31.6 ± 0.4	-15.4 ± 0.7	5.5 ± 0.6	32.0 ± 1.2
48.8	146.7 ± 0.5	29.0 ± 0.6	-74.1 ± 0.8	144.5 ± 0.8	38.9 ± 0.8	-19.5 ± 0.7	7.6 ± 1.1	40.0 ± 1.3
58.6	145.0 ± 0.7	29.5 ± 1.1	-75.5 ± 0.7	145.5 ± 1.2	46.3 ± 0.9	-20.9 ± 0.9	6.6 ± 0.7	49.9 ± 1.3
68.4	146.5 ± 1.0	30.3 ± 1.7	-72.2 ± 0.7	151.8 ± 1.3	55.1 ± 0.4	-22.9 ± 0.6	14.3 ± 0.5	55.5 ± 1.5
78.1	147.2 ± 0.6	32.2 ± 0.7	-66.6 ± 0.7	145.8 ± 0.6	62.0 ± 0.4	-29.2 ± 0.6	9.6 ± 0.8	63.5 ± 1.1
87.9	147.8 ± 2.2	26.9 ± 0.5	-65.5 ± 1.1	151.8 ± 0.7	68.5 ± 0.9	-34.5 ± 1.2	14.0 ± 1.3	62.0 ± 1.5
97.7	153.1 ± 0.7	27.3 ± 0.4	-67.0 ± 0.8	155.8 ± 0.7	79.5 ± 1.0	-37.5 ± 0.6	16.4 ± 0.8	79.4 ± 1.1
107.4	154.5 ± 0.6	23.7 ± 0.4	-62.5 ± 0.8	155.7 ± 0.9	86.8 ± 0.3	-40.8 ± 0.7	15.8 ± 0.3	83.2 ± 0.8
117.2	157.0 ± 0.7	24.0 ± 0.6	-59.3 ± 0.4	159.1 ± 0.8	94.2 ± 0.4	-44.6 ± 0.5	13.8 ± 0.5	90.4 ± 1.0
127.0	157.3 ± 0.2	21.7 ± 0.3	-55.7 ± 0.4	157.8 ± 0.5	100.4 ± 0.8	-46.0 ± 0.4	12.6 ± 0.5	98.7 ± 1.0
136.7	162.4 ± 0.4	19.7 ± 0.3	-47.6 ± 0.4	164.0 ± 0.7	108.3 ± 0.5	-48.6 ± 0.5	19.1 ± 0.7	105.0 ± 0.8
146.5	164.6 ± 0.3	19.7 ± 0.6	-44.8 ± 0.2	166.0 ± 0.6	116.4 ± 0.4	-49.7 ± 0.7	17.7 ± 0.5	112.4 ± 1.0
156.3	166.6 ± 0.4	22.3 ± 0.4	-39.5 ± 0.3	154.7 ± 0.6	123.7 ± 0.7	-50.2 ± 0.2	14.2 ± 0.2	120.7 ± 0.9
166.0	169.2 ± 1.4	13.6 ± 2.2	-40.9 ± 4.5	167.9 ± 1.5	129.6 ± 5.4	-55.4 ± 1.5	13.8 ± 0.3	131.7 ± 2.3
175.8	171.7 ± 1.1	15.6 ± 0.5	-34.4 ± 0.9	174.3 ± 0.6	137.0 ± 1.1	-54.3 ± 0.6	17.5 ± 0.8	140.1 ± 0.9
185.5	174.4 ± 1.0	13.9 ± 0.5	-34.2 ± 1.0	176.4 ± 0.7	146.6 ± 1.0	-53.9 ± 0.6	13.8 ± 1.6	153.7 ± 1.1
195.3	175.4 ± 2.1	15.4 ± 0.7	-27.2 ± 3.7	175.1 ± 1.1	154.5 ± 1.7	-51.9 ± 0.6	5.6 ± 1.6	156.7 ± 1.3
205.1	179.8 ± 0.7	15.3 ± 0.6	-23.1 ± 0.3	182.8 ± 0.8	161.3 ± 0.3	-52.0 ± 0.7	20.4 ± 0.7	168.1 ± 1.2
214.8	182.3 ± 0.3	16.6 ± 0.4	-20.6 ± 0.3	182.6 ± 0.7	171.2 ± 0.6	-52.3 ± 0.2	19.0 ± 0.3	173.0 ± 1.0
224.6	184.3 ± 0.5	27.6 ± 0.5	-15.2 ± 0.4	189.1 ± 0.6	180.1 ± 0.5	-37.4 ± 0.2	17.4 ± 0.4	198.0 ± 0.9
234.4	191.3 ± 0.8	15.3 ± 0.6	-20.2 ± 0.7	192.8 ± 0.7	187.2 ± 0.4	-53.8 ± 0.5	20.7 ± 0.8	198.7 ± 1.3
244.1	186.3 ± 0.3	15.0 ± 0.5	-15.6 ± 0.4	193.6 ± 0.7	198.2 ± 0.8	-51.3 ± 0.6	20.3 ± 0.4	199.0 ± 0.9

Table F.29: SBB - Impedance Values at 53 m/s and 2.1 MPa

Freq.	Re(H_{xx})	Re(H_{xy})	Re(H_{yx})	Re(H_{yy})	Im(H_{xx})	Im(H_{xy})	Im(H_{yx})	Im(H_{yy})
Hz	MN/m	MN/m	MN/m	MN/m	MN/m	MN/m	MN/m	MN/m
9.8	206.7 ± 0.3	-5.4 ± 1.1	-69.2 ± 0.5	226.5 ± 0.8	3.8 ± 0.7	-3.9 ± 1.0	3.5 ± 1.4	9.9 ± 1.3
19.5	209.1 ± 1.0	-2.0 ± 1.2	-69.1 ± 1.4	228.2 ± 2.2	8.6 ± 0.8	-4.6 ± 0.9	0.1 ± 1.1	12.8 ± 1.6
29.3	207.3 ± 0.9	-7.0 ± 0.6	-74.3 ± 0.7	240.1 ± 1.3	15.3 ± 0.5	-8.6 ± 0.4	4.0 ± 0.8	17.9 ± 1.4
39.1	206.9 ± 1.0	-4.4 ± 0.3	-68.6 ± 0.9	228.6 ± 0.7	23.6 ± 0.6	-14.8 ± 0.3	3.0 ± 1.0	28.7 ± 0.9
48.8	207.5 ± 0.4	-8.0 ± 0.4	-69.2 ± 0.9	229.6 ± 1.0	28.3 ± 1.5	-18.0 ± 0.4	-1.4 ± 0.8	37.8 ± 1.1
58.6	208.7 ± 0.7	-4.9 ± 0.7	-71.7 ± 2.1	228.8 ± 1.2	30.7 ± 1.0	-23.2 ± 0.8	-3.4 ± 0.9	45.1 ± 1.7
68.4	207.9 ± 0.3	-4.6 ± 0.4	-70.5 ± 1.1	233.9 ± 1.2	37.1 ± 0.8	-23.7 ± 0.8	1.0 ± 0.3	43.3 ± 1.4
78.1	210.5 ± 0.4	-2.4 ± 0.5	-58.8 ± 1.1	231.1 ± 1.4	44.9 ± 0.6	-26.1 ± 0.9	2.7 ± 0.7	56.0 ± 0.9
87.9	209.4 ± 1.0	-8.4 ± 0.6	-59.5 ± 0.7	238.6 ± 1.2	48.3 ± 1.2	-32.3 ± 0.8	2.3 ± 1.6	53.2 ± 1.4
97.7	212.8 ± 0.6	-9.9 ± 0.4	-64.6 ± 1.0	240.7 ± 0.5	57.3 ± 0.6	-33.9 ± 0.2	-0.7 ± 0.9	74.8 ± 1.1
107.4	212.6 ± 0.7	-11.7 ± 0.4	-62.9 ± 0.6	242.1 ± 0.9	60.7 ± 0.9	-36.8 ± 0.8	-1.1 ± 0.5	80.4 ± 0.9
117.2	212.5 ± 0.5	-11.8 ± 0.7	-61.7 ± 0.4	246.7 ± 0.7	65.3 ± 0.3	-37.9 ± 0.7	-2.4 ± 0.6	88.8 ± 1.2
127.0	214.9 ± 0.1	-13.9 ± 0.4	-59.3 ± 0.5	245.7 ± 0.9	70.4 ± 0.3	-40.2 ± 0.5	-7.6 ± 0.7	95.2 ± 1.0
136.7	215.7 ± 0.3	-13.6 ± 0.6	-50.2 ± 0.4	249.2 ± 0.7	79.7 ± 0.7	-41.7 ± 0.4	2.0 ± 0.6	99.6 ± 1.2
146.5	216.1 ± 0.3	-14.4 ± 0.5	-49.9 ± 0.1	259.0 ± 0.4	85.0 ± 0.5	-43.6 ± 0.5	0.7 ± 0.4	107.0 ± 0.9
156.3	218.1 ± 0.5	-12.7 ± 0.4	-46.2 ± 0.4	252.0 ± 0.6	92.2 ± 0.2	-45.6 ± 0.6	-1.8 ± 0.3	114.7 ± 0.8
166.0	218.5 ± 3.7	-18.3 ± 1.9	-50.5 ± 2.1	261.4 ± 2.3	96.1 ± 1.5	-47.5 ± 2.3	-3.5 ± 3.7	122.7 ± 2.1
175.8	219.5 ± 1.1	-18.0 ± 0.7	-42.2 ± 1.1	266.3 ± 0.9	101.8 ± 1.1	-46.7 ± 0.7	0.1 ± 1.4	127.1 ± 1.0
185.5	219.4 ± 1.1	-16.6 ± 0.5	-45.8 ± 1.7	267.2 ± 0.6	112.4 ± 1.7	-48.3 ± 0.8	-8.9 ± 0.5	149.1 ± 1.1
195.3	227.1 ± 3.0	-17.1 ± 0.9	-20.9 ± 1.5	263.7 ± 0.9	111.6 ± 1.6	-46.9 ± 0.9	-16.7 ± 3.6	141.2 ± 1.2
205.1	227.6 ± 0.6	-16.7 ± 0.8	-31.9 ± 0.4	279.1 ± 0.6	121.7 ± 0.4	-46.9 ± 0.3	-0.5 ± 0.3	156.5 ± 0.9
214.8	229.6 ± 0.5	-14.4 ± 0.4	-31.0 ± 0.5	279.6 ± 0.5	130.3 ± 0.7	-46.6 ± 0.6	-2.5 ± 0.6	159.3 ± 1.1
224.6	231.7 ± 0.8	-10.7 ± 0.6	-28.1 ± 0.6	321.5 ± 0.5	137.7 ± 0.8	-38.7 ± 0.6	-2.9 ± 0.5	168.9 ± 1.0
234.4	236.5 ± 0.3	-16.9 ± 0.7	-31.8 ± 0.3	288.1 ± 0.7	142.2 ± 0.3	-49.0 ± 0.5	-3.3 ± 0.5	178.9 ± 0.9
244.1	236.7 ± 0.7	-14.2 ± 0.6	-24.5 ± 0.7	289.4 ± 0.8	148.3 ± 1.2	-47.6 ± 0.5	-6.1 ± 0.6	172.4 ± 0.8

Table F.30: SBB - Impedance Values at 53 m/s and 2.9 MPa

Freq.	Re(H_{xx})	Re(H_{xy})	Re(H_{yx})	Re(H_{yy})	Im(H_{xx})	Im(H_{xy})	Im(H_{yx})	Im(H_{yy})
Hz	MN/m	MN/m	MN/m	MN/m	MN/m	MN/m	MN/m	MN/m
9.8	238.3 ± 0.9	-20.5 ± 0.8	-68.4 ± 0.5	287.7 ± 2.1	5.7 ± 1.0	-2.1 ± 0.6	2.3 ± 1.3	9.4 ± 1.6
19.5	239.1 ± 0.8	-19.4 ± 1.0	-67.1 ± 0.3	286.1 ± 0.9	11.8 ± 0.6	-4.4 ± 0.8	1.8 ± 1.9	12.0 ± 1.2
29.3	240.7 ± 0.6	-23.3 ± 0.5	-73.4 ± 0.4	301.1 ± 1.7	15.4 ± 0.8	-7.2 ± 0.5	0.8 ± 0.6	18.6 ± 1.8
39.1	241.6 ± 1.0	-20.1 ± 0.5	-67.7 ± 1.0	291.6 ± 0.8	22.8 ± 0.5	-13.3 ± 0.4	-0.3 ± 1.3	28.0 ± 1.7
48.8	242.7 ± 0.5	-22.9 ± 0.9	-69.8 ± 0.9	293.6 ± 0.7	25.5 ± 1.1	-15.2 ± 1.0	-0.7 ± 0.8	33.6 ± 1.1
58.6	242.2 ± 0.4	-20.3 ± 0.8	-68.2 ± 0.6	292.4 ± 1.3	30.4 ± 1.2	-19.4 ± 1.2	-4.1 ± 0.7	42.6 ± 1.9
68.4	242.9 ± 0.7	-20.9 ± 0.4	-68.2 ± 0.4	297.5 ± 1.8	33.5 ± 0.7	-18.1 ± 0.7	-4.1 ± 1.5	40.1 ± 1.9
78.1	241.8 ± 0.8	-20.1 ± 0.7	-66.1 ± 0.4	293.3 ± 0.6	44.6 ± 0.7	-17.8 ± 0.6	0.1 ± 0.8	57.0 ± 1.4
87.9	243.4 ± 1.1	-23.3 ± 1.4	-63.8 ± 1.6	303.3 ± 1.0	44.2 ± 1.6	-24.7 ± 0.7	-0.6 ± 1.0	50.6 ± 1.9
97.7	246.1 ± 0.7	-22.3 ± 0.3	-66.1 ± 0.8	303.2 ± 1.2	51.7 ± 0.5	-28.8 ± 0.7	-6.5 ± 0.9	69.0 ± 1.0
107.4	248.8 ± 0.5	-25.2 ± 0.5	-66.0 ± 0.8	303.5 ± 0.8	54.8 ± 0.5	-30.8 ± 0.5	-8.8 ± 1.1	75.3 ± 1.2
117.2	249.1 ± 0.5	-24.3 ± 0.7	-64.3 ± 0.5	309.6 ± 1.0	60.4 ± 0.4	-33.0 ± 0.7	-9.7 ± 0.2	82.3 ± 0.9
127.0	251.8 ± 0.9	-25.9 ± 0.3	-63.6 ± 0.7	308.0 ± 0.9	65.6 ± 1.0	-34.6 ± 0.8	-14.4 ± 0.4	88.4 ± 0.9
136.7	251.5 ± 0.4	-24.2 ± 0.2	-54.9 ± 0.4	311.5 ± 0.5	70.4 ± 0.5	-35.2 ± 0.4	-5.3 ± 0.3	92.0 ± 0.9
146.5	252.2 ± 0.3	-23.0 ± 0.3	-55.6 ± 0.6	314.1 ± 0.5	74.8 ± 0.3	-37.1 ± 0.2	-7.2 ± 0.4	99.7 ± 1.0
156.3	253.8 ± 0.2	-23.6 ± 0.3	-53.8 ± 0.5	317.3 ± 0.7	80.2 ± 0.7	-39.1 ± 0.4	-10.0 ± 0.5	106.5 ± 1.1
166.0	258.0 ± 1.4	-28.2 ± 2.8	-58.3 ± 3.9	324.9 ± 3.3	85.2 ± 4.4	-41.1 ± 3.0	-12.6 ± 2.7	112.1 ± 3.5
175.8	257.3 ± 1.1	-27.5 ± 0.9	-49.3 ± 1.2	326.5 ± 1.2	87.0 ± 1.6	-41.5 ± 0.9	-6.6 ± 1.5	118.4 ± 1.4
185.5	258.5 ± 1.0	-26.0 ± 0.6	-55.8 ± 0.7	329.8 ± 0.7	96.9 ± 0.9	-42.0 ± 0.5	-13.1 ± 0.7	138.9 ± 1.2
195.3	256.7 ± 2.7	-23.4 ± 0.9	-34.0 ± 2.0	327.6 ± 1.0	101.5 ± 0.8	-41.3 ± 0.6	-20.0 ± 0.8	134.4 ± 0.9
205.1	264.1 ± 0.5	-23.8 ± 0.6	-40.2 ± 0.3	340.4 ± 0.7	105.4 ± 0.7	-42.2 ± 0.2	-6.6 ± 0.6	145.4 ± 1.1
214.8	265.6 ± 0.2	-19.7 ± 0.5	-38.6 ± 0.1	340.6 ± 0.5	113.0 ± 1.0	-43.3 ± 0.6	-9.1 ± 0.4	151.9 ± 1.0
224.6	270.9 ± 0.4	-22.2 ± 0.8	-38.8 ± 0.4	400.8 ± 0.6	118.0 ± 0.5	-39.6 ± 0.5	-7.9 ± 0.4	157.9 ± 0.9
234.4	272.9 ± 0.5	-25.3 ± 0.8	-42.3 ± 0.4	357.6 ± 0.7	121.4 ± 1.0	-49.0 ± 1.0	-7.7 ± 1.1	172.7 ± 1.2
244.1	272.4 ± 0.9	-20.2 ± 0.6	-32.8 ± 0.2	352.5 ± 0.8	127.1 ± 1.0	-46.9 ± 0.5	-10.1 ± 0.5	162.5 ± 1.1

Table F.31: SBB - Impedance Values at 69 m/s and 0.7 MPa

Freq.	Re(H_{xx})	Re(H_{xy})	Re(H_{yx})	Re(H_{yy})	Im(H_{xx})	Im(H_{xy})	Im(H_{yx})	Im(H_{yy})
Hz	MN/m	MN/m	MN/m	MN/m	MN/m	MN/m	MN/m	MN/m
9.8	164.2 ± 2.3	39.8 ± 2.5	-85.8 ± 2.6	176.6 ± 2.1	8.9 ± 1.5	1.1 ± 1.4	7.1 ± 2.4	3.7 ± 2.9
19.5	167.0 ± 2.2	43.1 ± 1.3	-80.5 ± 1.3	169.8 ± 1.8	15.0 ± 1.8	-8.1 ± 2.0	6.0 ± 1.9	10.5 ± 3.0
29.3	165.9 ± 1.2	37.3 ± 1.1	-81.8 ± 1.7	172.8 ± 1.6	18.2 ± 0.7	-11.8 ± 0.9	5.4 ± 1.6	14.2 ± 3.0
39.1	167.2 ± 1.8	38.6 ± 1.0	-78.1 ± 1.0	170.3 ± 1.6	24.7 ± 1.5	-15.1 ± 1.6	3.9 ± 1.3	22.9 ± 1.4
48.8	165.9 ± 1.7	40.4 ± 1.2	-81.5 ± 0.6	172.5 ± 1.2	33.1 ± 1.2	-18.1 ± 2.2	9.6 ± 1.7	28.1 ± 2.2
58.6	167.2 ± 1.9	39.2 ± 2.1	-79.7 ± 1.8	169.7 ± 1.0	37.7 ± 1.1	-16.3 ± 0.6	9.0 ± 1.4	36.8 ± 1.2
68.4	165.1 ± 1.1	40.6 ± 0.9	-80.7 ± 1.1	175.4 ± 2.2	45.2 ± 0.5	-21.0 ± 1.2	14.6 ± 1.1	44.6 ± 2.5
78.1	164.8 ± 0.8	43.4 ± 1.4	-75.4 ± 1.1	171.0 ± 1.4	51.7 ± 1.1	-28.1 ± 2.2	9.7 ± 0.9	50.9 ± 2.8
87.9	168.8 ± 0.9	39.8 ± 1.3	-73.3 ± 1.9	176.4 ± 1.9	57.9 ± 1.3	-33.7 ± 1.7	11.5 ± 2.4	49.0 ± 3.1
97.7	170.1 ± 1.2	40.5 ± 0.6	-76.1 ± 1.1	178.8 ± 1.2	66.0 ± 0.5	-35.5 ± 1.0	17.3 ± 1.2	62.9 ± 1.2
107.4	171.4 ± 0.6	39.3 ± 0.7	-72.3 ± 0.9	177.9 ± 1.1	73.1 ± 0.6	-40.4 ± 0.7	18.0 ± 0.3	66.3 ± 1.0
117.2	172.3 ± 0.8	37.5 ± 0.5	-69.4 ± 0.4	179.7 ± 0.6	80.8 ± 0.4	-42.5 ± 0.6	18.5 ± 0.9	72.7 ± 1.2
127.0	174.2 ± 1.0	37.8 ± 0.5	-64.5 ± 0.5	177.9 ± 1.2	87.2 ± 0.6	-46.2 ± 0.6	18.7 ± 1.1	78.5 ± 1.3
136.7	177.5 ± 0.2	36.1 ± 0.5	-58.4 ± 0.5	184.6 ± 0.6	94.1 ± 0.5	-48.8 ± 0.4	25.1 ± 0.4	85.6 ± 1.1
146.5	179.0 ± 0.2	35.9 ± 0.3	-53.8 ± 0.4	182.6 ± 0.7	102.1 ± 0.2	-51.4 ± 0.3	22.7 ± 0.2	91.6 ± 0.9
156.3	180.3 ± 0.5	39.6 ± 0.4	-49.2 ± 0.7	175.6 ± 0.7	109.7 ± 0.3	-53.4 ± 0.4	20.8 ± 0.3	100.0 ± 0.9
166.0	183.5 ± 0.6	30.3 ± 0.6	-51.4 ± 0.9	183.0 ± 0.6	116.0 ± 0.6	-59.2 ± 0.4	22.0 ± 0.5	109.5 ± 1.1
175.8	186.5 ± 0.8	29.2 ± 0.6	-42.7 ± 0.7	194.0 ± 0.5	119.7 ± 1.0	-56.9 ± 0.7	24.0 ± 0.4	116.8 ± 0.9
185.5	189.0 ± 1.0	30.9 ± 0.9	-43.2 ± 1.4	191.9 ± 1.4	132.6 ± 1.0	-60.6 ± 0.7	20.8 ± 0.6	127.7 ± 1.3
195.3	185.8 ± 3.2	32.6 ± 1.0	-33.9 ± 1.9	191.8 ± 0.9	135.6 ± 1.0	-55.9 ± 0.9	15.5 ± 2.2	132.1 ± 1.3
205.1	195.3 ± 0.3	32.6 ± 0.8	-32.1 ± 0.8	200.0 ± 1.1	143.7 ± 1.1	-59.9 ± 1.0	30.0 ± 0.7	141.2 ± 1.1
214.8	198.2 ± 2.8	32.7 ± 5.6	-29.5 ± 1.9	201.2 ± 5.6	152.1 ± 2.7	-60.9 ± 6.1	30.4 ± 2.2	145.5 ± 4.5
224.6	203.1 ± 0.5	41.3 ± 0.4	-21.5 ± 0.6	218.6 ± 1.1	162.1 ± 1.1	-54.3 ± 1.1	28.7 ± 0.7	170.3 ± 1.0
234.4	212.8 ± 0.9	28.0 ± 1.0	-17.7 ± 0.9	210.0 ± 1.2	167.5 ± 1.2	-64.7 ± 0.7	36.4 ± 1.1	166.9 ± 0.9
244.1	206.3 ± 0.7	27.6 ± 0.9	-20.3 ± 0.9	209.8 ± 1.1	177.8 ± 0.7	-62.4 ± 0.6	36.0 ± 0.6	168.2 ± 1.2

Table F.32: SBB - Impedance Values at 69 m/s and 2.1 MPa

Freq.	Re(H_{xx})	Re(H_{xy})	Re(H_{yx})	Re(H_{yy})	Im(H_{xx})	Im(H_{xy})	Im(H_{yx})	Im(H_{yy})
Hz	MN/m	MN/m	MN/m	MN/m	MN/m	MN/m	MN/m	MN/m
9.8	196.6 ± 1.5	2.2 ± 1.8	-67.3 ± 2.9	219.4 ± 3.3	6.2 ± 1.1	-2.5 ± 1.0	1.2 ± 2.1	6.8 ± 1.9
19.5	197.6 ± 0.7	0.9 ± 0.9	-66.6 ± 1.4	218.6 ± 1.6	9.0 ± 0.7	-5.6 ± 1.4	2.4 ± 1.2	10.9 ± 2.0
29.3	197.1 ± 0.6	-1.0 ± 0.9	-70.2 ± 1.3	230.3 ± 1.7	13.5 ± 0.9	-7.8 ± 0.4	3.5 ± 1.1	14.4 ± 1.5
39.1	195.8 ± 0.4	2.8 ± 0.8	-67.4 ± 1.3	219.4 ± 1.2	16.8 ± 0.9	-10.6 ± 0.6	2.2 ± 1.4	22.4 ± 1.4
48.8	196.8 ± 0.7	1.3 ± 0.6	-68.4 ± 1.6	221.3 ± 1.3	21.9 ± 0.8	-14.2 ± 0.4	0.3 ± 1.5	30.5 ± 2.1
58.6	197.8 ± 0.6	1.1 ± 0.9	-66.1 ± 0.5	221.3 ± 2.0	23.9 ± 0.7	-14.7 ± 1.1	-2.5 ± 0.5	34.7 ± 1.5
68.4	197.1 ± 0.6	0.5 ± 0.6	-68.1 ± 0.9	225.1 ± 1.3	27.2 ± 0.6	-16.8 ± 0.8	0.1 ± 1.2	35.2 ± 1.6
78.1	198.8 ± 0.4	4.3 ± 0.5	-58.0 ± 0.8	227.1 ± 1.2	34.0 ± 0.2	-19.7 ± 0.7	1.8 ± 0.7	46.8 ± 1.2
87.9	198.7 ± 0.6	0.5 ± 0.6	-62.8 ± 0.7	228.1 ± 1.2	33.9 ± 1.2	-22.0 ± 0.6	1.4 ± 1.9	40.9 ± 1.2
97.7	199.4 ± 1.1	0.3 ± 0.9	-67.1 ± 0.5	229.3 ± 0.7	41.0 ± 0.7	-26.5 ± 0.5	3.9 ± 1.4	61.2 ± 1.2
107.4	198.4 ± 0.3	-0.9 ± 0.5	-64.6 ± 0.3	228.9 ± 0.7	43.7 ± 0.4	-28.4 ± 0.5	3.3 ± 0.4	63.9 ± 1.5
117.2	198.0 ± 0.2	-0.1 ± 0.6	-62.7 ± 0.5	233.1 ± 0.5	49.6 ± 0.2	-31.3 ± 0.5	0.6 ± 0.4	69.7 ± 1.1
127.0	198.4 ± 0.6	-0.8 ± 0.5	-60.8 ± 0.5	229.8 ± 1.1	53.3 ± 0.5	-32.7 ± 0.5	-4.7 ± 0.4	75.0 ± 0.9
136.7	198.5 ± 0.4	-0.8 ± 0.3	-50.8 ± 0.3	234.1 ± 0.4	59.7 ± 0.5	-34.8 ± 0.4	10.7 ± 0.5	79.3 ± 1.0
146.5	199.2 ± 0.2	-0.8 ± 0.4	-51.1 ± 0.4	235.2 ± 0.6	65.1 ± 0.3	-37.1 ± 0.2	8.4 ± 0.4	88.2 ± 1.0
156.3	199.8 ± 0.2	-0.9 ± 0.4	-48.3 ± 0.3	240.3 ± 0.6	70.8 ± 0.2	-39.1 ± 0.2	6.5 ± 0.3	93.7 ± 0.9
166.0	200.9 ± 0.4	-4.9 ± 0.4	-49.5 ± 0.5	241.1 ± 0.6	76.3 ± 0.3	-42.0 ± 0.2	4.2 ± 0.7	103.8 ± 1.0
175.8	199.9 ± 0.5	-4.5 ± 0.4	-39.7 ± 0.4	245.8 ± 0.6	81.3 ± 0.3	-42.3 ± 0.3	9.6 ± 0.8	104.8 ± 0.9
185.5	202.0 ± 0.5	-4.0 ± 0.5	-46.5 ± 0.8	245.1 ± 0.9	90.2 ± 0.8	-43.7 ± 0.3	1.8 ± 0.5	124.0 ± 1.1
195.3	197.2 ± 2.4	-2.5 ± 0.4	-28.3 ± 1.8	242.1 ± 0.8	91.0 ± 1.0	-41.8 ± 0.6	-5.8 ± 1.6	118.8 ± 1.3
205.1	204.5 ± 0.4	-3.2 ± 0.7	-28.1 ± 0.4	254.1 ± 0.6	98.2 ± 0.1	-44.3 ± 0.4	10.3 ± 0.3	131.5 ± 1.1
214.8	205.8 ± 0.7	-2.1 ± 2.5	-26.6 ± 0.6	254.1 ± 1.3	105.7 ± 0.8	-45.5 ± 1.3	9.9 ± 1.1	132.5 ± 2.7
224.6	209.2 ± 0.2	-2.8 ± 1.1	-22.0 ± 0.5	295.2 ± 0.5	112.6 ± 0.6	-39.5 ± 0.5	8.6 ± 0.3	144.0 ± 1.4
234.4	213.3 ± 0.5	-7.0 ± 0.7	-26.2 ± 0.4	262.4 ± 0.7	115.5 ± 0.5	-48.1 ± 0.4	9.6 ± 1.0	152.8 ± 1.3
244.1	213.3 ± 0.6	-6.0 ± 1.0	-17.8 ± 0.5	263.4 ± 1.2	124.2 ± 1.2	-48.2 ± 0.6	3.0 ± 0.7	149.1 ± 1.1

Table F.33: SBB - Impedance Values at 69 m/s and 2.9 MPa

Freq.	Re(H_{xx})	Re(H_{xy})	Re(H_{yx})	Re(H_{yy})	Im(H_{xx})	Im(H_{xy})	Im(H_{yx})	Im(H_{yy})
Hz	MN/m	MN/m	MN/m	MN/m	MN/m	MN/m	MN/m	MN/m
9.8	232.0 ± 0.9	-16.0 ± 1.7	-72.3 ± 0.8	273.2 ± 3.0	7.8 ± 1.9	-3.8 ± 2.9	7.4 ± 2.0	8.6 ± 4.8
19.5	231.9 ± 0.9	-13.1 ± 0.7	-68.6 ± 1.8	266.6 ± 1.0	11.1 ± 0.8	-3.1 ± 0.4	2.7 ± 0.7	8.2 ± 1.3
29.3	231.7 ± 1.3	-18.1 ± 0.7	-70.9 ± 1.4	285.3 ± 0.6	11.7 ± 0.5	-6.7 ± 0.8	1.8 ± 0.7	16.5 ± 2.2
39.1	231.9 ± 1.4	-14.4 ± 0.7	-66.7 ± 1.2	273.8 ± 0.9	16.1 ± 0.7	-9.5 ± 0.4	0.5 ± 1.0	23.5 ± 1.1
48.8	233.0 ± 0.5	-16.2 ± 0.8	-67.8 ± 0.9	278.4 ± 0.7	20.8 ± 0.5	-12.0 ± 0.3	-1.8 ± 0.8	29.4 ± 1.6
58.6	233.9 ± 0.6	-14.8 ± 0.8	-66.4 ± 0.5	274.0 ± 1.3	23.7 ± 0.4	-14.2 ± 0.7	-0.6 ± 0.6	35.3 ± 1.5
68.4	232.7 ± 0.4	-15.3 ± 0.4	-68.4 ± 0.3	280.2 ± 1.0	27.3 ± 0.4	-14.1 ± 0.5	-2.1 ± 0.4	35.2 ± 1.6
78.1	229.1 ± 0.7	-14.0 ± 0.3	-66.2 ± 0.3	278.9 ± 1.1	34.8 ± 0.6	-15.0 ± 0.7	3.0 ± 0.3	49.5 ± 1.3
87.9	235.9 ± 1.8	-17.2 ± 1.0	-65.3 ± 1.0	286.7 ± 1.0	28.1 ± 1.1	-20.7 ± 0.7	-0.5 ± 2.5	43.5 ± 1.4
97.7	235.7 ± 0.5	-15.0 ± 0.5	-66.7 ± 0.8	286.2 ± 0.8	40.3 ± 0.5	-24.2 ± 0.5	-5.8 ± 0.6	57.6 ± 1.4
107.4	235.8 ± 0.1	-15.8 ± 0.4	-64.8 ± 0.4	286.3 ± 0.7	42.3 ± 0.4	-25.5 ± 0.3	-5.2 ± 0.4	63.1 ± 1.1
117.2	236.9 ± 0.4	-16.8 ± 0.6	-64.5 ± 0.5	291.5 ± 1.1	47.1 ± 0.6	-28.6 ± 0.5	-7.1 ± 0.5	69.2 ± 1.1
127.0	237.1 ± 0.7	-16.4 ± 0.4	-62.1 ± 0.5	288.1 ± 0.7	51.7 ± 0.4	-29.8 ± 0.1	-9.6 ± 0.4	73.6 ± 0.8
136.7	238.8 ± 0.2	-16.9 ± 0.3	-53.0 ± 0.3	291.2 ± 0.5	54.3 ± 0.1	-31.4 ± 0.3	-1.2 ± 0.2	78.5 ± 0.9
146.5	239.8 ± 0.3	-16.1 ± 0.2	-53.1 ± 0.6	296.4 ± 0.6	58.2 ± 0.4	-32.8 ± 0.2	-1.6 ± 0.3	83.1 ± 0.9
156.3	241.0 ± 0.3	-17.0 ± 0.4	-51.7 ± 0.4	302.4 ± 0.6	63.1 ± 0.1	-35.9 ± 0.4	-6.3 ± 0.4	92.9 ± 1.0
166.0	243.1 ± 0.2	-21.3 ± 0.3	-54.2 ± 0.4	301.6 ± 0.6	67.0 ± 0.1	-37.1 ± 0.2	-8.6 ± 0.2	99.3 ± 0.8
175.8	243.9 ± 0.5	-18.2 ± 0.2	-47.4 ± 0.7	306.7 ± 0.5	66.0 ± 0.4	-35.7 ± 0.4	0.8 ± 0.2	100.0 ± 0.9
185.5	248.1 ± 0.8	-17.6 ± 0.3	-54.3 ± 1.5	304.8 ± 0.7	80.2 ± 0.8	-38.3 ± 0.5	-12.2 ± 0.8	122.5 ± 1.0
195.3	232.4 ± 1.3	-12.9 ± 0.7	-31.3 ± 1.6	303.1 ± 0.8	82.1 ± 0.4	-36.5 ± 0.4	-16.9 ± 0.8	113.2 ± 1.1
205.1	247.6 ± 0.5	-14.8 ± 0.6	-39.8 ± 0.5	316.4 ± 0.5	80.5 ± 0.3	-37.9 ± 0.6	-2.1 ± 0.2	126.0 ± 1.5
214.8	250.4 ± 0.5	-12.3 ± 1.8	-37.7 ± 0.9	314.6 ± 0.9	87.6 ± 1.1	-41.7 ± 0.9	-3.4 ± 0.6	128.6 ± 1.9
224.6	252.5 ± 1.1	-13.9 ± 1.0	-35.6 ± 0.5	369.1 ± 0.8	93.5 ± 0.2	-35.3 ± 0.6	-1.2 ± 0.9	133.5 ± 1.2
234.4	258.6 ± 0.5	-18.3 ± 0.9	-44.5 ± 0.5	329.5 ± 1.0	95.0 ± 0.7	-45.2 ± 0.5	-5.6 ± 0.6	147.3 ± 1.1
244.1	257.0 ± 0.3	-14.4 ± 0.5	-29.0 ± 0.4	326.4 ± 0.7	100.1 ± 0.5	-44.5 ± 0.5	-6.8 ± 0.5	139.3 ± 0.9

Table F.34: SBB - Impedance Values at 85 m/s and 0.7 MPa

Freq.	Re(H_{xx})	Re(H_{xy})	Re(H_{yx})	Re(H_{yy})	Im(H_{xx})	Im(H_{xy})	Im(H_{yx})	Im(H_{yy})
Hz	MN/m	MN/m	MN/m	MN/m	MN/m	MN/m	MN/m	MN/m
9.8	191.3 ± 2.1	36.7 ± 1.4	-93.3 ± 2.8	194.4 ± 6.2	12.5 ± 1.5	-6.1 ± 2.6	0.5 ± 4.2	-13.6 ± 7.0
19.5	190.5 ± 2.1	23.4 ± 4.0	-101.4 ± 5.3	205.7 ± 11.9	9.4 ± 2.1	-10.2 ± 3.7	-8.5 ± 3.1	5.7 ± 5.1
29.3	189.0 ± 1.4	33.2 ± 1.7	-84.4 ± 2.8	186.4 ± 3.3	13.9 ± 1.2	-15.8 ± 1.6	0.4 ± 2.0	13.3 ± 4.3
39.1	197.4 ± 1.6	25.6 ± 1.5	-91.4 ± 3.2	193.2 ± 4.1	20.4 ± 1.3	-14.7 ± 1.2	3.1 ± 2.0	19.9 ± 3.2
48.8	195.9 ± 1.6	26.1 ± 3.2	-99.4 ± 2.9	199.3 ± 5.8	17.9 ± 1.0	-20.4 ± 1.0	6.2 ± 4.1	11.2 ± 3.4
58.6	189.3 ± 1.4	29.9 ± 2.6	-97.7 ± 2.7	190.3 ± 1.8	26.7 ± 1.1	-24.3 ± 1.3	20.6 ± 3.1	20.9 ± 3.8
68.4	195.1 ± 1.3	30.9 ± 2.9	-83.9 ± 1.3	197.2 ± 3.5	35.6 ± 0.9	-26.0 ± 0.9	26.2 ± 1.5	36.5 ± 1.5
78.1	194.7 ± 1.1	27.7 ± 1.5	-83.2 ± 4.1	203.8 ± 2.1	31.9 ± 1.8	-30.6 ± 1.5	24.7 ± 2.4	38.6 ± 3.5
87.9	195.1 ± 1.2	27.8 ± 1.5	-94.6 ± 3.6	197.1 ± 2.3	37.7 ± 3.0	-32.8 ± 1.9	23.1 ± 2.5	36.0 ± 3.2
97.7	191.3 ± 1.1	23.9 ± 1.5	-69.6 ± 1.8	202.5 ± 3.2	41.9 ± 1.1	-32.4 ± 1.4	26.7 ± 1.3	42.7 ± 2.6
107.4	192.2 ± 1.1	19.2 ± 1.9	-69.7 ± 1.6	202.8 ± 2.2	47.4 ± 0.6	-37.3 ± 1.6	28.6 ± 0.9	49.5 ± 2.3
117.2	188.8 ± 0.4	22.7 ± 0.6	-59.9 ± 0.5	201.1 ± 1.3	55.2 ± 0.2	-39.8 ± 0.6	30.3 ± 0.6	47.6 ± 2.0
127.0	186.5 ± 1.0	21.9 ± 1.3	-57.7 ± 1.4	202.6 ± 2.4	60.1 ± 1.1	-39.9 ± 1.7	33.2 ± 0.9	55.8 ± 0.9
136.7	194.8 ± 0.9	18.6 ± 0.8	-69.3 ± 1.0	204.2 ± 1.2	58.2 ± 0.8	-44.5 ± 0.8	30.5 ± 0.9	64.1 ± 1.8
146.5	193.9 ± 0.7	18.9 ± 0.7	-58.7 ± 0.6	205.0 ± 0.9	67.8 ± 0.3	-44.6 ± 0.3	30.1 ± 0.5	70.2 ± 1.8
156.3	193.2 ± 0.2	24.8 ± 1.1	-48.3 ± 0.4	192.4 ± 0.9	75.0 ± 0.6	-47.5 ± 0.4	25.9 ± 0.4	77.0 ± 1.6
166.0	193.3 ± 0.3	14.3 ± 0.9	-52.2 ± 1.1	212.5 ± 1.5	81.3 ± 0.6	-48.5 ± 0.9	30.4 ± 0.6	78.6 ± 1.1
175.8	202.2 ± 1.5	13.9 ± 1.5	-59.5 ± 2.4	214.5 ± 1.4	73.8 ± 1.7	-50.6 ± 1.0	20.6 ± 1.6	87.5 ± 2.1
185.5	195.5 ± 1.6	19.4 ± 0.9	-36.6 ± 1.6	214.7 ± 2.2	102.7 ± 2.3	-50.6 ± 1.3	27.8 ± 1.1	86.4 ± 1.8
195.3	172.8 ± 1.7	17.5 ± 1.3	-44.0 ± 1.1	223.8 ± 1.8	85.3 ± 2.7	-39.9 ± 1.8	39.1 ± 2.7	98.6 ± 1.7
205.1	201.2 ± 1.0	18.8 ± 0.5	-37.8 ± 1.1	218.0 ± 1.6	103.3 ± 0.5	-49.6 ± 0.5	25.7 ± 0.9	105.9 ± 1.5
214.8	202.4 ± 0.6	22.0 ± 0.7	-28.9 ± 0.3	220.2 ± 1.2	115.5 ± 0.3	-48.7 ± 1.2	24.3 ± 0.6	109.5 ± 1.2
224.6	206.5 ± 0.6	33.0 ± 0.8	-18.5 ± 0.8	233.3 ± 2.1	124.3 ± 0.9	-49.1 ± 1.3	16.3 ± 0.7	141.5 ± 1.6
234.4	223.3 ± 0.8	17.0 ± 0.7	-19.8 ± 0.8	231.9 ± 1.2	123.8 ± 0.7	-57.7 ± 0.9	27.2 ± 0.8	126.5 ± 1.3
244.1	214.4 ± 0.6	24.4 ± 0.5	-29.5 ± 0.7	226.0 ± 1.1	143.6 ± 0.4	-55.8 ± 1.3	29.4 ± 1.1	131.9 ± 2.4

Table F.35: SBB - Impedance Values at 85 m/s and 2.1 MPa

Freq.	Re(H_{xx})	Re(H_{xy})	Re(H_{yx})	Re(H_{yy})	Im(H_{xx})	Im(H_{xy})	Im(H_{yx})	Im(H_{yy})
Hz	MN/m	MN/m	MN/m	MN/m	MN/m	MN/m	MN/m	MN/m
9.8	189.1 ± 0.7	8.1 ± 1.9	-65.0 ± 1.6	204.4 ± 2.5	6.8 ± 0.4	-0.1 ± 0.9	5.7 ± 1.7	5.2 ± 1.7
19.5	187.0 ± 0.6	6.2 ± 2.4	-59.1 ± 0.6	200.1 ± 2.2	7.9 ± 1.0	-7.2 ± 2.8	4.7 ± 1.2	8.7 ± 2.5
29.3	185.2 ± 0.4	3.5 ± 0.8	-65.7 ± 0.3	220.7 ± 1.3	9.9 ± 0.3	-5.7 ± 0.7	5.6 ± 1.0	12.7 ± 1.2
39.1	184.4 ± 0.6	5.7 ± 0.5	-63.7 ± 0.7	209.7 ± 0.7	12.3 ± 0.9	-9.3 ± 0.7	4.8 ± 0.3	18.7 ± 1.0
48.8	184.6 ± 0.9	7.4 ± 0.8	-59.1 ± 0.4	208.6 ± 0.7	15.5 ± 0.6	-9.5 ± 0.8	8.1 ± 0.9	21.5 ± 0.9
58.6	186.9 ± 0.6	5.1 ± 0.5	-64.2 ± 0.3	207.7 ± 1.0	15.3 ± 0.7	-10.4 ± 0.6	-1.4 ± 0.7	28.1 ± 1.6
68.4	184.6 ± 0.7	5.3 ± 0.4	-63.2 ± 0.5	213.0 ± 1.1	21.3 ± 0.7	-12.8 ± 0.3	1.4 ± 0.7	27.7 ± 1.0
78.1	189.9 ± 0.2	9.5 ± 0.5	-48.3 ± 0.6	209.6 ± 1.0	30.3 ± 0.4	-15.9 ± 0.7	-0.1 ± 0.3	35.5 ± 1.2
87.9	186.3 ± 0.4	6.8 ± 0.7	-54.8 ± 0.5	212.5 ± 1.6	27.7 ± 0.6	-15.0 ± 0.7	5.8 ± 0.4	31.8 ± 1.2
97.7	188.2 ± 0.2	6.5 ± 1.0	-57.5 ± 0.5	214.5 ± 1.1	36.3 ± 0.4	-19.2 ± 0.4	4.1 ± 0.6	47.1 ± 1.3
107.4	187.6 ± 0.3	7.7 ± 0.7	-57.0 ± 0.4	213.3 ± 0.6	38.9 ± 0.1	-21.4 ± 0.2	1.6 ± 0.2	50.8 ± 0.9
117.2	187.3 ± 0.3	7.5 ± 0.4	-57.8 ± 0.2	216.6 ± 0.5	41.7 ± 0.2	-23.1 ± 0.5	-0.6 ± 0.2	55.7 ± 1.2
127.0	184.7 ± 0.4	7.0 ± 0.3	-59.4 ± 0.4	213.6 ± 0.5	43.3 ± 0.2	-23.9 ± 0.4	-1.8 ± 0.4	60.0 ± 1.3
136.7	188.3 ± 0.3	7.7 ± 0.2	-48.6 ± 0.2	217.4 ± 0.6	48.0 ± 0.2	-25.5 ± 0.2	14.3 ± 0.2	64.8 ± 1.0
146.5	187.2 ± 0.2	7.6 ± 0.4	-49.1 ± 0.2	223.7 ± 0.7	54.0 ± 0.2	-28.5 ± 0.3	11.3 ± 0.2	69.8 ± 0.8
156.3	187.2 ± 0.2	10.1 ± 0.3	-45.9 ± 0.3	213.5 ± 0.5	59.6 ± 0.1	-29.6 ± 0.3	7.6 ± 0.1	75.1 ± 0.8
166.0	187.0 ± 0.1	5.8 ± 0.3	-48.7 ± 0.3	219.6 ± 0.5	64.0 ± 0.2	-32.1 ± 0.2	8.7 ± 0.2	82.2 ± 0.9
175.8	191.3 ± 0.4	4.9 ± 0.4	-44.2 ± 0.4	228.5 ± 0.7	62.1 ± 0.2	-33.5 ± 0.3	23.4 ± 0.4	84.9 ± 0.8
185.5	186.9 ± 0.3	7.7 ± 0.6	-48.1 ± 0.4	224.5 ± 0.8	73.8 ± 0.4	-33.7 ± 0.9	13.7 ± 0.4	101.5 ± 1.2
195.3	180.0 ± 1.8	8.7 ± 0.7	-53.0 ± 1.5	224.8 ± 0.6	78.6 ± 1.0	-32.3 ± 0.4	6.7 ± 0.9	98.5 ± 1.3
205.1	192.7 ± 0.4	7.5 ± 0.4	-29.5 ± 0.2	233.5 ± 0.5	82.6 ± 0.3	-36.1 ± 0.2	24.9 ± 0.4	107.5 ± 0.8
214.8	193.7 ± 0.2	9.5 ± 0.4	-24.9 ± 0.2	231.4 ± 0.8	90.2 ± 0.3	-37.1 ± 0.4	23.2 ± 0.3	110.1 ± 0.9
224.6	195.3 ± 0.1	10.9 ± 0.6	-21.3 ± 0.2	268.9 ± 0.7	93.9 ± 0.4	-30.1 ± 0.3	24.6 ± 0.1	120.7 ± 1.0
234.4	204.0 ± 0.3	7.2 ± 0.3	-27.0 ± 0.3	234.7 ± 0.6	99.5 ± 0.5	-39.4 ± 0.7	24.5 ± 0.5	127.1 ± 0.9
244.1	198.7 ± 0.1	7.8 ± 0.5	-13.6 ± 0.3	233.8 ± 0.7	103.1 ± 0.4	-39.4 ± 0.4	20.0 ± 0.5	122.8 ± 1.1

Table F.36: SBB - Impedance Values at 85 m/s and 2.9 MPa

Freq.	Re(H_{xx})	Re(H_{xy})	Re(H_{yx})	Re(H_{yy})	Im(H_{xx})	Im(H_{xy})	Im(H_{yx})	Im(H_{yy})
Hz	MN/m	MN/m	MN/m	MN/m	MN/m	MN/m	MN/m	MN/m
9.8	222.6 ± 1.1	-5.5 ± 1.9	-70.7 ± 0.7	255.7 ± 1.6	2.6 ± 1.4	-2.2 ± 2.3	8.0 ± 1.1	8.8 ± 2.2
19.5	220.6 ± 0.7	-8.3 ± 2.1	-67.9 ± 1.0	253.7 ± 1.9	4.8 ± 0.7	-5.5 ± 1.3	8.3 ± 1.1	10.4 ± 1.3
29.3	221.8 ± 1.2	-13.3 ± 1.6	-69.0 ± 0.8	271.9 ± 1.0	10.2 ± 0.4	-6.6 ± 1.1	4.2 ± 0.7	15.8 ± 1.2
39.1	220.8 ± 0.6	-8.1 ± 1.3	-65.7 ± 0.5	260.2 ± 1.8	15.0 ± 0.8	-8.2 ± 1.0	0.0 ± 0.8	20.3 ± 1.3
48.8	222.8 ± 0.6	-6.7 ± 1.5	-65.9 ± 0.6	260.0 ± 1.4	18.1 ± 1.0	-12.7 ± 1.1	0.7 ± 0.9	26.1 ± 1.9
58.6	223.9 ± 0.8	-6.8 ± 0.3	-66.2 ± 0.5	259.0 ± 0.9	18.3 ± 0.5	-13.3 ± 0.9	-0.2 ± 0.7	33.8 ± 1.2
68.4	221.7 ± 0.3	-6.9 ± 0.6	-66.7 ± 0.3	264.6 ± 0.8	21.1 ± 0.8	-12.3 ± 1.1	1.2 ± 0.8	29.8 ± 1.0
78.1	222.0 ± 0.8	-7.2 ± 1.2	-65.5 ± 0.4	262.9 ± 1.1	33.3 ± 0.4	-16.2 ± 0.3	6.6 ± 0.6	41.8 ± 1.3
87.9	227.3 ± 0.6	-7.7 ± 0.7	-62.1 ± 0.6	268.1 ± 1.0	26.1 ± 0.2	-17.9 ± 0.6	2.8 ± 0.2	38.2 ± 1.3
97.7	225.6 ± 0.5	-6.8 ± 0.7	-64.0 ± 0.6	269.7 ± 1.0	35.7 ± 0.4	-19.6 ± 0.6	-3.2 ± 0.5	50.4 ± 1.7
107.4	226.5 ± 0.3	-7.6 ± 0.6	-64.7 ± 0.5	270.7 ± 0.8	36.5 ± 0.4	-21.8 ± 0.3	-4.0 ± 0.8	55.5 ± 0.8
117.2	226.3 ± 0.3	-6.8 ± 0.3	-65.0 ± 0.3	274.1 ± 0.5	40.1 ± 0.3	-24.4 ± 0.6	-5.5 ± 0.5	60.6 ± 1.3
127.0	226.0 ± 0.2	-6.6 ± 0.6	-65.2 ± 0.6	272.1 ± 0.5	43.5 ± 0.4	-26.2 ± 0.5	-6.9 ± 0.7	64.7 ± 0.8
136.7	227.6 ± 0.2	-7.2 ± 0.6	-56.1 ± 0.2	274.6 ± 0.8	45.9 ± 0.3	-27.8 ± 0.3	6.1 ± 0.1	68.4 ± 0.8
146.5	227.3 ± 0.1	-6.0 ± 0.4	-55.6 ± 0.2	278.6 ± 0.6	50.2 ± 0.2	-29.5 ± 0.3	4.8 ± 0.3	71.8 ± 0.9
156.3	227.3 ± 0.1	-7.2 ± 0.4	-53.4 ± 0.2	287.9 ± 0.7	55.8 ± 0.2	-33.9 ± 0.4	0.2 ± 0.2	85.5 ± 0.9
166.0	229.9 ± 0.2	-10.6 ± 0.6	-54.8 ± 0.2	280.1 ± 0.5	59.5 ± 0.2	-35.0 ± 0.2	-0.2 ± 0.2	85.5 ± 0.8
175.8	234.2 ± 0.4	-10.2 ± 0.5	-52.1 ± 0.4	286.7 ± 0.7	57.7 ± 0.2	-34.7 ± 0.5	15.6 ± 0.3	88.6 ± 0.8
185.5	234.7 ± 0.4	-7.8 ± 0.3	-55.3 ± 0.1	281.8 ± 0.8	68.8 ± 0.5	-36.1 ± 0.4	1.4 ± 0.7	107.5 ± 0.9
195.3	219.3 ± 1.2	-4.0 ± 0.6	-35.1 ± 2.9	279.8 ± 0.7	76.8 ± 2.0	-33.2 ± 0.4	-26.7 ± 3.8	102.2 ± 1.2
205.1	236.7 ± 0.2	-7.0 ± 0.5	-37.4 ± 0.3	292.7 ± 0.7	72.4 ± 0.3	-36.9 ± 0.3	12.3 ± 0.2	112.5 ± 1.0
214.8	238.4 ± 0.1	-4.3 ± 0.5	-32.8 ± 0.3	288.1 ± 0.7	78.1 ± 0.3	-38.1 ± 0.3	9.1 ± 0.3	118.9 ± 1.1
224.6	242.1 ± 0.3	-7.1 ± 0.4	-33.4 ± 0.2	348.7 ± 0.5	82.4 ± 0.3	-33.1 ± 0.5	11.6 ± 0.4	125.9 ± 1.2
234.4	246.6 ± 0.2	-8.5 ± 0.4	-38.7 ± 0.4	301.4 ± 0.5	87.2 ± 0.3	-40.9 ± 0.5	5.1 ± 0.4	134.2 ± 1.0
244.1	242.4 ± 0.4	-5.9 ± 0.7	-22.7 ± 0.2	298.5 ± 0.7	88.9 ± 0.2	-38.7 ± 0.3	6.2 ± 0.6	126.5 ± 1.0

Table F.37: SB - Impedance Values at 38 m/s and 0.7 MPa

Freq.	Re(H_{xx})	Re(H_{xy})	Re(H_{yx})	Re(H_{yy})	Im(H_{xx})	Im(H_{xy})	Im(H_{yx})	Im(H_{yy})
Hz	MN/m	MN/m	MN/m	MN/m	MN/m	MN/m	MN/m	MN/m
9.8	120.5 ± 0.2	22.2 ± 0.1	-52.5 ± 0.1	124.1 ± 0.2	8.7 ± 0.2	-2.8 ± 0.3	3.0 ± 0.1	11.9 ± 0.3
19.5	122.0 ± 0.2	22.0 ± 0.2	-54.3 ± 0.1	123.8 ± 0.3	18.2 ± 0.1	-5.7 ± 0.1	2.5 ± 0.1	18.9 ± 0.4
29.3	122.0 ± 0.2	21.4 ± 0.1	-55.6 ± 0.3	129.6 ± 0.3	25.5 ± 0.2	-8.7 ± 0.2	5.2 ± 0.1	28.0 ± 0.2
39.1	122.4 ± 0.2	23.7 ± 0.2	-52.4 ± 0.1	125.6 ± 0.2	36.5 ± 0.2	-12.8 ± 0.2	2.8 ± 0.2	39.0 ± 0.3
48.8	124.6 ± 0.1	21.6 ± 0.3	-53.4 ± 0.2	127.5 ± 0.5	45.8 ± 0.2	-16.5 ± 0.2	3.3 ± 0.2	49.8 ± 0.3
58.6	124.3 ± 0.2	22.2 ± 0.3	-51.8 ± 0.2	128.3 ± 0.4	54.2 ± 0.1	-19.0 ± 0.2	3.8 ± 0.3	58.7 ± 0.3
68.4	125.7 ± 0.1	20.9 ± 0.3	-53.9 ± 0.1	132.9 ± 0.3	66.7 ± 0.1	-18.1 ± 0.2	6.9 ± 0.2	72.1 ± 0.3
78.1	127.4 ± 0.3	23.1 ± 0.1	-44.3 ± 0.2	129.9 ± 0.3	73.2 ± 0.1	-22.0 ± 0.1	4.0 ± 0.2	75.3 ± 0.3
87.9	131.4 ± 0.4	19.8 ± 0.3	-42.9 ± 0.4	139.4 ± 0.3	76.6 ± 0.2	-27.5 ± 0.2	14.5 ± 0.4	78.2 ± 0.4
97.7	133.3 ± 0.1	19.8 ± 0.2	-46.6 ± 0.2	140.3 ± 0.4	90.8 ± 0.2	-29.1 ± 0.4	4.9 ± 0.1	97.8 ± 0.4
107.4	135.4 ± 0.1	17.7 ± 0.4	-43.3 ± 0.2	144.1 ± 0.3	100.4 ± 0.3	-29.9 ± 0.3	5.0 ± 0.2	104.5 ± 0.3
117.2	134.2 ± 6.6	17.1 ± 4.4	-43.0 ± 8.7	147.0 ± 2.4	108.6 ± 9.9	-32.5 ± 1.9	5.0 ± 4.3	115.8 ± 3.4
127.0	140.7 ± 0.4	17.4 ± 0.2	-41.0 ± 0.4	148.3 ± 0.5	115.6 ± 0.5	-33.0 ± 0.4	-0.2 ± 0.5	121.6 ± 0.2
136.7	145.8 ± 0.3	17.0 ± 0.1	-33.1 ± 0.2	154.9 ± 0.3	124.8 ± 0.3	-34.6 ± 0.2	11.5 ± 0.4	129.9 ± 0.3
146.5	147.1 ± 0.2	17.3 ± 0.2	-27.6 ± 0.1	157.4 ± 0.3	132.1 ± 0.2	-34.3 ± 0.2	7.8 ± 0.2	139.2 ± 0.3
156.3	148.3 ± 0.1	21.1 ± 0.1	-25.3 ± 0.1	148.4 ± 0.2	141.5 ± 0.2	-31.9 ± 0.1	1.9 ± 0.1	146.4 ± 0.2
166.0	151.4 ± 0.2	16.2 ± 0.2	-25.2 ± 0.0	161.4 ± 0.2	149.2 ± 0.3	-38.6 ± 0.1	1.9 ± 0.2	159.6 ± 0.2
175.8	149.7 ± 0.5	17.3 ± 0.1	-22.7 ± 0.4	165.7 ± 0.2	164.6 ± 0.3	-35.6 ± 0.2	11.8 ± 0.2	168.7 ± 0.3
185.5	155.3 ± 0.3	21.2 ± 0.3	-27.7 ± 0.5	170.4 ± 0.2	170.8 ± 0.4	-37.1 ± 0.1	0.1 ± 0.2	186.4 ± 0.5
195.3	158.2 ± 0.4	24.0 ± 0.3	-29.0 ± 0.8	169.7 ± 0.4	180.0 ± 0.6	-32.4 ± 0.5	-0.8 ± 0.7	191.2 ± 0.3
205.1	166.1 ± 0.5	25.3 ± 0.3	-19.5 ± 0.3	179.8 ± 0.3	188.6 ± 0.5	-36.2 ± 0.1	17.8 ± 0.2	205.6 ± 0.4
214.8	164.1 ± 1.0	28.4 ± 0.6	-8.7 ± 0.8	178.4 ± 0.5	199.5 ± 0.7	-34.4 ± 0.3	15.2 ± 0.5	213.2 ± 0.3
224.6	164.9 ± 0.6	42.3 ± 0.5	-11.6 ± 0.7	178.5 ± 0.6	215.4 ± 0.6	-18.1 ± 0.6	12.9 ± 0.8	211.0 ± 0.4
234.4	154.8 ± 23.8	32.2 ± 4.1	-29.8 ± 29.6	194.9 ± 4.4	237.0 ± 15.9	-29.4 ± 5.3	30.6 ± 16.6	252.2 ± 6.6
244.1	170.8 ± 1.2	27.9 ± 0.8	-13.6 ± 1.3	205.9 ± 1.1	242.0 ± 1.9	-35.9 ± 0.9	25.9 ± 2.1	246.6 ± 1.2

Table F.38: SB - Impedance Values at 38 m/s and 2.1 MPa

Freq.	Re(H_{xx})	Re(H_{xy})	Re(H_{yx})	Re(H_{yy})	Im(H_{xx})	Im(H_{xy})	Im(H_{yx})	Im(H_{yy})
Hz	MN/m	MN/m	MN/m	MN/m	MN/m	MN/m	MN/m	MN/m
9.8	208.0 ± 0.5	-16.1 ± 0.8	-70.0 ± 0.5	256.6 ± 1.5	8.0 ± 0.8	-2.4 ± 1.0	2.9 ± 0.8	12.3 ± 1.0
19.5	211.7 ± 0.5	-15.3 ± 0.9	-70.5 ± 0.4	254.3 ± 0.7	15.7 ± 0.3	-4.1 ± 1.0	2.8 ± 0.3	14.7 ± 0.8
29.3	214.5 ± 0.4	-20.8 ± 0.3	-72.7 ± 0.4	266.4 ± 0.2	22.1 ± 0.5	-8.2 ± 0.8	3.1 ± 0.3	21.6 ± 0.6
39.1	212.3 ± 0.4	-16.8 ± 0.5	-67.2 ± 0.3	259.0 ± 0.4	30.8 ± 0.4	-12.1 ± 0.7	-1.1 ± 0.4	34.2 ± 0.5
48.8	216.0 ± 0.3	-17.7 ± 0.4	-70.1 ± 0.3	261.2 ± 0.6	38.8 ± 0.3	-13.8 ± 0.4	0.1 ± 0.2	43.7 ± 0.5
58.6	216.1 ± 0.3	-17.2 ± 0.8	-68.1 ± 0.6	259.5 ± 0.4	46.4 ± 0.2	-16.9 ± 0.4	-1.8 ± 0.5	51.1 ± 0.2
68.4	217.9 ± 0.2	-18.4 ± 0.4	-70.7 ± 0.5	265.8 ± 1.1	53.5 ± 0.3	-17.1 ± 0.5	-4.0 ± 0.2	54.7 ± 0.7
78.1	219.8 ± 0.4	-13.5 ± 0.8	-61.5 ± 0.5	265.3 ± 0.6	64.1 ± 0.3	-15.4 ± 0.8	0.3 ± 0.6	74.6 ± 0.5
87.9	223.5 ± 0.6	-16.4 ± 0.5	-57.6 ± 1.3	270.7 ± 0.3	59.2 ± 0.6	-21.0 ± 0.7	7.7 ± 1.1	67.2 ± 0.3
97.7	222.5 ± 0.6	-15.8 ± 0.4	-67.3 ± 0.3	272.9 ± 0.3	75.9 ± 0.4	-24.7 ± 0.5	-4.7 ± 0.4	86.6 ± 0.5
107.4	225.9 ± 0.6	-16.5 ± 1.1	-64.8 ± 0.4	273.8 ± 0.5	83.5 ± 0.7	-26.9 ± 0.3	-5.8 ± 0.5	93.5 ± 1.1
117.2	64.4 ± 60.0	-5.9 ± 111.1	-6.4 ± 57.6	134.5 ± 264	77.2 ± 76.0	-216.5 ± 325	118.8 ± 58.2	173.4 ± 125
127.0	232.8 ± 0.8	-15.1 ± 0.5	-66.8 ± 0.8	278.4 ± 0.5	95.7 ± 0.8	-31.2 ± 0.4	-9.4 ± 0.4	109.6 ± 0.5
136.7	233.9 ± 0.1	-13.9 ± 0.3	-53.6 ± 0.3	281.2 ± 0.5	100.9 ± 0.4	-31.7 ± 0.2	3.3 ± 0.4	117.2 ± 0.3
146.5	235.2 ± 0.4	-13.8 ± 0.2	-50.4 ± 0.1	290.1 ± 0.3	107.5 ± 0.2	-33.4 ± 0.3	-1.1 ± 0.3	128.4 ± 0.4
156.3	236.2 ± 0.2	-8.8 ± 0.3	-47.7 ± 0.4	286.0 ± 0.5	114.6 ± 0.3	-34.3 ± 0.2	-6.8 ± 0.3	137.2 ± 0.5
166.0	239.0 ± 0.2	-14.3 ± 0.2	-49.3 ± 0.4	293.9 ± 0.3	121.9 ± 0.3	-39.8 ± 0.1	-8.6 ± 0.3	149.7 ± 0.4
175.8	239.7 ± 0.7	-12.7 ± 0.3	-44.2 ± 0.3	297.8 ± 0.8	131.3 ± 0.6	-39.4 ± 0.2	4.9 ± 0.9	156.6 ± 0.4
185.5	243.1 ± 0.3	-8.6 ± 0.2	-49.2 ± 0.7	302.9 ± 0.8	138.7 ± 0.4	-41.5 ± 0.2	-8.7 ± 0.7	177.6 ± 0.7
195.3	251.0 ± 1.7	-4.5 ± 0.4	-54.5 ± 2.0	305.0 ± 0.7	153.2 ± 0.5	-42.2 ± 0.4	-10.6 ± 0.5	181.0 ± 0.4
205.1	254.3 ± 0.8	-4.7 ± 0.5	-36.6 ± 0.9	317.9 ± 0.8	149.7 ± 0.5	-45.4 ± 0.3	3.9 ± 0.3	194.1 ± 0.9
214.8	252.7 ± 1.3	-1.5 ± 0.6	-25.6 ± 0.6	320.9 ± 1.1	157.1 ± 0.6	-47.2 ± 0.3	1.5 ± 1.1	200.7 ± 0.6
224.6	256.9 ± 0.7	5.8 ± 1.2	-28.4 ± 0.9	356.4 ± 1.4	170.9 ± 1.5	-42.5 ± 0.5	1.6 ± 1.6	189.3 ± 1.2
234.4	262.1 ± 160	-152.8 ± 72	90.6 ± 105.3	132.9 ± 100	66.0 ± 124.1	18.1 ± 38.9	-97.2 ± 272	143.4 ± 61.0
244.1	265.0 ± 0.9	-5.1 ± 1.7	-22.5 ± 1.3	347.9 ± 2.5	189.2 ± 2.6	-51.3 ± 1.4	4.9 ± 3.6	221.2 ± 2.0

Table F.39: SB - Impedance Values at 38 m/s and 2.9 MPa

Freq.	Re(H_{xx})	Re(H_{xy})	Re(H_{yx})	Re(H_{yy})	Im(H_{xx})	Im(H_{xy})	Im(H_{yx})	Im(H_{yy})
Hz	MN/m	MN/m	MN/m	MN/m	MN/m	MN/m	MN/m	MN/m
9.8	242.5 ± 1.3	-28.8 ± 1.3	-70.3 ± 1.5	309.0 ± 2.6	7.3 ± 0.6	-2.9 ± 1.6	4.3 ± 0.9	12.9 ± 2.0
19.5	246.0 ± 0.6	-29.8 ± 0.1	-69.6 ± 0.2	306.7 ± 0.4	16.9 ± 0.5	-5.2 ± 0.5	0.8 ± 0.5	13.0 ± 0.6
29.3	249.6 ± 0.7	-34.5 ± 0.3	-73.6 ± 0.4	327.3 ± 0.3	22.3 ± 0.6	-7.8 ± 0.7	-0.5 ± 0.5	22.2 ± 0.4
39.1	247.9 ± 0.2	-30.7 ± 0.2	-68.6 ± 0.6	314.7 ± 0.4	30.5 ± 0.6	-12.0 ± 0.6	-4.4 ± 0.1	31.9 ± 0.7
48.8	250.7 ± 0.3	-31.5 ± 0.4	-71.3 ± 0.3	318.1 ± 0.5	36.8 ± 0.3	-13.8 ± 0.4	-4.9 ± 0.4	39.8 ± 0.8
58.6	253.4 ± 0.4	-31.1 ± 0.4	-70.7 ± 0.3	317.7 ± 0.7	43.4 ± 0.3	-14.9 ± 0.2	-7.1 ± 0.5	48.2 ± 0.5
68.4	255.0 ± 0.3	-31.1 ± 0.8	-73.5 ± 0.3	323.7 ± 0.7	51.6 ± 0.4	-15.6 ± 0.2	-9.9 ± 0.3	49.1 ± 0.6
78.1	252.3 ± 0.2	-32.7 ± 0.3	-76.1 ± 0.4	315.3 ± 0.4	57.6 ± 0.4	-15.8 ± 0.5	-7.1 ± 0.5	63.9 ± 0.6
87.9	262.1 ± 1.0	-31.2 ± 0.4	-64.9 ± 0.8	330.1 ± 0.7	54.3 ± 1.4	-20.3 ± 0.2	0.6 ± 0.8	61.4 ± 0.6
97.7	260.0 ± 0.2	-29.3 ± 0.4	-70.8 ± 0.2	330.1 ± 0.5	69.8 ± 0.3	-24.0 ± 0.5	-11.9 ± 0.4	79.5 ± 0.4
107.4	263.3 ± 0.7	-29.8 ± 0.8	-70.7 ± 0.7	331.6 ± 0.6	76.3 ± 0.7	-25.7 ± 0.4	-12.0 ± 0.6	85.8 ± 0.4
117.2	248.0 ± 21.9	76.7 ± 67.1	-89.4 ± 14.4	380.1 ± 50.4	46.1 ± 24.9	97.3 ± 101.9	16.1 ± 24.7	-39.8 ± 92.6
127.0	270.4 ± 0.9	-27.8 ± 0.5	-72.4 ± 0.8	336.2 ± 0.3	86.8 ± 0.8	-30.1 ± 0.3	-15.6 ± 0.6	101.1 ± 0.3
136.7	271.1 ± 0.3	-26.8 ± 0.2	-62.0 ± 0.3	339.0 ± 0.2	90.8 ± 0.4	-31.6 ± 0.3	-3.6 ± 0.5	107.4 ± 0.3
146.5	271.6 ± 0.2	-25.4 ± 0.2	-59.1 ± 0.4	344.6 ± 0.3	96.3 ± 0.2	-32.9 ± 0.1	-8.8 ± 0.3	117.1 ± 0.2
156.3	272.3 ± 0.3	-23.5 ± 0.2	-57.4 ± 0.2	352.2 ± 0.3	103.0 ± 0.4	-36.3 ± 0.2	-13.0 ± 0.2	127.4 ± 0.2
166.0	274.8 ± 0.4	-28.4 ± 0.3	-59.3 ± 0.3	354.9 ± 0.3	108.8 ± 0.1	-40.4 ± 0.1	-14.5 ± 0.3	137.8 ± 0.5
175.8	277.6 ± 0.3	-26.4 ± 0.3	-54.9 ± 0.4	357.6 ± 0.4	116.0 ± 0.2	-40.5 ± 0.3	-0.7 ± 0.4	143.1 ± 0.3
185.5	279.4 ± 0.4	-21.0 ± 0.5	-57.9 ± 0.5	361.7 ± 0.3	125.7 ± 0.3	-43.9 ± 0.3	-14.6 ± 0.3	165.3 ± 0.5
195.3	288.0 ± 0.3	-18.0 ± 0.4	-63.9 ± 0.9	364.9 ± 0.3	139.3 ± 0.6	-45.4 ± 0.4	-13.0 ± 1.1	166.3 ± 0.4
205.1	289.7 ± 0.4	-18.5 ± 0.3	-44.0 ± 0.7	377.3 ± 0.4	130.8 ± 0.6	-48.0 ± 0.1	-2.0 ± 0.1	176.6 ± 0.5
214.8	286.1 ± 0.5	-13.8 ± 0.4	-35.5 ± 0.9	378.0 ± 0.8	138.8 ± 0.7	-50.8 ± 0.3	-7.5 ± 0.5	189.5 ± 0.8
224.6	291.1 ± 1.1	-13.4 ± 0.8	-39.3 ± 0.9	430.3 ± 0.7	150.5 ± 0.3	-49.2 ± 0.6	-5.2 ± 1.1	167.4 ± 1.2
234.4	299.1 ± 28.0	-19.5 ± 62.1	-30.8 ± 25.1	282.3 ± 73.1	152.6 ± 9.5	51.1 ± 36.0	3.0 ± 32.2	299.8 ± 69.0
244.1	299.4 ± 1.8	-18.9 ± 0.7	-30.3 ± 1.1	409.6 ± 0.7	167.0 ± 0.4	-52.1 ± 1.0	-0.3 ± 2.6	204.9 ± 1.5

Table F.40: SB - Impedance Values at 53 m/s and 0.7 MPa

Freq.	Re(H_{xx})	Re(H_{xy})	Re(H_{yx})	Re(H_{yy})	Im(H_{xx})	Im(H_{xy})	Im(H_{yx})	Im(H_{yy})
Hz	MN/m	MN/m	MN/m	MN/m	MN/m	MN/m	MN/m	MN/m
9.8	140.6 ± 0.4	28.8 ± 0.7	-61.7 ± 0.1	142.5 ± 0.4	7.9 ± 0.3	-3.3 ± 0.5	2.6 ± 0.2	9.4 ± 0.4
19.5	142.2 ± 0.3	29.6 ± 0.1	-63.6 ± 0.2	141.2 ± 0.5	15.6 ± 0.3	-4.8 ± 0.4	2.0 ± 0.2	17.3 ± 0.4
29.3	143.5 ± 0.3	26.7 ± 0.3	-65.5 ± 0.6	148.7 ± 0.3	22.0 ± 0.3	-8.2 ± 0.2	4.1 ± 0.3	23.8 ± 0.5
39.1	142.7 ± 0.2	30.4 ± 0.4	-62.0 ± 0.3	144.5 ± 0.3	30.3 ± 0.2	-12.4 ± 0.5	2.9 ± 0.4	33.2 ± 0.4
48.8	143.5 ± 0.2	29.9 ± 0.6	-63.5 ± 0.4	144.8 ± 0.5	39.7 ± 0.3	-15.7 ± 0.4	5.2 ± 0.1	41.6 ± 0.2
58.6	143.1 ± 0.3	29.7 ± 0.2	-61.7 ± 0.2	144.9 ± 0.3	47.0 ± 0.3	-19.5 ± 0.7	4.6 ± 0.2	50.1 ± 0.5
68.4	145.4 ± 0.2	28.6 ± 0.6	-63.5 ± 0.3	150.4 ± 0.6	58.8 ± 0.2	-16.6 ± 0.4	10.4 ± 0.4	61.1 ± 0.4
78.1	145.1 ± 0.6	33.0 ± 0.2	-54.6 ± 0.3	145.0 ± 0.2	64.4 ± 0.2	-23.1 ± 0.3	4.9 ± 0.3	66.0 ± 0.8
87.9	146.8 ± 0.7	28.3 ± 0.5	-53.0 ± 1.2	154.7 ± 0.5	66.7 ± 1.4	-27.9 ± 0.2	14.3 ± 0.8	65.8 ± 0.8
97.7	150.1 ± 0.5	28.3 ± 0.4	-57.4 ± 0.4	154.8 ± 0.6	79.2 ± 0.4	-29.9 ± 0.6	8.7 ± 0.2	82.8 ± 0.3
107.4	152.1 ± 0.3	27.3 ± 0.3	-55.5 ± 0.2	157.1 ± 0.5	88.1 ± 0.3	-31.9 ± 0.3	9.0 ± 0.2	88.5 ± 0.5
117.2	155.3 ± 0.5	27.6 ± 0.3	-53.5 ± 0.3	159.5 ± 0.6	97.0 ± 0.4	-35.1 ± 0.2	7.2 ± 0.2	97.5 ± 0.4
127.0	155.9 ± 0.3	26.3 ± 0.3	-51.2 ± 0.3	160.2 ± 0.2	100.6 ± 0.4	-35.8 ± 0.2	7.1 ± 0.4	103.0 ± 0.3
136.7	159.4 ± 0.1	25.3 ± 0.2	-43.6 ± 0.3	167.3 ± 0.3	109.4 ± 0.5	-37.3 ± 0.2	17.3 ± 0.2	110.4 ± 0.3
146.5	160.5 ± 0.2	25.6 ± 0.2	-39.9 ± 0.2	169.3 ± 0.3	116.1 ± 0.4	-38.3 ± 0.2	14.5 ± 0.4	118.3 ± 0.5
156.3	161.8 ± 0.2	29.1 ± 0.2	-35.9 ± 0.3	158.7 ± 0.3	125.1 ± 0.3	-37.3 ± 0.1	9.8 ± 0.2	124.8 ± 0.4
166.0	164.6 ± 1.9	21.7 ± 1.2	-36.5 ± 1.4	172.1 ± 1.2	130.7 ± 1.5	-42.9 ± 1.1	11.1 ± 1.6	135.6 ± 1.4
175.8	161.9 ± 0.7	22.6 ± 0.6	-29.7 ± 0.6	174.8 ± 0.6	145.0 ± 0.7	-40.7 ± 0.4	19.3 ± 0.5	143.8 ± 0.6
185.5	167.4 ± 0.3	24.1 ± 0.4	-33.0 ± 0.8	180.5 ± 0.6	149.1 ± 0.5	-41.9 ± 0.2	12.7 ± 0.7	157.0 ± 0.6
195.3	169.3 ± 0.7	28.0 ± 0.4	-31.0 ± 0.9	178.1 ± 0.3	159.7 ± 0.4	-39.1 ± 0.6	10.4 ± 0.5	160.9 ± 0.4
205.1	175.8 ± 0.3	25.7 ± 0.4	-21.9 ± 0.4	186.7 ± 0.5	163.2 ± 0.5	-40.1 ± 0.7	25.2 ± 0.4	171.8 ± 0.5
214.8	173.5 ± 0.2	28.7 ± 0.3	-12.6 ± 0.4	184.2 ± 0.4	173.2 ± 0.3	-39.0 ± 0.2	22.7 ± 0.5	178.5 ± 0.3
224.6	173.5 ± 0.4	42.2 ± 0.2	-11.7 ± 0.2	181.7 ± 0.3	186.6 ± 0.4	-26.2 ± 0.3	19.4 ± 0.3	171.7 ± 0.5
234.4	170.5 ± 0.5	27.5 ± 0.4	-12.3 ± 0.5	196.6 ± 0.2	197.9 ± 0.4	-37.8 ± 0.2	32.8 ± 0.2	200.6 ± 0.3
244.1	174.3 ± 0.6	26.5 ± 0.3	-12.1 ± 0.5	199.3 ± 0.4	208.9 ± 0.2	-33.2 ± 0.4	31.5 ± 0.7	204.5 ± 0.2

Table F.41: SB - Impedance Values at 53 m/s and 2.1 MPa

Freq.	Re(H_{xx})	Re(H_{xy})	Re(H_{yx})	Re(H_{yy})	Im(H_{xx})	Im(H_{xy})	Im(H_{yx})	Im(H_{yy})
Hz	MN/m	MN/m	MN/m	MN/m	MN/m	MN/m	MN/m	MN/m
9.8	211.3 ± 0.7	-9.5 ± 0.5	-76.6 ± 1.0	244.7 ± 0.7	5.6 ± 1.0	-1.4 ± 1.4	8.6 ± 0.6	9.0 ± 1.3
19.5	213.5 ± 0.6	-8.5 ± 1.4	-75.4 ± 0.5	243.5 ± 0.5	13.2 ± 0.8	-3.8 ± 0.7	2.3 ± 0.3	11.3 ± 0.6
29.3	216.9 ± 0.6	-13.9 ± 0.5	-80.0 ± 0.7	258.9 ± 1.3	20.1 ± 0.6	-8.7 ± 0.5	5.2 ± 1.2	18.3 ± 0.7
39.1	215.4 ± 0.6	-10.4 ± 0.5	-75.0 ± 0.8	247.6 ± 1.0	28.2 ± 0.7	-12.9 ± 0.5	-0.1 ± 0.4	29.8 ± 0.7
48.8	218.3 ± 0.8	-12.9 ± 0.9	-76.2 ± 0.5	249.0 ± 1.6	35.3 ± 0.5	-18.1 ± 1.2	0.6 ± 0.6	38.6 ± 1.5
58.6	217.9 ± 0.9	-11.5 ± 1.0	-75.4 ± 0.4	246.1 ± 1.0	41.8 ± 1.1	-19.2 ± 1.0	0.1 ± 0.4	46.2 ± 0.7
68.4	219.4 ± 0.7	-14.7 ± 0.7	-77.1 ± 0.8	253.0 ± 1.0	48.1 ± 0.4	-17.8 ± 0.8	-2.8 ± 0.6	49.2 ± 0.7
78.1	221.0 ± 0.2	-8.9 ± 0.4	-67.0 ± 0.7	254.1 ± 0.5	58.0 ± 0.7	-19.8 ± 0.7	2.1 ± 0.6	63.3 ± 0.7
87.9	224.8 ± 1.7	-13.4 ± 0.9	-63.2 ± 1.8	256.2 ± 0.9	56.5 ± 0.7	-25.3 ± 1.0	9.2 ± 1.8	56.7 ± 0.6
97.7	223.5 ± 0.4	-14.4 ± 0.6	-72.7 ± 0.8	260.6 ± 0.9	68.3 ± 0.2	-26.3 ± 0.5	-3.5 ± 0.5	77.6 ± 0.6
107.4	226.2 ± 0.5	-15.8 ± 0.6	-70.9 ± 0.4	260.7 ± 0.6	75.7 ± 0.2	-29.1 ± 0.6	-3.7 ± 0.3	82.1 ± 0.6
117.2	229.3 ± 0.5	-14.9 ± 0.3	-72.3 ± 0.3	265.7 ± 0.6	80.9 ± 0.3	-30.0 ± 0.5	-6.7 ± 0.3	90.8 ± 0.4
127.0	231.4 ± 0.7	-14.7 ± 0.7	-73.6 ± 0.8	265.4 ± 0.3	84.7 ± 0.8	-30.6 ± 0.5	-7.3 ± 0.7	95.5 ± 0.7
136.7	231.5 ± 0.6	-13.1 ± 0.3	-60.9 ± 0.2	268.1 ± 0.2	91.1 ± 0.2	-31.3 ± 0.2	5.3 ± 0.2	100.6 ± 0.4
146.5	232.4 ± 0.4	-13.5 ± 0.4	-59.3 ± 0.7	276.8 ± 0.3	96.8 ± 0.3	-32.6 ± 0.3	1.4 ± 0.3	108.2 ± 0.3
156.3	232.7 ± 0.4	-9.4 ± 0.4	-55.6 ± 0.5	270.4 ± 0.4	104.3 ± 0.2	-33.2 ± 0.2	-3.6 ± 0.2	115.2 ± 0.5
166.0	233.6 ± 2.0	-12.7 ± 3.2	-57.1 ± 1.1	276.0 ± 3.0	111.5 ± 1.3	-38.2 ± 3.4	-3.3 ± 2.0	122.2 ± 2.8
175.8	236.2 ± 1.0	-15.6 ± 0.6	-52.2 ± 0.5	281.2 ± 0.3	120.9 ± 0.3	-35.5 ± 0.7	10.5 ± 0.7	127.9 ± 0.6
185.5	239.5 ± 0.5	-10.6 ± 0.3	-55.2 ± 0.7	281.8 ± 0.8	124.8 ± 0.2	-37.9 ± 0.6	-4.0 ± 0.3	146.5 ± 0.6
195.3	244.3 ± 1.2	-8.1 ± 0.7	-60.1 ± 1.5	281.3 ± 0.5	132.8 ± 1.0	-35.9 ± 0.2	-5.4 ± 0.6	145.1 ± 0.6
205.1	248.1 ± 0.3	-7.4 ± 0.6	-41.6 ± 0.4	291.0 ± 0.5	134.1 ± 0.3	-38.5 ± 0.5	8.3 ± 0.5	156.8 ± 0.3
214.8	245.2 ± 0.5	-4.1 ± 0.3	-31.4 ± 0.6	288.2 ± 0.4	141.4 ± 0.5	-37.8 ± 0.4	4.6 ± 0.4	163.8 ± 0.8
224.6	247.2 ± 0.1	2.7 ± 0.2	-34.0 ± 0.4	319.7 ± 0.5	151.2 ± 0.3	-32.6 ± 0.2	4.0 ± 0.3	146.4 ± 0.5
234.4	241.9 ± 0.9	-5.0 ± 0.4	-42.1 ± 0.4	300.6 ± 0.6	160.6 ± 0.6	-39.0 ± 0.4	9.8 ± 1.0	183.5 ± 0.6
244.1	250.6 ± 0.4	-2.9 ± 0.5	-28.8 ± 0.4	304.0 ± 0.4	164.3 ± 0.3	-35.5 ± 0.7	4.8 ± 0.6	184.6 ± 0.4

Table F.42: SB - Impedance Values at 53 m/s and 2.9 MPa

Freq.	Re(H_{xx})	Re(H_{xy})	Re(H_{yx})	Re(H_{yy})	Im(H_{xx})	Im(H_{xy})	Im(H_{yx})	Im(H_{yy})
Hz	MN/m	MN/m	MN/m	MN/m	MN/m	MN/m	MN/m	MN/m
9.8	241.7 ± 0.3	-25.9 ± 0.6	-73.5 ± 0.9	297.9 ± 0.6	0.9 ± 0.9	-1.7 ± 0.7	-0.3 ± 0.7	11.2 ± 1.2
19.5	245.6 ± 0.9	-26.9 ± 0.8	-74.3 ± 1.1	296.7 ± 1.3	13.3 ± 0.4	-2.9 ± 0.4	-1.0 ± 0.7	11.5 ± 1.0
29.3	251.9 ± 0.6	-35.3 ± 0.5	-76.9 ± 1.1	314.0 ± 0.5	20.4 ± 1.0	-8.9 ± 0.7	1.2 ± 1.5	16.9 ± 1.0
39.1	246.3 ± 0.8	-28.6 ± 0.7	-72.8 ± 1.0	301.5 ± 0.5	28.5 ± 0.6	-12.7 ± 0.6	-3.0 ± 0.6	27.9 ± 0.5
48.8	248.4 ± 0.5	-31.2 ± 0.4	-75.4 ± 1.2	305.0 ± 1.6	32.2 ± 0.3	-14.4 ± 0.5	-3.7 ± 0.5	35.4 ± 1.7
58.6	249.2 ± 1.1	-29.3 ± 1.1	-75.3 ± 0.7	303.5 ± 1.7	37.4 ± 0.7	-18.7 ± 0.7	-7.3 ± 1.1	41.4 ± 1.7
68.4	250.7 ± 0.8	-30.4 ± 1.1	-77.6 ± 0.8	308.5 ± 0.9	43.9 ± 0.6	-17.3 ± 1.2	-8.0 ± 0.9	39.5 ± 1.5
78.1	248.5 ± 0.7	-32.2 ± 0.4	-80.4 ± 0.9	299.3 ± 0.7	52.3 ± 0.7	-15.0 ± 0.5	-4.5 ± 0.6	56.2 ± 1.0
87.9	252.7 ± 1.8	-31.5 ± 0.5	-72.4 ± 1.0	312.7 ± 0.6	51.5 ± 1.3	-22.9 ± 0.7	1.6 ± 2.7	50.0 ± 0.8
97.7	255.1 ± 0.6	-31.1 ± 0.5	-77.3 ± 0.4	313.9 ± 0.8	62.6 ± 0.5	-23.9 ± 0.6	-10.7 ± 0.8	69.3 ± 0.9
107.4	257.8 ± 0.2	-32.0 ± 0.6	-76.4 ± 0.4	316.4 ± 0.5	68.2 ± 0.5	-24.1 ± 0.3	-11.6 ± 0.6	74.3 ± 0.5
117.2	259.8 ± 0.4	-30.9 ± 0.3	-77.7 ± 0.5	320.3 ± 0.4	72.3 ± 0.3	-26.3 ± 0.3	-15.2 ± 0.9	82.2 ± 0.4
127.0	262.4 ± 0.5	-29.8 ± 0.2	-79.7 ± 0.4	319.2 ± 0.2	75.7 ± 0.4	-27.3 ± 0.3	-16.2 ± 0.5	85.9 ± 0.3
136.7	261.6 ± 0.4	-28.2 ± 0.3	-67.9 ± 0.5	321.1 ± 0.4	82.6 ± 0.4	-28.4 ± 0.1	-4.2 ± 0.5	89.8 ± 0.3
146.5	262.7 ± 0.4	-26.5 ± 0.2	-66.8 ± 0.3	325.9 ± 0.3	87.1 ± 0.5	-28.8 ± 0.2	-7.9 ± 0.4	96.9 ± 0.3
156.3	263.6 ± 0.7	-24.6 ± 0.2	-64.7 ± 0.5	329.6 ± 0.2	93.0 ± 0.3	-31.6 ± 0.4	-11.3 ± 0.4	105.1 ± 0.5
166.0	266.6 ± 2.6	-30.1 ± 3.5	-71.3 ± 1.5	332.0 ± 4.1	95.6 ± 2.8	-35.7 ± 4.5	-10.5 ± 3.0	112.0 ± 3.2
175.8	264.3 ± 0.8	-28.0 ± 0.5	-62.0 ± 0.2	331.9 ± 0.6	106.6 ± 0.7	-32.7 ± 0.6	1.6 ± 0.7	115.3 ± 0.7
185.5	268.8 ± 0.7	-23.0 ± 0.4	-64.1 ± 0.7	333.2 ± 0.7	111.6 ± 0.7	-35.8 ± 0.5	-10.9 ± 0.6	135.4 ± 0.2
195.3	272.0 ± 1.4	-19.4 ± 0.5	-70.5 ± 1.2	333.6 ± 0.7	120.0 ± 0.9	-35.2 ± 0.3	-11.6 ± 0.6	133.6 ± 0.4
205.1	277.9 ± 0.6	-18.8 ± 0.8	-50.1 ± 0.4	341.8 ± 0.4	119.9 ± 0.3	-37.0 ± 0.2	0.1 ± 0.3	144.2 ± 0.5
214.8	274.8 ± 0.7	-15.1 ± 0.4	-42.6 ± 0.5	339.6 ± 0.3	125.8 ± 0.7	-39.2 ± 0.3	-5.2 ± 0.4	154.9 ± 0.5
224.6	276.2 ± 0.5	-11.5 ± 0.3	-45.9 ± 0.2	387.9 ± 0.3	135.0 ± 0.4	-36.7 ± 0.5	-5.0 ± 0.4	132.4 ± 0.2
234.4	271.9 ± 0.8	-19.5 ± 0.6	-53.7 ± 1.3	358.5 ± 0.6	142.7 ± 0.9	-42.3 ± 0.6	-3.1 ± 1.7	175.8 ± 0.5
244.1	279.8 ± 0.3	-14.1 ± 0.2	-39.9 ± 0.5	356.5 ± 0.4	145.6 ± 0.8	-38.4 ± 0.4	-4.1 ± 0.2	171.0 ± 0.7

Table F.43: SB - Impedance Values at 69 m/s and 0.7 MPa

Freq.	Re(H_{xx})	Re(H_{xy})	Re(H_{yx})	Re(H_{yy})	Im(H_{xx})	Im(H_{xy})	Im(H_{yx})	Im(H_{yy})
Hz	MN/m	MN/m	MN/m	MN/m	MN/m	MN/m	MN/m	MN/m
9.8	160.8 ± 0.5	36.9 ± 0.6	-68.1 ± 0.7	160.7 ± 0.7	7.3 ± 0.4	-1.9 ± 0.3	0.2 ± 0.8	9.1 ± 1.1
19.5	160.5 ± 0.5	38.4 ± 0.5	-67.9 ± 0.5	158.5 ± 0.7	13.2 ± 0.3	-2.8 ± 0.4	1.7 ± 0.3	13.8 ± 0.6
29.3	161.8 ± 0.2	37.1 ± 0.4	-68.7 ± 0.7	166.8 ± 0.4	20.0 ± 0.6	-7.4 ± 0.7	1.6 ± 0.7	20.5 ± 0.5
39.1	163.3 ± 0.6	41.1 ± 0.4	-67.5 ± 0.2	162.2 ± 0.5	26.6 ± 0.7	-11.8 ± 0.4	2.8 ± 1.1	27.2 ± 1.2
48.8	163.2 ± 0.7	40.6 ± 0.8	-67.9 ± 0.6	163.1 ± 0.9	34.5 ± 1.4	-13.8 ± 0.4	3.6 ± 0.6	35.7 ± 0.9
58.6	162.3 ± 0.6	40.1 ± 0.7	-67.2 ± 0.5	161.5 ± 0.8	40.1 ± 0.6	-17.8 ± 0.3	3.7 ± 0.6	41.0 ± 1.0
68.4	163.3 ± 0.5	39.4 ± 1.2	-70.3 ± 0.9	162.5 ± 0.5	48.0 ± 0.5	-17.2 ± 0.5	8.1 ± 0.4	50.1 ± 1.1
78.1	162.5 ± 0.4	44.1 ± 0.7	-62.0 ± 0.5	163.2 ± 0.9	54.4 ± 0.5	-20.7 ± 0.4	5.8 ± 0.5	54.9 ± 0.7
87.9	167.4 ± 0.8	41.3 ± 0.4	-66.8 ± 1.3	166.7 ± 0.6	60.0 ± 1.4	-27.4 ± 0.5	10.1 ± 1.5	55.9 ± 1.3
97.7	165.4 ± 0.7	42.3 ± 0.5	-62.5 ± 0.5	169.5 ± 0.8	68.0 ± 0.2	-28.8 ± 0.3	12.3 ± 0.5	68.6 ± 0.3
107.4	167.7 ± 0.2	39.0 ± 0.4	-61.5 ± 0.6	171.4 ± 0.9	74.5 ± 0.7	-31.4 ± 0.7	14.1 ± 0.3	75.7 ± 0.6
117.2	169.3 ± 0.4	42.2 ± 0.3	-59.2 ± 0.2	172.8 ± 0.6	82.8 ± 0.5	-35.5 ± 0.4	14.4 ± 0.4	81.8 ± 0.3
127.0	169.7 ± 0.6	40.4 ± 0.4	-57.6 ± 0.3	172.1 ± 0.4	87.6 ± 0.6	-36.9 ± 0.2	14.0 ± 0.4	89.2 ± 0.6
136.7	173.0 ± 0.6	40.9 ± 0.4	-52.0 ± 0.3	177.1 ± 0.3	96.9 ± 0.3	-40.2 ± 0.3	20.1 ± 0.3	96.9 ± 0.4
146.5	174.1 ± 0.6	41.4 ± 0.3	-47.7 ± 0.3	178.8 ± 0.4	104.2 ± 0.2	-41.6 ± 0.5	19.0 ± 0.5	104.0 ± 0.5
156.3	174.5 ± 0.2	44.9 ± 0.3	-44.7 ± 0.5	169.6 ± 0.4	111.1 ± 0.6	-42.5 ± 0.3	18.3 ± 0.1	110.4 ± 0.4
166.0	176.0 ± 0.1	37.1 ± 0.3	-42.9 ± 0.6	182.5 ± 0.5	119.9 ± 0.5	-47.3 ± 0.1	22.5 ± 0.3	119.0 ± 0.3
175.8	173.5 ± 0.7	38.0 ± 0.2	-36.1 ± 0.6	184.5 ± 0.5	134.5 ± 0.8	-46.1 ± 0.4	25.4 ± 0.6	127.7 ± 0.4
185.5	180.3 ± 0.4	38.8 ± 0.6	-37.5 ± 0.3	191.8 ± 0.8	136.6 ± 0.3	-48.2 ± 0.6	24.7 ± 0.4	138.2 ± 0.5
195.3	180.6 ± 0.7	42.1 ± 0.6	-34.6 ± 0.5	191.6 ± 0.4	145.6 ± 0.4	-45.1 ± 0.6	28.9 ± 0.3	144.7 ± 0.6
205.1	187.3 ± 0.4	42.1 ± 0.4	-27.3 ± 0.4	196.5 ± 0.6	154.3 ± 0.8	-47.8 ± 0.7	35.7 ± 0.3	153.4 ± 0.5
214.8	187.0 ± 1.4	44.0 ± 2.6	-19.4 ± 2.4	198.0 ± 1.0	166.8 ± 3.0	-48.0 ± 1.1	39.8 ± 0.8	160.0 ± 2.5
224.6	188.3 ± 0.3	58.7 ± 0.6	-14.7 ± 0.4	194.0 ± 0.6	177.3 ± 0.2	-38.0 ± 0.6	34.2 ± 0.3	151.7 ± 0.4
234.4	186.4 ± 0.7	40.5 ± 0.8	-7.4 ± 1.0	212.4 ± 0.7	187.1 ± 0.8	-46.2 ± 0.3	47.0 ± 0.3	181.3 ± 0.7
244.1	192.6 ± 0.4	40.5 ± 0.6	-6.2 ± 0.3	214.0 ± 0.8	199.5 ± 0.4	-44.1 ± 0.7	53.4 ± 0.4	185.1 ± 0.3

Table F.44: SB - Impedance Values at 69 m/s and 2.1 MPa

Freq.	Re(H_{xx})	Re(H_{xy})	Re(H_{yx})	Re(H_{yy})	Im(H_{xx})	Im(H_{xy})	Im(H_{yx})	Im(H_{yy})
Hz	MN/m	MN/m	MN/m	MN/m	MN/m	MN/m	MN/m	MN/m
9.8	217.1 ± 1.0	7.2 ± 1.2	-88.7 ± 1.9	246.0 ± 1.3	4.2 ± 1.1	0.1 ± 1.3	1.4 ± 2.2	6.8 ± 1.4
19.5	219.0 ± 1.3	6.6 ± 1.7	-82.8 ± 0.8	241.4 ± 0.6	8.9 ± 0.8	-4.4 ± 1.9	0.4 ± 0.5	11.2 ± 1.0
29.3	219.9 ± 1.0	0.9 ± 0.8	-89.2 ± 1.0	253.6 ± 1.8	15.7 ± 0.9	-9.7 ± 1.1	3.8 ± 1.2	14.5 ± 1.9
39.1	219.2 ± 2.3	2.3 ± 1.2	-86.0 ± 2.7	244.5 ± 1.6	25.5 ± 0.6	-15.3 ± 1.2	-0.5 ± 0.9	24.3 ± 1.1
48.8	223.7 ± 1.6	1.8 ± 0.7	-83.8 ± 1.2	246.4 ± 0.7	32.5 ± 0.9	-22.0 ± 1.6	5.1 ± 0.9	32.7 ± 1.6
58.6	220.8 ± 1.1	5.3 ± 0.3	-83.6 ± 1.2	244.2 ± 1.0	37.3 ± 0.8	-20.1 ± 2.0	4.0 ± 1.0	41.1 ± 2.0
68.4	224.2 ± 1.0	0.2 ± 0.7	-84.0 ± 1.0	248.5 ± 0.6	42.7 ± 0.8	-20.1 ± 1.1	2.3 ± 1.0	41.2 ± 0.7
78.1	223.6 ± 1.1	5.8 ± 1.8	-75.4 ± 1.0	249.3 ± 1.1	52.2 ± 1.5	-23.7 ± 1.8	9.4 ± 0.6	54.3 ± 1.1
87.9	226.0 ± 1.1	2.0 ± 1.7	-74.1 ± 2.3	249.7 ± 2.1	52.6 ± 3.2	-28.4 ± 0.3	8.0 ± 1.9	50.9 ± 0.6
97.7	225.5 ± 1.5	1.4 ± 0.8	-80.0 ± 0.3	253.2 ± 0.7	60.6 ± 1.0	-31.3 ± 1.8	6.0 ± 0.9	65.0 ± 0.4
107.4	229.0 ± 0.7	-1.5 ± 0.2	-78.8 ± 1.3	252.2 ± 1.0	71.1 ± 0.9	-34.6 ± 0.5	4.3 ± 0.4	73.4 ± 0.6
117.2	229.9 ± 0.7	-0.2 ± 1.2	-75.4 ± 1.3	254.6 ± 0.8	75.0 ± 0.8	-37.1 ± 0.8	2.3 ± 0.5	78.9 ± 1.0
127.0	233.0 ± 0.9	-1.5 ± 0.7	-73.8 ± 1.0	255.2 ± 0.9	79.0 ± 0.8	-39.1 ± 0.6	5.6 ± 0.9	84.7 ± 0.6
136.7	232.8 ± 0.5	-2.6 ± 0.4	-64.6 ± 0.7	257.4 ± 0.4	86.5 ± 0.7	-39.9 ± 0.3	11.4 ± 1.6	92.1 ± 0.5
146.5	233.1 ± 0.5	-3.8 ± 0.4	-62.9 ± 0.7	267.1 ± 0.3	92.2 ± 0.7	-42.0 ± 0.4	8.5 ± 0.5	100.5 ± 0.5
156.3	233.9 ± 0.8	-0.4 ± 0.5	-58.3 ± 0.6	262.0 ± 0.5	99.6 ± 0.2	-43.1 ± 0.4	3.9 ± 0.3	105.9 ± 0.4
166.0	237.0 ± 0.5	-7.1 ± 0.6	-60.9 ± 1.0	266.6 ± 0.7	105.3 ± 0.5	-47.5 ± 0.4	2.0 ± 0.4	115.7 ± 0.9
175.8	233.5 ± 1.4	-7.9 ± 0.5	-56.6 ± 1.3	270.3 ± 0.9	114.5 ± 1.4	-45.9 ± 1.0	15.3 ± 0.9	120.7 ± 1.1
185.5	238.9 ± 1.0	-3.7 ± 1.3	-55.8 ± 0.9	274.4 ± 0.9	118.2 ± 0.4	-46.7 ± 0.4	6.0 ± 1.0	135.0 ± 0.7
195.3	240.5 ± 1.1	-0.3 ± 0.5	-58.2 ± 1.3	272.8 ± 1.1	123.7 ± 1.2	-45.4 ± 0.8	8.0 ± 0.8	135.2 ± 0.9
205.1	247.9 ± 1.1	-2.7 ± 1.0	-45.2 ± 0.5	282.2 ± 1.1	131.4 ± 0.6	-50.0 ± 0.5	15.4 ± 0.7	146.1 ± 0.8
214.8	247.2 ± 4.0	-0.1 ± 0.7	-39.0 ± 1.0	280.0 ± 1.3	136.1 ± 0.7	-50.3 ± 1.8	12.9 ± 2.5	150.5 ± 1.3
224.6	246.5 ± 0.5	4.5 ± 0.9	-35.4 ± 0.9	311.6 ± 0.7	147.0 ± 0.8	-46.0 ± 1.2	11.7 ± 0.4	131.6 ± 0.3
234.4	243.0 ± 1.6	-5.2 ± 0.8	-40.6 ± 1.9	293.3 ± 0.6	154.4 ± 0.9	-49.5 ± 0.4	16.7 ± 0.9	167.9 ± 1.1
244.1	251.4 ± 0.6	-4.6 ± 0.6	-29.6 ± 0.7	292.9 ± 0.6	157.7 ± 0.6	-45.7 ± 0.6	15.4 ± 0.8	167.1 ± 0.9

Table F.45: SB - Impedance Values at 69 m/s and 2.9 MPa

Freq.	Re(H_{xx})	Re(H_{xy})	Re(H_{yx})	Re(H_{yy})	Im(H_{xx})	Im(H_{xy})	Im(H_{yx})	Im(H_{yy})
Hz	MN/m	MN/m	MN/m	MN/m	MN/m	MN/m	MN/m	MN/m
9.8	231.9 ± 0.5	-11.9 ± 1.2	-68.1 ± 0.7	277.6 ± 2.2	1.0 ± 0.8	-1.2 ± 0.5	0.1 ± 0.7	10.5 ± 0.8
19.5	235.9 ± 0.5	-9.4 ± 0.7	-69.2 ± 0.3	274.3 ± 1.1	12.4 ± 1.0	-5.5 ± 0.7	3.3 ± 0.7	8.2 ± 0.7
29.3	236.2 ± 0.7	-12.9 ± 1.3	-71.0 ± 0.9	289.1 ± 2.0	16.7 ± 0.6	-8.6 ± 1.2	4.2 ± 1.7	14.3 ± 1.5
39.1	232.6 ± 1.0	-9.8 ± 0.5	-67.7 ± 1.0	279.7 ± 1.5	23.6 ± 0.6	-11.9 ± 0.7	0.1 ± 0.6	22.2 ± 1.2
48.8	237.5 ± 0.4	-13.3 ± 0.3	-67.1 ± 0.7	278.6 ± 2.0	26.2 ± 0.5	-17.0 ± 0.9	-0.3 ± 0.7	29.5 ± 0.9
58.6	237.6 ± 0.7	-10.0 ± 1.1	-64.7 ± 0.9	277.0 ± 2.0	28.1 ± 0.5	-18.8 ± 0.5	-7.5 ± 0.5	35.2 ± 1.3
68.4	239.9 ± 0.3	-10.8 ± 0.9	-66.1 ± 0.8	281.5 ± 1.7	33.7 ± 0.8	-18.5 ± 0.3	-7.8 ± 0.7	35.2 ± 0.9
78.1	238.5 ± 0.6	-13.5 ± 0.2	-67.2 ± 1.5	273.7 ± 0.9	43.3 ± 0.5	-17.7 ± 0.8	-0.6 ± 1.0	50.2 ± 0.9
87.9	240.6 ± 1.7	-14.5 ± 0.9	-62.4 ± 2.0	286.0 ± 1.0	43.4 ± 1.8	-25.6 ± 0.7	2.7 ± 0.5	43.5 ± 1.1
97.7	240.1 ± 0.4	-12.6 ± 0.6	-65.7 ± 0.8	287.8 ± 0.5	50.0 ± 0.5	-26.9 ± 0.4	-5.6 ± 0.6	61.0 ± 0.5
107.4	243.1 ± 0.4	-15.2 ± 0.5	-62.9 ± 0.4	285.8 ± 0.9	55.0 ± 0.2	-29.8 ± 0.7	-6.9 ± 0.5	64.9 ± 0.9
117.2	243.7 ± 0.6	-13.4 ± 0.4	-63.2 ± 0.7	289.2 ± 0.9	59.2 ± 0.4	-32.2 ± 0.4	-10.9 ± 0.3	72.0 ± 1.4
127.0	244.4 ± 0.8	-15.5 ± 0.3	-64.1 ± 0.3	288.6 ± 0.5	60.2 ± 0.8	-32.3 ± 0.4	-13.5 ± 0.6	76.7 ± 0.9
136.7	243.5 ± 0.4	-14.1 ± 0.4	-55.6 ± 0.6	290.2 ± 0.6	68.2 ± 0.3	-34.3 ± 0.3	-1.1 ± 1.2	82.2 ± 0.5
146.5	243.8 ± 0.2	-12.9 ± 0.6	-55.2 ± 0.4	293.8 ± 0.6	72.5 ± 0.6	-35.6 ± 0.4	-5.7 ± 0.8	88.9 ± 0.2
156.3	243.9 ± 0.3	-11.9 ± 0.2	-53.0 ± 0.3	297.7 ± 0.5	79.2 ± 0.3	-37.7 ± 0.3	-8.4 ± 0.4	95.3 ± 0.1
166.0	246.6 ± 0.2	-18.6 ± 0.2	-56.7 ± 0.2	301.8 ± 0.5	83.8 ± 0.2	-40.0 ± 0.2	-10.3 ± 0.4	102.3 ± 0.4
175.8	243.8 ± 0.8	-16.1 ± 0.3	-50.2 ± 0.5	302.4 ± 0.6	91.4 ± 1.1	-38.5 ± 0.2	2.9 ± 1.0	107.2 ± 0.9
185.5	247.3 ± 0.5	-13.3 ± 0.5	-56.9 ± 0.7	306.3 ± 0.7	96.1 ± 0.2	-41.3 ± 0.6	-9.0 ± 0.8	124.7 ± 0.7
195.3	249.7 ± 1.5	-10.2 ± 0.5	-66.4 ± 1.5	306.8 ± 0.8	105.5 ± 2.3	-42.8 ± 0.8	-6.9 ± 1.7	124.6 ± 0.7
205.1	256.6 ± 0.5	-11.4 ± 0.9	-41.9 ± 0.6	313.1 ± 0.9	102.8 ± 0.5	-43.7 ± 0.5	2.6 ± 0.9	132.0 ± 1.1
214.8	250.5 ± 1.3	-7.0 ± 3.0	-33.3 ± 1.6	312.3 ± 2.0	110.5 ± 2.0	-44.7 ± 2.5	1.1 ± 1.0	136.5 ± 2.1
224.6	255.8 ± 0.6	-9.3 ± 0.7	-36.0 ± 0.3	363.8 ± 0.9	119.2 ± 0.7	-43.5 ± 0.8	-1.5 ± 0.6	118.4 ± 0.4
234.4	253.9 ± 0.6	-15.9 ± 1.2	-41.6 ± 0.8	333.3 ± 0.5	123.7 ± 0.9	-47.9 ± 0.9	3.9 ± 1.4	158.5 ± 0.6
244.1	259.8 ± 0.3	-13.4 ± 0.5	-29.2 ± 0.1	328.0 ± 0.9	129.1 ± 0.4	-44.3 ± 0.7	-0.5 ± 0.7	154.4 ± 1.0

Table F.46: SB - Impedance Values at 85 m/s and 0.7 MPa

Freq.	Re(H_{xx})	Re(H_{xy})	Re(H_{yx})	Re(H_{yy})	Im(H_{xx})	Im(H_{xy})	Im(H_{yx})	Im(H_{yy})
Hz	MN/m	MN/m	MN/m	MN/m	MN/m	MN/m	MN/m	MN/m
9.8	186.3 ± 2.1	40.1 ± 1.7	-74.7 ± 1.3	188.7 ± 2.9	5.8 ± 1.3	-3.0 ± 3.8	-2.7 ± 1.2	7.4 ± 2.5
19.5	187.6 ± 2.5	39.4 ± 1.7	-73.7 ± 0.9	184.3 ± 1.3	11.5 ± 1.8	-9.7 ± 1.7	0.5 ± 1.4	18.9 ± 1.5
29.3	192.5 ± 1.8	43.8 ± 2.1	-77.1 ± 1.7	191.7 ± 2.3	18.7 ± 2.2	-3.6 ± 1.2	-4.3 ± 2.0	16.2 ± 2.6
39.1	190.1 ± 0.7	46.0 ± 0.7	-76.8 ± 1.1	190.4 ± 1.7	23.9 ± 0.9	-9.1 ± 1.1	-0.1 ± 1.4	21.5 ± 0.8
48.8	191.3 ± 0.6	45.8 ± 1.2	-77.6 ± 0.6	189.2 ± 0.9	26.9 ± 1.2	-10.6 ± 1.3	5.7 ± 0.8	29.5 ± 1.3
58.6	188.1 ± 1.1	44.0 ± 1.2	-75.4 ± 1.4	189.4 ± 1.1	31.5 ± 1.0	-15.3 ± 0.9	4.8 ± 0.5	33.5 ± 0.5
68.4	189.0 ± 0.6	43.5 ± 0.8	-77.7 ± 0.7	190.6 ± 1.3	37.0 ± 0.5	-18.7 ± 0.4	5.2 ± 0.8	41.9 ± 0.9
78.1	188.6 ± 0.2	47.2 ± 0.8	-68.0 ± 0.9	190.3 ± 0.5	42.4 ± 0.5	-20.9 ± 1.2	6.4 ± 0.7	50.0 ± 0.7
87.9	189.8 ± 0.9	45.3 ± 0.6	-76.4 ± 0.9	191.7 ± 0.3	52.0 ± 0.5	-25.5 ± 1.0	3.6 ± 1.1	50.4 ± 0.9
97.7	189.3 ± 0.5	45.9 ± 0.7	-74.3 ± 0.5	199.2 ± 0.4	55.2 ± 0.9	-24.0 ± 0.7	9.2 ± 0.9	59.2 ± 0.9
107.4	191.3 ± 0.9	46.7 ± 0.6	-75.2 ± 0.9	197.4 ± 0.5	61.4 ± 0.9	-28.8 ± 0.5	10.5 ± 0.8	63.9 ± 1.0
117.2	190.8 ± 0.6	46.4 ± 0.5	-71.3 ± 0.5	199.4 ± 0.7	70.1 ± 0.3	-31.6 ± 0.7	9.4 ± 0.3	72.0 ± 0.3
127.0	189.5 ± 0.7	49.9 ± 0.4	-67.9 ± 0.2	194.1 ± 0.5	74.4 ± 0.3	-32.9 ± 0.9	11.5 ± 0.5	76.5 ± 0.9
136.7	189.2 ± 0.4	51.2 ± 0.4	-63.3 ± 0.6	198.2 ± 0.4	84.0 ± 0.6	-33.8 ± 0.4	9.6 ± 0.5	82.3 ± 0.5
146.5	192.2 ± 0.9	52.6 ± 0.6	-61.8 ± 0.3	200.0 ± 0.8	88.9 ± 0.4	-38.4 ± 0.7	16.5 ± 0.1	90.8 ± 0.4
156.3	193.6 ± 0.3	53.1 ± 0.5	-59.3 ± 0.2	199.5 ± 0.4	95.2 ± 0.2	-39.9 ± 0.3	20.6 ± 0.2	96.1 ± 0.5
166.0	196.0 ± 0.2	47.0 ± 0.4	-59.9 ± 0.4	207.0 ± 0.6	102.7 ± 0.5	-44.3 ± 0.3	19.8 ± 0.5	102.0 ± 0.8
175.8	192.1 ± 0.3	49.7 ± 0.6	-56.9 ± 0.4	205.4 ± 0.3	116.3 ± 0.5	-45.3 ± 0.8	20.8 ± 0.1	115.2 ± 0.6
185.5	200.7 ± 0.3	51.5 ± 0.2	-55.6 ± 1.1	213.9 ± 1.0	117.4 ± 0.4	-50.0 ± 0.9	30.7 ± 1.1	121.3 ± 0.6
195.3	200.6 ± 0.4	52.2 ± 1.1	-49.3 ± 0.8	213.7 ± 0.4	123.8 ± 0.5	-48.0 ± 0.3	30.1 ± 0.4	127.1 ± 0.6
205.1	203.2 ± 0.6	54.2 ± 1.2	-47.1 ± 0.6	214.3 ± 0.6	133.7 ± 0.6	-48.7 ± 0.6	30.1 ± 0.3	136.7 ± 0.8
214.8	199.7 ± 0.5	56.4 ± 0.6	-41.3 ± 0.5	217.3 ± 0.8	144.3 ± 0.5	-49.3 ± 0.5	33.0 ± 0.4	143.4 ± 0.9
224.6	202.7 ± 0.3	74.7 ± 0.5	-38.2 ± 0.6	218.6 ± 0.4	157.5 ± 0.5	-46.0 ± 0.9	29.0 ± 0.6	138.5 ± 0.6
234.4	198.6 ± 0.6	54.2 ± 0.6	-36.2 ± 0.7	232.0 ± 1.1	165.7 ± 1.0	-52.0 ± 0.8	47.9 ± 0.6	165.7 ± 0.6
244.1	209.4 ± 0.5	57.8 ± 0.6	-29.6 ± 0.3	233.2 ± 0.6	174.4 ± 0.4	-53.4 ± 0.7	49.7 ± 0.2	172.5 ± 0.7

Table F.47: SB - Impedance Values at 85 m/s and 2.1 MPa

Freq.	Re(H_{xx})	Re(H_{xy})	Re(H_{yx})	Re(H_{yy})	Im(H_{xx})	Im(H_{xy})	Im(H_{yx})	Im(H_{yy})
Hz	MN/m	MN/m	MN/m	MN/m	MN/m	MN/m	MN/m	MN/m
9.8	217.5 ± 1.5	24.7 ± 2.1	-78.2 ± 1.8	244.1 ± 3.9	8.3 ± 2.3	-3.1 ± 2.2	-4.7 ± 2.0	9.0 ± 3.0
19.5	223.2 ± 1.4	20.0 ± 3.9	-78.3 ± 1.7	234.0 ± 4.0	9.4 ± 1.6	-5.6 ± 0.3	-3.9 ± 1.1	14.7 ± 2.7
29.3	226.8 ± 2.4	20.8 ± 2.1	-77.7 ± 1.3	241.3 ± 1.9	15.6 ± 0.9	-6.9 ± 1.7	-6.6 ± 0.9	14.1 ± 1.8
39.1	224.8 ± 0.6	24.4 ± 1.6	-78.4 ± 1.3	240.9 ± 3.4	19.0 ± 1.3	-12.9 ± 1.8	-5.6 ± 1.5	19.5 ± 2.5
48.8	222.2 ± 0.6	23.8 ± 0.7	-81.5 ± 1.7	239.3 ± 1.4	21.5 ± 1.3	-15.2 ± 2.3	5.8 ± 1.0	27.2 ± 1.6
58.6	222.3 ± 1.0	23.2 ± 1.4	-79.5 ± 1.6	241.3 ± 1.1	29.9 ± 1.2	-20.3 ± 0.6	1.4 ± 1.3	35.1 ± 1.5
68.4	222.6 ± 0.4	23.1 ± 0.9	-81.9 ± 1.1	240.8 ± 2.2	33.7 ± 0.8	-22.2 ± 1.1	3.1 ± 1.2	41.0 ± 1.5
78.1	224.1 ± 0.7	26.1 ± 1.0	-72.0 ± 0.7	245.5 ± 1.4	39.5 ± 0.5	-22.2 ± 1.0	6.1 ± 0.8	51.1 ± 0.8
87.9	224.1 ± 0.9	25.5 ± 1.1	-85.3 ± 1.5	247.3 ± 1.0	45.9 ± 0.9	-30.8 ± 0.7	7.9 ± 1.3	48.8 ± 1.3
97.7	223.5 ± 0.7	20.7 ± 0.5	-77.3 ± 0.6	248.8 ± 1.8	49.7 ± 1.3	-31.0 ± 0.6	6.5 ± 0.7	58.4 ± 1.2
107.4	222.0 ± 0.3	23.4 ± 0.3	-77.4 ± 1.1	248.2 ± 1.4	53.0 ± 1.0	-32.1 ± 1.4	13.8 ± 1.2	60.6 ± 1.0
117.2	224.1 ± 0.5	20.8 ± 0.1	-74.7 ± 0.5	250.8 ± 0.9	62.2 ± 0.4	-39.6 ± 0.6	7.8 ± 0.4	68.7 ± 1.6
127.0	223.5 ± 0.3	24.0 ± 0.7	-71.1 ± 0.6	243.0 ± 1.0	65.4 ± 0.4	-38.7 ± 0.8	8.9 ± 0.6	75.4 ± 0.4
136.7	224.0 ± 0.8	25.3 ± 0.7	-66.4 ± 0.5	244.0 ± 0.4	75.1 ± 0.7	-42.0 ± 0.7	4.7 ± 0.9	80.4 ± 0.4
146.5	226.8 ± 1.5	24.5 ± 0.5	-61.8 ± 1.1	252.7 ± 1.0	77.3 ± 1.0	-45.8 ± 0.7	15.1 ± 0.4	87.9 ± 0.6
156.3	227.3 ± 0.6	19.1 ± 0.6	-62.1 ± 0.2	258.7 ± 0.5	83.3 ± 0.5	-45.7 ± 1.2	17.4 ± 0.7	91.6 ± 0.5
166.0	228.6 ± 0.4	15.1 ± 0.9	-60.4 ± 0.4	257.0 ± 0.9	90.1 ± 0.7	-48.6 ± 1.1	13.5 ± 0.5	96.0 ± 0.9
175.8	224.1 ± 0.6	18.0 ± 1.2	-59.7 ± 0.3	256.7 ± 1.1	103.1 ± 0.5	-52.2 ± 1.1	15.1 ± 0.6	111.2 ± 1.5
185.5	236.6 ± 1.0	14.5 ± 1.5	-57.7 ± 1.0	265.7 ± 0.8	101.1 ± 1.5	-53.1 ± 1.8	29.4 ± 1.6	115.6 ± 1.2
195.3	232.2 ± 0.9	19.6 ± 1.4	-46.9 ± 1.2	261.3 ± 1.1	113.1 ± 1.5	-54.2 ± 1.1	22.1 ± 0.3	120.4 ± 1.2
205.1	236.0 ± 0.6	18.1 ± 1.1	-48.9 ± 0.5	268.0 ± 0.8	114.8 ± 0.8	-55.3 ± 0.7	20.2 ± 0.9	133.0 ± 1.2
214.8	234.4 ± 0.9	16.6 ± 1.0	-44.2 ± 0.8	273.8 ± 1.1	121.6 ± 0.4	-58.2 ± 0.8	19.6 ± 0.9	138.4 ± 0.6
224.6	235.8 ± 0.3	26.2 ± 1.3	-41.4 ± 0.4	296.4 ± 0.7	131.4 ± 0.6	-55.8 ± 0.3	19.7 ± 0.2	117.1 ± 0.9
234.4	233.2 ± 0.8	13.4 ± 1.0	-43.4 ± 0.6	284.1 ± 0.9	136.9 ± 0.6	-60.0 ± 0.4	28.5 ± 1.1	155.1 ± 1.4
244.1	239.6 ± 0.2	13.4 ± 0.9	-33.1 ± 0.3	281.7 ± 1.1	141.1 ± 0.4	-58.3 ± 1.1	28.4 ± 0.2	160.6 ± 1.2

Table F.48: SB - Impedance Values at 85 m/s and 2.9 MPa

Freq.	Re(H_{xx})	Re(H_{xy})	Re(H_{yx})	Re(H_{yy})	Im(H_{xx})	Im(H_{xy})	Im(H_{yx})	Im(H_{yy})
Hz	MN/m	MN/m	MN/m	MN/m	MN/m	MN/m	MN/m	MN/m
9.8	228.4 ± 1.3	-2.9 ± 1.0	-66.0 ± 1.0	261.0 ± 0.9	7.6 ± 0.9	-5.2 ± 0.7	-3.1 ± 1.4	13.5 ± 3.4
19.5	233.5 ± 0.9	-0.5 ± 1.0	-69.9 ± 0.6	263.3 ± 1.4	10.9 ± 0.4	-2.7 ± 0.9	0.7 ± 1.6	9.0 ± 1.9
29.3	233.0 ± 1.1	-3.1 ± 0.5	-67.3 ± 1.8	265.6 ± 1.1	15.2 ± 0.5	-4.8 ± 0.4	-6.9 ± 0.4	16.0 ± 1.6
39.1	236.3 ± 0.8	-2.0 ± 0.1	-69.8 ± 0.6	265.4 ± 1.4	15.4 ± 0.8	-9.8 ± 0.4	-8.5 ± 0.8	21.1 ± 0.6
48.8	232.9 ± 0.4	0.0 ± 0.5	-71.2 ± 0.7	262.2 ± 1.2	17.7 ± 0.4	-11.2 ± 0.9	0.3 ± 1.3	28.5 ± 0.5
58.6	234.2 ± 0.4	-0.2 ± 0.4	-69.6 ± 0.7	266.1 ± 1.0	24.1 ± 0.9	-14.3 ± 0.8	-2.8 ± 1.4	34.1 ± 1.2
68.4	234.7 ± 0.6	-0.5 ± 0.7	-73.6 ± 0.8	269.1 ± 1.0	25.7 ± 0.5	-16.8 ± 0.6	-2.8 ± 0.4	39.1 ± 0.7
78.1	232.4 ± 0.6	-3.0 ± 0.4	-68.6 ± 0.4	260.9 ± 0.6	32.1 ± 0.7	-16.1 ± 1.0	4.2 ± 0.5	51.2 ± 0.3
87.9	238.3 ± 0.7	-2.2 ± 0.6	-75.2 ± 1.0	272.3 ± 0.9	34.2 ± 0.7	-24.9 ± 0.5	-2.8 ± 1.0	48.2 ± 0.7
97.7	235.4 ± 0.6	-1.4 ± 0.4	-68.7 ± 0.8	274.1 ± 0.9	36.7 ± 0.2	-23.4 ± 0.7	-0.2 ± 0.7	55.0 ± 1.0
107.4	232.4 ± 0.8	-1.1 ± 0.7	-74.1 ± 0.9	274.4 ± 1.0	39.2 ± 0.7	-23.8 ± 0.9	6.6 ± 0.7	56.6 ± 1.4
117.2	235.6 ± 0.8	-3.8 ± 0.6	-67.4 ± 0.8	278.6 ± 1.2	46.0 ± 0.2	-29.6 ± 0.5	-1.8 ± 0.6	67.3 ± 0.8
127.0	233.7 ± 0.3	0.5 ± 0.4	-66.6 ± 0.5	270.7 ± 0.9	46.7 ± 0.5	-29.2 ± 0.8	-0.2 ± 0.4	70.4 ± 0.9
136.7	233.2 ± 0.3	1.8 ± 0.3	-61.5 ± 1.1	269.4 ± 0.8	53.4 ± 0.6	-31.8 ± 0.4	-4.0 ± 0.6	76.2 ± 0.5
146.5	233.9 ± 0.6	3.2 ± 0.7	-55.7 ± 0.6	270.9 ± 0.8	58.1 ± 0.3	-33.2 ± 0.7	6.8 ± 0.4	82.7 ± 0.7
156.3	234.0 ± 0.3	-2.1 ± 0.3	-59.7 ± 0.2	289.8 ± 0.5	63.1 ± 0.4	-35.2 ± 0.5	9.1 ± 0.3	85.4 ± 0.6
166.0	233.6 ± 0.3	-5.2 ± 0.4	-59.0 ± 0.8	286.8 ± 0.8	67.4 ± 0.7	-36.2 ± 0.8	5.1 ± 0.4	90.1 ± 1.0
175.8	228.5 ± 0.4	-3.1 ± 1.0	-57.9 ± 0.4	285.1 ± 0.8	78.4 ± 0.6	-37.5 ± 0.4	6.7 ± 0.2	102.0 ± 0.9
185.5	236.9 ± 1.0	-2.6 ± 0.6	-54.9 ± 0.7	292.3 ± 0.9	79.0 ± 0.8	-40.7 ± 0.8	18.9 ± 1.6	109.5 ± 0.5
195.3	237.6 ± 1.0	-0.8 ± 0.5	-46.7 ± 0.8	293.4 ± 1.2	83.8 ± 0.7	-39.2 ± 0.5	13.7 ± 0.2	110.4 ± 0.4
205.1	238.7 ± 0.4	-1.5 ± 1.0	-48.2 ± 0.5	299.1 ± 1.1	88.3 ± 0.3	-40.5 ± 0.5	11.8 ± 0.3	120.6 ± 0.6
214.8	236.5 ± 0.4	-1.5 ± 0.7	-42.8 ± 0.4	299.2 ± 0.9	94.2 ± 0.8	-45.3 ± 0.5	10.0 ± 0.7	128.2 ± 0.9
224.6	238.7 ± 0.5	2.3 ± 0.3	-43.0 ± 0.8	340.3 ± 0.9	102.8 ± 0.5	-43.0 ± 0.5	9.5 ± 0.8	103.9 ± 0.5
234.4	231.5 ± 1.5	-6.3 ± 0.3	-44.1 ± 0.6	318.4 ± 1.0	106.4 ± 1.1	-45.8 ± 1.0	18.1 ± 1.5	145.9 ± 0.7
244.1	241.2 ± 0.7	-4.2 ± 0.8	-34.6 ± 0.4	309.5 ± 0.6	110.8 ± 0.3	-44.4 ± 0.3	15.8 ± 0.3	145.5 ± 0.7

APPENDIX G

ADDITIONAL ROTORDYNAMIC COEFFICIENT FIGURES

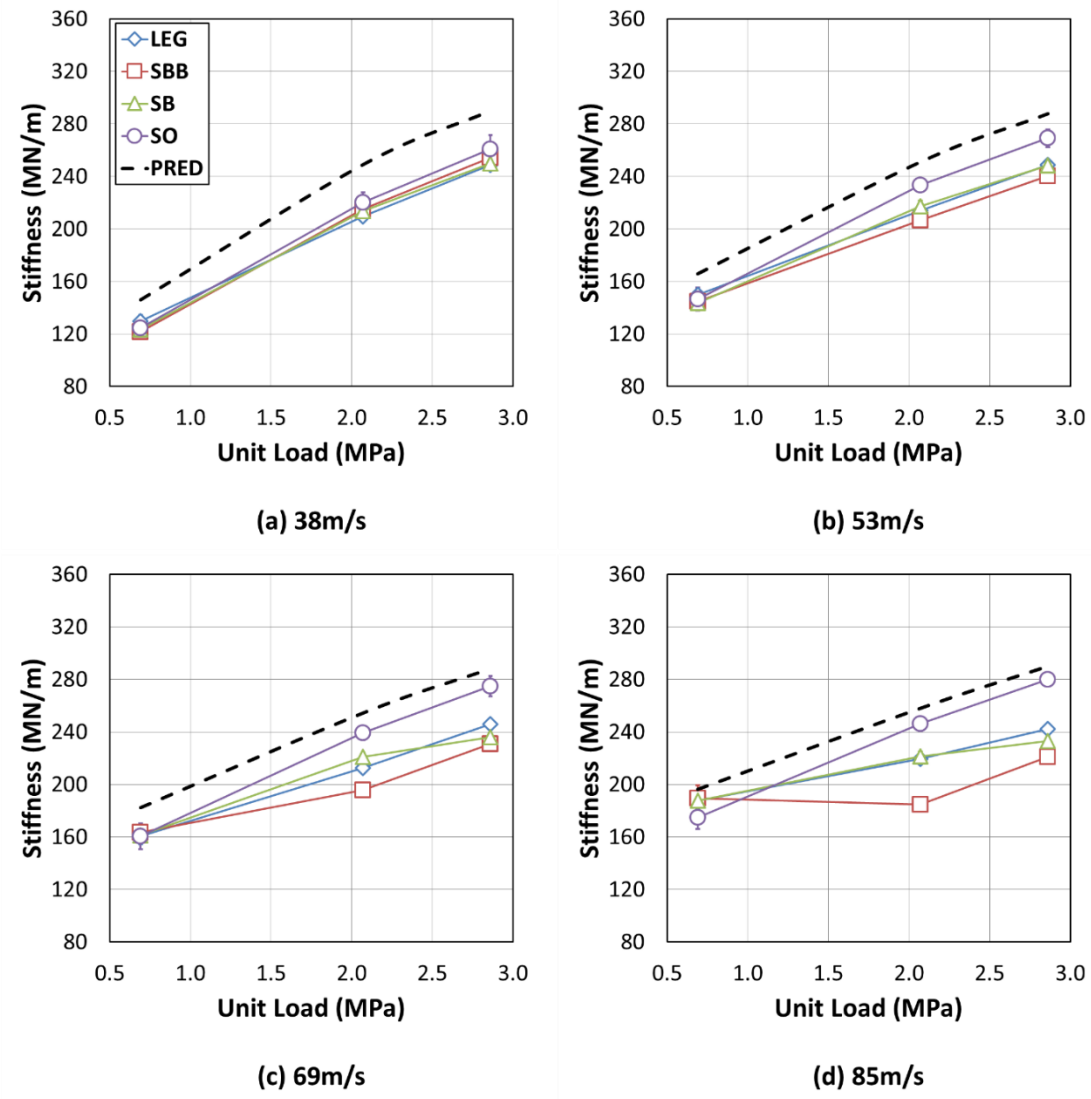

Figure G.1: K_{xx} - Measured and Predicted Direct Stiffness in the Direction Perpendicular to Load as a Function of Load for Speeds of (a) 38, (b) 53, (c) 69, and (d) 85 m/s

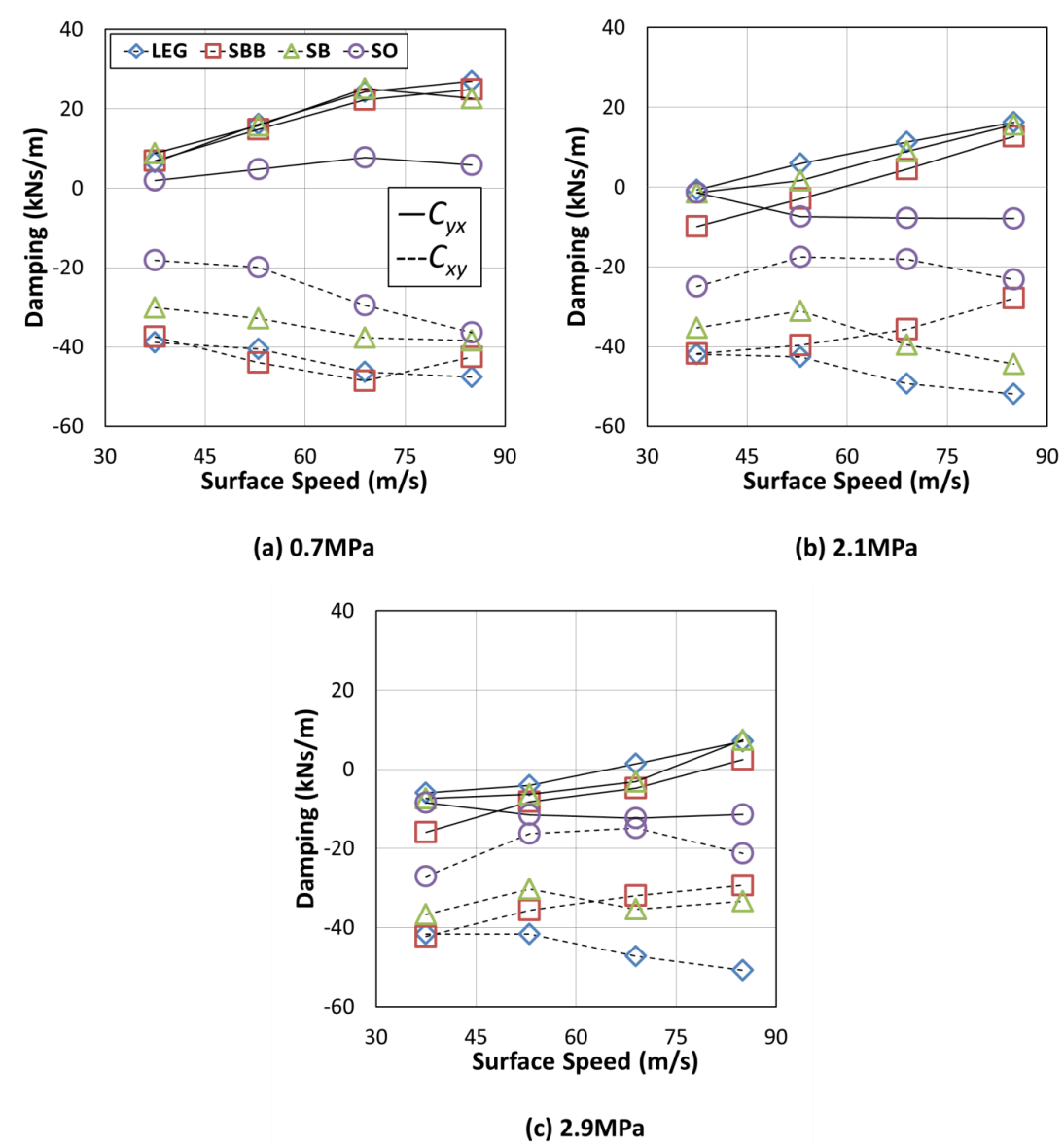

Figure G.2: C_{xy} & C_{yx} - Measured Cross-Coupled Damping as a Function of Speed for Unit Loads of (a) 0.7, (b) 2.1, and (c) 2.9 MPa (Not Shown: Predicted C_{xy} and $C_{yx} \approx$ Zero)

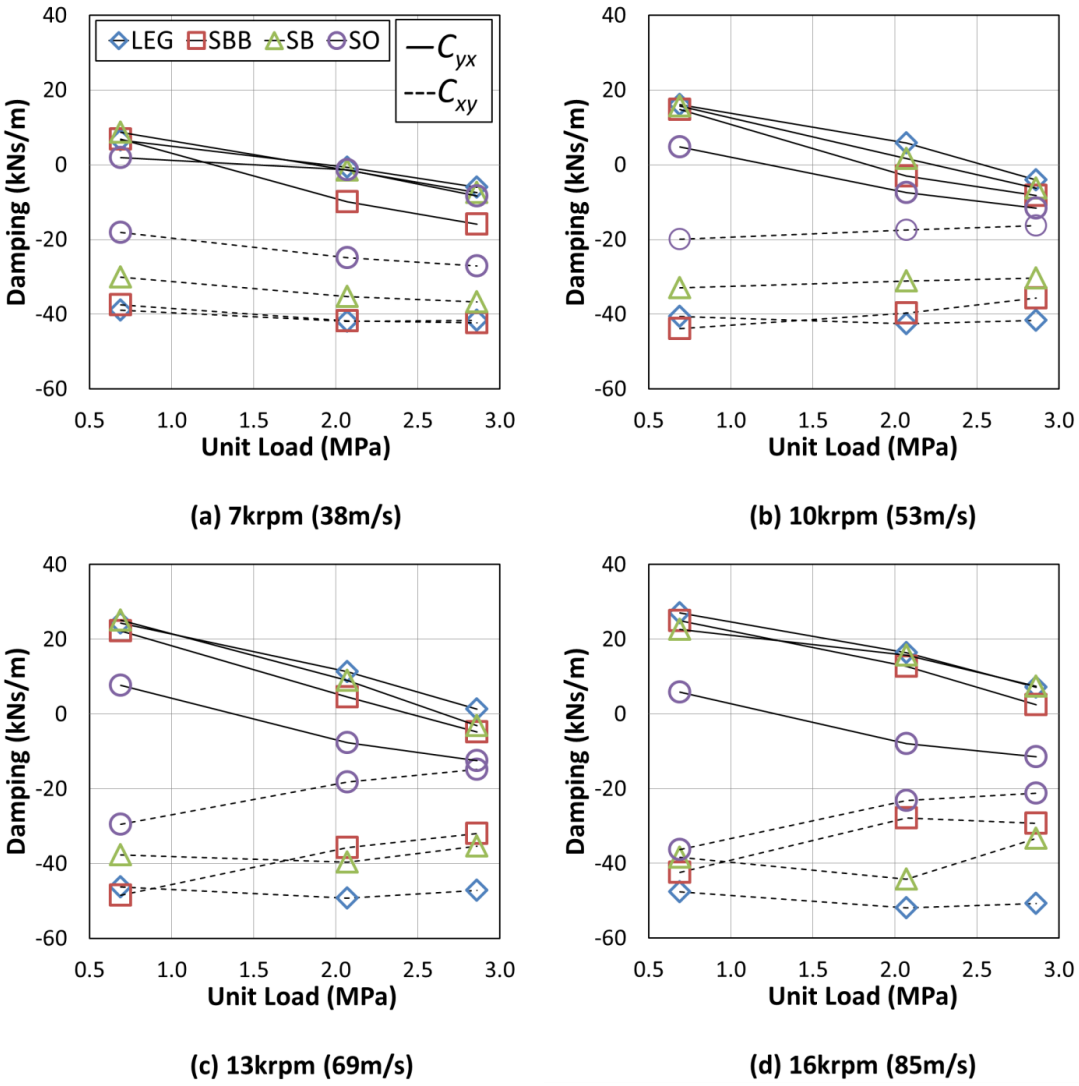

Figure G.3: C_{xy} & C_{yx} - Measured Cross-Coupled Damping as a Function of Load for Speeds of (a) 38, (b) 53, (c) 69, and (d) 85 m/s (Not Shown: Predicted C_{xy} and $C_{yx} \approx$ Zero)

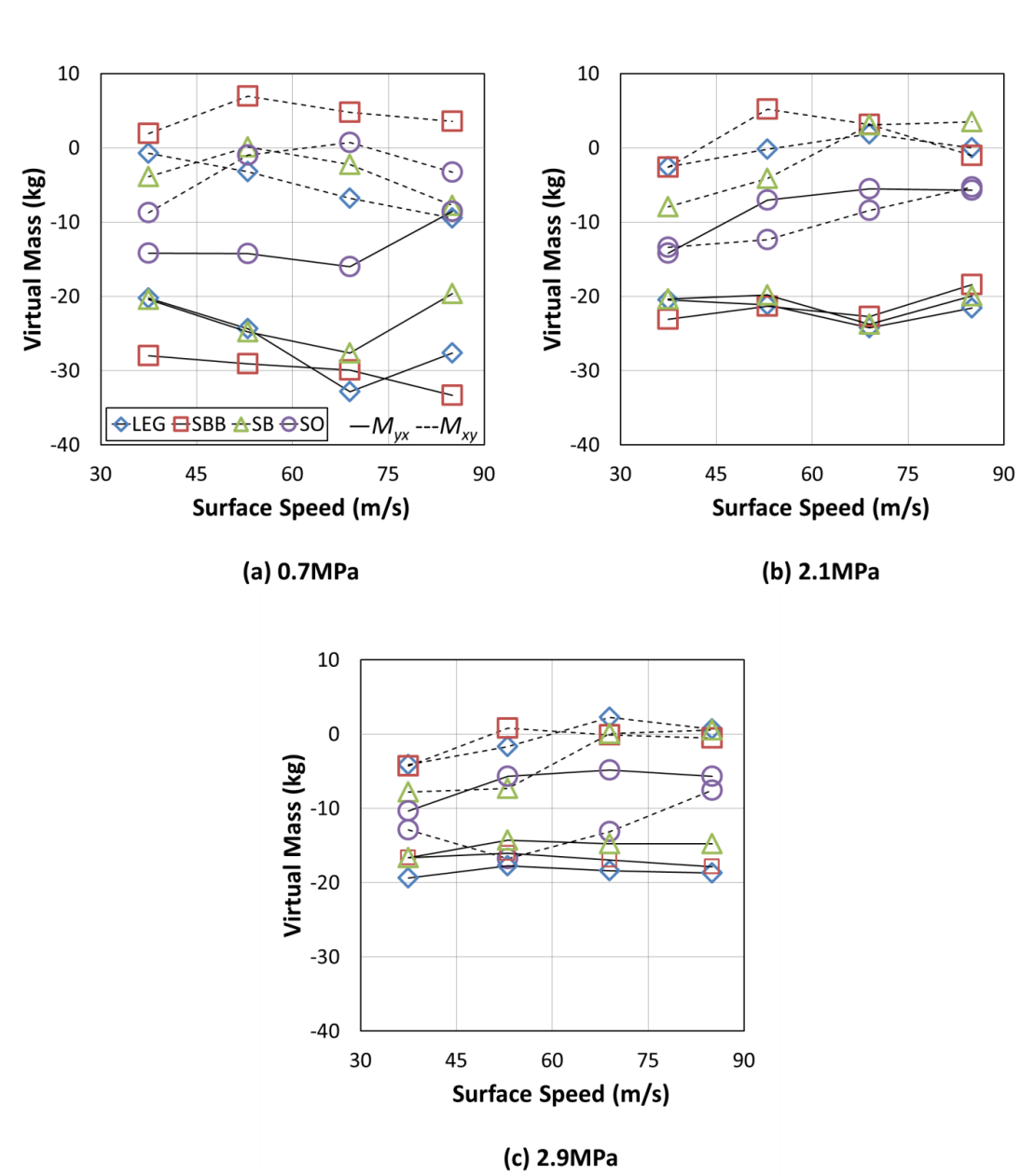

Figure G.4: M_{xy} & M_{yx} - Measured Cross-Coupled Virtual Mass as a Function of Speed for Unit Loads of (a) 0.7, (b) 2.1, and (c) 2.9 MPa (Not Shown: Predicted M_{xy} and $M_{yx} \approx$ Zero)